Espen Oland

Nonlinear Control of Fixed-Wing Unmanned Aerial Vehicles

Thesis for the degree of Philosophiae Doctor

Trondheim, November 2014

Norwegian University of Science and Technology
Faculty of Information Technology, Mathematics
and Electrical Engineering
Department of Engineering Cybernetics

NTNU – Trondheim
Norwegian University of
Science and Technology

NTNU
Norwegian University of Science and Technology

Thesis for the degree of Philosophiae Doctor

Faculty of Information Technology, Mathematics and Electrical Engineering
Department of Engineering Cybernetics

ISBN 978-82-326-0564-4 (printed ver.)
ISBN 978-82-326-0565-1 (electronic ver.)
ISSN 1503-8181

Doctoral theses at NTNU, 2014:326

Printed by NTNU-trykk

Summary

This thesis considers the problem of controlling fixed-wing unmanned aerial vehicles (UAVs). By estimating the higher order derivatives of the angle of attack and sideslip, the rotational and translational systems become decoupled. This allows a rotational control law to be designed first, followed by a speed controller. This decoupling also allows the dynamics to remain in their original form, such that control laws derived for general classes of Euler-Lagrange systems can be applied for flight control.

Several quaternion-based control laws are derived to point the speed in a desired direction. Specifically, a sliding surface controller, a backstepping controller, a PD+ controller and an adaptive backstepping controller are derived and presented in this thesis. The adaptive backstepping controller in particular enables adaptive control in the presence of actuator saturation, which is known for having a deteriorating effect on the adaptive update laws. The approach uses a reference signal to move the saturation from the plant to the reference, such that the update laws are unaffected by the actuator saturation. The same approach is applied for an adaptive speed controller. Two additional speed controllers are also derived, namely a model-based proportional controller and a model-based proportional-integral controller. Using the proposed decoupling, it allows the deflection angles to enter into the translational dynamics, and can be removed from the closed loop system using the thrust.

Through an analysis of the rotational control laws, it is observed that the airspeed directly affects the aerodynamic moments, such that by increasing the airspeed, saturation of the deflection angles can be avoided. This property is exploited by designing a reference speed that increases whenever the deflection angles cross a predefined threshold, and tracks a desired speed otherwise. By following the reference speed, the saturation problem of the deflection angles are moved to the translational system. This means that if the UAV has sufficiently thrust available, saturation of the deflection angles can be avoided.

With the possibility of pointing the airspeed in a desired direction and moving with a desired airspeed, the system is augmented with guidance. Using a mapping of the position tracking errors to one axis, a desired quaternion and angular velocity are found that facilitates waypoint tracking. The same idea is extended to trajectory tracking using a saturated control law that enables a UAV to track a point that is moving as a function of time. This is further extended to formation flight. By taking basis in rigid body dynamics, it enables desired positions, velocities and accelerations for any number of followers to be found relative to a virtual leader. These desired vectors are then mapped to controllable states, which then are tracked using the proposed control solutions.

In order to point the airspeed in a desired direction, multiple reference frames are required. This results in a composite quaternion and a corresponding angular velocity. From this structure, it is observed that behavioral control can be facilitated through the desired quaternion and angular velocity. Multiple tasks can be defined as simple rotations that are defined relative each other, and can be arranged in a hierarchy. This structure ensures that the primary task will always be fulfilled, and where lower level tasks will be completed successively. This approach fits per-

fectly with the subsumption architecture by Rodney Brooks, who derived methods for creating truly autonomous agents using behavioral control. The subsumption architecture is applied to a group of UAVs which fly through a city without colliding with each other, the buildings nor the ground, while tracking a series of waypoints. It is also applied for a terrain avoidance maneuver. The use of composite quaternion rotations enable multiple problems to be solved in a modular fashion, and can be used to make truly autonomous unmanned aerial vehicles.

Preface

This thesis is submitted in partial fulfillment of the requirements for Philosophiae Doctor Degree (PhD) at the Norwegian University of Science and Technology (NTNU), and is a result of research conducted at the Department of Technology at Narvik University College (NUC) from October 2010 to March 2014. The research has been funded by the Norwegian Research Council and is part of the Arctic Earth Observation and Surveillance Technologies project 195143/I60.

First and foremost I would like to thank my supervisor Dr. Raymond Kristiansen who has introduced me to the wonders of control theory, and who has guided me through this project. Throughout this project he has helped me with many technical challenges and shaped my way of thinking. I would also like to thank Professor Jan Tommy Gravdahl who has helped me with both technical and administrative problems. Whenever I have had any problems, he has quickly helped me to solve them and been a good support throughout this work. I am also grateful for interesting discussions with Professor Thor Inge Fossen, who helped me to truly define the control problem which enabled me to solve the problem of flight control. I would also like to thank Professor Andrea Serrani who I worked with during my stay at The Ohio State University (OSU). Much of my results can be contributed to our collaboration.

My best friend and good colleague Rune Schlanbusch has also been invaluable. Whenever I have had any technical problems, he has been quick to provide aid and never turned me down. My colleague Tom Stian Andersen has also provided me with help, and I will always be envious of his 3D modeling skills. I would also like to thank the library at NUC, especially Ellen Julin, Torild Rones, Unni Trondsen and Sidsel Kruuse-Meyer, who have provided me with all the literature that I have required for this work. Additionally, I would like to thank the library at the University of Agder, who provided me with a copy of the paper "On aërial locomotion" from 1864 at great expense for them, even though I have no direct affiliation with them.

Lastly I would like to thank my beautiful wife Siri and my two fantastic daughters Elise and Victoria. Siri for supporting me throughout these years, Elise for being so kind and gentle and Victoria for being full of character and as stubborn as her father. I would also like to thank my mother and father, Anne-Lise and Gunnar who have given me a good childhood and who have supported me in pursuing a technical degree. I am also grateful for my brother and friend Geir Arne who always has a spark in his eyes and is the only one who can make me laugh till I cry. I would also like to thank my mother and father in law, Eva and Steinar for accepting me into their family, and I appreciate all the support and aid we have received throughout the years.

Contents

List of Figures

Chapter 1

Introduction

> I am well convinced that 'Aerial Navigation' will form a most prominent feature in the progress of civilization.
>
> Sir George Cayley, 1804

An unmanned aerial vehicle (UAV) can be defined as a rigid body that uses aerodynamic forces and moments to produce lift and flies autonomously. This thesis considers fixed-wing UAVs that have wings that are fixed to the fuselage such that they resemble conventional aircraft, except that they fly autonomously without human interactions. The problem of flight control can be defined as pointing the speed in a desired direction, and move with a positive desired airspeed. This basic problem can be decomposed into two parts: a rotational problem of pointing the speed direction in a desired direction; and a translational problem of obtaining a desired airspeed. Each part can be solved by designing a rotational and translational controller which together enable a fixed-wing UAV to reach any point in Euclidean space, that in general can be moving.

1.1 Anatomy of a fixed-wing UAV

The body frame of a fixed-wing UAV can be defined as having its x axis aligned with the fuselage, the y axis pointing through the right wing and the z axis pointing downwards, completing the orthonormal system. The attitude (or orientation) of the body frame can be related to an inertial frame using a rotation matrix. The rotation matrix can be parameterized using *e.g.* quaternions, Rodrigues parameters or Euler angles. For aircraft, the use of Euler angles through the roll, pitch and yaw angles are well established and easy to visualize. The roll angle is defined as a rotation around the x axis, the pitch angle around the new y axis and the yaw angle around the new z axis (*cf.* Egeland and Gravdahl (2002)). Through these three rotations, the attitude of the body can be related to an inertial frame.

Figure 1.1 shows a standard configuration of a fixed-wing UAV. The UAV has four actuators: a propeller that produces thrust which can be used to control the

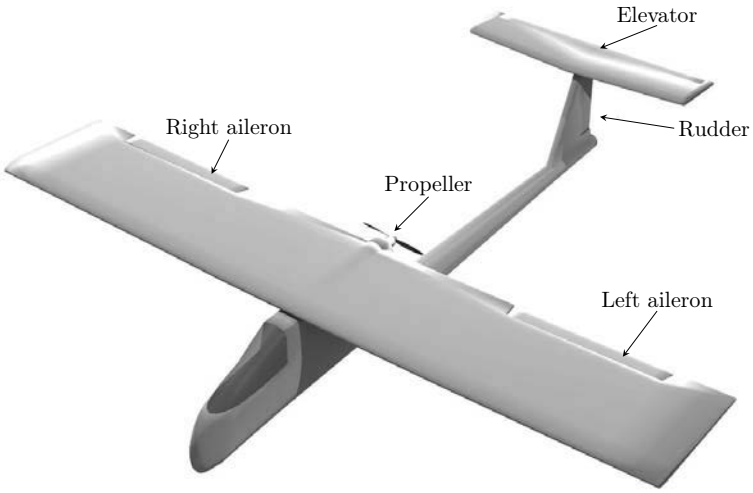

Figure 1.1: Standard configuration of a fixed-wing UAV. The propeller generates thrust which enables the airspeed to be controlled, while the aileron, elevator and rudder generate aerodynamic moments which can be used to control the orientation of the UAV (illustration by Tom Stian Andersen).

airspeed of the aircraft, and three control surfaces, namely aileron, elevator and rudder which can be used for rotational control. Note that the aileron consists of two parts, a left and right aileron that work in pairs in order to change the roll angle of the aircraft. The rudder is located at the back of the fuselage and is used to change the yaw angle, while the elevator is used to change the pitch angle of the aircraft. By changing the deflection angle of a control surface, aerodynamic moments will be generated, which results in an angular velocity that changes the orientation of the body. By changing the rotation speed of the propeller, the thrust can be increased or decreased, enabling the speed to be controlled. Early work on aerial locomotion is presented in Boulton (1864), where the author depicts using a screw motion (propeller) similar to that of steamboats in order to obtain aerial propulsion. The author also consider the energy requirement to produce enough lift to compensate for the gravity, and advocated the use of gun-cotton until a new power source could be found. Today, propellers are powered by either a combustion engine or using an electric power source, but the basic idea by Boulton (1864) of using a propeller is still employed by many aircraft.

The shape of the wing is called an airfoil and is illustrated in Figure 1.2, and due to the incoming airflow as the aircraft moves through the air, a lift force will be generated that is perpendicular to the direction of motion. This lift force is the

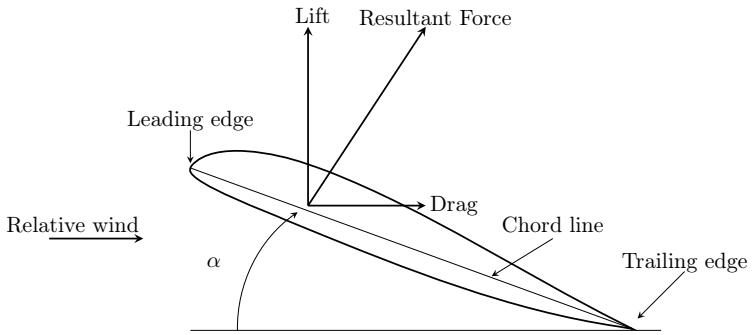

Figure 1.2: Illustration of an airfoil. As the UAV moves through the air with a positive airspeed, a lift force is generated that can be used to compensate for the gravity vector, while the wing introduces a drag component that must be compensated for using the thrust. By changing the angle of attack, α, the direction of the resulting force vector can be changed and used to move in any direction.

basic force that enables flight. Drag is another aerodynamic force that is aligned with the opposite direction of motion and serves as a damping force to slow down the aircraft. In order to obtain a desired airspeed the available thrust must therefore be larger than the drag, a force that increases as a function of the airspeed squared. The lift and drag are functions of the angle of attack. The angle of attack is defined as the angle between the chord line and the direction of relative motion, where the chord line is the line going from the leading edge to the trailing edge of the airfoil. By increasing the angle of attack (up to a limit), the lift force will be increased, which can be used to increase the altitude of the aircraft. Another important angle is the sideslip angle, which is defined as the angle between the centerline of the fuselage and the incoming airflow. Together, the angle of attack and the sideslip angle relate the direction of the airspeed to the body frame and are of great importance for flight control.

The lift vector can be tilted by rolling or *banking* the aircraft. While the roll angle is defined as a rotation around the x-axis of the body frame, the bank angle is defined as a rotation around the velocity vector. The ailerons, which were first presented in Boulton (1868), allows the aircraft to change the roll angle and consequently the bank angle, which results in improved lateral control compared to using only a yaw maneuver. For this reason, the three main angles that are used for flight control are the angle of attack, sideslip and bank angle. It is therefore common to use these angles as state variables.

1.2 Underactuation

In general the dynamics of a rigid body can be decomposed into rotational and translational dynamics. The rotational dynamics describe the changes in orienta-

tion and the angular velocity, while the translational dynamics describe the changes in position and velocity relative to an inertial frame. A free flying rigid body has six degrees of freedom. It can translate along three axes and rotate around each of these axes. In the case of a *fully-actuated* rigid body; the number of actuators are equal to the degrees of freedom, such that the control problem can be solved using any of the general control laws derived for Euler-Lagrange systems (*cf.* Paden and Panja (1988), Slotine and Li (1988), Ortega *et al.* (1998), Bloch *et al.* (2000), Luyckx *et al.* (2001), Kyrkjebø and Pettersen (2005), Mei *et al.* (2011) and Loría (2013)). In the case of a rigid body with fewer actuators than degrees of freedom, the rigid body is said to be *underactuated* –*cf.* Reyhanoglu *et al.* (1999). This means that the vehicle cannot follow an arbitrary trajectory, but must move as constrained by its actuators. For example, an aircraft must fly in a circular motion to reach a position that initially is to the left of the aircraft. It cannot move directly sideways[1].

The fact that fixed-wing UAVs and conventional aircraft are underactuated is rarely mentioned when designing control laws for flight control, even though they share similar constraints as autonomous underwater vehicles (AUVs) that commonly are defined as being underactuated. To stress this point, consider the actuator configuration of a fixed-wing UAV. It has four actuators: thrust for translational control and three control surfaces for rotational control; and has six degrees of freedom. With fewer actuators than degrees of freedom, a fixed-wing UAV is underactuated which complicates the controller design. Due to this underactuation it is not possible to control all degrees of freedom directly. Instead, it is possible to map the desired states from the *unactuated* to the *actuated* states, which can be controlled using known methods. This is the purpose of the guidance system, which is a standard component in any flight system. Consider the problem of altitude control. The only way of generating a lift force is by changing the angle of attack (and consequently the orientation). For this reason, the altitude error can be mapped to a desired angle of attack which then can be tracked using the elevator to generate aerodynamic moments that aligns the angle of attack with its desired value. Had the vehicle been fully-actuated it would simply have generated a lift force directly to obtain the desired altitude, instead of using the angle of attack as a state variable.

Accepting the fact that fixed-wing UAVs are underactuated, it allows the results from other underactuated rigid bodies to be applied. Underactuated control has received much attention such as *e.g.* ships, AUVs, quadrotors, planar vertical take-off and landing aircraft, spacecraft, the pendubot system, hovercraft and surface vehicles (*cf.* Wichlund *et al.* (1995), Leonard (1995), Godhavn and Egeland (1995), Spong (1998), Pettersen and Egeland (1999), Olfati-Saber (2001), Bullo and Lynch (2001), Aguiar and Pascoal (2002), Fantoni and Lozano (2002), Fossen *et al.* (2003), Børhaug and Pettersen (2005*a*), Breivik and Fossen (2005), Arrichiello *et al.* (2006*b*), Tayebi and McGilvray (2006), Aguiar and Hespanha (2007), Refsnes *et al.* (2007), Lee *et al.* (2007), Roberts and Tayebi (2009), Hua *et al.* (2009), López-Martínez *et al.* (2010), Lee *et al.* (2010), Toshimura *et al.* (2011) and references therein). The different control solutions that have been derived for these vehicles,

[1] An aircraft can experience small changes in the lateral direction through the aerodynamic forces, but these forces are too small to be used for lateral control.

have exploited the knowledge about underactuation, and used that as a starting point for controller design. In the particular case of controlling ships and AUVs, the problem is solved by finding a desired orientation, angular velocity and speed that make the position (and velocity) tracking errors converge to zero. These results can easily be adapted for flight control and have served as an inspiration for this thesis.

Another way of defining actuation is presented in Tedrake (2009). The general form of a second order dynamical system can be written as

$$\ddot{\mathbf{q}} = \mathbf{f}_1(\mathbf{q}, \dot{\mathbf{q}}, t) + \mathbf{f}_2(\mathbf{q}, \dot{\mathbf{q}}, t)\mathbf{u} \tag{1.1}$$

where $\mathbf{q}$ is a vector of positions, $\dot{\mathbf{q}} := \frac{d}{dt}\mathbf{q}$ is a vector of velocities, t is time and $\mathbf{u}$ is the control vector.

Definition 1.1 (fully actuated) *A control system described by (1.1) is said to be fully-actuated in the configuration $(\mathbf{q}, \dot{\mathbf{q}}, t)$ if it is able to command an instantaneous acceleration in an arbitrary direction in $\mathbf{q}$:*

$$rank(\mathbf{f}_2(\mathbf{q}, \dot{\mathbf{q}}, t)) = dim(\mathbf{q}). \tag{1.2}$$

Definition 1.2 (Underactuated) *A control system described by (1.1) is underactuated in the configuration $(\mathbf{q}, \dot{\mathbf{q}}, t)$ if it is not able to command an instantaneous acceleration in an arbitrary direction in $\mathbf{q}$:*

$$rank(\mathbf{f}_2(\mathbf{q}, \dot{\mathbf{q}}, t)) < dim(\mathbf{q}). \tag{1.3}$$

From a control perspective, this means that a fully actuated vehicle is able to track an arbitrary trajectory which may not be possible for an underactuated vehicle. Imposing certain constraints on the trajectory allows an underactuated vehicle to track it, but in order to perform the tracking, the errors of the unactuated states must be mapped to the actuated states. For aircraft, this means that the desired position and velocity errors relative to a desired trajectory must be mapped to a desired speed, orientation, angular velocity and accelerations. These desired states can then be tracked using the available actuators.

1.3 Flight Control

The first autopilot was designed by the Sperry Corporation in 1912 (Dyer (2001)). Since then, much research has been performed on aircraft control and many different methods have been derived. Recent results on control of fixed-wing UAVs are presented in Ren and Beard (2003), Ren and Beard (2004) and Ren and Atkins (2005) where problems such as unknown autopilot constants, actuator constraints and trajectory tracking are solved. The authors consider the kinematic model which they decouple into two parts: one for altitude and one for motion in the xy-plane. This enables the authors to apply the results from mobile robots that received much attention during the 1990's and early 2000 (*cf.* Kanayama *et al.* (1990), Samson (1995), Fierro and Lewis (1997), Jiang *et al.* (2001) and Tanner and Kyria (2002)). By applying the results from mobile robots, the problem of flight control becomes simple. Other results on kinematic UAV control include among others Betser *et al.*

(2005), Hao *et al.* (2005), Jeyaraman *et al.* (2005), Xie *et al.* (2005), Ambrosino *et al.* (2006) and Beard and Humpherys (2011). When using kinematic control, the second order dynamics of the system is ignored such that the UAV is controlled directly using the airspeed and the angular velocity. In truth, the UAV requires torques and thrust to change the angular velocity and airspeed which must be accounted for when designing the control laws.

Nonlinear dynamic inversion (NDI) is considered one of the prominent methods for controlling aircraft and has resulted in publications such as Lane and Stengel (1988), Snell *et al.* (1992), Stiharu-Alexe and Stiharu-Alexe (1993), Ngo and Doman (2001), Ito *et al.* (2002), Yu *et al.* (2009) and Rizwan *et al.* (2011). In essence, the method consists of an inner-outer loop, where an outer loop consists of slow variables (angles), while an inner loop consists of fast variables (angular velocities). By applying the time-scale separation principle –*cf.* Reiner *et al.* (1996) the fast variables can be treated as constants in the outer loop. This simplifies the problem and enables the desired angles to be used for generating desired angular velocities, which then are sent through a linear filter to generate desired angular accelerations. By inverting the dynamics, the deflection angles that correspond to the desired angular accelerations are found, which then can be used to control the aircraft. As a simple example of the NDI approach, consider the linearized roll dynamics which can be written as (Honeywell and Lockheed Martin (1996))

$$\dot{p} = L_p p + L_{\delta_a} \delta_a \tag{1.4}$$

where p is the roll rate, L_p and L_{δ_a} are the linearized damping and aileron efficiency coefficients respectively, while δ_a is the deflection angle of the ailerons. To find the deflection angle of the ailerons (1.4) can be inverted as

$$\delta_a = \frac{1}{L_{\delta_a}} \left(\dot{p} - L_p p \right). \tag{1.5}$$

To find a control law; δ_a can be replaced by the commanded one, δ_a^{com}, $\dot{p}$ can be replaced by a desired angular acceleration $\dot{p}^{des}$, the roll rate, p, can be replaced by the measured value p^{meas}, such that the commanded deflection angle is found as

$$\delta_a^{com} = \frac{1}{L_{\delta_a}} \left(\dot{p}^{des} - L_p p^{meas} \right). \tag{1.6}$$

Inserting (1.6) into (1.4) assuming that $\delta_a = \delta_a^{com}$, $p = p^{meas}$ it follows that $\dot{p} = \dot{p}^{des}$, indicating that by using dynamic inversion, the correct output can be found. However, since actuator dynamics, measurement noise, parameter uncertainty and actuator saturation must be accounted for, this will rarely be true and can only be considered an ideal case. Several papers have dealt with NDI using nonlinear aerodynamics to allow the model to be valid for the whole flight regime. The method has therefore been augmented with adaptive control and robustness to address these issues –*cf.* Wang and Stengel (2000), Wang and Stengel (2005), MacKunis *et al.* (2010) and Sieberling *et al.* (2010).

Model predictive control (Slegers *et al.* (2006)), feedback linearization (Charlet *et al.* (1988), Hauser *et al.* (1992)) and backstepping (*cf.* Krstić *et al.* (1995))

are other methods that are applied for flight control[2]). Especially backstepping has received much attention with regards to flight control with results such as Härkegård and Glad (2000), Lee and Kim (2001), Farrell *et al.* (2005), Robinson (2007) and Sonneveldt *et al.* (2009*a*).

Rewriting the translational dynamics by defining the angle of attack, sideslip and bank angle as state variables (*cf.* Honeywell and Lockheed Martin (1996)), the system can be put on a lower triangular form to facilitate backstepping design under certain assumptions. This results in an *aggregated* dynamics that looses the good properties of the rotation matrices, cross products and becomes singular at certain angles. Another major problem, is that the deflection angles enter through both the aerodynamic forces and moments. The aggregated dynamics can be written on the form

$$\dot{\mathbf{x}}_1 = f_1(\mathbf{x}_1, \mathbf{u}) + g_1(\mathbf{x}_1)\mathbf{x}_2 \tag{1.7}$$
$$\dot{\mathbf{x}}_2 = f_2(\mathbf{x}_1, \mathbf{x}_2) + g_2(\mathbf{x}_1, \mathbf{x}_2)\mathbf{u} \tag{1.8}$$

where $\mathbf{x}_1$ represents the angle of attack, the sideslip angle and the bank angle, $\mathbf{x}_2$ represents the angular velocity and $\mathbf{u}$ represents the deflection angles that are used for control. This enables $\mathbf{x}_2$ to be used as virtual control to stabilize the $\mathbf{x}_1$ system, while $\mathbf{u}$ can be used to stabilize the new system that is designed during the backstepping process. The important point is that the deflection angles that also are part of the $\mathbf{x}_1$ system must be assumed to be constant during the first step of the backstepping design which is valid by invoking the time-scale separation principle (Reiner *et al.* (1996)). Since the correct deflection angles at a given time-step are not directly available, the deflection angles from the previous time-step can be used when stabilizing the $\mathbf{x}_1$ system. Naturally this introduces small errors to the system that can be considered negligible using time-scale separation.

Quaternion-based approaches for flight control are presented in *e.g.* Ngo and Doman (2001), Doman and Ngo (2002), Johnson *et al.* (2008) and Sobolic and How (2009). In Ngo and Doman (2001) and Doman and Ngo (2002) quaternions are used in the outer loop to generate angular velocity commands which then are sent to an inner loop where the deflection angles are found. In Sobolic and How (2009) and Johnson *et al.* (2008) quaternion-based control laws are derived to enable transition between leveled flight and hover for fixed-wing UAVs. Quaternion-based control has also received much attention for other mechanical systems such as spacecraft, AUVs, vertical-take-off and landing (VTOL) UAVs or general rigid bodies (*cf.* Wen and Kreutz-Delgado (1991), Fjellstad (1994), Pettersen and Egeland (1996), Akella *et al.* (2005), Tayebi (2008), Kristiansen (2008), Roberts and Tayebi (2009), Schlanbusch (2012) and references therein).

1.3.1 Adaptive Control

With unknown aerodynamics, the aerodynamic model must be estimated which can be done through adaptive control. One of the first results on adaptive control is presented in Simon (1956) where the author apply the certainty equivalence

[2]Note that NDI and feedback-linearization are essentially the same (*cf.* MacKunis *et al.* (2010)

principle to design a controller with unknown parameters. The author estimated the parameters, and then used the estimated parameters as part of the control law as if they were the true parameters. As pointed out in Becker *et al.* (1985), the estimated parameters are not necessarily the true values. This results in a degradation and a sub-optimal solution by using the certainty equivalence principle, and has resulted in more research on adaptive control using an adaptive update law in works such as Leonessa *et al.* (2001), Sonneveldt (2010) and Hovakimyan *et al.* (2011). Even though the coefficients don't necessarily converge to their true values, the impact of modeling imperfection is dealt with by the control law and the adaptive update law, and in a Lyapunov sense, the impact of the modeling uncertainty does not affect the stability of the resulting equilibria.

A different problem with adaptive control is actuator saturation. When the actuators go into saturation, the adaptive update law "believes" that it has converged to the correct values, which is not true. This leads to a deterioration of the closed loop system.

1.3.2 Actuator Saturation

Actuator saturation is a common and significant nonlinearity that affects the flight controller and can have dire consequences. For flight control, saturation resulted in the YF-22 crash in 1992 and the Gripen JAS aircraft in 1993, where rate constraints resulted in pilot induced oscillations making the closed loop system unstable (Dornheim (1992), Murray (1999), Bak (2000)). It has also been blamed as a contributing factor to the Chernobyl nuclear plant accident in 1986 as discussed in Stein (2003). It is therefore critical to take actuator constraints into account when designing control laws. Note that actuator saturation is not only a bad quality, and it has been shown in Sourlas *et al.* (1994) that the disturbance rejection qualities of a system with saturation is better than that of a system without saturation.

A well-known approach to deal with the saturation nonlinearity is anti-windup. Originally the phenomenon of integrator *windup* was observed when using PID control with saturation. When the actuators are in saturation, the integrator term will continue to integrate the error, resulting in a large windup that must be removed when the actuators have desaturated. There are two basic approaches to this problem: back calculation and conditional integration (clamping). Back-calculation uses a feedback loop to discharge the integrator while the actuators are in saturation, while conditional integration simply stops the integrator while the actuators are in saturation.

When designing a control law using Lyapunov theory, the stability of the resulting equilibria usually assume infinite actuation. This means that if the saturation nonlinearity is not accounted for during the design, it can result in an unstable closed loop system. In Akella *et al.* (2005) a quaternion-based control law is designed for a general rigid body that takes both magnitude and rate saturation into account. Using a filter to estimate the angular velocity together with the natural bounds on the unit-quaternion, ensures that the required control action always remain within its bounds by properly choosing the gains and desired trajectories.

In Annaswamy and Wong (1997) the authors account for the saturation nonlinearity when designing the adaptive update laws for a linear plant. This results

in global stability[3] when the plant is open loop stable[4] and minimum phase[5], and locally stable[6] otherwise. For flight control, a recent method that has received some attention is the use of command filtered backstepping (Farrell *et al.* (2005)). Instead of using the virtual control in the next step of the backstepping process, it is instead sent through a saturated filter that ensures that its output remains within its bounds. This is used to ensure that all the tracking errors are small enough to make the actuators operate in their linear regions. As stated, the impact of actuator saturation is especially important for adaptive control. Roughly speaking, an adaptive update law is simply an integrator that integrates up the error. Similarly as for integrator windup, saturation will result in a system degradation that must be accounted for. In Johnson and Calise (2000) this problem was handled by feeding back the difference between the commanded and actual actuator signal to a reference generator. This ensures that the reference signal will deviate from the desired trajectory whenever the actuators are in saturation, such that the adaptive update law will not "see" the actuator saturation. The same result was extended in Johnson and Calise (2001) and Johnson and Calise (2002) and later applied in a quaternion framework with applications to adaptive spacecraft control in Tandale and Valasek (2005). The idea has also been applied in Lavretsky and Hovakimyan (2004), where the actuators can become bounded by a virtual bound chosen arbitrarily, such that the deflection angles never go into saturation.

1.3.3 Decoupling

The dynamics of an aircraft are strongly coupled since the deflection angles enter both through the aerodynamic forces and moments. Due to the strong coupling, a decoupling method is required. A common decoupling method is to assume that the roll and sideslip angles are zero. This represents a normal flight condition and enables the nonlinear dynamics to be decoupled into a longitudinal and a lateral system (*cf.* Stevens and Lewis (2003) and Lavretsky and Wise (2013)). The longitudinal motion is described by pitching and translation in the $x - y$ plane, while the lateral motion is described by rolling, sideslipping and yawing. Hence, the longitudinal/lateral decoupling results in two systems that contain mixed sets of both translational and rotational states, and is a well established approach that is common in the literature.

Instead of decoupling the nonlinear dynamics into a *longitudinal* and a *lateral* system, it can be decoupled into a *rotational* and a *translational* system. By approximating the higher order derivatives of the angle of attack and sideslip angle, it allows the rotational controller to be designed first, followed by a speed controller. The use of filters for flight control is common for both backstepping and nonlinear dynamic inversion. When using the NDI approach, the desired angles are compared with the measured angles producing an error. This error is sent through a filter to generate a desired angular velocity. Similarly, the error in angular velocity is sent

[3]The origin is stable for any initial conditions.

[4]The origin is stable in the absence of feedback.

[5]A transfer function is said to be minimum phase when it has all zeros in the open-left half plane (Khalil (2002)).

[6]The origin is stable with unknown region of attraction (Khalil (2002)).

through another filter to generate the desired angular acceleration. By inverting the dynamics, the control signal can be found. This approach results in an inner-outer loop, where the inner loop is the fast variables (angular velocities), while the outer loop contains the slow variables (angles). Instead of filtering the errors, it is possible to filter the angle of attack and sideslip angle directly. This removes the need for an outer loop, and it enables the desired trajectory to be defined relative to an inertial frame. A similar idea is presented in Breivik and Fossen (2005) where the authors correct the desired angles with the angle of attack and sideslip before filtering the desired attitude to obtain the higher order derivatives.

In Kaminer *et al.* (1998) an integrated approach to guidance and control is presented. The authors present a method for designing controllers for UAVs that enables them to track trajectories relative to an inertial frame. They design trimmed trajectories (at equilibrium) that are parameterized by the linear speed, yaw rate and flight path angle[7], which then enable a UAV to track them. With basis in the angle of attack and the sideslip angle, the authors trim the trajectories to enable leveled flight and to enable the UAV to track a helix trajectory. In order to trim the trajectory, the authors require the angular acceleration between the body frame and the inertial frame. Since the angular acceleration is not directly available from sensor measurements, they approximate it using a linear filter. For this reason, the filtering of the angle of attack and the sideslip angle to find their higher order derivatives, share many similarities with the results by Kaminer *et al.* (1998).

1.4 Guidance

The flight system requires inputs that the controllers can track in order to complete a mission objective. Guidance is defined by Shneydor (1998) as the process for guiding the path of an object towards a given point, which in general may be moving. One of the most well known guidance laws is proportional navigation (PN) and has received much attention for missiles and aircraft –*cf.* Murtaugh and Criel (1966), Guelman (1971), Yang and Yang (1995), Palumbo *et al.* (2010). By generating acceleration commands that are proportional to the line-of-sight rate, the missile or aircraft will be able to intercept a desired point in finite time. The basic idea has served as an inspiration to similar guidance laws as presented in Baba *et al.* (1993), Park *et al.* (2004), Breivik and Fossen (2008) and Dhananjay and Kristiansen (2012). Another way of looking at line-of-sight based guidance such as PN, is to map all the position errors to one axis. By aligning the speed direction with that axis, it is a simple matter of moving with a positive speed to make the error go to zero.

The problem of tracking a desired angle of attack, sideslip angle and bank angle can be solved using the NDI control law as presented previously. One issue with using a desired angle of attack and sideslip angle, is that these angles are defined relative to a body frame, and not an inertial frame. An intermediate step is therefore required to go from a desired trajectory defined relative to an inertial frame to obtain the desired angle of attack, sideslip angle and bank angle. For example in Sonneveldt (2010), the presented solution requires an additional step

[7]The angle between the horizontal plane and the velocity vector.

in the backstepping process in order to map the desired trajectory to trackable variables. So from a guidance point of view, it can be argued that UAVs should be able to track trajectories defined relative to an inertial frame, *i.e.* the output from the guidance should be directly trackable by the control solution.

Autonomous underwater vehicles and fixed-wing UAVs share similar constraints; guidance laws derived for AUVs can therefore be directly applied for fixed-wing UAVs by properly designing the control laws. Some recent results on guidance for autonomous underwater vehicles are presented in Børhaug and Pettersen (2005*a*), Børhaug and Pettersen (2005*b*), Breivik and Fossen (2005), Breivik and Fossen (2007) and Breivik and Fossen (2009). In Breivik and Fossen (2005), the authors show how to derive guidance commands that enable an AUV to perform path following in three dimensions while Børhaug and Pettersen (2005*a*) show how to perform waypoint tracking. The output from these guidance laws are desired pitch and yaw angles together with a desired speed which can be used for flight control if the controller is properly designed. Some recent results on guidance methods for UAVs are presented in Osborne and Rysdyk (2005), Rysdyk (2006), Sato *et al.* (2006), and Nelson *et al.* (2007). In Nelson *et al.* (2007) a guidance law is designed that enables path following of straight lines, circular arcs and orbits. The authors also show how wind can be accounted for, an issue that is also addressed in works such as Osborne and Rysdyk (2005) and Rysdyk (2006).

1.5 Behavioral Control

With the possibility of guiding a UAV to any position that in general can be moving, how can this be extended to make an agent truly autonomous? By simply allowing a UAV or an agent to follow a predefined trajectory, the autonomy of the agent becomes constrained by its programming. To exceed its programming and to behave like a truly autonomous agent, behavioral control can be applied.

Some of the first works on behavioral-based control was by Reynolds (1987) who derived a computer model of bird flocks with application to computer graphics. Reynolds started with the fact that any individual bird that is part of a flock has two balanced opposing behaviors as described in Shaw (1975): the desire to stay close to the flock, and the desire to avoid collision within the flock. Flocking behavior has been studied intensively, where it is argued that by flying in a flock the individual birds increase their chances of survival from predators, have an increased chance of finding a mate and an increased probability for finding food (Werner and Dyer (1993)). Consider Figure 1.3 which shows a flock of snow geese. To simulate the flock, three behaviors that lead to a simulated flocking behavior were defined by Reynolds (1987) with decreasing precedence as

1. Collision avoidance: avoid collisions with nearby flockmates
2. Velocity matching: attempt to match velocity with nearby flockmates
3. Flock centering: attempt to stay close to nearby flockmates.

Each of these behaviors can be treated as a desired acceleration, which can be used to find a weighted averaged for the whole flock, producing a total acceleration to

Figure 1.3: Snow geese in flight. Consider the impressive feat of performing collision avoidance while moving with high speed as part of a flock (reproduced with permission by Stephen L. Tabone).

facilitate the flocking behavior. The basic idea of behavioral control has generated a multitude of publications on different methods for performing coordination of a group of agents (*cf.* Jadbabaie *et al.* (2003), Fax and Murray (2004), Ihle *et al.* (2006), Olfati-Saber *et al.* (2007), Ren and Beard (2008), Yang *et al.* (2008), Qu (2009), Tsourdos *et al.* (2011), Xargay *et al.* (2012), Lewis *et al.* (2014) and references therein). Using averaged accelerations, Reynolds (1987) presented an example of what can happen if the averaged acceleration from multiple tasks are used to direct an agent. Consider a grid-based city where the agent is located at an intersection. One behavior tells the agent to move North, while another behavior tells the agent to move East. Each of these behaviors alone would provide a good choice, but the averaged combination of moving North-East would result in a collision.

Instead of using an averaged approach, it is possible to use a parallel approach. The subsumption architecture by Rodney Brooks as presented in Brooks (1986), Brooks (1990), Brooks (1991*a*), Brooks (1991*b*) enables the problem of controlling an agent in a complex dynamic environment to be divided into several simple behaviors or tasks that can be arranged in a hierarchy. By letting a higher level task *subsume* or suppress the conflicting parts of the lower level tasks, it can be used to ensure that the primary task always will be fulfilled. As the primary task is completed, the secondary task will be fully pursued and so on until all the tasks have

been completed. This enables several simple behaviors to be defined and arranged in a hierarchy. Consider for example behaviors such as: wander around aimlessly, avoid obstacles, move to a desired position, and map an area. Any of these behaviors alone would result in an apparent unintelligent motion for the agent, but by using the subsumption architecture, it will make the agent appear intelligent as it purposely moves from point A to B while mapping the area and avoiding obstacles. As stated in Brooks (1991*a*), "*intelligence is in the eye of the observer*", such that if an agent is able to move around in a complex dynamic environment without collisions, it will appear intelligent, which is the purpose of the behavioral control method. The modularity approach to the subsumption architecture makes it very attractive. Each task is designed individually and can be fully tested before augmenting the system with additional tasks. By adding an addition task or *layer*, the apparent level of intelligence will be further augmented. The basic idea has resulted in the null-space-based behavioral (NSB) control method as presented in Antonelli *et al.* (2005*b*), Arrichiello (2006) and Arrichiello *et al.* (2006*b*). It adheres to the principle of layered control, but where it is only the conflicting velocity components that are removed by projecting them onto the nullspace. The reference velocity vector is found as the sum of the individual task velocity vectors, producing a reference that ensures that the primary task is always fulfilled. When controlling fixed-wing UAVs, the use of a reference velocity vector is not directly applicable since UAVs are underactuated with only translational control in one direction. To apply this approach to underactuated vehicles, the reference velocity vector must be mapped to a desired orientation and speed which has been done in work such as Arrichiello *et al.* (2006*a*) where the approach was applied to a formation of underactuated surface vessels. The NSB approach has also been applied to problems such as control of mobile robots (Antonelli *et al.* (2005*a*), Antonelli *et al.* (2006), Antonelli *et al.* (2008), Arrichiello *et al.* (2009)) performing spacecraft reconfiguration (Schlanbusch *et al.* (2008), Oland *et al.* (2010), Schlanbusch and Oland (2013)) and control of quadrotors (Oland *et al.* (2013*b*)).

1.5.1 Formation Flight

One behavior in particular that is very interesting is formation flight. When snow geese migrate for the winter to warmer climates they maintain a V-formation as shown in Figure 1.4. This has several purposes. Flying as part of a flock reduces the probability of being killed by predators. Predators may stalk lone individuals more successfully than those in flocks, since the use of flocks have an increased sensing range and are therefore better to assess their surroundings (Goldman (1980)). Furthermore, predators are more likely to attack birds at the edges of the formation, making the central birds relatively safe. The use of a V-formation also reduces the drag of the birds flying in the wake of the leader (central front bird). This reduction in drag reduces the amount of energy required, and thereby increasing the potential traveling distance. As pointed out in Lissaman and Shollenberger (1970), 25 birds flying in a V-formation can theoretically increase their range by 70% compared to a single bird flying alone.

This means that by using a close formation of aircraft, the operational radius can be greatly increased, as compared to a single aircraft. By constraining the

Figure 1.4: Snow geese in formation (reproduced with permission by Stephen L. Tabone)

aircraft to the same altitude, Blake (2002) shows that the theoretical range increase for nine aircraft flying in a V-formation is 80%. Introducing other constraints such as turbulence, actuator constraints, etc. reduces this value. To maintain a close formation is very challenging, and manned formation flight is mainly done for obtaining a visual line of sight and attack purposes. Figure 1.5 shows nine Red Arrows maintain a V-formation together with two Spitfires during an air show in 2005. Maintaining such a close formation is considered an impressive feat and requires many years of practice for a human pilot. For unmanned aerial vehicles, it is possible to derive control laws that enable the UAVs to position themselves appropriately where they can exploit the drag reduction, and thereby increase their operational range. This actually makes UAVs better suited than manned flight for observation in the arctic regions, and hence a formation of UAVs can travel farther than a single UAV.

From a control perspective, the use of formations for aircraft, spacecraft, ships, and quadrotors has received much attention (*cf.* Giulietti *et al.* (2000), Fierro *et al.* (2001), Borrelli *et al.* (2004), Song *et al.* (2005), Dogan and Venkataramanan (2005), Betser *et al.* (2005), Arrichiello *et al.* (2006*a*), Campa *et al.* (2007), Paul *et al.* (2008), Kristiansen (2008), Cui *et al.* (2010), Abdessameud and Tayebi (2010), Schlanbusch (2012), and Guerrero *et al.* (2012)). It poses an interesting control problem, while its applications have the potential for energy savings, redundancy, line of sight communication, improved coverage of a region and 3D sensor measurements. Hence, the use of multiple UAVs can obtain an increased capacity compared

Figure 1.5: Red arrows flying in a V-formation together with two Spitfire aircraft (reproduced with courtesy to Andrew P. Clarke)

with that of a single UAV.

1.5.2 Collision Avoidance

With multiple agents flying in a formation or a flock, collision avoidance is an important behavior that must be maintained at all times. The problem of collision avoidance can be defined as maintaining the relative distance between two agents above a threshold. If the relative distance goes to zero, the agents will collide. Consider the case of an obstacle between an agent and its desired position. The obvious method of avoiding the collision is to move directly away from the obstacle which thereby increases the relative distance, but then the secondary objective of reaching the desired position will not be fulfilled. Another way of avoiding collision is to move perpendicular to the line of sight vector between the agent and the obstacle, which will result in a circular motion around any obstacle. Not only will this avoid collision, but it can also enable the agent to reach its desired position after it has moved around the obstacle.

Collision avoidance has received a lot of attention the last decades, and has resulted in solutions such as the artificial potential field method (Khatib (1986)), navigation functions (Rimon and Koditschek (1992)) and the NSB method (Antonelli *et al.* (2005*b*)). The artificial potential field method by Khatib (1986) is

intuitively simple, as an attractive potential is placed at the desired position, while a repulsive potential is placed around the obstacle. By following the negative gradient of the total potential field, the agent is able to reach the desired position without colliding with the obstacle. The beauty of the artificial potential field method is that it provides both a path planning method and a control law at the same time, and is a very popular approach (*cf.* Kim and Khosla (1992), Kyriakopoulos *et al.* (1995), Ge and Cui (2000), Paul *et al.* (2008), Chunyu *et al.* (2009), Qu (2009), Siciliano *et al.* (2010) and references therein). Even though it is simple, the potential field approach has several drawbacks, such as its inability to pass through narrow gaps, the possibility of getting stuck at a local minimum and becoming trapped, as discussed in Koren and Borenstein (1991). The navigation function was derived in Rimon and Koditschek (1992) to counter this, and is an extension of the potential field method which ensures that the agent will move to the desired position, while avoiding local minima. For flight control, the navigation function was extended for nonholonomic vehicles in Roussos *et al.* (2010), where it is applied to an aircraft-like nonholonomic vehicle with velocity constraints[8].

1.6 Applications

Unmanned aerial vehicles have become very popular the last decade with both military and civilian applications. The Predator UAV as shown in Figure 1.6, was initially designed for observation and reconnaissance and entered active duty in 1995, and has since then been retrofitted with armaments and been applied for several military campaigns. The main motivation has been to reduce the loss of American lives, and instead of using a human pilot that must be inside the UAV, a human operator can remotely control the UAV from any location without fearing for his life. This makes the UAVs expendable (although expensive) drones that can ensure aerial superiority. A Predator moving at high speed makes relatively little noise, and by launching a Hellfire missile that is supersonic, no sound will be heard before the missile hits its target, thus making the Predator UAV a formidable weapon.

Civilian applications of UAVs include *e.g.* autonomous mapping, search and rescue, communication relay and 3D mapping (*cf.* Templeton *et al.* (2007), Goodrich *et al.* (2007), Waharte and Trigoni (2010), Dixon and Frew (2007), Burdakov *et al.* (2010), Cetin and Zagli (2012), Rogers and Finn (2013) and references therein). Another application is crop monitoring and pest control and is often highlighted as one of the most potential civilian applications of UAVs (*cf.* Huang *et al.* (2009) and Zhu *et al.* (2010)). Using UAVs to monitor a field, it enables the exact detection of where the pests are emerging which then can be combated using a targeted spraying of pesticide to protect the crop. Not only is it faster using UAVs over a large area than using conventional methods, it also enables large savings in pesticide, since it

[8]Underactuated vehicles have an acceleration constraint also known as a second order nonholonomic constraint, while in general when speaking of a nonholonomic constraint, it is the first order nonholonomic constraint that is considered, which is a velocity constraint (*cf.* Bloch *et al.* (2007)). Due to gravity and aerodynamic sideslip forces, an aircraft will always possess small velocity components along the unactuated axes, such that an aircraft is to be considered an underactuated vehicle with second order nonholonomic constraints.

Figure 1.6: An MQ-1 Predator armed with an AGM-114 Hellfire missile flies a training mission (Courtesy to the U.S. Airforce).

is no longer required to spray the whole field, only where the pests are emerging. UAVs can also be used to perform *in-situ* measurements which has resulted in many papers on the subject such as Kuroki *et al.* (2010), Wegener *et al.* (2004) and Šmídl and Hofman (2013), where it is argued that using multiple UAVs as a mobile sensor network will be less expensive and more accurate compared to ground-based sensors. In Subchan *et al.* (2008) the problem of tracking a cloud of contaminant was studied, and they propose an algorithm to track the contaminant cloud based on waypoints to map the entry and exit points of the cloud to track the cloud itself. Real-time particle tracking is presented in Oland and Kristiansen (2013*c*) where multiple UAVs move in a formation to locate the points of a volcanic ash plume with highest density to provide real-time inputs to analytical plume models.

1.7 Contribution and Scope of Thesis

This thesis considers the problem of controlling fixed-wing UAVs. It presents several rotational and translational control laws that together with different guidance methods enable waypoint tracking, trajectory tracking, formation flight and behavioral control. In particular, a quaternion framework is presented which enables

multiple problems to be dealt with in a modular fashion. Through the desired quaternion and angular velocity, several different tasks can be defined and fused together using the subsumption theory. To facilitate control of a fixed-wing UAV, a filter is applied to find the higher order derivatives of the angle of attack and the sideslip angle. This enables a rotational controller to be designed first, followed by a speed controller. The airspeed dynamics are found by taking basis in the Euclidean norm and enables singularity-free speed controllers to be derived. The presented approach does not apply an inner-outer loop, and enables control of the UAV directly relative to an inertial frame.

By maintaining the dynamics in their original form, it enables control laws derived for general classes of Euler-Lagrange systems to be directly applied. This thesis considers the work by Kristiansen (2008) and Schlanbusch (2012) as a starting point, where quaternion-based control laws are derived to change the orientation of spacecraft. By using the proposed decoupling, the control laws are adapted to the case of flight control, which then enable the airspeed to be pointed in a desired direction. Together with singularity-free speed controllers, a UAV is able to obtain any desired orientation, angular velocity and speed.

1.7.1 Contributions and Summary

- Chapter 2: Based on previous work on aircraft (*cf.* Etkin (1972), Stevens and Lewis (2003) and Stengel (2004)), the mathematical modeling of fixed-wing UAVs is presented in this chapter. It is also shown how the speed direction can be related to an inertial frame through a composite quaternion rotation. The rotational and translational dynamics are then written in a form that facilitates controller design by decoupling the systems. Two sets of dynamics are presented: one that assumes that the aerodynamics are perfectly known together with infinite actuation, and one that accounts for the unknown aerodynamics and the actuator constraints.

- Chapter 3: By using the proposed decoupling, a number of controllers are derived and presented in this chapter. For rotational control, a backstepping controller, a sliding surface controller and a PD+ controller are adapted to the case of flight control based on Kristiansen *et al.* (2009*b*), Slotine and Li (1987) and Paden and Panja (1988) respectively. An adaptive backstepping controller is also derived, which accounts for the unknown aerodynamics and the actuator constraints. It adapts the idea by Johnson and Calise (2000) and uses a reference trajectory to move the saturation problem from the plant to the reference. Through a comparison of the controllers, it is found that the PD+ controller, the sliding surface controller and the backstepping controller produce almost similar results when the gains are chosen appropriately. This is due to the saturation of the deflection angles. It is also observed that by using a reference trajectory that deviates from a desired trajectory whenever the actuators are in saturation, results in improved performance compared to that of tracking a desired trajectory. Specifically, the reference trajectory can be designed such that the control deficiency of one actuator can become

mapped to the other actuators through the reference trajectory. This results in increased actuation that makes the errors converge faster to zero.

For speed control, model-based proportional and proportional-integral controllers are derived using standard Lyapunov methods. An adaptive speed controller that accounts for uncertain aerodynamics and actuator constraints is also presented. It is also observed that the rotational control laws are dependent on the airspeed, such that at higher airspeeds a smaller deflection angle is required to produce a desired moment. This fact is exploited by designing a reference airspeed that increases whenever the deflection angles cross a predefined threshold, such that by tracking this reference speed, the deflection angles can be kept within their bounds under certain assumptions.

- Chapter 4: Several guidance laws that produce the desired states are presented in this chapter. A waypoint guidance method is derived which maps the position error to one axis, resulting in a desired quaternion and angular velocity. By tracking the desired states, a set containing all the points in a shell around the origin is shown to be uniformly asymptotically stable. A similar idea is applied for trajectory tracking, where a virtual saturated translational controller is designed to make the position and velocity errors go to zero. The outputs from the virtual controller are then mapped to desired states that can be tracked using the control laws from Chapter 3. The trajectory tracking solution is then extended to formation flight by defining desired trajectories relative to a virtual leader, which by tracking, enable the UAVs to maintain a rigid formation.

- Chapter 5: Behavioral control of fixed-wing UAVs using composite quaternion rotations is presented in this chapter. From the previous chapters, it is observed that several quaternions can be multiplied together where the quaternions and corresponding angular velocities can be treated individually. This is used to design a behavioral control method that fits nicely into the framework by Brooks (1986), where it is possible to define multiple tasks and arrange them in a hierarchy. This enables different quaternions to be designed for performing collision avoidance, ground avoidance and waypoint tracking. By suppressing the inactive quaternions, it is shown that the solution enables multiple UAVs to perform waypoint tracking while moving through a city without colliding with the buildings, the ground nor each other.

- Appendix A: This appendix presents the YF-22 UAV model that is used in all the simulations, and contains all the aerodynamic coefficients that are used in the modeling.

- Appendix B: This appendix presents the aggregated dynamics which is commonly used as a basis when designing flight controllers.

- Appendix C: This appendix shows how the aerodynamics can be extended to be more accurate than the common representation; an extension that fits nicely into the framework of this thesis.

- Appendix D: This appendix presents different definitions and theorems that are employed in this thesis.

- Appendix E: This appendix contains detailed proofs of the theorems and lemmas that are presented throughout this thesis.

1.7.2 Delimitations

This thesis makes several assumptions in order to maintain focus on the individual contributions and are stated as they are required. On a general level, it is assumed that all states are perfectly known at all time, the body is rigid such that the inertia matrix and mass are known and constant, and the direction and magnitude of the wind is assumed to be known. Furthermore, actuator dynamics are not taken into account such that the actuators produce a given force or moment instantaneously. No rate saturation is therefore considered, and the actuators are only limited by magnitude saturations.

The problem of state estimation can be solved by applying recent results on nonlinear observer design by Grip *et al.* (2013) or using an Extended Kalman Filter (EKF) as in Kingston and Beard (2004). The wind can be estimated by using the algorithm presented in Langelaan *et al.* (2010) while rate saturation is considered in work such as Tandale and Valasek (2005) and Akella *et al.* (2005).

1.7.3 Publications

The following list contains the publications that have been written during the course of this work.

- Oland, E., T. S. Andersen and R. Kristiansen (2014). Subsumption Architecture applied to Flight Control using Composite Rotations. Submitted to Automatica.

- Oland, E. and R. Kristiansen (2014). A Decoupled Approach for Flight Control. Submitted to Journal of Guidance, Control, and Dynamics.

- Oland, E. and R. Kristiansen (2014). Trajectory Tracking of an Underactuated Fixed-wing UAV. In: *Proceedings of the ICNPAA Congress on Mathematical Problems in Engineering Aerospace and Sciences* (In Press), Narvik, Norway.

- Oland, E., T. S. Andersen and R. Kristiansen (2014). Actuator Desaturation for a Fixed-wing UAV using Speed Modification. In: *Proceedings of the ICNPAA Congress on Mathematical Problems in Engineering Aerospace and Sciences* (In Press), Narvik, Norway.

- Oland, E. and R. Kristiansen (2014). Adaptive Flight Control with Constrained Actuation. In: Proceedings of the American Control Conference, Portland, OR, USA.

- Oland, E., R. Schlanbusch and R. Kristiansen (2013). Underactuated Waypoint Tracking of a Fixed-wing UAV. In: *Proceedings of the 2nd RED-UAS, Workshop on Research, Education and Development of Unmanned Aerial Systems*, Compiegne, France.
- Oland, E. and T.S. Andersen and R. Kristiansen (2013). Underactuated Control of Quadrotors with Collision Avoidance. In: *Proceedings of the 2nd RED-UAS, Workshop on Research, Education and Development of Unmanned Aerial Systems*, Compiegne, France.
- Oland, E. and R. Kristiansen (2013). Real-time Particle Tracking using a Formation of UAVs. In *Proceedings of the 2nd RED-UAS, Workshop on Research, Education and Development of Unmanned Aerial Systems*, Compiegne, France.
- Oland, E. and R. Kristiansen (2013). Collision and Terrain Avoidance for UAVs using the Potential Field Method. In: *Proceedings of the 34th IEEE Aerospace Conference*, Big Sky, Montana, USA.
- Oland, E. and R. Kristiansen (2013). Quaternion-based Backstepping control of a Fixed-wing Unmanned Aerial Vehicle. In: *Proceedings of the 34th IEEE Aerospace Conference*, Big Sky, Montana, USA.
- Oland, E. and R. Kristiansen (2013). Underactuated Translational Control of a Rigid Spacecraft. In: *Proceedings of the 34th IEEE Aerospace Conference*, Big Sky, Montana, USA.
- Schlanbusch, R. and E. Oland (2013). Spacecraft Formation Reconfiguration with Dynamic Collision Avoidance. In: *Proceedings of the 34th IEEE Aerospace Conference*, Big Sky, Montana, USA.
- Kristiansen, R., E. Oland and D. Narayanachar (2012). Operational Concepts in UAV Formation Monitoring of Industrial Emissions. In: *Proceedings of the 3rd IEEE International Conference on Cognitive Infocommunications*, Kosice, Slovakia.
- Kristiansen, R., R. Schlanbusch and E. Oland (2011). PD+ Based Spacecraft Attitude Tracking with Magnetometer Rate Feedback. In: *Proceedings of the 50th IEEE Conference on Decision and Control (CDC)*, Orlando, FL.

Note that this thesis only considers fixed-wing UAVs, while some of the publications consider other underactuated rigid bodies. The research approach for this project has been to study how other underactuated rigid bodies are controlled, and apply that knowledge for flight control. To maintain a strong focus, these results are not included in this thesis.

Chapter 2

Modeling

> Quaternions came from Hamilton after his really good work had been done; and, though beautifully ingenious, have been an unmixed evil to those who have touched them in any way, including Clerk Maxwell.
>
> Lord Kelvin, 1892

This chapter is based on Oland *et al.* (2013*a*), Oland and Kristiansen (2014*a*) and Oland and Kristiansen (2014*b*) and presents the complete model for a fixed-wing UAV, including both rotational and translational dynamics. To facilitate controller design, two different models are presented: one that assumes that the aerodynamics are perfectly known together with infinite actuation, and one model that takes the aerodynamic uncertainty into account together with the constrained actuation.

2.1 Preliminaries

Bold Greek or Latin letters are vectors $\mathbf{x} \in \mathbb{R}^n$ and bold capital Greek or Latin letters are matrices $\mathbf{X} \in \mathbb{R}^{n \times m}$, and scalars are non-bold. The time derivative of a vector is denoted as $\dot{\mathbf{x}} = d\mathbf{x}/dt$ and the Euclidean length is written as $||\mathbf{x}|| = \sqrt{\mathbf{x}^\top \mathbf{x}}$. Superscripts denote the reference frame of a vector such that $\mathbf{v}^B$ is a vector in frame B. The rotation matrix is denoted $\mathbf{R}_A^B \in \mathcal{SO}(3) = \{\mathbf{R} \in \mathbb{R}^{3\times 3} : \mathbf{R}^\top \mathbf{R} = \mathbf{I}, \det(\mathbf{R}) = 1\}$, which rotates a vector from frame A to frame B and where $\mathbf{I}$ denotes the identity matrix of sufficient dimension depending on the context. The angular velocity vector is denoted $\boldsymbol{\omega}_{B,A}^C \in \mathbb{R}^3$, which represents the angular velocity of frame A relative to frame B referenced in frame C. Angular velocities between different frames can be added together as $\boldsymbol{\omega}_{A,D}^B = \boldsymbol{\omega}_{A,C}^B + \boldsymbol{\omega}_{C,D}^B$ (*cf.* Egeland and Gravdahl (2002)). The time derivative of the rotation matrix is found as $\dot{\mathbf{R}}_A^B = \mathbf{R}_A^B \mathbf{S}(\boldsymbol{\omega}_{B,A}^A)$ where the cross product operator $\mathbf{S}(\cdot)$ is such that for two arbitrary vectors $\mathbf{v}_1, \mathbf{v}_2 \in \mathbb{R}^3$, $\mathbf{S}(\mathbf{v}_1)\mathbf{v}_2 = \mathbf{v}_1 \times \mathbf{v}_2$, $\mathbf{S}(\mathbf{v}_1)\mathbf{v}_2 = -\mathbf{S}(\mathbf{v}_2)\mathbf{v}_1$, $\mathbf{S}(\mathbf{v}_1)\mathbf{v}_1 = \mathbf{0}$ and

$\mathbf{v}_1^\top \mathbf{S}(\mathbf{v}_2)\mathbf{v}_1 = 0$ and with $\mathbf{v}_1 = \begin{bmatrix} v_1 & v_2 & v_3 \end{bmatrix}^\top$ the cross-product operator is defined as

$$\mathbf{S}(\mathbf{v}_1) = \begin{bmatrix} 0 & -v_3 & v_2 \\ v_3 & 0 & -v_1 \\ -v_2 & v_1 & 0 \end{bmatrix}. \tag{2.1}$$

The rotation matrix can be parameterized by quaternions as invented by Hamilton (1844), where the quaternion that represents a rotation from frame A to frame B is denoted $\mathbf{q}_{B,A} \in \mathcal{S}^3 = \{\mathbf{q} \in \mathbb{R}^4 : \mathbf{q}^\top \mathbf{q} = 1\}$, and can be written on vector form as

$$\mathbf{q}_{B,A} = \begin{bmatrix} \eta_{B,A} & \boldsymbol{\epsilon}_{B,A}^\top \end{bmatrix}^\top = \begin{bmatrix} \cos(\frac{\vartheta_{B,A}}{2}) & \mathbf{k}_{B,A}^\top \sin(\frac{\vartheta_{B,A}}{2}) \end{bmatrix}^\top \tag{2.2}$$

which performs a rotation of an angle $\vartheta_{B,A}$ around the unit vector $\mathbf{k}_{B,A}$, and the inverse quaternion is defined as $\mathbf{q}_{A,B} = \begin{bmatrix} \eta_{B,A} & -\boldsymbol{\epsilon}_{B,A}^\top \end{bmatrix}^\top$. The scalar part is denoted $\eta_{B,A}$ and the vector part as $\boldsymbol{\epsilon}_{B,A} \in \mathbb{R}^3$, enabling the rotation matrix to be constructed as

$$\mathbf{R}_A^B = \mathbf{I} + 2\eta_{B,A}\mathbf{S}(\boldsymbol{\epsilon}_{B,A}) + 2\mathbf{S}^2(\boldsymbol{\epsilon}_{B,A}). \tag{2.3}$$

For a general quaternion $\mathbf{q} = \begin{bmatrix} \eta & \epsilon_1 & \epsilon_2 & \epsilon_3 \end{bmatrix}^\top$, the rotation matrix can also be constructed using the quaternion components as

$$\mathbf{R} = \begin{bmatrix} \eta^2 + \epsilon_1^2 - \epsilon_2^2 - \epsilon_3^2 & 2(\epsilon_1\epsilon_2 - \eta\epsilon_3) & 2(\epsilon_1\epsilon_3 + \eta\epsilon_2) \\ 2(\epsilon_1\epsilon_2 + \eta\epsilon_3) & \eta^2 - \epsilon_1^2 + \epsilon_2^2 - \epsilon_3^2 & 2(\epsilon_2\epsilon_3 - \eta\epsilon_1) \\ 2(\epsilon_1\epsilon_3 - \eta\epsilon_2) & 2(\epsilon_2\epsilon_3 + \eta\epsilon_1) & \eta^2 - \epsilon_1^2 - \epsilon_2^2 + \epsilon_3^2 \end{bmatrix}. \tag{2.4}$$

To ensure that the resulting quaternion maintains the unit length property, composite rotations are found using the quaternion product as (*cf.* Egeland and Gravdahl (2002))

$$\mathbf{q}_{A,C} = \mathbf{q}_{A,B} \otimes \mathbf{q}_{B,C} = \mathbf{T}(\mathbf{q}_{A,B})\mathbf{q}_{B,C} \tag{2.5}$$

where

$$\mathbf{T}(\mathbf{q}_{A,B}) = \begin{bmatrix} \eta_{A,B} & -\boldsymbol{\epsilon}_{A,B}^\top \\ \boldsymbol{\epsilon}_{A,B} & \eta_{A,B}\mathbf{I} + \mathbf{S}(\boldsymbol{\epsilon}_{A,B}) \end{bmatrix} \tag{2.6}$$

while the quaternion kinematics is given as

$$\dot{\mathbf{q}}_{B,A} = \frac{1}{2}\mathbf{q}_{B,A} \otimes \begin{bmatrix} 0 \\ \boldsymbol{\omega}_{B,A}^A \end{bmatrix} = \frac{1}{2}\mathbf{T}(\mathbf{q}_{B,A}) \begin{bmatrix} 0 \\ \boldsymbol{\omega}_{B,A}^A \end{bmatrix}. \tag{2.7}$$

2.2 Reference Frames

Several basic reference frames are required to describe the rotational and translational dynamics of a fixed-wing UAV. Additional frames are defined as they are required.

North East Down (NED): This frame is denoted $\mathcal{F}^n$ and is treated as an inertial frame. The $\mathbf{x}^n$ axis points North, $\mathbf{y}^n$ points East while $\mathbf{z}^n$ completes the right-handed orthonormal reference frame by pointing down toward the center of the Earth. Flying with low speed in a local region, the centripetal and Coriolis effects of the Earth can be ignored (*cf.* Stevens and Lewis (2003)), enabling NED frame to be treated as an inertial frame, which makes the Laws of Newton valid. This is also known as flat-Earth approximation.

East North Up (ENU): This frame is denoted $\mathcal{F}^u$ and is treated as an inertial frame. The $\mathbf{x}^u$ axis points East, $\mathbf{y}^u$ points North while $\mathbf{z}^u$ completes the right-handed orthonormal reference frame by pointing up relative to the center of the Earth. This reference frame is only used for visualizations of trajectories since it fits better with the human perception than that of the NED frame.

Body Frame: This frame is denoted $\mathcal{F}^b$ and has its origin in the center of mass of the rigid body. The $\mathbf{x}^b$ axis is aligned with the fuselage, $\mathbf{y}^b$ goes through the right wing, while $\mathbf{z}^b = \mathbf{x}^b \times \mathbf{y}^b$ completes the right handed orthonormal frame. This reference frame is fixed to the rigid body.

Stability Frame: This frame is denoted $\mathcal{F}^s$ and is initially aligned with the body frame. The $\mathbf{x}^s$ axis is found through a left-handed rotation around the $\mathbf{y}^b$ axis, $\mathbf{y}^s = \mathbf{y}^b$ and $\mathbf{z}^s = \mathbf{x}^s \times \mathbf{y}^s$. The stability frame is an intermediate frame used to find the wind frame and is in general used for studying the flight dynamics.

Wind Frame: This frame is denoted $\mathcal{F}^w$ and is initially aligned with the body frame. The wind frame is defined such that the airspeed, V_a, is aligned along the $\mathbf{x}^w$ axis, which is found through the rotation of the angle of attack to the stability frame, and by an additional rotation around the $\mathbf{z}^s$ axis by the sideslip angle β. The relation between the body, stability and wind is shown in Figure 2.1.

2.3 Translational Kinematics and Dynamics

The kinematics of the ground velocity is defined as (*cf.* Stevens and Lewis (2003))

$$\dot{\mathbf{p}}^n = \mathbf{R}_b^n \mathbf{v}^b \tag{2.8}$$

$$\mathbf{v}_r^b = \mathbf{v}^b - \mathbf{R}_n^b \mathbf{w}^n \tag{2.9}$$

where $\mathbf{p}^n$ is the position of the UAV relative to the Earth and where $\mathbf{v}^b$ is the ground velocity vector in the body frame. To account for the wind, let the velocity vector relative to the surrounding air be denoted[1] $\mathbf{v}_r^b := \begin{bmatrix} u & v & w \end{bmatrix}^\top$ with $\mathbf{w}^n$ as the wind vector. The ground speed and airspeed are denoted respectively as V_g and V_a and

[1] From now on called the relative velocity vector.

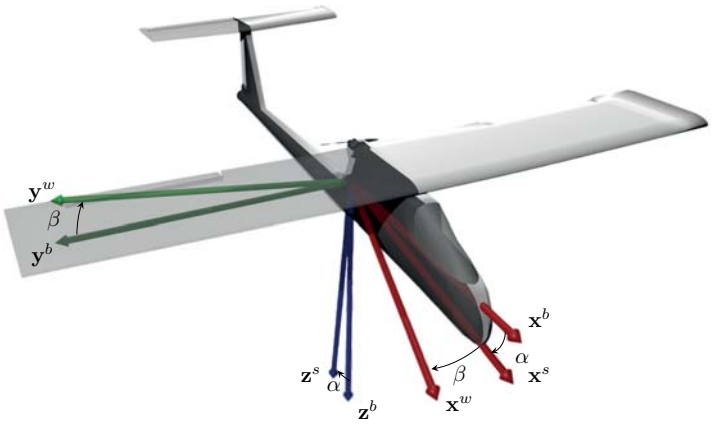

Figure 2.1: The body, stability and wind frame. By using the angle of attack and the sideslip angle, the relation between the body frame and the direction of the airspeed is obtained (illustration by Tom Stian Andersen).

are given as

$$V_g = ||\mathbf{v}^b|| = \sqrt{(\mathbf{v}^b)^\top \mathbf{v}^b} \tag{2.10}$$

$$V_a = ||\mathbf{v}_r^b|| = \sqrt{(\mathbf{v}_r^b)^\top \mathbf{v}_r^b}. \tag{2.11}$$

The direction of the ground speed tells how the UAV moves relative to the ground, which is important from a guidance perspective, while the airspeed affects the aerodynamic forces and moments and is therefore important from a control perspective. The wind triangle in Figure 2.2 shows the relation between the air, ground and wind velocity vectors where $\mathbf{v}_r^n := \mathbf{R}_b^n \mathbf{v}_r^b$ and $\mathbf{v}_g^n := \mathbf{R}_b^n \mathbf{v}^b$.

The relative velocity vector can be rotated to the wind frame as

$$\mathbf{v}_r^w = \mathbf{R}_b^w \mathbf{v}_r^b = \mathbf{R}_b^w \begin{bmatrix} V_a \\ 0 \\ 0 \end{bmatrix} \tag{2.12}$$

where the airspeed is aligned along the $\mathbf{x}^w$ axis and where the rotation matrix is defined as

$$\mathbf{R}_b^w = \begin{bmatrix} \cos(\alpha)\cos(\beta) & \sin(\beta) & \sin(\alpha)\cos(\beta) \\ -\cos(\alpha)\sin(\beta) & \cos(\beta) & -\sin(\alpha)\sin(\beta) \\ -\sin(\alpha) & 0 & \cos(\alpha) \end{bmatrix} \tag{2.13}$$

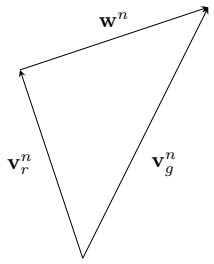

Figure 2.2: The wind triangle shows the relation between the air, ground and wind velocity vectors.

with the angle of attack and the sideslip angles defined respectively as

$$\alpha = \tan^{-1}\left(\frac{w}{u}\right) \tag{2.14}$$

$$\beta = \sin^{-1}\left(\frac{v}{V_a}\right). \tag{2.15}$$

Remark 2.1 *With zero wind, the airspeed and ground speed coincide. Hence the control problem reduces to that of aligning the wind frame in a desired direction and move with a positive airspeed.*

By treating the NED frame as an inertial frame, the translational dynamics are found through Newton's Second law as (*cf.* Stevens and Lewis (2003))

$$\dot{\mathbf{v}}^b = \frac{1}{m}(\mathbf{f}_{thrust}^b + \mathbf{R}_w^b \mathbf{f}_{aero}^w) + \mathbf{R}_n^b \mathbf{f}_g^n - \mathbf{S}(\boldsymbol{\omega}_{n,b}^b)\mathbf{v}^b \tag{2.16}$$

where m is the mass, $\mathbf{f}_{thrust}^b := \begin{bmatrix} T & 0 & 0 \end{bmatrix}^\top$ is the thrust vector with T as the total thrust, $\mathbf{f}_{aero}^w$ is the aerodynamic forces acting on the rigid body, $\mathbf{f}_g^n := \begin{bmatrix} 0 & 0 & g \end{bmatrix}^\top$ is the gravity vector where g is the acceleration due to the gravity and $\boldsymbol{\omega}_{n,b}^b := \begin{bmatrix} p & q & r \end{bmatrix}^\top$ is the angular velocity vector. The aerodynamic force vector can be defined as (*cf.* Etkin (1972), Stengel (2004), Campa *et al.* (2007))

$$\mathbf{f}_{aero}^w := \begin{bmatrix} -D & Y & -L \end{bmatrix}^\top = \frac{1}{2}\rho S V_a^2 \begin{bmatrix} -C_D & C_Y & -C_L \end{bmatrix}^\top \tag{2.17}$$

$$C_D := C_{D_0} + C_{D_\alpha}\alpha + \frac{\bar{c}}{2V_a}C_{D_q}q + C_{D_{\delta_e}}\delta_e \tag{2.18}$$

$$C_Y := C_{Y_0} + C_{Y_\beta}\beta + \frac{b}{2V_a}C_{Y_p}p + \frac{b}{2V_a}C_{Y_r}r + C_{Y_{\delta_a}}\delta_a + C_{Y_{\delta_r}}\delta_r \tag{2.19}$$

$$C_L := C_{L_0} + C_{L_\alpha}\alpha + \frac{\bar{c}}{2V_a}C_{L_q}q + C_{L_{\delta_e}}\delta_e \tag{2.20}$$

where D is the drag, Y is the sideforce, L is the lift, ρ is the air density, S is the wing area, $C_{(\cdot)}$ are aerodynamic coefficients, b is the wing span, $\bar{c}$ is the mean aerodynamic chord and $\delta_a, \delta_e, \delta_r$ are the deflection angles of the aileron, elevator and rudder respectively which are used for rotational control. The drag force, D, is aligned along the negative $\mathbf{x}^w$ axis, the sideforce, Y, along the $\mathbf{y}^w$ axis and the lift, L, along the negative $\mathbf{z}^w$ axis. Note that the drag is always positive and provides damping to the system.

Remark 2.2 *The aerodynamic representation that is used in this section is linear in the angle of attack and the sideslip angle, and is therefore only valid close to leveled flight. A set of coefficients representing the aerodynamics of the* YF-*22* UAV *are given in Appendix A as described in Campa* et al. *(2007). A more detailed discussion regarding aerodynamic modeling is given in Appendix C and details procedures for obtaining more accurate aerodynamic models that can be used together with the control laws that are derived in this thesis.*

Assumption 2.1 *It is assumed that the wind vector is constant or slowly varying.*

Assumption 2.2 *It is assumed that the airspeed is lower bounded as* $V_a \geq \beta_v > 0$ *and that* $u > 0 \ \forall \ t \geq t_0$.

Assumption 2.2 is a common assumption, which in essence states that the aircraft has a positive speed above stall speed which is a requirement for flight. The assumption that $u > 0 \ \forall \ t \geq t_0$ states that the aircraft is moving forward, and as such is another reasonable assumption. Using Assumption 2.1, it follows that $\dot{\mathbf{w}}^n \approx \mathbf{0}$, enabling the relative acceleration to be found by differentiating (2.9) and using (2.16) as

$$\dot{\mathbf{v}}_r^b = \frac{1}{m}(\mathbf{f}_{thrust}^b + \mathbf{R}_w^b \mathbf{f}_{aero}^w) + \mathbf{R}_n^b \mathbf{f}_g^n - \mathbf{S}(\boldsymbol{\omega}_{n,b}^b)\mathbf{v}_r^b, \tag{2.21}$$

while the linear acceleration is found by differentiating (2.11), inserting (2.21) and using that $(\mathbf{v}_r^b)^\top \mathbf{S}(\boldsymbol{\omega}_{n,b}^b)\mathbf{v}_r^b = 0$ as

$$\dot{V}_a = \frac{u}{mV_a}T + \frac{(\mathbf{v}_r^b)^\top}{V_a}(\frac{1}{m}\mathbf{R}_w^b \mathbf{f}_{aero}^w + \mathbf{R}_n^b \mathbf{f}_g^n). \tag{2.22}$$

Remark 2.3 *The derivation of the aggregated translational dynamics* $(\dot{V}_a, \dot{\alpha}, \dot{\beta})$ *is given in Appendix B. When solving for the thrust, the inverse dynamics become singular when* α *or* β *are equal to* $\pm\pi/2$*, which can be avoided by using (2.22).*

Remark 2.4 *The translational dynamics (2.21) can be written in terms of angle of attack and the sideslip rates such that (cf. (B.4))*

$$\dot{\alpha} = f(\mathbf{q}_{n,b}, \boldsymbol{\omega}_{n,b}^b, V_a, \alpha, \beta, T, \delta_e) \tag{2.23}$$

$$\dot{\beta} = f(\mathbf{q}_{n,b}, \boldsymbol{\omega}_{n,b}^b, V_a, \alpha, \beta, T, \delta_a, \delta_r). \tag{2.24}$$

When using $\boldsymbol{\omega}_{n,b}^b$ to stabilize the angle of attack and the sideslip angle, the deflection rates must be sufficiently fast to enable the time-scale separation principle to be applied (cf. Reiner et al. *(1996)) and the errors they introduce must be assumed to be negligible. The stabilization of the angular velocity is then done in the next step through the deflection angles. This is currently the common approach for flight control and has resulted in a wealth of research (cf. Lane and Stengel (1988), Reiner* et al. *(1996), Lee and Kim (2001), Farrell* et al. *(2005), Shin and Kim (2006), Ju and Tsai (2007), Sonneveldt* et al. *(2009a)) all constrained by the inherent limitations of angular representation, time-scale separation and deflection angles in the translational dynamics. Since the rotational dynamics are independent of the thrust, it is in this thesis proposed to first solve the rotation problem and then the translation problem. With a control law stabilizing the rotational dynamics through $\delta_a, \delta_e, \delta_r$, the translational control problem becomes trivial.*

Remark 2.5 *With thrust only available along the $\mathbf{x}^b$ axis, the aircraft is clearly underactuated. Instead of controlling all the velocity components (u, v, w) it is possible to control the airspeed, V_a, and use the rotation matrix $\mathbf{R}_b^w$ to map the control problem from $\mathbb{R}^3 \times \mathcal{SO}(3)$ to $\mathbb{R}^1 \times \mathcal{SO}(3)$ and with quaternions it becomes mapped to $\mathbb{R}^1 \times \mathcal{S}^3$.*

2.4 Rotational Kinematics and Dynamics

The rotational kinematics are derived using quaternions as (*cf.* Egeland and Gravdahl (2002))

$$\dot{\mathbf{q}}_{n,b} = \frac{1}{2}\mathbf{q}_{n,b} \otimes \begin{bmatrix} 0 \\ \boldsymbol{\omega}_{n,b}^b \end{bmatrix} \tag{2.25}$$

which represents the orientation of the body frame relative to the NED frame. The angular acceleration of the UAV is found using Euler's momentum equation as (*cf.* Stengel (2004))

$$\mathbf{J}\dot{\boldsymbol{\omega}}_{n,b}^b = -\mathbf{S}(\boldsymbol{\omega}_{n,b}^b)\mathbf{J}\boldsymbol{\omega}_{n,b}^b + \boldsymbol{\tau}_{aero}^b \tag{2.26}$$

where the inertia matrix is defined as

$$\mathbf{J} = \begin{bmatrix} J_{xx} & 0 & -J_{xz} \\ 0 & J_{yy} & 0 \\ -J_{xz} & 0 & J_{zz} \end{bmatrix} \tag{2.27}$$

where J_{xx}, J_{yy}, J_{zz} and J_{xz} represent constant inertia components. The aerodynamic moments can be written as (*cf.* Etkin (1972), Stengel (2004), Campa *et al.* (2007))

$$\boldsymbol{\tau}_{aero}^b = \mathbf{f}(\mathbf{x}) - \mathbf{D}(\mathbf{x})\boldsymbol{\omega}_{n,b}^b + \mathbf{G}(\mathbf{x})\mathbf{u} \tag{2.28}$$

where $\mathbf{x} = \begin{bmatrix} V_a & \alpha & \beta \end{bmatrix}^\top$ and $\mathbf{u} = \begin{bmatrix} \delta_a & \delta_e & \delta_r \end{bmatrix}^\top$ is the control signal. The aerodynamic vector $\mathbf{f}(\mathbf{x})$ is defined as

$$\mathbf{f}(\mathbf{x}) = \frac{1}{2}\rho S V_a^2 \begin{bmatrix} b(C_{l_0} + C_{l_\beta}\beta) \\ \bar{c}(C_{m_0} + C_{m_\alpha}\alpha) \\ b(C_{n_0} + C_{n_\beta}\beta) \end{bmatrix} \tag{2.29}$$

and the damping matrix is defined as

$$\mathbf{D}(\mathbf{x}) = -\frac{1}{2}\rho S V_a^2 \begin{bmatrix} \frac{b^2}{2V_a}C_{l_p} & 0 & \frac{b^2}{2V_a}C_{l_r} \\ 0 & \frac{\bar{c}^2}{2V_a}C_{m_q} & 0 \\ \frac{b^2}{2V_a}C_{n_p} & 0 & \frac{b^2}{2V_a}C_{n_r} \end{bmatrix}. \tag{2.30}$$

Note that $\mathbf{D}(\mathbf{x})$ is positive definite for all $V_a > 0$. The control effectiveness matrix is defined as

$$\mathbf{G}(\mathbf{x}) = \frac{1}{2}\rho S V_a^2 \begin{bmatrix} bC_{l_{\delta_a}} & 0 & bC_{l_{\delta_r}} \\ 0 & \bar{c}C_{m_{\delta_e}} & 0 \\ bC_{n_{\delta_a}} & 0 & bC_{n_{\delta_r}} \end{bmatrix} \tag{2.31}$$

which has full rank as long as $V_a > 0$ and $C_{m_{\delta_e}}(C_{l_{\delta_a}}C_{n_{\delta_r}} - C_{l_{\delta_r}}C_{n_{\delta_a}}) \neq 0$. Inserting (2.28) into (2.26), the angular acceleration becomes

$$\mathbf{J}\dot{\boldsymbol{\omega}}_{n,b}^b = -\mathbf{S}(\boldsymbol{\omega}_{n,b}^b)\mathbf{J}\boldsymbol{\omega}_{n,b}^b + \mathbf{f}(\mathbf{x}) - \mathbf{D}(\mathbf{x})\boldsymbol{\omega}_{n,b}^b + \mathbf{G}(\mathbf{x})\mathbf{u}. \tag{2.32}$$

2.5 Total System

Let the aerodynamic force vector (2.17) be rewritten as

$$\mathbf{f}_{aero}^w = \mathbf{f}_2(\mathbf{x}, \boldsymbol{\omega}_{n,b}^b) + \mathbf{G}_2(\mathbf{x})\mathbf{u} \tag{2.33}$$

where

$$\mathbf{f}_2(\mathbf{x}, \boldsymbol{\omega}_{n,b}^b) = \frac{1}{2}\rho S V_a^2 \begin{bmatrix} -(C_{D_0} + C_{D_\alpha}\alpha + \frac{\bar{c}}{2V_a}C_{D_q}q) \\ C_{Y_0} + C_{Y_\beta}\beta + \frac{b}{2V_a}C_{Y_p}p + \frac{b}{2V_T}C_{Y_r}r \\ -(C_{L_0} + C_{L_\alpha}\alpha + \frac{\bar{c}}{2V_a}C_{L_q}q) \end{bmatrix} \tag{2.34}$$

and

$$\mathbf{G}_2(\mathbf{x}) = \frac{1}{2}\rho S V_a^2 \begin{bmatrix} 0 & -C_{D_{\delta_e}} & 0 \\ C_{Y_{\delta_a}} & 0 & C_{Y_{\delta_r}} \\ 0 & -C_{L_{\delta_e}} & 0 \end{bmatrix}, \tag{2.35}$$

then the total system can be written using (2.21) and (2.32) as

$$\begin{bmatrix} \dot{\mathbf{v}}_r^b \\ \mathbf{J}\dot{\boldsymbol{\omega}}_{n,b}^b \end{bmatrix} = \begin{bmatrix} \frac{1}{m}\left(\begin{bmatrix} T \\ 0 \\ 0 \end{bmatrix} + \mathbf{R}_w^b(\mathbf{f}_2(\mathbf{x}, \boldsymbol{\omega}_{n,b}^b) + \mathbf{G}_2(\mathbf{x})\mathbf{u})\right) + \mathbf{R}_n^b\mathbf{f}_g^n - \mathbf{S}(\boldsymbol{\omega}_{n,b}^b)\mathbf{v}_r^b \\ -\mathbf{S}(\boldsymbol{\omega}_{n,b}^b)\mathbf{J}\boldsymbol{\omega}_{n,b}^b + \mathbf{f}(\mathbf{x}) - \mathbf{D}(\mathbf{x})\boldsymbol{\omega}_{n,b}^b + \mathbf{G}(\mathbf{x})\mathbf{u} \end{bmatrix}. \tag{2.36}$$

For this system there are four actuators, the thrust, T, that is acting along the $\mathbf{x}^b$ axis, and three deflection angles, $\mathbf{u} = \begin{bmatrix} \delta_a & \delta_e & \delta_r \end{bmatrix}^\top$ that produce moments as well as affecting the aerodynamic drag, lift and sideforce. A critical issue with this model, and control of aircraft in general, is that the elevator, δ_e, and the thrust are producing forces along the $\mathbf{x}^b$ axis, an issue that often is ignored by simplifying

the aerodynamics or solved by using values for the elevator from the previous time-step. This represents a strong coupling between the rotational and translational systems that must be accounted for when designing the control laws. The common approach to address this issue, is to divide the system into a slow system and a fast system, where the deflection angles are treated as constants in the slow system, and are only "active" in the fast system. This means that the elevator is assumed to be constant when designing the speed controller. To be precise, the common approach is to solve the translational dynamics first, followed by the rotational dynamics. By studying the dynamics (2.36), it is evident that the thrust only appears in the translational dynamics, while the deflection angles are part of both systems. A better approach which will be followed in this thesis would therefore be to first control the rotational system and then the translational system. With the deflection angles available from the control law, their impact on the translational system can be removed from the closed loop dynamics using the thrust.

Remark 2.6 *For some aircraft, the thrust is not directly aligned along the* $\mathbf{x}^b$ *axis, but is rotated by a small angle relative to the* $\mathbf{x}^b$ *axis. When this is the case, aerodynamic pitching moments are generated by the thrust which thereby increases the coupling between the systems.*

2.6 Decoupling the Rotational and Translational Systems

The objective of pointing the speed in a desired direction can be performed through rotational control. More precisely, this can be achieved by pointing the wind frame in a desired direction. To relate the wind frame to the NED frame, it is possible to rotate from NED to body using the attitude (*e.g.* roll, pitch, yaw or $\mathbf{q}_{b,n}$), and to rotate from the body frame to the wind frame, it is possible to use the angle of attack and the sideslip angle. Using these angles, the relation between the wind frame and the NED frame can be established such that the airspeed can be pointed in a desired direction relative to the NED frame. The decoupling will first be presented from an Euler perspective since it is more easily understood, and then it will be presented using quaternions.

2.6.1 Motivation from an Euler Perspective

The motion of a particle moving in $\mathbb{R}^3$ can be expressed using a flight path angle (γ), a course angle (χ), and a speed. In the vertical plane, the flight path angle is the difference between the pitch angle (θ) and the angle of attack, $\gamma = \theta - \alpha$, while in the horizontal plane, the course angle is the sum of the yaw angle (ψ) and the sideslip angle, $\chi = \psi + \beta$ (*cf.* Stengel (2004)). To control the direction of motion of the particle, let a desired flight path and course angle be defined by γ_d, χ_d, and let the flight path and course errors be defined as

$$\tilde{\gamma} := \gamma - \gamma_d = \theta - \alpha - \gamma_d \tag{2.37}$$

$$\tilde{\chi} := \chi - \chi_d = \psi + \beta - \chi_d. \tag{2.38}$$

By differentiating (2.37)-(2.38) twice, the deflection angles enter the system through $\ddot{\theta}$ and $\ddot{\psi}$, where the higher order derivatives of γ_d and χ_d are found using linear

filters. The angle of attack and the sideslip angle are functions of the relative velocity vector, such that the second derivative of the angle of attack and the sideslip angle are found from the second derivative of the relative velocity vector, which is not available. To remedy this issue, let the tracking error be rewritten as

$$\tilde{\gamma} = \theta - \theta_d \tag{2.39}$$

$$\tilde{\chi} = \psi - \psi_d \tag{2.40}$$

where $\theta_d := \gamma_d + \alpha$ and $\psi_d := \chi_d - \beta$. Instead of using a filter to find the higher order derivatives of the desired flight path and course angles, it can be used on the desired pitch and yaw angles (θ_d, ψ_d). This enables the higher order derivatives of the angle of attack and the sideslip angle to be approximated using a linear filter, which simplifies the control problem. Note that the relations (2.37)-(2.38) are only valid when the roll angle (ϕ) and the sideslip angle are equal to zero, such that this represents a particular case. Quaternions will therefore be used to generalize the results.

In Fossen (2011) the author shows how the sideslip angle can be used for guidance purposes for ships and the same approach is proposed for controlling underactuated AUVs in Breivik and Fossen (2005), where the authors apply the particular case for finding the desired pitch and yaw angle. In Kaminer *et al.* (1998), the authors use a filter to find the angular acceleration of the body frame relative to the NED frame, and use it to trim the desired trajectory and apply it to control a fixed-wing UAV. The approach by Kaminer *et al.* (1998) is in many ways similar to what is presented here, except that they estimate the angular acceleration of the body relative to NED and not the higher order derivatives of the sideslip angle and angle of attack.

2.6.2 Quaternion Representation

The rotation from the wind frame to the body frame can be written using quaternions as

$$\mathbf{q}_{b,w} = \mathbf{q}_{b,s} \otimes \mathbf{q}_{s,w} \tag{2.41}$$

where the two quaternions are defined as

$$\mathbf{q}_{b,s} := \begin{bmatrix} \cos\left(\frac{\alpha}{2}\right) & 0 & -\sin\left(\frac{\alpha}{2}\right) & 0 \end{bmatrix}^\top \tag{2.42}$$

$$\mathbf{q}_{s,w} := \begin{bmatrix} \cos\left(\frac{\beta}{2}\right) & 0 & 0 & \sin\left(\frac{\beta}{2}\right) \end{bmatrix}^\top, \tag{2.43}$$

and this enables the wind frame to be related to the NED frame through the composite quaternion rotation as

$$\mathbf{q}_{n,w} = \mathbf{q}_{n,b} \otimes \mathbf{q}_{b,s} \otimes \mathbf{q}_{s,w} = \mathbf{q}_{n,b} \otimes \mathbf{q}_{b,w}. \tag{2.44}$$

Higher order derivatives of the angle of attack and the sideslip angle can be approximated using linear filters. In Yip *et al.* (1996), the authors show that higher order derivatives of the virtual control signals that are used as part of the backstepping

process, can be approximated by linear filters which greatly simplifies the controller design. For flight control, this approach has been applied in works such as Farrell *et al.* (2005) and Sonneveldt *et al.* (2009*b*). A linear filter can be chosen as (*cf.* Fossen (2011))

$$\dot{\mathbf{x}}_d = \mathbf{A}_d \mathbf{x}_d + \mathbf{B}_d r \tag{2.45}$$

with

$$\mathbf{A}_d = \begin{bmatrix} 0 & 1 & 0 \\ 0 & 0 & 1 \\ -\omega_n^3 & -(2\zeta+1)\omega_n^2 & -(2\zeta+1)\omega_n \end{bmatrix} \tag{2.46}$$

$$\mathbf{B}_d = \begin{bmatrix} 0 & 0 & \omega_n^3 \end{bmatrix}^\top \tag{2.47}$$

where ζ is the relative damping ratio, ω_n is the natural frequency and r is the reference signal being either the angle of attack or the sideslip angle. The state vector can be chosen as $\mathbf{x}_d = \begin{bmatrix} \alpha & \dot{\alpha} & \ddot{\alpha} \end{bmatrix}^\top$ in the case of the angle of attack and as $\mathbf{x}_d = \begin{bmatrix} \beta & \dot{\beta} & \ddot{\beta} \end{bmatrix}^\top$ for the sideslip angle. With the higher order derivatives of the angle of attack and the sideslip angle, the angular velocity of the wind frame relative to the body frame is found as (*cf.* Stevens and Lewis (2003))

$$\boldsymbol{\omega}_{b,w}^w = \begin{bmatrix} 0 \\ 0 \\ \dot{\beta} \end{bmatrix} + \begin{bmatrix} \cos(\beta) & \sin(\beta) & 0 \\ -\sin(\beta) & \cos(\beta) & 0 \\ 0 & 0 & 1 \end{bmatrix} \begin{bmatrix} 0 \\ -\dot{\alpha} \\ 0 \end{bmatrix} = \begin{bmatrix} -\dot{\alpha}\sin(\beta) \\ -\dot{\alpha}\cos(\beta) \\ \dot{\beta} \end{bmatrix} \tag{2.48}$$

and the angular acceleration is found through direct differentiation as

$$\dot{\boldsymbol{\omega}}_{b,w}^w = \begin{bmatrix} -\ddot{\alpha}\sin(\beta) - \dot{\alpha}\dot{\beta}\cos(\beta) \\ -\ddot{\alpha}\cos(\beta) + \dot{\alpha}\dot{\beta}\sin(\beta) \\ \ddot{\beta} \end{bmatrix}. \tag{2.49}$$

It is also possible to include saturation in the filter to ensure that the output remains bounded, which is important for the stability of the resulting tracking errors. The higher order derivatives can also be found by other methods such as *e.g.* a high gain observer (*cf.* Khalil (2002)). With the second derivative of a desired trajectory together with the angular velocity and acceleration of the wind frame relative to the body frame, it simplifies the problem of pointing the airspeed in a desired direction.

2.7 Actuator Saturation and Unknown Aerodynamics

The dynamics (2.21) and (2.32) represent a perfect scenario with infinite actuation and perfectly known aerodynamic models. To incorporate saturation into the dynamics, let the saturation function for a vector $\mathbf{v} := \begin{bmatrix} v_1 & v_2 & v_3 \end{bmatrix}^\top$ be defined as

$$\sigma(\mathbf{v}) := \begin{bmatrix} \sigma(v_1) & \sigma(v_2) & \sigma(v_3) \end{bmatrix}^\top \tag{2.50}$$

where the saturation operator works on a component level and is defined as

$$\sigma(v_i) := \begin{cases} v_{max} & \text{if } v_i \geq v_{max} \\ v_i & \text{if } v_{min} < v_i < v_{max} \\ v_{min} & \text{if } v_i \leq v_{min} \end{cases} \tag{2.51}$$

where $i = 1, 2, 3$, v_{max} and v_{min} denote the maximum and minimum values of the output. In the case of the thrust, it can be bounded between zero and a maximum value denoted T_{max}, such that

$$\sigma(T) := \begin{cases} T_{max} & \text{if } T \geq T_{max} \\ T & \text{if } 0 < T < T_{max} \\ 0 & \text{if } T \leq 0 \end{cases} \tag{2.52}$$

while the deflection angles can be bounded between a minium and maximum deflection angle such that

$$\sigma(\mathbf{u}) := \begin{bmatrix} \sigma(\delta_a) & \sigma(\delta_e) & \sigma(\delta_r) \end{bmatrix}^\top \tag{2.53}$$

and by letting δ represent an arbitrary deflection angle, its component-level saturation becomes

$$\sigma(\delta_i) := \begin{cases} \delta_{max} & \text{if } \delta \geq \delta_{max} \\ \delta & \text{if } \delta_{min} < \delta < \delta_{max} \\ \delta_{min} & \text{if } \delta \leq \delta_{min} \end{cases} \tag{2.54}$$

where $i = a, e, r$, δ_{min} and δ_{max} denote the minimum and maximum deflection angles respectively.

The thrust force vector can now be redefined as $\mathbf{f}^b_{thrust} = \begin{bmatrix} \sigma(T) & 0 & 0 \end{bmatrix}^\top$ such that the acceleration becomes (*cf.* (2.22))

$$\dot{V}_a = \frac{u}{mV_a}\sigma(T) + \frac{(\mathbf{v}^b_r)^\top}{V_a}\left(\frac{1}{m}\mathbf{R}^b_w\mathbf{f}^w_{aero} + \mathbf{R}^b_n\mathbf{f}^n_g\right). \tag{2.55}$$

To facilitate adaptive control, let the aerodynamic force vector be rewritten as $\mathbf{f}^w_{aero} = \boldsymbol{\Phi}_1\boldsymbol{\theta}_1$, where $\boldsymbol{\theta}_1$ is a vector of coefficients, while $\boldsymbol{\Phi}_1 = \boldsymbol{\Phi}_1(V_a, \alpha, \beta, \boldsymbol{\omega}^b_{n,b}, \mathbf{u})$ is a known matrix. Let the error between the saturated and commanded thrust be defined as $\tilde{T} = \sigma(T) - T$, and let the difference between the estimated and true aerodynamic coefficients be defined as $\tilde{\boldsymbol{\theta}}_1 = \hat{\boldsymbol{\theta}}_1 - \boldsymbol{\theta}_1$; then the acceleration becomes

$$\dot{V}_a = \frac{u}{mV_a}T + \frac{u}{mV_a}\tilde{T} + \frac{(\mathbf{v}^b_r)^\top}{V_a}\left(\frac{1}{m}\mathbf{R}^b_w\boldsymbol{\Phi}_1\hat{\boldsymbol{\theta}}_1 - \frac{1}{m}\mathbf{R}^b_w\boldsymbol{\Phi}_1\tilde{\boldsymbol{\theta}}_1 + \mathbf{R}^b_n\mathbf{f}^n_g\right). \tag{2.56}$$

For the rotational dynamics (2.26), the aerodynamic moments can be redefined as

$$\boldsymbol{\tau}^b_{aero} = \mathbf{f}(\mathbf{x}) - \mathbf{D}(\mathbf{x})\boldsymbol{\omega}^b_{n,b} + \mathbf{G}(\mathbf{x})\sigma(\mathbf{u}) \tag{2.57}$$

and by defining the error between the saturated and the actual command signal as $\tilde{\mathbf{u}} = \sigma(\mathbf{u}) - \mathbf{u}$, it enables the aerodynamic moments to be rewritten as

$$\boldsymbol{\tau}^b_{aero} = \mathbf{f}(\mathbf{x}) - \mathbf{D}(\mathbf{x})\boldsymbol{\omega}^b_{n,b} + \mathbf{G}(\mathbf{x})\mathbf{u} + \mathbf{G}(\mathbf{x})\tilde{\mathbf{u}}. \tag{2.58}$$

The aerodynamic moments are unknown and can be written as

$$\boldsymbol{\tau}^b_{aero} = \boldsymbol{\Phi}_2\boldsymbol{\theta}_2 + \boldsymbol{\Phi}_3\boldsymbol{\theta}_3 \tag{2.59}$$

where $\boldsymbol{\Phi}_2 = \boldsymbol{\Phi}_2(V_a, \alpha, \beta, \boldsymbol{\omega}^b_{n,b})$ and $\boldsymbol{\Phi}_3 = \boldsymbol{\Phi}_3(V_a, \delta_a, \delta_e, \delta_r)$ are two known matrices based on the aerodynamical moments, and $\boldsymbol{\theta}_2$ contains the coefficients of $\mathbf{f}(\mathbf{x})$ and $\mathbf{D}(\mathbf{x})$, while the control effectiveness coefficients are contained in $\boldsymbol{\theta}_3$. Now let the error between the estimated values and actual values be defined as $\tilde{\boldsymbol{\theta}}_2 = \hat{\boldsymbol{\theta}}_2 - \boldsymbol{\theta}_2$ and $\tilde{\boldsymbol{\theta}}_3 = \hat{\boldsymbol{\theta}}_3 - \boldsymbol{\theta}_3$ such that the angular acceleration becomes

$$\mathbf{J}\dot{\boldsymbol{\omega}}^b_{n,b} = -\mathbf{S}(\boldsymbol{\omega}^b_{n,b})\mathbf{J}\boldsymbol{\omega}^b_{n,b} + \boldsymbol{\Phi}_2\hat{\boldsymbol{\theta}}_2 + \hat{\mathbf{G}}(\mathbf{x})\mathbf{u} + \hat{\mathbf{G}}(\mathbf{x})\tilde{\mathbf{u}} - \boldsymbol{\Phi}_2\tilde{\boldsymbol{\theta}}_2 - \boldsymbol{\Phi}_3\tilde{\boldsymbol{\theta}}_3 \tag{2.60}$$

where the control effectiveness matrix has been reconstructed using the estimated aerodynamic coefficients.

Remark 2.7 *The aerodynamic coefficients that constitute the control effectiveness matrix are contained in $\boldsymbol{\theta}_3$. To facilitate the design of a control law, it is vital that the control coefficients never change sign by crossing zero since this will result in a singularity. Hence, the control coefficients are separated from the rest of the aerodynamics to enable projection of the coefficients to ensure that they become bounded to a convex set.*

Remark 2.8 *The saturation nonlinearity is commonly implemented using the* $\tanh(\cdot)$ *function. This ensures that the saturation function is smooth, such that there exist solutions to the differential equations (2.56) and (2.60).*

2.8 Summary

In this chapter two different translational and rotational models have been derived. The first model assumes infinite actuation and perfect aerodynamic modeling, while the second includes actuator constraints and the unknown aerodynamics. Using a filter to estimate the higher order derivatives of the angle of attack and the sideslip angle, the rotational and translational systems become decoupled, which is an important property that simplifies the controller design.

Chapter 3

Controller Design

> Without uncertainty there is no need for feedback.
>
> K. J. Åström, 1999

This chapter is based on Oland *et al.* (2013*a*), Oland and Kristiansen (2013*b*), Oland and Kristiansen (2014*a*), Oland *et al.* (2014*a*) and Oland *et al.* (2014*b*). In this chapter several attitude and speed controllers are derived for the problem of flight control. For attitude control, an integrator backstepping controller, a sliding surface controller and a PD+ controller are derived and modified to be applicable for flight control. For speed control, a simple proportional speed controller is derived using standard Lyapunov methods, while a proportional-integral speed controller is derived based on backstepping. Adaptive backstepping controllers are also derived for the rotational and translational systems where the actuator saturation and unknown aerodynamics are accounted for. It is also observed that the control signals for the attitude controllers are directly dependent on the airspeed of the UAV, a property that is exploited by designing a reference speed that makes the UAV increase its speed whenever the actuators are about to reach saturation, resulting in desaturation of the deflection angles.

3.1 Control Objective

From Chapter 2 it is apparent that the wind frame must be aligned in a desired direction and that the airspeed must be positive to enable flight. Let the desired frame be defined through $\mathbf{q}_{n,d} \in \mathcal{S}^3$ and $\boldsymbol{\omega}^d_{n,d}, \dot{\boldsymbol{\omega}}^d_{n,d} \in \mathcal{L}_\infty$ which in general can be time-varying; then the attitude tracking error can be written as

$$\mathbf{q}_{d,w} = \mathbf{q}_{d,n} \otimes \mathbf{q}_{n,b} \otimes \mathbf{q}_{b,w} \tag{3.1}$$

with the error kinematics as

$$\dot{\mathbf{q}}_{d,w} = \frac{1}{2}\mathbf{q}_{d,w} \otimes \begin{bmatrix} 0 \\ \boldsymbol{\omega}^w_{d,w} \end{bmatrix} \tag{3.2}$$

which has two equilibria at $\mathbf{q}^{\star}_{d,w} = \begin{bmatrix}\pm 1 & 0 & 0 & 0\end{bmatrix}^{\top}$ that physically represent the same orientation, but mathematically they are different. From a control perspective it is more intuitive to control the attitude relative to the origin. Based on the work by Kristiansen *et al.* (2009*a*), let an error function be defined as

$$\mathbf{e}_{q\pm} = \begin{bmatrix} 1 \mp \eta_{d,w} \\ \boldsymbol{\epsilon}_{d,w} \end{bmatrix} \in \mathcal{S}^3_e \tag{3.3}$$

where $\mathcal{S}^3_e = \{\begin{bmatrix}1 \mp \eta_{d,w} & \boldsymbol{\epsilon}^{\top}_{d,w}\end{bmatrix}^{\top} \mid \mathbf{q}_{d,w} \in \mathcal{S}^3\}$ with the kinematics as

$$\dot{\mathbf{e}}_{q\pm} = \mathbf{T}_e(\mathbf{e}_{q\pm})\mathbf{R}^w_b\boldsymbol{\omega}^b_{d,w} \tag{3.4}$$

$$\mathbf{T}_e(\mathbf{e}_{q\pm}) = \frac{1}{2}\begin{bmatrix} \pm\boldsymbol{\epsilon}^{\top}_{d,w} \\ \eta_{d,w}\mathbf{I} + \mathbf{S}(\boldsymbol{\epsilon}_{d,w}) \end{bmatrix} \tag{3.5}$$

$$\boldsymbol{\omega}^b_{d,w} = \boldsymbol{\omega}^b_{n,b} - \mathbf{R}^b_d\boldsymbol{\omega}^d_{n,d} + \mathbf{R}^b_w\boldsymbol{\omega}^w_{b,w}, \tag{3.6}$$

where $\boldsymbol{\omega}^b_{d,w} \coloneqq \begin{bmatrix}\omega_x & \omega_y & \omega_z\end{bmatrix}^{\top}$. Equation (3.6) can be differentiated, and by inserting (2.32) the rotational error dynamics become[1]

$$\begin{aligned}\mathbf{J}\dot{\boldsymbol{\omega}}^b_{d,w} =& -\mathbf{S}(\boldsymbol{\omega}^b_{n,b})\mathbf{J}\boldsymbol{\omega}^b_{n,b} + \mathbf{f}(\mathbf{x}) - \mathbf{D}(\mathbf{x})\boldsymbol{\omega}^b_{n,b} + \mathbf{G}(\mathbf{x})\mathbf{u} \\ &- \mathbf{J}\mathbf{R}^b_d\mathbf{S}(\boldsymbol{\omega}^d_{b,d})\boldsymbol{\omega}^d_{n,d} - \mathbf{J}\mathbf{R}^b_d\dot{\boldsymbol{\omega}}^d_{n,d} + \mathbf{J}\mathbf{R}^b_w\dot{\boldsymbol{\omega}}^w_{b,w},\end{aligned} \tag{3.7}$$

and by using (3.6) and that $\boldsymbol{\omega}^d_{b,d} = \boldsymbol{\omega}^d_{n,d} - \boldsymbol{\omega}^d_{n,b}$ the error dynamics become

$$\begin{aligned}\mathbf{J}\dot{\boldsymbol{\omega}}^b_{d,w} =& -\mathbf{S}(\boldsymbol{\omega}^b_{n,b})\mathbf{J}\boldsymbol{\omega}^b_{n,b} + \mathbf{f}(\mathbf{x}) - \mathbf{D}(\mathbf{x})\boldsymbol{\omega}^b_{d,w} - \mathbf{D}(\mathbf{x})(\mathbf{R}^b_d\boldsymbol{\omega}^d_{n,d} - \mathbf{R}^b_w\boldsymbol{\omega}^w_{b,w}) \\ &+ \mathbf{G}(\mathbf{x})\mathbf{u} + \mathbf{J}\mathbf{S}(\boldsymbol{\omega}^b_{n,b})\mathbf{R}^b_d\boldsymbol{\omega}^d_{n,d} - \mathbf{J}\mathbf{R}^b_d\dot{\boldsymbol{\omega}}^d_{n,d} + \mathbf{J}\mathbf{R}^b_w\dot{\boldsymbol{\omega}}^w_{b,w}.\end{aligned} \tag{3.8}$$

Let a desired speed profile be defined through $V_d, \dot{V}_d \in \mathcal{L}_\infty$ which in general can be time-varying, and let a speed error function be defined as $\tilde{V} = V_a - V_d$. By differentiating the speed error and by inserting (2.22) the error dynamics become

$$\dot{\tilde{V}} = \frac{u}{mV_a}T + \frac{(\mathbf{v}^b_r)^{\top}}{V_a}(\frac{1}{m}\mathbf{R}^b_w\mathbf{f}^w_{aero} + \mathbf{R}^b_n\mathbf{f}_g) - \dot{V}_d. \tag{3.9}$$

Hence, the control objective is to make $(\tilde{V}, \mathbf{e}_{q\pm}, \boldsymbol{\omega}^b_{d,w}) \to (0, \mathbf{0}, \mathbf{0})$, which will ensure that the UAV moves with a desired positive airspeed and tracks a desired attitude and angular velocity. To facilitate controller design, a few assumptions are required that will be used as they are needed.

Assumption 3.1 *The aerodynamics are perfectly known.*

Assumption 3.2 *The desired trajectory is designed such that it can be tracked by the* UAV *with its inherent actuator limitations.*

Assumption 3.3 *The signs of the coefficients for the control effectiveness matrix are known.*

[1] The term $\frac{d}{dt}\mathbf{J}\mathbf{R}^b_w\boldsymbol{\omega}^w_{b,w} = \mathbf{J}\mathbf{R}^b_w\mathbf{S}(\boldsymbol{\omega}^w_{b,w})\boldsymbol{\omega}^w_{b,w} + \mathbf{J}\mathbf{R}^b_w\dot{\boldsymbol{\omega}}^w_{b,w} = \mathbf{J}\mathbf{R}^b_w\dot{\boldsymbol{\omega}}^w_{b,w}$.

Assumption 3.4 *The desired trajectory is persistently exciting, i.e., there exist positive constants, μ and T such that (cf. Panteley* et al. *(2001))*

$$\mu \mathbf{I} \leq \int_t^{t+T} \mathbf{\Phi}(\tau)\mathbf{\Phi}^\top(\tau)d\tau, \quad \forall\ t \geq 0. \tag{3.10}$$

Assumption 3.1 can be relaxed by introducing adaptive control (*cf.* Slotine and Li (1991), Krstić *et al.* (1995), Farrell *et al.* (2005), Sonneveldt *et al.* (2009*a*), Hovakimyan and Cao (2010)) which will be done later in this chapter. Assumption 3.2 is a reasonable assumption, since it is only natural to track trajectories that the UAV actually can track. That is, the desired trajectory does not move faster than the angular velocity that the control surfaces can produce. Hence, it is reasonable to claim that if the actuators have gone into saturation, since the desired trajectory is slower than the UAV, the tracking error will eventually go to zero, resulting in a desaturation of the actuators. Assumption 3.3 is also a reasonable assumption that is often required for adaptive control (*cf.* Krstić *et al.* (1995)). In essence, Assumption 3.3 states that when changing a deflection angle by a certain degree, the direction of the resulting aerodynamic moment is known. Assumption 3.4 states that motion of the UAV must be sufficiently rich, in the sense that it contains enough frequencies to enable the adaptive controller to estimate the unknown coefficients (Boyd and Sastry (1986)). This is a standard assumption that is required for adaptive control and can be facilitated by superimposing a sinusoidal signal onto the desired trajectory (*cf.* Stepanyan and Hovakimyan (2007) and van Oort *et al.* (2010)).

3.2 Rotational Controllers

To facilitate controller design, an assumption and a few lemmas are required as presented below:

Lemma 3.1 *Let Assumption 2.2 hold. Then the airspeed, V_a, is uniformly globally ultimately bounded for any T.*

Proof. The proof is given in Appendix E.1. ■

Lemma 3.2 *Let Assumption 2.2 hold. Then the angular velocity $\boldsymbol{\omega}_{n,b}^b$ of the system (2.32) is uniformly globally ultimately bounded for any $\mathbf{u}$.*

Proof. The proof is given in Appendix E.2 ■

Lemma 3.3 *Let Assumption 2.2 hold. Then the angular velocity $\boldsymbol{\omega}_{b,w}^w$ is bounded.*

Proof. The proof is given in Appendix E.3. ■

Lemma 3.2 is a direct result of the aerodynamic damping together with the fact that the deflection angles are physical bounded. Lemma 3.3 follows as a consequence of Lemma 3.1, Lemma 3.2 and the fact that the thrust and deflection angles are bounded. Similar arguments can be applied to show that $\dot{\boldsymbol{\omega}}_{b,w}^w$ is bounded, but then the actuators must have rate constraints which are not considered in this thesis. Instead it can be enforced by applying saturation when approximating the higher order derivatives of the angle of attack and the sideslip angle.

Assumption 3.5 *sign*$(\eta_{d,w}(t)) = $ *sign*$(\eta_{d,w}(t_0))\ \forall\ t \geq t_0$.

Assumption 3.5 divides the rotation sphere into two halves enabling the controller to be derived while focusing on only one of the two equilibria of the quaternion error. This assumption can be relaxed by introducing hybrid switching as shown in Schlanbusch *et al.* (2011). To generalize the following lemma, it considers an arbitrary quaternion $\mathbf{q} = \begin{bmatrix}\eta & \boldsymbol{\epsilon}^\top\end{bmatrix}^\top$.

Lemma 3.4 *Given that sign*$(\eta(t)) = $ *sign*$(\eta(t_0))\ \forall\ t \geq t_0$*, then the following inequality holds:*

$$\mathbf{e}_{q\pm}^\top \mathbf{T}_e(\mathbf{e}_{q\pm})\mathbf{T}_e^\top(\mathbf{e}_{q\pm})\mathbf{e}_{q\pm} \geq \frac{1}{8}\mathbf{e}_{q\pm}^\top \mathbf{e}_{q\pm}. \tag{3.11}$$

Proof. The proof is given in Kristiansen *et al.* (2009*a*) and Schlanbusch *et al.* (2012*a*) and is reproduced in Appendix E.4. ■

3.2.1 Quaternion-based Backstepping Controller

Backstepping control is presented in Krstić *et al.* (1995), and is a method for controlling nonlinear systems in strict feedback form. As opposed to feedback-linearization, the use of backstepping enables the removal of undesirable terms while maintaining the good terms. For example the term $\mathbf{D}(\mathbf{x})\boldsymbol{\omega}_{d,w}^b$ in (3.8) can be considered a good term since it provides damping of the angular velocity error and can therefore be maintained in the closed loop dynamics. Quaternion-based backstepping has been applied for spacecraft control in Kristiansen *et al.* (2009*b*) and can be adapted to flight control by taking basis in the error dynamics (3.4) and (3.8) which are in strict-feedback form. The results are summarized in the following theorem:

Theorem 3.1 *Let Assumptions 2.2, 3.1, 3.2 and 3.5 hold. Given* $\mathbf{q}_{n,d} \in \mathcal{S}^3$ *and* $\boldsymbol{\omega}_{n,d}^d, \dot{\boldsymbol{\omega}}_{n,d}^d \in \mathcal{L}_\infty$*, then the dual equilibrium points* $(\mathbf{e}_{q\pm}, \mathbf{z}) = (\mathbf{0}, \mathbf{0})$ *of the dynamics (2.25) and (2.32) in closed loop with the controller*

$$\begin{aligned}\mathbf{u} = {} & \mathbf{G}^{-1}(\mathbf{x})(\mathbf{J}\mathbf{R}_d^b\dot{\boldsymbol{\omega}}_{n,d}^d - \mathbf{J}\mathbf{S}(\boldsymbol{\omega}_{n,b}^b)\mathbf{R}_d^b\boldsymbol{\omega}_{n,d}^d + \mathbf{S}(\boldsymbol{\omega}_{n,b}^b)\mathbf{J}\boldsymbol{\omega}_{n,b}^b - \mathbf{f}(\mathbf{x}) \\ & + \mathbf{D}(\mathbf{x})(\mathbf{R}_d^b\boldsymbol{\omega}_{n,d}^d - \mathbf{R}_w^b\boldsymbol{\omega}_{b,w}^w - k_q\mathbf{R}_w^b\mathbf{T}_e^\top\mathbf{e}_q) - \mathbf{J}\mathbf{R}_w^b\dot{\boldsymbol{\omega}}_{b,w}^w \\ & - k_q\mathbf{J}\mathbf{R}_w^b\mathbf{S}(\boldsymbol{\omega}_{b,w}^w)\mathbf{T}_e^\top\mathbf{e}_q - \frac{k_q}{2}\mathbf{J}\mathbf{R}_w^b\dot{\boldsymbol{\epsilon}}_{d,w} - \mathbf{R}_w^b\mathbf{T}_e^\top\mathbf{e}_q - k_\omega\mathbf{z})\end{aligned} \tag{3.12}$$

$$\mathbf{z} = \boldsymbol{\omega}_{n,b}^b - \mathbf{R}_d^b\boldsymbol{\omega}_{n,d}^d + \mathbf{R}_w^b\boldsymbol{\omega}_{b,w}^w + k_q\mathbf{R}_w^b\mathbf{T}_e^\top\mathbf{e}_q \tag{3.13}$$

where $k_q > 0$*,* $k_\omega > 0$*, are uniformly exponentially stable.*

Proof. The proof is given in Appendix E.5. ■

Remark 3.1 *As* $(\mathbf{e}_q, \mathbf{z}) \to (\mathbf{0}, \mathbf{0})$ *if follows from (3.13) that* $\boldsymbol{\omega}_{d,w}^b = \boldsymbol{\omega}_{n,b}^b - \mathbf{R}_d^b\boldsymbol{\omega}_{n,d}^d + \mathbf{R}_w^b\boldsymbol{\omega}_{b,w}^w \to \mathbf{0}$*, and thereby completing the control objective.*

Using this control law, it enables the UAV to point its airspeed in any desired direction which in general can be moving. Note that the airspeed must be positive in order to invert the control effectiveness matrix $\mathbf{G}(\mathbf{x})$, and it is assumed to have full rank which is true for the aerodynamic coefficients that are defined in Appendix A (even though they are for a specific flight condition). Note that all the rotational controllers that are derived in this chapter share many similarities with the dynamic inversion approach, since the angular velocity dynamics are inverted to find the control signals that make the errors go to zero.

3.2.2 Paden and Panja PD+ Controller

Takegaki and Arimoto (1981) proposed a very simple solution to the problem of robot position control and the result was later extended to trajectory tracking in Paden and Panja (1988) where the authors applied the Matrosov theorem (*cf.* Theorem D.4) to prove stability of the tracking errors. Both controllers are passivity-based (*cf.* Ortega and Spong (1989)) as emphasized in Berghuis and Nijmeijer (1993), meaning that the control law exploits the physical structure of the robot and reshapes the robots natural energy to achieve its control objective. The result by Paden and Panja has later been applied for spacecraft control in works such as Kristiansen *et al.* (2008*a*), Kristiansen *et al.* (2011) and Schlanbusch *et al.* (2012*b*). In this section, the control solution is adapted to the problem of flight control which is summarized in the following theorem:

Theorem 3.2 *Let Assumptions 2.2, 3.1, 3.2 and 3.5 hold. Given* $\mathbf{q}_{n,d} \in \mathcal{S}^3$ *and* $\boldsymbol{\omega}^d_{n,d}, \dot{\boldsymbol{\omega}}^d_{n,d} \in \mathcal{L}_\infty$*, then the dual equilibrium points* $(\mathbf{e}_{q\pm}, \boldsymbol{\omega}^b_{d,w}) = (\mathbf{0}, \mathbf{0})$ *of the dynamics (2.25) and (2.32) in closed loop with the controller*

$$\begin{aligned}\mathbf{u} = \mathbf{G}^{-1}(\mathbf{x})(&\mathbf{J}\mathbf{R}^b_d\dot{\boldsymbol{\omega}}^d_{n,d} - \mathbf{J}\mathbf{S}(\boldsymbol{\omega}^b_{n,b})\mathbf{R}^b_d\boldsymbol{\omega}^d_{n,d} + \mathbf{S}(\boldsymbol{\omega}^b_{n,b})\mathbf{J}\boldsymbol{\omega}^b_{n,b} - \mathbf{f}(\mathbf{x}) \\ &+ \mathbf{D}(\mathbf{x})(\mathbf{R}^b_d\boldsymbol{\omega}^d_{n,d} - \mathbf{R}^b_w\boldsymbol{\omega}^w_{b,w}) - \mathbf{J}\mathbf{R}^b_w\dot{\boldsymbol{\omega}}^w_{b,w} - k_q\mathbf{R}^b_w\mathbf{T}_e^\top\mathbf{e}_q - k_\omega\boldsymbol{\omega}^b_{d,w})\end{aligned} \tag{3.14}$$

where $k_q > 0$ *and* $k_\omega > 0$*, are uniformly asymptotically stable.*

Proof. The proof is given in Appendix E.6. ■

Notice the relatively simple structure of the controller. It consists of several nonlinear terms to remove the undesirable terms from the error dynamics (3.8) together with a proportional and a derivative term to make the tracking errors go to zero (the last two terms).

Corollary 3.1 *The dual equilibrium points* $(\mathbf{e}_{q\pm}, \boldsymbol{\omega}^b_{d,w}) = (\mathbf{0}, \mathbf{0})$ *of the dynamics (2.25) and (2.32) in closed loop with (3.14) can be shown to be uniformly exponentially stable by invoking Lemma 3 from Panteley* et al. *(2001) by following the same lines as shown in Schlanbusch (2012) Theorem* 3.3.

3.2.3 Sliding Surface Controller

The sliding surface controller by Slotine and Li (1987) is another passivity-based controller. Instead of tracking the desired trajectory directly, a reference trajectory

is defined which when tracked, obtains desirable reduced order dynamics. The difference between the actual and the reference trajectory is called the sliding surface. The method has received much attention and has resulted in a new branch of nonlinear controllers called sliding mode control which employs switching to remain on the sliding surface. Note that the sliding surface controller that is presented in Slotine and Li (1987) is a continuous controller and is not to be confused with the discontinuous sliding mode controller as presented in Slotine and Li (1991). The sliding surface controller is adapted to the case of flight control and is summarized in the following theorem:

Theorem 3.3 *Let assumptions 2.2, 3.1, 3.2 and 3.5 hold. Given* $\mathbf{q}_{n,d} \in \mathcal{S}^3$ *and* $\boldsymbol{\omega}^d_{n,d}, \dot{\boldsymbol{\omega}}^d_{n,d} \in \mathcal{L}_\infty$*, then the dual equilibrium points* $(\mathbf{e}_{q\pm}, \mathbf{s}) = (\mathbf{0}, \mathbf{0})$ *of the dynamics (2.25) and (2.32) in closed loop with the controller*

$$\begin{aligned}
\mathbf{u} =& \mathbf{G}^{-1}(\mathbf{x})(\mathbf{J}\dot{\boldsymbol{\omega}}^b_{n,r} + \mathbf{D}(\mathbf{x})\boldsymbol{\omega}^b_{n,r} + \mathbf{S}(\boldsymbol{\omega}^b_{n,b})\mathbf{J}\boldsymbol{\omega}^b_{n,b} - \mathbf{f}(\mathbf{x}) - k_s\mathbf{s} \\
& - k_q\mathbf{R}^b_w\mathbf{T}^\top_e\mathbf{e}_q) && (3.15)\\
\mathbf{s} =& \boldsymbol{\omega}^b_{n,b} - \boldsymbol{\omega}^b_{n,r} && (3.16)\\
\boldsymbol{\omega}^b_{n,r} =& \mathbf{R}^b_d\boldsymbol{\omega}^d_{n,d} - \mathbf{R}^b_w\boldsymbol{\omega}^w_{b,w} - \boldsymbol{\Lambda}\mathbf{R}^b_w\mathbf{T}^\top_e\mathbf{e}_q && (3.17)\\
\dot{\boldsymbol{\omega}}^b_{n,r} =& \mathbf{R}^b_d\dot{\boldsymbol{\omega}}^d_{n,d} - \mathbf{S}(\boldsymbol{\omega}^b_{n,b})\mathbf{R}^b_d\boldsymbol{\omega}^d_{n,d} - \mathbf{R}^b_w\dot{\boldsymbol{\omega}}^w_{b,w} \\
& - \boldsymbol{\Lambda}\mathbf{R}^b_w\mathbf{S}(\boldsymbol{\omega}^w_{b,w})\mathbf{T}^\top_e\mathbf{e}_q - \frac{1}{2}\boldsymbol{\Lambda}\mathbf{R}^b_w\dot{\boldsymbol{\epsilon}}_{d,w} && (3.18)
\end{aligned}$$

where $k_q > 0$ *and* $k_s > 0$*,* $\boldsymbol{\Lambda} = \lambda\mathbf{I}$*,* $\lambda > 0$*, are uniformly exponentially stable.*

Proof. The proof is given in Appendix E.7. ■

Remark 3.2 *As* $(\mathbf{e}_q, \mathbf{s}) \to (\mathbf{0}, \mathbf{0})$ *if follows from (3.16) that* $\boldsymbol{\omega}^b_{d,w} = \boldsymbol{\omega}^b_{n,b} - \mathbf{R}^b_d\boldsymbol{\omega}^d_{n,d} + \mathbf{R}^b_w\boldsymbol{\omega}^w_{b,w} \to \mathbf{0}$*, and thereby completing the control objective.*

Remark 3.3 *As pointed out in Kristiansen* et al. *(2008a), the backstepping controller and the sliding surface controller are the same controller if the gains are chosen appropriately.*

3.2.4 Adaptive Backstepping Controller with Constrained Actuation

Assumption 3.1 has enabled the preceding controllers to be derived. In this section, this assumption will be relaxed to create a more realistic controller that doesn't assume that the aerodynamics are known. This section takes basis in the results by Johnson and Calise (2000) and Tandale and Valasek (2005) and presents a method for performing adaptive control of a fixed-wing UAV in the presence of the saturation nonlinearity. The basic idea with this approach is to design a reference trajectory which deviates from the desired trajectory whenever the actuators are in saturation. This ensures that the adaptive update laws are not affected by the saturation nonlinearity which has a deteriorating effect on the parameter estimation. To take saturation and unknown aerodynamics into account when designing the control law, the dynamic model (2.60) is used.

Let a reference trajectory be defined through $\mathbf{q}_{n,r}, \boldsymbol{\omega}^r_{n,r}, \dot{\boldsymbol{\omega}}^r_{n,r}$ with the kinematics as

$$\dot{\mathbf{q}}_{n,r} = \frac{1}{2}\mathbf{q}_{n,r} \otimes \begin{bmatrix} 0 \\ \boldsymbol{\omega}^r_{n,r} \end{bmatrix}, \tag{3.19}$$

where $\dot{\boldsymbol{\omega}}^r_{n,r}$ can be designed such that the reference trajectory tracks the desired trajectory. The reference tracking error can be defined as $\mathbf{q}_{d,r} = \mathbf{q}_{d,n} \otimes \mathbf{q}_{n,r}$ with a corresponding error function as

$$\mathbf{e}_{q_r\pm} = \begin{bmatrix} 1 \mp \eta_{d,r} \\ \boldsymbol{\epsilon}_{d,r} \end{bmatrix} \tag{3.20}$$

and with the error kinematics as

$$\dot{\mathbf{e}}_{q_r\pm} = \mathbf{T}_{e_r}(\mathbf{e}_{q_r\pm})\boldsymbol{\omega}^r_{d,r} = \mathbf{T}_{e_r}(\mathbf{e}_{q_r\pm})(\boldsymbol{\omega}^r_{n,r} - \mathbf{R}^r_d\boldsymbol{\omega}^d_{n,d}) \tag{3.21}$$

$$\mathbf{T}_{e_r}(\mathbf{e}_{q_r\pm}) = \frac{1}{2}\begin{bmatrix} \pm\boldsymbol{\epsilon}^\top_{d,r} \\ \eta_{d,r}\mathbf{I} + \mathbf{S}(\boldsymbol{\epsilon}_{d,r}) \end{bmatrix}. \tag{3.22}$$

Assumption 3.6 *$sign(\eta_{d,r}(t)) = sign(\eta_{d,r}(t_0))\ \forall\ t \geq t_0$.*

Assumption 3.7 *$sign(\eta_{r,w}(t)) = sign(\eta_{r,w}(t_0))\ \forall\ t \geq t_0$.*

These assumptions allow the rotation sphere to be divided into two halves and enable Lemma 3.4 to be applied.

Lemma 3.5 *Let Assumption 3.6 hold and a continuous bounded vector be defined as $\boldsymbol{\xi}_1 = f_1(\tilde{\mathbf{u}})$ with $f_1(\mathbf{0}) = \mathbf{0}$. Given $\mathbf{q}_{n,d} \in \mathcal{S}^3$ and $\boldsymbol{\omega}^d_{n,d}, \dot{\boldsymbol{\omega}}^d_{n,d} \in \mathcal{L}_\infty$, then the dual equilibrium points $(\mathbf{e}_{q_r\pm}, \mathbf{z}_r) = (\mathbf{0}, \mathbf{0})$ using the reference*

$$\dot{\mathbf{q}}_{n,r} = \frac{1}{2}\mathbf{q}_{n,r} \otimes \begin{bmatrix} 0 \\ \boldsymbol{\omega}^r_{n,r} \end{bmatrix} \tag{3.23}$$

$$\dot{\boldsymbol{\omega}}^r_{n,r} = \mathbf{R}^r_d\dot{\boldsymbol{\omega}}^d_{n,d} - \mathbf{S}(\boldsymbol{\omega}^r_{n,r})\mathbf{R}^r_d\boldsymbol{\omega}^d_{n,d} - k_1\frac{\dot{\boldsymbol{\epsilon}}_{d,r}}{2} - \mathbf{T}^\top_{e_r}\mathbf{e}_{q_r} - k_2\mathbf{z}_r + \boldsymbol{\xi}_1 \tag{3.24}$$

$$\mathbf{z}_r = \boldsymbol{\omega}^r_{n,r} - \mathbf{R}^r_d\boldsymbol{\omega}^d_{n,d} + k_1\mathbf{T}^\top_{e_r}\mathbf{e}_{q_r} \tag{3.25}$$

where $k_1 > 0$, $k_2 > 0$, are uniformly asymptotically stable when $\boldsymbol{\xi}_1 = \mathbf{0}$.

Proof. The proof is given in Appendix E.8. ■

Remark 3.4 *As $(\mathbf{e}_{q_r}, \mathbf{z}_r) \to (\mathbf{0}, \mathbf{0})$ if follows from (3.25) that $\boldsymbol{\omega}^r_{n,r} \to \mathbf{R}^r_d\boldsymbol{\omega}^d_{n,d}$ ensuring that the reference tracks the desired angular velocity.*

Remark 3.5 *The vector $\boldsymbol{\xi}_1 = f_1(\tilde{\mathbf{u}})$ becomes non-zero when the actuators are in saturation. This will result in a divergence of the reference trajectory away from the desired trajectory to accommodate for the actuator saturation. Using Assumption 3.2 it follows that $\tilde{\mathbf{u}} \to \mathbf{0}$ in finite time, such that the reference trajectory will converge to the desired trajectory again. Hence, the vector $\boldsymbol{\xi}_1$ can be used to move the saturation problem from the plant to the reference.*

Remark 3.6 *Since the reference trajectory can be designed with infinite actuation (i.e. no bound on $\dot{\boldsymbol{\omega}}^r_{n,r}$), it is also possible to show that the origin is uniformly practically exponentially stable (cf. Grøtli (2010)). The gains can be increased to infinity, making the errors go to a small ball around the origin that can be made arbitrarily small (cf. Chaillet (2006)). Due to the physical constraints of the control surfaces, practical stability cannot be applied to prove stability of the resulting equilibria for the rotational control laws; since by increasing the gains toward infinity makes the actuators go into saturation.*

Assumption 3.1 can now be relaxed. Let the reference trajectory be defined by (3.19) and (3.24) such that the attitude tracking error can be redefined as

$$\mathbf{q}_{r,w} \coloneqq \mathbf{q}_{r,n} \otimes \mathbf{q}_{n,b} \otimes \mathbf{q}_{b,w} \tag{3.26}$$

with the error function as $\mathbf{e}_{q\pm} \coloneqq \begin{bmatrix} 1 \mp \eta_{r,w} & \boldsymbol{\epsilon}^\top_{r,w} \end{bmatrix}^\top$ which has the error kinematics as

$$\dot{\mathbf{e}}_{q\pm} = \mathbf{T}_e(\mathbf{e}_{q\pm})\mathbf{R}^w_b \boldsymbol{\omega}^b_{r,w} \tag{3.27}$$

$$\boldsymbol{\omega}^b_{r,w} = \boldsymbol{\omega}^b_{n,b} - \mathbf{R}^b_r \boldsymbol{\omega}^r_{n,r} + \mathbf{R}^b_w \boldsymbol{\omega}^w_{b,w}. \tag{3.28}$$

Note that the desired angular velocity, $\boldsymbol{\omega}^d_{n,d}$, is *subsumed*[2] by the reference $\boldsymbol{\omega}^r_{n,r}$, a property that is exploited in Chapter 5. Differentiating (3.28) and inserting (2.60) and (3.24) the error dynamics become

$$\begin{aligned}
\mathbf{J}\dot{\boldsymbol{\omega}}^b_{r,w} = &- \mathbf{S}(\boldsymbol{\omega}^b_{n,b})\mathbf{J}\boldsymbol{\omega}^b_{n,b} + \boldsymbol{\Phi}_2\hat{\boldsymbol{\theta}}_2 + \hat{\mathbf{G}}(\mathbf{x})\mathbf{u} + \hat{\mathbf{G}}(\mathbf{x})\tilde{\mathbf{u}} - \boldsymbol{\Phi}_2\tilde{\boldsymbol{\theta}}_2 - \boldsymbol{\Phi}_3\tilde{\boldsymbol{\theta}}_3 \\
&+ \mathbf{J}\mathbf{S}(\boldsymbol{\omega}^b_{n,b})\mathbf{R}^b_r\boldsymbol{\omega}^r_{n,r} - \mathbf{J}\mathbf{R}^b_r(\mathbf{R}^r_d\dot{\boldsymbol{\omega}}^d_{n,d} - \mathbf{S}(\boldsymbol{\omega}^r_{n,r})\mathbf{R}^r_d\boldsymbol{\omega}^d_{n,d} \\
&- k_1\frac{\dot{\boldsymbol{\epsilon}}_{d,r}}{2} - \mathbf{T}^\top_{e_r}\mathbf{e}_{q_r} - k_2\mathbf{z}_r + \boldsymbol{\xi}_1) + \mathbf{J}\mathbf{R}^b_w\dot{\boldsymbol{\omega}}^w_{b,w}.
\end{aligned} \tag{3.29}$$

The function $\boldsymbol{\xi}_1$ can now be used to remove the saturation problem during the derivation of the controller, an adaptive update law can be designed to deal with the unknown coefficients and a control law can be designed to make the tracking errors go to zero. This is formalized through the following theorem:

Theorem 3.4 *Let Assumptions 2.2, 3.2, 3.3, 3.4 and 3.7 hold. Given $\mathbf{q}_{n,d}, \boldsymbol{\omega}^d_{n,d}$, $\dot{\boldsymbol{\omega}}^d_{n,d} \in \mathcal{L}_\infty$, then the dual equilibrium points $(\mathbf{e}_{q\pm}, \mathbf{z}, \tilde{\boldsymbol{\theta}}_2, \tilde{\boldsymbol{\theta}}_3) = (\mathbf{0}, \mathbf{0}, \mathbf{0}, \mathbf{0})$ of the dynamics (2.25) and (2.60) in closed loop with the controller, bounded function and*

[2]Oxford Dictionaries define "subsume" as: "include or absorb (something) into something else". The point here is that the desired angular velocity has become a part of the reference angular velocity, and is thereby subsumed by the reference.

update laws

$$\begin{aligned}\mathbf{u} = \hat{\mathbf{G}}^{-1}(\mathbf{x})(&\mathbf{S}(\boldsymbol{\omega}^b_{n,b})\mathbf{J}\boldsymbol{\omega}^b_{n,b} - \boldsymbol{\Phi}_2\hat{\boldsymbol{\theta}}_2 + \mathbf{J}(-\mathbf{S}(\boldsymbol{\omega}^b_{n,b})\mathbf{R}^b_r\boldsymbol{\omega}^r_{n,r} \\ &+ \mathbf{R}^b_r(\mathbf{R}^r_d\dot{\boldsymbol{\omega}}^d_{n,d} - \mathbf{S}(\boldsymbol{\omega}^r_{n,r})\mathbf{R}^r_d\boldsymbol{\omega}^d_{n,d} - k_1\frac{\dot{\boldsymbol{\epsilon}}_{d,r}}{2} - \mathbf{T}^\top_{e_r}\mathbf{e}_{q_r} - k_2\mathbf{z}_r) \\ &- k_3\mathbf{R}^b_w\mathbf{S}(\boldsymbol{\omega}^w_{b,w})\mathbf{T}^\top_e\mathbf{e}_q - \frac{k_3}{2}\mathbf{R}^b_w\dot{\boldsymbol{\epsilon}}_{r,w} - \mathbf{R}^b_w\mathbf{T}^\top_e\mathbf{e}_q - \mathbf{R}^b_w\dot{\boldsymbol{\omega}}^w_{b,w} - k_4\mathbf{z})) \end{aligned} \tag{3.30}$$

$$\boldsymbol{\xi}_1 = \mathbf{R}^r_b\mathbf{J}^{-1}\hat{\mathbf{G}}(\mathbf{x})\tilde{\mathbf{u}} \tag{3.31}$$

$$\tilde{\mathbf{u}} = \sigma(\mathbf{u}) - \mathbf{u} \tag{3.32}$$

$$\dot{\hat{\boldsymbol{\theta}}}_2 = \boldsymbol{\Gamma}_2\boldsymbol{\Phi}_2^\top\mathbf{J}^{-1}\mathbf{z} \tag{3.33}$$

$$\dot{\hat{\boldsymbol{\theta}}}_3 = \mathrm{proj}(\boldsymbol{\Gamma}_3\boldsymbol{\Phi}_3^\top\mathbf{J}^{-1}\mathbf{z}) \tag{3.34}$$

$$\mathbf{z} = \boldsymbol{\omega}^b_{r,w} + k_3\mathbf{R}^b_w\mathbf{T}^\top_e\mathbf{e}_q \tag{3.35}$$

$$\mathbf{z}_r = \boldsymbol{\omega}^r_{n,r} - \mathbf{R}^r_d\boldsymbol{\omega}^d_{n,d} + k_1\mathbf{T}^\top_{e_r}\mathbf{e}_{q_r} \tag{3.36}$$

with $k_1 > 0$, $k_2 > 0$, $k_3 > 0$, $k_4 > 0$, $\boldsymbol{\Gamma}_3 = \boldsymbol{\Gamma}_3^\top > \mathbf{0}$ and $\boldsymbol{\Gamma}_2 = \boldsymbol{\Gamma}_2^\top > \mathbf{0}$, are uniformly asymptotically stable even in the presence of unknown aerodynamics and actuator constraints.

Proof. The proof is given in Appendix E.9. ■

The modeling uncertainty is handled through the adaptive update laws (3.33)-(3.34) and the saturation problem is moved to the reference trajectory through (3.31). Note that the saturation problem is not solved, but it has been moved to the reference trajectory such that stability of the origin is not affected by the saturation nonlinearity.

Remark 3.7 *When the actuators have desaturated, it follows from Lemma 3.5 that $(\mathbf{e}_{q_r}, \mathbf{z}_r) \to (\mathbf{0}, \mathbf{0})$ such that $\mathbf{q}_{n,r} \to \mathbf{q}_{n,d}$ and $\boldsymbol{\omega}^r_{n,r} \to \mathbf{R}^r_d\boldsymbol{\omega}^d_{n,d}$. As $(\mathbf{e}_q, \mathbf{z}) \to (\mathbf{0}, \mathbf{0})$ it follows using Lemma 3.5 and (3.35) that $\boldsymbol{\omega}^b_{r,w} \to \boldsymbol{\omega}^b_{d,w} \to \mathbf{0}$ and thereby completing the control objective.*

Remark 3.8 *The projection operator is used in (3.34) to ensure that the estimated control effectiveness matrix never becomes singular by constraining the estimated coefficients to a convex set which is possible using Assumption 3.3 (cf. Krstić* et al. *(1995)).*

Remark 3.9 *The good property of the damping matrix $\mathbf{D}(\mathbf{x})$ is not exploited in this control law, since its coefficients are allowed to change sign, which can have a destabilizing effect.*

Remark 3.10 *When Assumption 3.4 does not hold, it follows from the stability proof that $\tilde{\boldsymbol{\theta}}_2$ and $\tilde{\boldsymbol{\theta}}_3$ are uniformly bounded, and by applying Barbalat's Lemma (cf. Slotine and Li (1991)) it can be shown that $(\mathbf{e}_{q\pm}, \mathbf{z}) \to (\mathbf{0}, \mathbf{0})$ as $t \to \infty$.*

The vital parameter during this derivation is the vector $\boldsymbol{\xi}_1$ which must be bounded and go to zero in finite time. In the proceeding lemmas, the boundedness of the control law will be studied. With the control law bounded, and the

fact that the actuators will desaturate in finite time, it can be shown that $\boldsymbol{\xi}_1$ is a bounded vector that will go to zero in finite time.

Lemma 3.6 *The control law (3.30) is bounded.*

Proof. The proof is given in Appendix E.10. ■

Lemma 3.7 *The function (3.31) is bounded.*

Proof. The proof is given in Appendix E.11. ■

To summarize, the control law (3.30) makes the dual equilibrium point $(\mathbf{e}_{q\pm}, \mathbf{z}, \tilde{\boldsymbol{\theta}}_2, \tilde{\boldsymbol{\theta}}_3) = (\mathbf{0}, \mathbf{0}, \mathbf{0}, \mathbf{0})$ uniformly asymptotically stable even in the presence of actuator constraints and unknown aerodynamics. The function $\boldsymbol{\xi}_1$ is a bounded function and will go to zero in finite time. Since it is only natural to track feasible trajectories, it is reasonable to assume that the UAV will eventually make the tracking error small enough such that the deflection angles will desaturate, making $\boldsymbol{\xi}_1 \to \mathbf{0}$. The reference trajectory tracks the desired trajectory asymptotically, and as the actuators have desaturated, the reference will track the desired trajectory exponentially. When all errors have gone to zero, the control objective of making $\mathbf{q}_{n,w} \to \mathbf{q}_{n,d}$ and $\boldsymbol{\omega}^b_{d,w} \to \mathbf{0}$ is completed.

3.3 Translational Controllers

The objective of the translational control laws is to make the UAV track a desired speed profile. In this section three different speed controllers are derived. First a proportional controller, then a proportional-integral controller based on backstepping and finally an adaptive speed controller that accounts for the unknown aerodynamics and actuator saturation.

3.3.1 Proportional Airspeed Controller

By differentiating $V_a = ||\mathbf{v}^b_r||$, the acceleration is found as shown in (2.22). This expression enables a relatively simple proportional speed controller to be derived as shown in the following theorem:

Theorem 3.5 *Let Assumptions 2.2, 3.1 and 3.2 hold. Given a desired trajectory defined by $V_d, \dot{V}_d \in \mathcal{L}_\infty$, then the origin $\tilde{V} = 0$ of the dynamics (2.22) in closed loop with the controller*

$$T = \frac{mV_a}{u}\left(\dot{V}_d - \kappa_p(V_a - V_d) - \frac{(\mathbf{v}^b_r)^\top}{V_a}\left(\frac{1}{m}\mathbf{R}^b_w \mathbf{f}^w_{aero} + \mathbf{R}^b_n \mathbf{f}^n_g\right)\right), \tag{3.37}$$

where $\kappa_p > 0$, is uniformly exponentially stable.

Proof. The proof is given in Appendix E.12. ■

3.3.2 Proportional-Integral Airspeed Controller

The proportional speed controller can be augmented with integral control using backstepping as shown in the following theorem:

Theorem 3.6 *Let Assumptions 2.2, 3.1 and 3.2 hold. Given a desired trajectory defined by $V_d, \dot{V}_d \in \mathcal{L}_\infty$ with the tracking errors $x_1 = \int_0^t \tilde{V}(\tau))d\tau$, $x_2 = \tilde{V}(t)$ and $z = x_2 + \kappa_1 x_1$ with $\kappa_1 > 0$ and the dynamics (2.22) in closed loop with the speed controller*

$$\begin{aligned} T =& \frac{mV_a}{u}\left(\dot{V}_d - \kappa_p(V_a - V_d) - \kappa_i \int_0^t (V_a - V_d(\tau))d\tau \right. \\ & \left. - \frac{(\mathbf{v}_r^b)^\top}{V_a}\left(\frac{1}{m}\mathbf{R}_w^b \mathbf{f}_{aero}^w + \mathbf{R}_n^b \mathbf{f}_g^n\right)\right) \end{aligned} \tag{3.38}$$

where $\kappa_p > 0$ and $\kappa_i > 0$, then the origin $(x_1, z) = (0, 0)$ is uniformly exponentially stable.

Proof. The proof is given in Appendix E.13. ■

Remark 3.11 *As $x_1, z \to 0$ it follows that $x_2 \to 0$ and thereby completing the control objective of making $\tilde{V} \to 0$.*

Remark 3.12 *Using integral action with constrained actuation can make the system unstable (cf. Åström and Rundqwist (1989)), but can however easily be handled by using conditional integration (cf. Visioli (2003)); i.e. the integrator is switched off whenever the thrust is in saturation.*

Remark 3.13 *The main reason for introducing integral control is to make the closed loop system robust with regards to uncertainties. It should be noted that the rotational control laws also can be augmented with integral control following the same lines as in Kristiansen* et al. *(2008b).*

3.3.3 Adaptive Proportional Airspeed Controller with Constrained Thrust

Using the same procedure as for the adaptive backstepping controller in Section 3.2.4, it is possible to design an adaptive speed controller that accounts for the thrust constraint and unknown aerodynamics. The speed dynamics (2.56) are therefore used in this section. Let a reference airspeed be denoted V_r which shall be used to move the saturation problem from the plant to the reference where $\dot{V}_r$ is to be designed. Let the desired speed profile be defined through $V_d, \dot{V}_d$ and the tracking error as $\tilde{V}_r := V_r - V_d$, then the reference acceleration can be designed as shown in the following lemma:

Lemma 3.8 *Let a continuous bounded function be defined as $\xi_2 = f_2(\tilde{T})$ with $f_2(0) = 0$. Given a desired speed profile defined by $V_d, \dot{V}_d \in \mathcal{L}_\infty$, then the origin $\tilde{V}_r = 0$ using the reference acceleration*

$$\dot{V}_r = \dot{V}_d - \kappa_r(V_d - V_r) + \xi_2 \tag{3.39}$$

where $\kappa_r > 0$, is uniformly globally asymptotically stable when $\xi_2 = 0$.

Proof. The proof is given in Appendix E.14. ■

Instead of tracking the desired speed, the speed controller can track the reference speed which is found through integration of (3.39). This enables the reference to take the actuator saturation into account, and move it out of the closed loop system. The speed error can be redefined as $\tilde{V} := V_a - V_r$ which can be forced to zero by using the adaptive speed controller presented in the following theorem:

Theorem 3.7 *Let Assumptions 2.2, 3.2 and 3.4 hold. Given a desired speed profile defined by $V_d, \dot{V}_d \in \mathcal{L}_\infty$, then the origin $(\tilde{V}, \tilde{\boldsymbol{\theta}}_1) = (0, \mathbf{0})$ of the dynamics (2.56) in closed loop with the controller and update law*

$$T = \frac{mV_a}{u}(\dot{V}_d - \kappa_r \tilde{V}_r - \kappa_p \tilde{V} - \frac{(\mathbf{v}_r^b)^\top}{V_a}(\frac{1}{m}\mathbf{R}_w^b \boldsymbol{\Phi}_1 \hat{\boldsymbol{\theta}}_1 + \mathbf{R}_n^b \mathbf{f}_g^n)) \tag{3.40}$$

$$\dot{\hat{\boldsymbol{\theta}}}_1 = \frac{\tilde{V}}{mV_a}\boldsymbol{\Gamma}_1 \boldsymbol{\Phi}_1^\top \mathbf{R}_b^w \mathbf{v}_r^b \tag{3.41}$$

$$\xi_2 = \frac{u}{mV_a}\tilde{T} \tag{3.42}$$

$$\tilde{T} = \sigma(T) - T \tag{3.43}$$

where $\kappa_r > 0$, $\kappa_p > 0$ and $\boldsymbol{\Gamma}_1 = \boldsymbol{\Gamma}_1^\top > \mathbf{0}$, is uniformly asymptotically stable even in the presence of unknown aerodynamics and constrained actuation.

Proof. The proof is given in Appendix E.15. ■

Remark 3.14 *When Assumption 3.4 does not hold, it follows from the stability proof that $\tilde{\boldsymbol{\theta}}_1$ is uniformly bounded, and by applying Barbalat's Lemma (cf. Slotine and Li (1991)) it can be shown that $\tilde{V} \to 0$ as $t \to \infty$.*

To show that the reference airspeed will track the desired airspeed, ξ_2 must be shown to be a bounded function that converges to zero. This is shown through the following lemmas:

Lemma 3.9 *The control law (3.40) is bounded.*

Proof. The proof is given in Appendix E.16. ■

Lemma 3.10 *The function (3.42) is bounded.*

Proof. The proof is given in Appendix E.17. ■

To summarize, the reference speed deviates from the desired speed whenever the thrust is in saturation. Since the desired speed profile is designed such that it is possible for the UAV to track it with its inherent actuator limitations, it follows that the thrust will desaturate in finite time. As the thrust desaturates, the function ξ_2 goes to zero, making the reference converge to the desired trajectory. The control law (3.40) makes the airspeed track the reference airspeed which eventually will converge to the desired airspeed. Hence, it follows that the tracking error $(V_a - V_r) \to (V_a - V_d) \to 0$ which thereby completes the control objective.

3.4 Simulations

To validate the different control solutions that have been presented in this chapter, several simulations have been conducted. The UAV model that is employed is the YF-22 UAV from Campa *et al.* (2007) where the stabilizer is treated as an elevator and its aerodynamic model is reproduced in Appendix A. The UAV has the thrust constrained as $0 \leq T \leq 250$ N and the deflection angles are bounded as $-0.3491 \leq \delta_a, \delta_e, \delta_r \leq 0.3491$ radians.

3.4.1 Attitude Maneuver

Let the initial states be given as $\mathbf{q}_{n,b}(0) = \begin{bmatrix} 0 & 0 & 0 & 1 \end{bmatrix}^\top$, $\boldsymbol{\omega}^b_{n,b}(0) = \begin{bmatrix} 0.1 & -0.2 & 0 \end{bmatrix}^\top$ rad/s, $\mathbf{p}^n(0) = \begin{bmatrix} 0 & 0 & -100 \end{bmatrix}^\top$ m, $\mathbf{v}^b(0) = \begin{bmatrix} 25 & 0 & 0 \end{bmatrix}^\top$ m/s, $\mathbf{w}^n = \begin{bmatrix} 10 & 0 & 0 \end{bmatrix}^\top$ m/s. With the initial attitude the UAV is pointing along the negative $\mathbf{x}^n$ axis, such that by defining $\mathbf{q}_{n,d} = \begin{bmatrix} 1 & 0 & 0 & 0 \end{bmatrix}^\top$, the objective is to perform a rotation of π radians such that the wind frame becomes aligned with the NED frame resulting in leveled flight. The desired angular velocity and acceleration are set equal to zero and the desired airspeed is set to $V_d = 40$ m/s. All gains are chosen through empirical testing to obtain the desired performance.

Sliding Surface Control

Consider the case of using the sliding surface controller (3.15) in conjunction with the proportional speed controller (3.37) where the gains are chosen as $k_q = 2$, $k_s = 2$, $\mathbf{\Lambda} = \mathbf{I}$ and $\kappa_p = 2$.

Figure 3.1 shows the attitude error, angular velocity error and the deflection angles. The attitude error goes quickly to zero, and the same applies for the angular velocity error. Note that the deflection angle of the rudder goes into saturation as the UAV performs a rotation of π radians. Also note that due to the control effectiveness matrix, there is a strong coupling between the aileron and rudder, such that both actuators can be used to produce yaw moments. This makes the rudder and aileron work together in producing the required moments. As the attitude and angular velocity tracking errors have converged to zero, the deflection angles go to small values close to zero to compensate for the aerodynamic vector $\mathbf{f}(\mathbf{x})$. The airspeed tracking error and thrust are shown in Figure 3.2. The airspeed error converges exponentially to zero, and the thrust converges to a constant value maintaining the desired airspeed. The position of the UAV is shown in Figure 3.3. Remember that the objective is simply to align the wind frame with the NED frame such that the UAV moves along the $\mathbf{x}^n$ axis which is apparent from Figure 3.3. Also note that the z component converges to a constant, such that the UAV obtains leveled flight.

To better visualize the results, let the orientation of the body relative to the NED frame be defined through the roll (ϕ), pitch (θ) and yaw (ψ) angles. This is visualized in Figure 3.4 where the initial yaw angle is π radians which converges close to zero. In fact it is only the roll angle that goes to zero. When the roll angle is zero, there exists a simple relation between the yaw angle and the course angle as $\chi = \psi + \beta$, and between the pitch angle and the flight path angle as $\gamma = \theta - \alpha$.

Figure 3.4 shows that the pitch and yaw angles do not converge to zero, but to the angle of attack and the negative sideslip angle. This is highlighted in the bottom plot, where it is seen that the roll, flight path and course angles all converge to zero. The plot in the middle shows the angle of attack and sideslip angle during the maneuver, where it is seen that the sideslip angle is as large as about 0.42 radians while the UAV performs its attitude maneuver. Also note that the angle of attack does not go to zero, but converges to about 0.0617 radians which produces enough lift to compensate for the gravity. Conversely, with the angle of attack and sideslip angle bounded and converging to small values, it follows through (2.14) and (2.15) that the linear velocity components v, w remain bounded throughout the maneuver.

Backstepping Control

Consider the case of using the backstepping controller (3.12) in conjunction with the proportional speed controller (3.37) with the gains $k_q = 2$, $k_\omega = 2$ and $\kappa_p = 2$. The attitude and angular velocity tracking errors are shown in Figure 3.5 where all the errors converge quickly to zero. There are some oscillations on the angular velocity error which is due to the actuator saturation. If the actuators had infinite torque available, the angular velocity error would have converged exponentially to zero without oscillations. The same argument also applies for the other controllers. The airspeed has a similar response as for the simulation of the sliding surface controller and is therefore omitted for both the backstepping and the PD+ simulation.

PD+ Control

Consider the PD+ controller (3.14) in conjunction with the proportional speed controller (3.37) with the gains $k_q = 25$, $k_\omega = 25$ and $\kappa_p = 2$. The attitude and angular velocity tracking errors are shown in Figure 3.6 where all the errors go to zero. The PD+ controller is in saturation only 10 s, and as such it results in less oscillatory motion than that of the backstepping controller. On the other hand, it has a slower convergence rate than the backstepping controller, something that can be remedied by tuning the gains.

3.4.2 Adaptive Control with Actuator Constraints

Consider the case of using the adaptive backstepping controller (3.30) in conjunction with the adaptive speed controller (3.40) with the gains gains as $k_1 = k_2 = k_3 = k_4 = 2$, $\kappa_r = 2$, $\kappa_p = 4$. The aerodynamic coefficients have an initial 50% mismatch relative their true values and the adaptive gain matrices are chosen as $\mathbf{\Gamma}_1 = \mathbf{\Gamma}_2 = \mathbf{\Gamma}_3 = 0.001\mathbf{I}$. Let the fixed-wing UAV have the initial conditions: $\mathbf{q}_{n,b}(0) = \begin{bmatrix}0.5 & 0.5 & 0.5 & 0.5\end{bmatrix}^\top$, $\boldsymbol{\omega}^b_{n,b}(0) = \begin{bmatrix}0 & 0 & 0\end{bmatrix}^\top$ rad/s, $\mathbf{v}^b(0) = \begin{bmatrix}30 & 0 & 0\end{bmatrix}^\top$ m/s, $\mathbf{w}^n = \begin{bmatrix}10 & 0 & 0\end{bmatrix}^\top$ m/s, $\mathbf{p}^n(0) = \begin{bmatrix}0 & 0 & -100\end{bmatrix}^\top$ m, with the desired airspeed $V_d = 50$ m/s, desired attitude $\mathbf{q}_{n,d}(0) = \begin{bmatrix}1 & 0 & 0 & 0\end{bmatrix}^\top$ and desired angular velocity $\boldsymbol{\omega}^d_{n,d} = \begin{bmatrix}0 & 0 & 0.05\end{bmatrix}^\top$ rad/s. The desired angular acceleration and desired linear acceleration are set equal to zero. Hence, the UAV will track a circular trajectory and move with a constant airspeed.

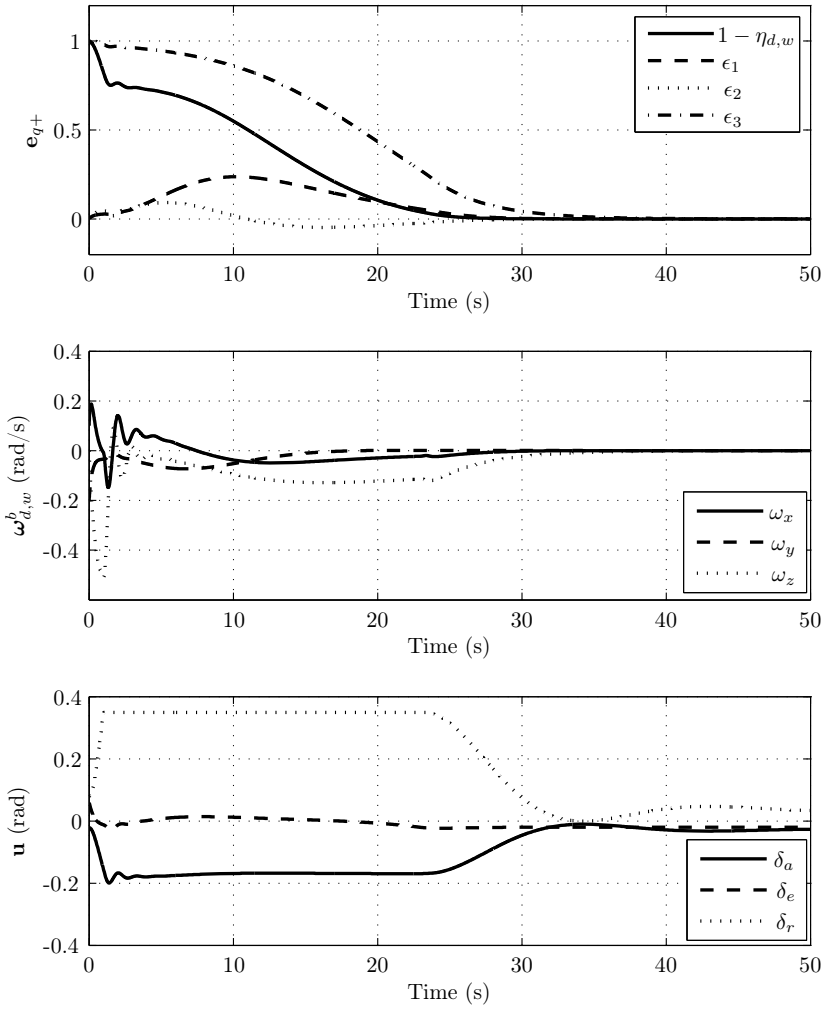

Figure 3.1: Attitude error, angular velocity error and deflection angles using the sliding surface controller.

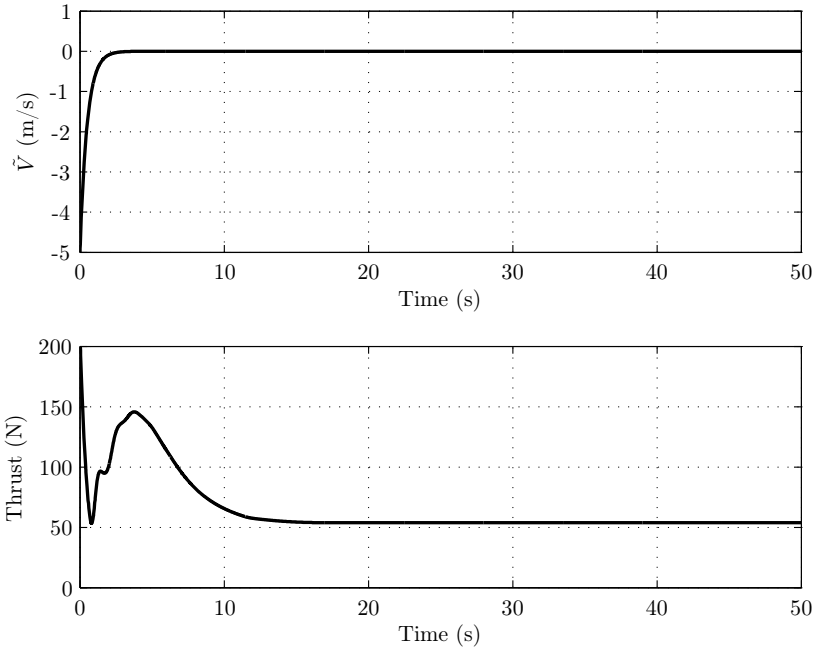

Figure 3.2: Airspeed tracking error and thrust using the proportional speed controller.

Figure 3.7 shows the attitude errors, angular velocity errors and deflection angles. The top plot shows the attitude error between the reference and the desired trajectory and the second plot shows the angular velocity error between the reference and the desired trajectory. The third plot shows the attitude error between the wind frame and the reference trajectory frame while the fourth plot shows the angular velocity error between the wind and the reference trajectory frame. All errors converge to zero. Even though the actuators move into saturation as shown in the bottom plot, the system is able to adapt to the unknown aerodynamics and make the tracking errors converge to zero.

Figure 3.8 shows the difference between the adaptive and a non-adaptive controller in the presence of unknown aerodynamics. It becomes quite evident that the non-adaptive case contains more oscillatory motion and therefore has a higher energy requirement than that of the adaptive control law. Consequently, the fuel expenditure would be increased using a non-adaptive speed controller. The speed tracking errors go to zero using both controllers, and the thrust go into saturation during the initial maneuver before converging to about 64 N to maintain the desired airspeed.

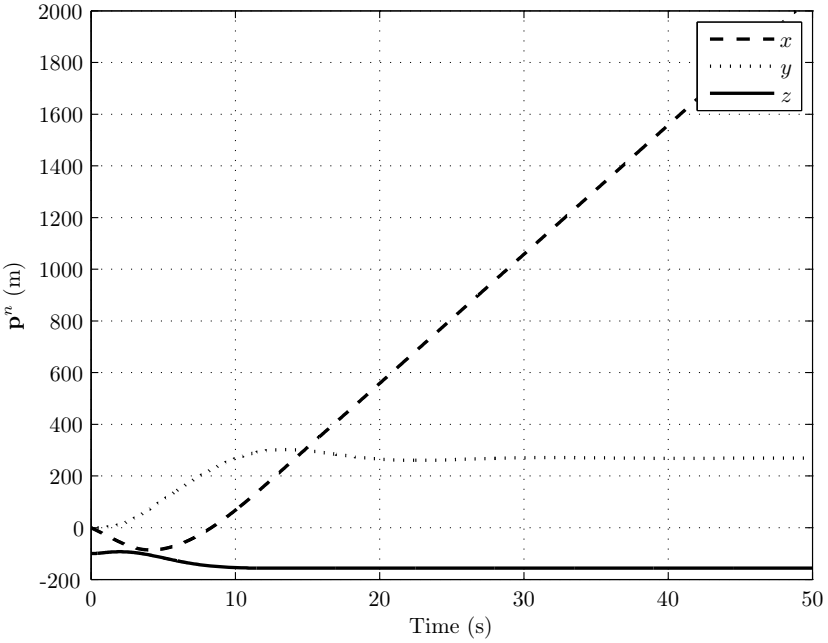

Figure 3.3: Position of the UAV. Since no guidance is applied, the UAV will only point its wind frame in the $\mathbf{x}^n$ direction, which is evident from the simulation as the position in the $\mathbf{x}^n$ direction increases, while the other two go to constant values indicating leveled flight.

3.4.3 Comparison of Rotational Controllers

To enable a comparison between the rotational controllers, consider the problem of tracking a reference $\dot{\mathbf{q}}_{n,d} = \frac{1}{2}\mathbf{q}_{n,d} \otimes \begin{bmatrix} 0 \\ \boldsymbol{\omega}^d_{n,d} \end{bmatrix}$ where $\mathbf{q}_{n,d}(0) = \begin{bmatrix} 0 & 0 & 0 & 1 \end{bmatrix}^\top$, $\boldsymbol{\omega}^d_{n,d} = \begin{bmatrix} 0 & 0 & 0.5 \end{bmatrix}^\top$ and $\dot{\boldsymbol{\omega}}^d_{n,d} = \mathbf{0}$ using the proportional speed controller (3.37) with $\kappa_p = 2$ and a desired airspeed of $V_d = 50$ m/s. The UAV has the following initial conditions: $\mathbf{v}^b(0) = \begin{bmatrix} 25 & 0 & 0 \end{bmatrix}^\top$ m/s, $\mathbf{w}^n = \begin{bmatrix} 10 & 0 & 0 \end{bmatrix}^\top$ m/s, $\mathbf{q}_{n,b}(0) = \begin{bmatrix} 1 & 0 & 0 & 0 \end{bmatrix}^\top$ and $\boldsymbol{\omega}^b_{n,b}(0) = \begin{bmatrix} 0 & 0 & 1 \end{bmatrix}^\top$ rad/s.

The response from the Lyapunov function $V = \frac{1}{2}\mathbf{e}_q^\top \mathbf{e}_q + \frac{1}{2}(\boldsymbol{\omega}^b_{d,w})^\top \boldsymbol{\omega}^b_{d,w}$ will be used to compared the different controllers. Even though some of the controllers have been derived with a different Lyapunov function, the control objective is to make $(\mathbf{e}_q, \boldsymbol{\omega}^b_{d,w}) \to (\mathbf{0}, \mathbf{0})$, and as such, this provides a good measure for comparison.

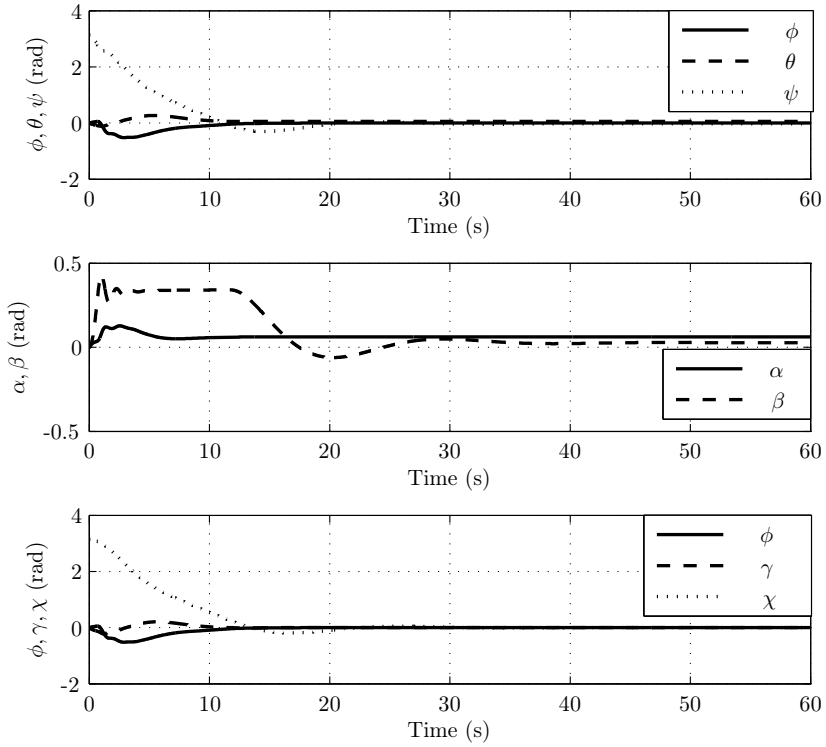

Figure 3.4: Angular representation. The top plot shows the roll, pitch and yaw angles of the UAV. The middle plot shows the angle of attack and the sideslip angle, while the bottom plot shows the roll, flight path and course angles.

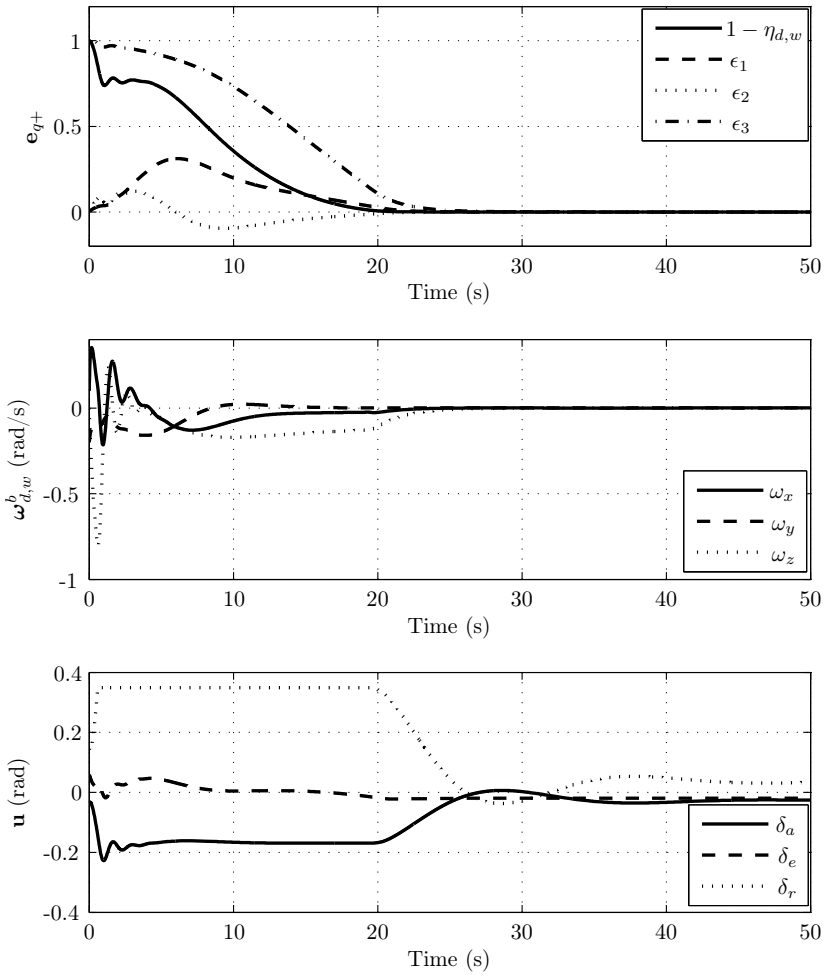

Figure 3.5: Attitude error, angular velocity error and deflection angles using the backstepping controller.

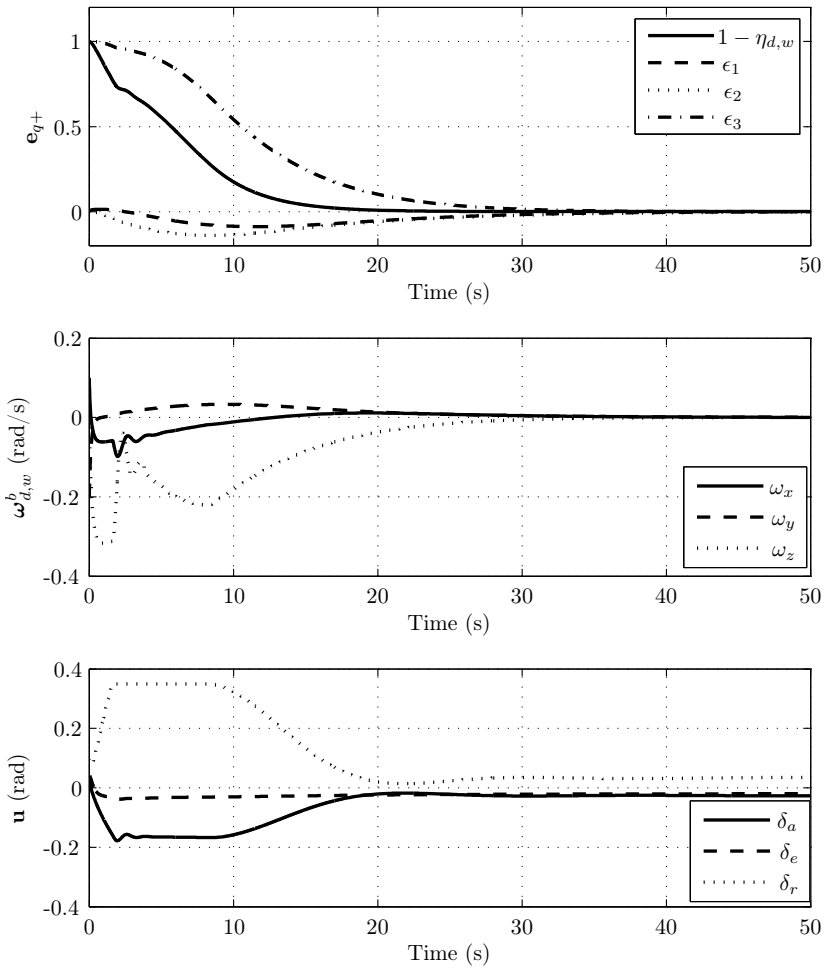

Figure 3.6: Attitude error, angular velocity error and deflection angles using the PD+ controller.

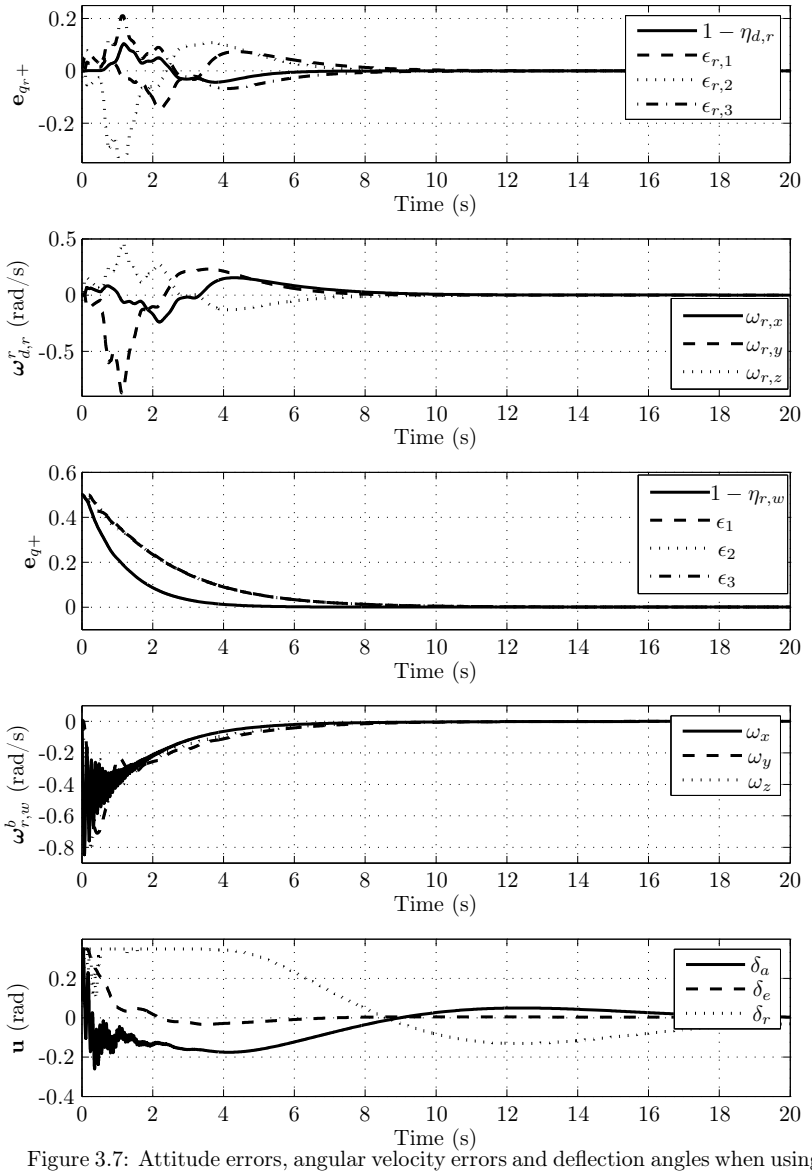

Figure 3.7: Attitude errors, angular velocity errors and deflection angles when using the adaptive attitude controller.

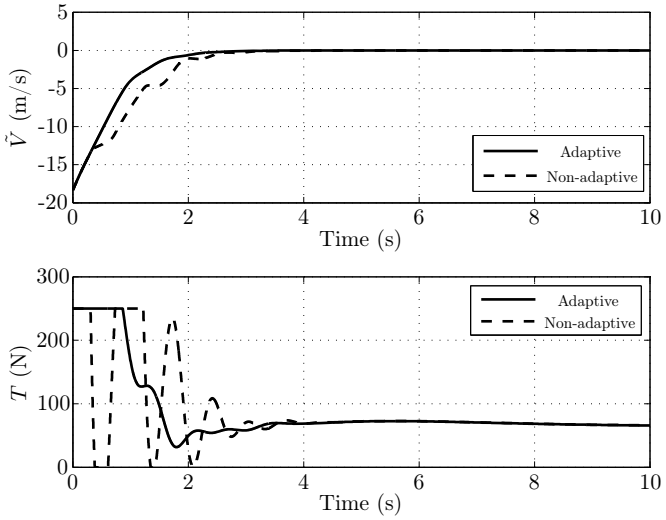

Figure 3.8: Adaptive vs. non-adaptive speed control.

Backstepping vs. Sliding Surface

Consider the backstepping controller (3.12) with the gains $k_q = 2$ and $k_\omega = 2$ and the sliding surface controller (3.15) with the gains $k_q = 2$, $k_s = 2$ and $\lambda = 2$. The top plot in Figure 3.9 shows that both controllers behave identically with the selected gains, and the Lyapunov function goes to zero. The fact that they behave identically is also supported by Remark 3.3. Since the two controllers behave identically with these gains, the rest of the comparisons will go in two directions. One part will compare the backstepping controller with the adaptive backstepping controller using a reference signal, while the other part will compare the PD+ controller with the sliding surface controller.

Backstepping vs. Adaptive Backstepping using a Reference Signal

Consider the the backstepping controller (3.12) with the gains $k_q = 2$ and $k_\omega = 2$, and the adaptive backstepping controller (3.30) using the reference signal (3.19) and (3.24) with the gains $k_1 = k_2 = k_3 = k_4 = 2$. To enable a fair comparison, the coefficients are assumed to be perfectly known such that the adaptive part of the control law is not considered. This reduces the comparison to that of a backstepping controller with and without a reference signal that makes the reference deviate from the desired trajectory whenever the actuators are in saturation. As shown in the middle plot in Figure 3.9, using the reference signal results in improved performance compared to that of the standard backstepping controller. To better understand this, the actuator signals are shown for both controllers in Figure 3.10, where it is

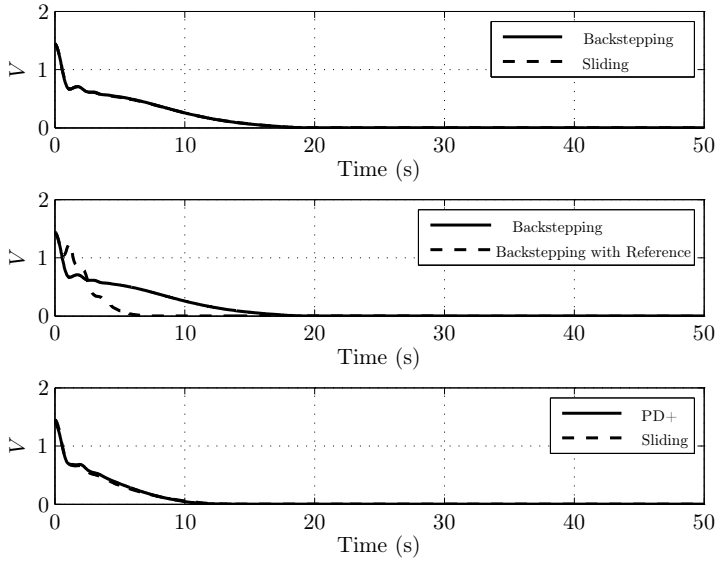

Figure 3.9: Comparison between rotational controllers using the Lyapunov function $V = \frac{1}{2}\mathbf{e}_q^\top \mathbf{e}_q + \frac{1}{2}(\boldsymbol{\omega}_{d,w}^b)^\top \boldsymbol{\omega}_{d,w}^b$ as a measure of performance. The top plot shows the backstepping controller and the sliding surface controller with similar gains. Both controllers obtain identical convergence to zero. The middle plot shows the backstepping controller with and without a reference signal. By using the reference, increased performance can be obtained. The bottom plot compares the sliding surface controller to the PD+ controller, where the controllers obtain similar results with the selected gains.

seen that the controller using the reference, employs more control action from the elevator than the standard backstepping controller. The nonlinear function (3.31) can in the case of rudder saturation be written as

$$\boldsymbol{\xi}_1 = \frac{1}{2}\rho S V_a^2 \mathbf{R}_b^r \mathbf{J}^{-1} \begin{bmatrix} b\hat{C}_{l_{\delta_a}} & 0 & b\hat{C}_{l_{\delta_r}} \\ 0 & \bar{c}\hat{C}_{m_{\delta_e}} & 0 \\ b\hat{C}_{n_{\delta_a}} & 0 & b\hat{C}_{n_{\delta_r}} \end{bmatrix} \begin{bmatrix} 0 \\ 0 \\ \sigma(\delta_r) - \delta_r \end{bmatrix}. \tag{3.44}$$

From (3.44) it is evident that the control deficiency of the rudder becomes mapped to the other axes through $\hat{\mathbf{G}}(\mathbf{x})$ and $\mathbf{R}_b^r$. This fact enables more control action to be applied from the other actuators, and thus the errors convergence faster to zero using the reference signal.

PD+ vs. Sliding Surface

Consider the gains for the PD+ controller as $k_q = 50$ and $k_\omega = 25$ and for the sliding surface controller $k_q = 50$, $k_s = 25$ and $\lambda = 1$. The bottom plot in Figure 3.9

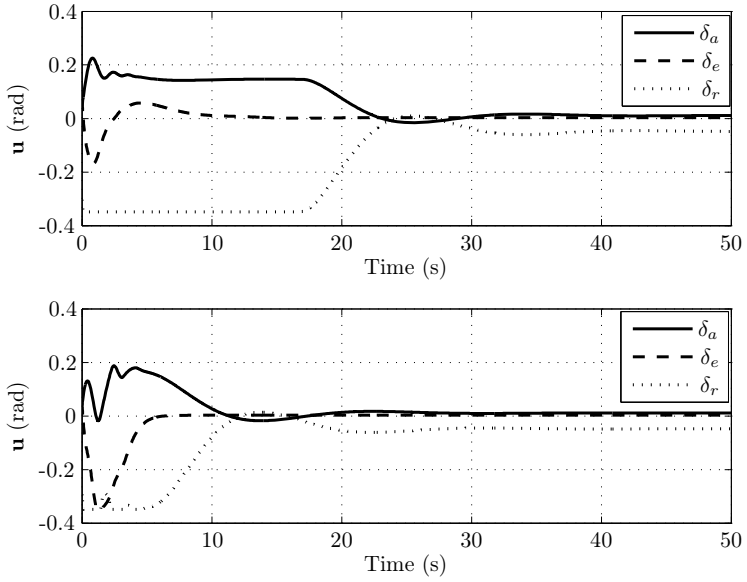

Figure 3.10: Actuator signals when using the backstepping controller with and without a reference. In the top plot, no reference signal is used, and the rudder remains in saturation for about 18 seconds. In the bottom plot, a reference signal is used which moves parts of the control deficiency to the other actuators. Using the reference signal, the rudder remains in saturation for only about 6 seconds.

shows the Lyapunov function for both controllers. With the selected gains, the two controllers produce approximately similar responses, something that is due to the saturation of the deflection angles. To visualize the difference between the two controllers, the saturation is removed, and the λ gain is changed. In the top plot of Figure 3.11 it is evident that when there is sufficient actuation available, a better performance of the sliding surface controller can be obtained compared to that of the PD+ controller. But, with actuator saturation as shown in the bottom plot of Figure 3.11, the two controllers result in similar performance.

Conclusion

The main findings from this comparison is that in general, even though the control laws have been derived using different techniques, the saturation nonlinearity makes the trajectories almost identical. Some improved performance of one controller relative to another can be obtained by fine-tuning the gains, but in general there is little to gain. Noise has also been added to the signals without any comparable differences between the trajectories. The use of a reference trajectory that deviates from the desired trajectory whenever the actuators are in saturation, results in

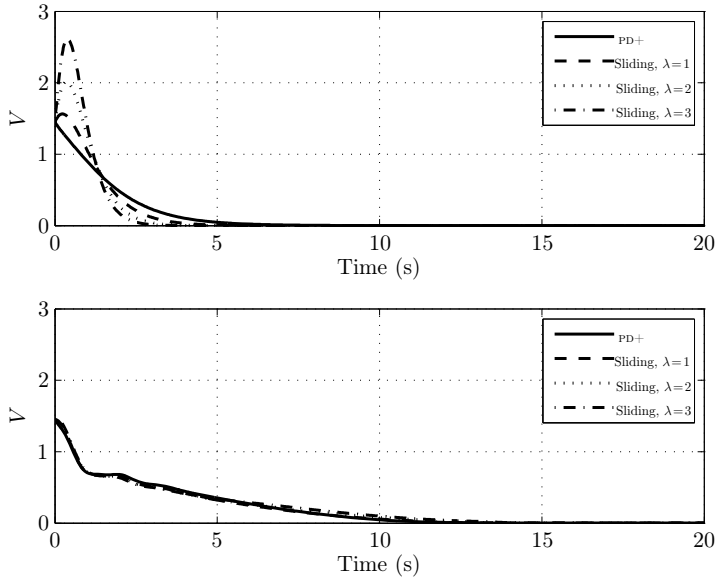

Figure 3.11: Comparison between the sliding surface controller and the PD+ controller. In the top plot, the actuator saturation is removed, which shows that by changing the gain λ, faster convergence of the errors to zero can be obtained. In the bottom plot, actuator saturation is included, where it is evident that even by changing the gain λ the two controllers obtain similar results.

improved performance compared to using standard methods.

3.4.4 Comparison of Speed Controllers

Consider a case of comparing the proportional speed controller (3.37) with the proportional-integrator controller (3.38). Let the fixed-wing UAV have the initial conditions: $\mathbf{q}_{n,b}(0) = \begin{bmatrix}1 & 0 & 0 & 0\end{bmatrix}^\top$, $\boldsymbol{\omega}^b_{n,b}(0) = \begin{bmatrix}0 & 0 & 0\end{bmatrix}^\top$ rad/s, $\mathbf{v}^b(0) = \begin{bmatrix}25 & 0 & 0\end{bmatrix}^\top$ m/s, $\mathbf{w}^n = \begin{bmatrix}10 & 0 & 0\end{bmatrix}^\top$ m/s, $\mathbf{p}^n(0) = \begin{bmatrix}0 & 0 & -100\end{bmatrix}^\top$ m, with the desired airspeed $V_d = 40$ m/s, desired attitude $\mathbf{q}_{n,d}(0) = \begin{bmatrix}1 & 0 & 0 & 0\end{bmatrix}^\top$ and desired angular velocity $\boldsymbol{\omega}^d_{n,d} = \begin{bmatrix}0 & 0 & 0.01\end{bmatrix}^\top$ rad/s. The desired angular acceleration and desired linear acceleration are set equal to zero. The sliding surface controller is used for rotational control with the gains $k_q = 2$, $k_s = 2$, $\mathbf{\Lambda} = \mathbf{I}$, while the speed controllers have the gains $\kappa_1 = 2$, $\kappa_2 = 2$, such that $\kappa_p = 4$ and $\kappa_i = 5$ (*cf.* Appendix E.13). Hence, the UAV will track a circular trajectory and move with a constant airspeed.

A simulation has been performed where the aerodynamics are perfectly mod-

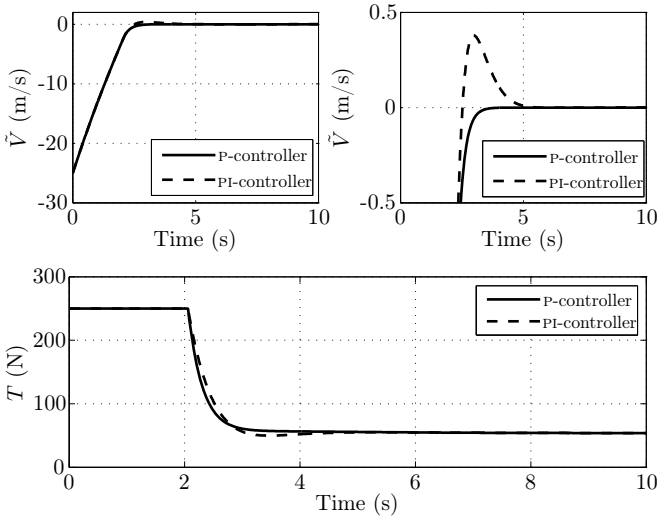

Figure 3.12: P vs. PI controller with perfect modeling.

eled and is shown in Figure 3.12. Both controllers quickly make the speed tracking error converge to zero, but the speed controller with the integral term has a slight overshoot of about 0.4 m/s during the initial convergence, which is typical for PI controllers. The thrust for both controllers are almost the same and converge to a constant value as the tracking error has converged to zero. The main reason for introducing an integral term to the airspeed controller, is to increase its robustness to uncertainties and poor modeling. Figure 3.13 shows the results of a simulation that was performed where the drag is chosen as 50% of its true value. This introduces an off-set that is apparent in Figure 3.13 where the proportional controller does not make the tracking error converge to zero, but to -0.3237 m/s. The PI controller makes the tracking error converge to zero, even though there is an error in the drag term. From both simulations it is apparent that the thrust reaches its bound of 250 N, while the airspeed converges to zero. As pointed out in Remark 3.12, conditional integration must be used to avoid large overshoots due to the saturation of the thrust. This has been implemented for the PI controller, but to show the impact of integration when the actuators saturate, an additional simulation has been performed with results as shown in Figure 3.14. Without conditional integration, the PI controller makes the speed error diverge by about 15 m/s before converging again, while the PI controller with condition integration only has a small overshoot of about 0.5 m/s.

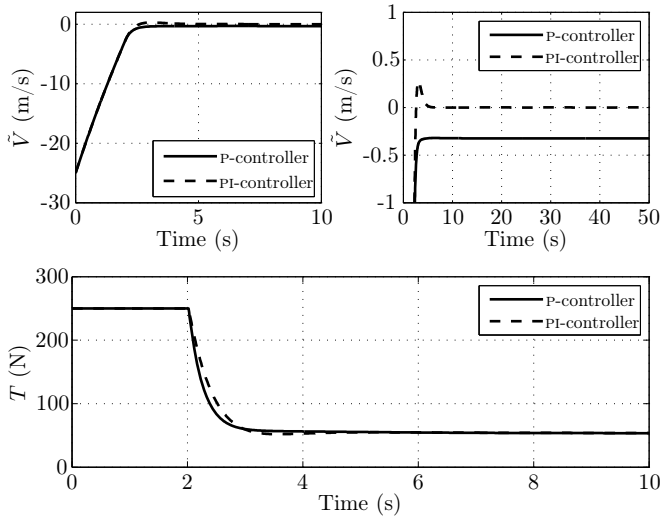

Figure 3.13: P vs. PI controller with uncertainty.

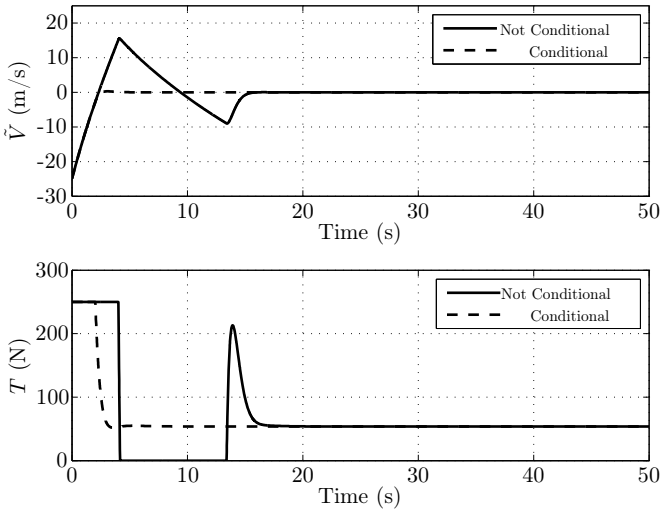

Figure 3.14: With and without conditional integration.

3.5 Actuator Desaturation using Speed Modification

In this section, it is established that the airspeed of an aircraft directly affects the deflection angles which are used for rotational control. Hence, by increasing the airspeed, smaller deflection angles are required to produce a given aerodynamic moment. A reference airspeed is therefore designed, which makes the aircraft increase its speed whenever the deflection angles are getting close to saturation, which directly can be used to avoid saturation of the actuators. Rate saturation is not considered.

Stall speed, V_s, is the minimum speed required for steady leveled flight. If the airspeed drops below the stall speed, it results in a loss of control of the aircraft. As the aircraft performs a banking maneuver, the stall speed increases, meaning that a higher airspeed is required to maintain leveled flight. When the aircraft performs a banking maneuver, the airspeed must be larger than $\frac{1}{\sqrt{\cos(\mu)}}V_s$ where μ is the bank angle to maintain leveled flight (*cf.* Phillips (2010)). For example if the aircraft performs a banking maneuver with a bank angle of 60°, the stall speed is increased by 41.4% and is illustrated in Figure 3.15. Hence, it is of utmost importance to keep this in mind when designing control laws for aircraft. From a control perspective, the rotational control laws are designed to point the wind frame in a desired direction, while the speed controller is designed to track a desired speed profile. For waypoint tracking, the airspeed is typically set to a constant value above the stall speed. Instead of choosing the airspeed as a constant value, it can be used as an additional degree of freedom, whose purpose is to avoid saturation of the deflection angles. It is quite intuitive, that at larger airspeeds, a smaller deflection is required to produce aerodynamic moments, than at low airspeeds. Hence, whenever the deflection angles reach a threshold, a reference airspeed can be increased to ensure that the deflection angles remain within their bounds.

3.5.1 Speed Modification

Consider the sliding surface attitude controller (3.15) which can be written as

$$\begin{aligned}\mathbf{u} =&\mathbf{G}^{-1}(\mathbf{x})(\mathbf{J}\dot{\boldsymbol{\omega}}^b_{n,r} + \mathbf{D}(\mathbf{x})\boldsymbol{\omega}^b_{n,r} + \mathbf{S}(\boldsymbol{\omega}^b_{n,b})\mathbf{J}\boldsymbol{\omega}^b_{n,b} - \mathbf{f}(\mathbf{x}) - k_s\mathbf{s} \\ &- k_q\mathbf{R}^b_w\mathbf{T}_e^\top\mathbf{e}_q)\end{aligned} \tag{3.45}$$

where

$$\mathbf{G}^{-1}(\mathbf{x}) = \frac{2}{\rho S V_a^2}\begin{bmatrix} bC_{l_{\delta_a}} & 0 & bC_{l_{\delta_r}} \\ 0 & \bar{c}C_{m_{\delta_e}} & 0 \\ bC_{n_{\delta_a}} & 0 & bC_{n_{\delta_r}} \end{bmatrix}^{-1}. \tag{3.46}$$

Note that the inverse control effectiveness matrix contains the square of the airspeed in the denominator. By increasing the airspeed, the magnitude of the control signal is reduced[3] which can be used to regain control of an aircraft after the deflection angles have gone into saturation. Let $V_a \to \infty$, then any of the control signals

[3]The right hand side of (3.45)

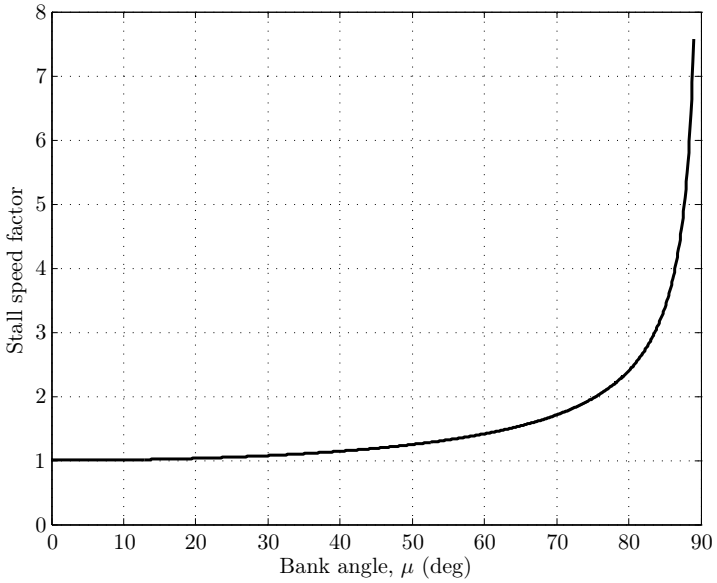

Figure 3.15: Stall speed factor as a function of bank angle.

(3.12), (3.14) or (3.15) can be written as

$$\mathbf{u} = -\mathbf{G}^{-1}(\mathbf{x})\mathbf{f}(\mathbf{x}) \tag{3.47}$$

since the term $\frac{1}{V_a^2}$ will dominate every term except $\mathbf{f}(\mathbf{x})$[4]. Note that

$$\mathbf{D}(\mathbf{x}) = -\frac{1}{2}\rho S V_a^2 \begin{bmatrix} \frac{b^2}{2V_a}C_{l_p} & 0 & \frac{b^2}{2V_a}C_{l_r} \\ 0 & \frac{\bar{c}^2}{2V_a}C_{m_q} & 0 \\ \frac{b^2}{2V_a}C_{n_p} & 0 & \frac{b^2}{2V_a}C_{n_r} \end{bmatrix} \tag{3.48}$$

where V_a^2 is canceled, but due to the airspeed in the denominator inside the matrix, it will make this matrix also go to zero. The aerodynamic vector $\mathbf{f}(\mathbf{x})$ is defined as (*cf.* equation (2.29))

$$\mathbf{f}(\mathbf{x}) = \frac{1}{2}\rho S V_a^2 \begin{bmatrix} b(C_{l_0} + C_{l_\beta}\beta) \\ \bar{c}(C_{m_0} + C_{m_\alpha}\alpha) \\ b(C_{n_0} + C_{n_\beta}\beta) \end{bmatrix} \tag{3.49}$$

which is a function of the angle of attack and the sideslip angle. As $V_a \to \infty$ it follows from (2.15) that $\beta \to 0$. Similarly, by assuming that $u >> w$ it follows that

[4]In the case of the sliding surface controller with sufficiently high airspeed, the terms $\mathbf{G}^{-1}(\mathbf{x})(\mathbf{J}\dot{\boldsymbol{\omega}}^b_{n,r} + \mathbf{D}(\mathbf{x})\boldsymbol{\omega}^b_{n,r} + \mathbf{S}(\boldsymbol{\omega}^b_{n,b})\mathbf{J}\boldsymbol{\omega}^b_{n,b} - k_s\mathbf{s} - k_q\mathbf{R}^b_w\mathbf{T}_e^\top\mathbf{e}_q)$ can be approximated to zero.

$\alpha \to 0$ using (2.14). Hence, by making the airspeed go to infinity, the control signal reduces to

$$\mathbf{u} = -\begin{bmatrix} bC_{l_{\delta_a}} & 0 & bC_{l_{\delta_r}} \\ 0 & \bar{c}C_{m_{\delta_e}} & 0 \\ bC_{n_{\delta_a}} & 0 & bC_{n_{\delta_r}} \end{bmatrix}^{-1} \begin{bmatrix} bC_{l_0} \\ \bar{c}C_{m_0} \\ bC_{n_0} \end{bmatrix} \tag{3.50}$$

which is within the actuator bounds. This means that actuator saturation is not necessarily due to a poorly designed attitude control law, but it can be that the aircraft is moving too slow, a notion that corresponds well with the definition of the stall speed.

This analysis can serve as a basis when designing the reference airspeed that the speed controller should track. Intuitively, the airspeed should be increased whenever the deflection angles are in saturation, or are above a chosen threshold. Let a saturation function be defined as

$$\sigma_{mod}(\mathbf{u}) := \begin{bmatrix} \sigma_{mod}(\delta_a) & \sigma_{mod}(\delta_e) & \sigma_{mod}(\delta_r) \end{bmatrix}^\top \tag{3.51}$$

where

$$\sigma_{mod}(\delta) := \begin{cases} \delta_{mod} & \text{if } \delta \geq \delta_{mod} \\ \delta & \text{if } -\delta_{mod} < \delta < \delta_{mod} \\ -\delta_{mod} & \text{if } \delta \leq -\delta_{mod} \end{cases} \tag{3.52}$$

where δ represents any of the three deflection angles. The modified limit $\delta_{mod} \in \left[0, \delta_{max}\right]$ is used to define the threshold when the speed modification is active where δ_{max} is the physical actuator constraint. Let a dead-zone nonlinearity be defined as

$$\tilde{\mathbf{u}}_{mod} := \begin{bmatrix} u_1 & u_2 & u_3 \end{bmatrix}^\top = \mathbf{u} - \sigma_{mod}(\mathbf{u}), \tag{3.53}$$

which is zero while $-\delta_{mod} \leq \delta_a, \delta_e, \delta_r \leq \delta_{mod}$, and non-zero otherwise. A reference airspeed that can be used to avoid actuator saturation can now be designed as shown in the following theorem:

Theorem 3.8 *Let Assumptions 2.2, 3.1, 3.2 and 3.5 hold, and let the speed error be defined as $\tilde{V} = V_a - V_r$. Given the dynamics (2.25) and (2.32) in closed loop with the sliding surface controller (3.15) and the airspeed controller (3.37) together with the reference airspeed*

$$\dot{V}_r = \dot{V}_d - \kappa_r(V_r - V_d) + \kappa_u u_{max} \tag{3.54}$$

$$u_{max} = \max\{|u_1|, |u_2|, |u_3|\} \tag{3.55}$$

where $\kappa_r > 0$, $\kappa_u > 0$ are gains, then the dual equilibrium points $(\mathbf{e}_{q\pm}, \mathbf{s}, \tilde{V}) = (\mathbf{0}, \mathbf{0}, 0)$ are uniformly exponentially stable. Furthermore, the reference airspeed asymptotically tracks the desired airspeed and the deflection angles will desaturate in finite time.

Proof. The proof is given in Appendix E.18. ■

Corollary 3.2 *Theorem 3.8 also holds for the backstepping controller (3.12) and the* PD+ *controller (3.14).*

Assumption 3.8 *Let the thrust be unconstrained.*

Corollary 3.3 *Let Assumption 3.8 hold. Using Theorem 3.8, then the maximum deflection angle is defined through δ_{mod} and saturation is avoided.*

Remark 3.15 *Since the main objective of a speed controller is to track a desired speed profile, which often is chosen as a constant, it can be used as an additional degree of freedom by applying Theorem 3.8. In essence, the saturation problem is moved from the rotational to the translational dynamics, where it is important that the aircraft has enough thrust available to compensate for the deflection angle saturation through speed modification.*

3.5.2 Simulation

Consider the case of tracking a series of waypoints using the speed controller (3.37) with the reference airspeed (3.54) together with a sliding surface controller (3.15) with the gains as $\kappa_u = 10^5, \kappa_r = 2, \kappa_p = 2, k_q = 2, k_s = 2$ and $\mathbf{\Lambda} = 0.5\mathbf{I}$. Let the fixed-wing UAV have the initial conditions: $\mathbf{q}_{n,b}(0) = \begin{bmatrix}1 & 0 & 0 & 0\end{bmatrix}^\top$, $\boldsymbol{\omega}^b_{n,b}(0) = \begin{bmatrix}0 & 0 & 0\end{bmatrix}^\top$ rad/s, $\mathbf{v}^b(0) = \begin{bmatrix}30 & 0 & 0\end{bmatrix}^\top$ m/s, $\mathbf{w}^n = \begin{bmatrix}10 & 0 & 0\end{bmatrix}^\top$ m/s, $\mathbf{p}^n(0) = \begin{bmatrix}0 & 0 & 0\end{bmatrix}^\top$ m, with the desired airspeed $V_d = 40$ m/s. The deflection angles are bounded as $-0.3491 \leq \delta_a, \delta_e, \delta_r \leq 0.3491$ radians while the modified limit is defined as $\delta_{mod} = 0.5\delta_{max}$. The objective is to track a series of waypoints while keeping the deflection angles within their actuation zone. The first and second waypoints are chosen respectively as $\mathbf{p}^n_{wp,1} = \begin{bmatrix}2000 & 1000 & -1000\end{bmatrix}^\top$ m and $\mathbf{p}^n_{wp,2} = \begin{bmatrix}-2000 & 4000 & -1000\end{bmatrix}^\top$ m. The waypoint guidance law is presented in Chapter 4, but is used in this simulation to produce jumps in the tracking error such that the deflection angles go into saturation unless the problem is addressed through speed modification.

Assume that the thrust is unconstrained. This crude assumption enables the maximum deflection angles to be directly defined through δ_{mod} and saturation will be avoided. By including a thrust constraint, the deflection angles may go into saturation and will require some time before they desaturate. In Figure 3.16 the attitude and angular velocity errors are shown which both go to zero. Note that there are spikes in the tracking error at about 52 s, which is due to the switching to the next waypoint. In the bottom plot, the deflection angles are shown, which keep within the bounds defined through δ_{mod}, and saturation of the actuators have therefore been avoided. Normally the actuators would have gone into saturation during the switching, but due to the reference airspeed the saturation has been avoided. In the top plot of Figure 3.17 the position tracking error is shown, which go toward zero, and switches at about 52 s. In the middle plot, the airspeed error is shown. Note that this is the error between the reference and the actual airspeed. Observe that the airspeed error increases to about 70 m/s during the switching to the next waypoint which is due to the increase in the reference airspeed as shown

in Figure 3.18. This ensures that the deflection angles of the actuators remain below δ_{mod}. The thrust, since it has no upper bound, goes as high as 1180 N. This makes the speed modification happen almost instantly, and thereby ensuring that the deflection angles do not go into saturation. In Figure 3.18 the reference airspeed is shown, which goes as high as about 135 m/s before converging to the constant desired airspeed of 40 m/s. Hence, the reference airspeed is only active when the deflection angles are exceeding a predefined limit, and can therefore be used as a tool to keep them within a desired bound.

Consider the case when the thrust is bounded by 250 N, which is a more realistic scenario. From simulations with leveled flight using the model by Campa *et al.* (2007), the maximum airspeed that can be obtained is 140.8 m/s. Considering Figure 3.18, the reference speed is below this value, such that it is reasonable to assume that in finite time, even with constrained actuation, the deflection angles will desaturate.

3.6 Summary

In this chapter several control laws have been derived for both rotational and translational control. These control laws enable the UAV to track a desired attitude and angular velocity that are defined relative to the North East Down frame and track a desired speed profile. Problems such as unknown aerodynamics and actuator constraints have been addressed through the use of a reference trajectory. The control laws that have been presented in this chapter enable the UAV to point the airspeed in a desired direction. The desired airspeed, attitude, angular velocity and acceleration can be defined through a guidance law to complete any mission objective, which will be done in the next chapter.

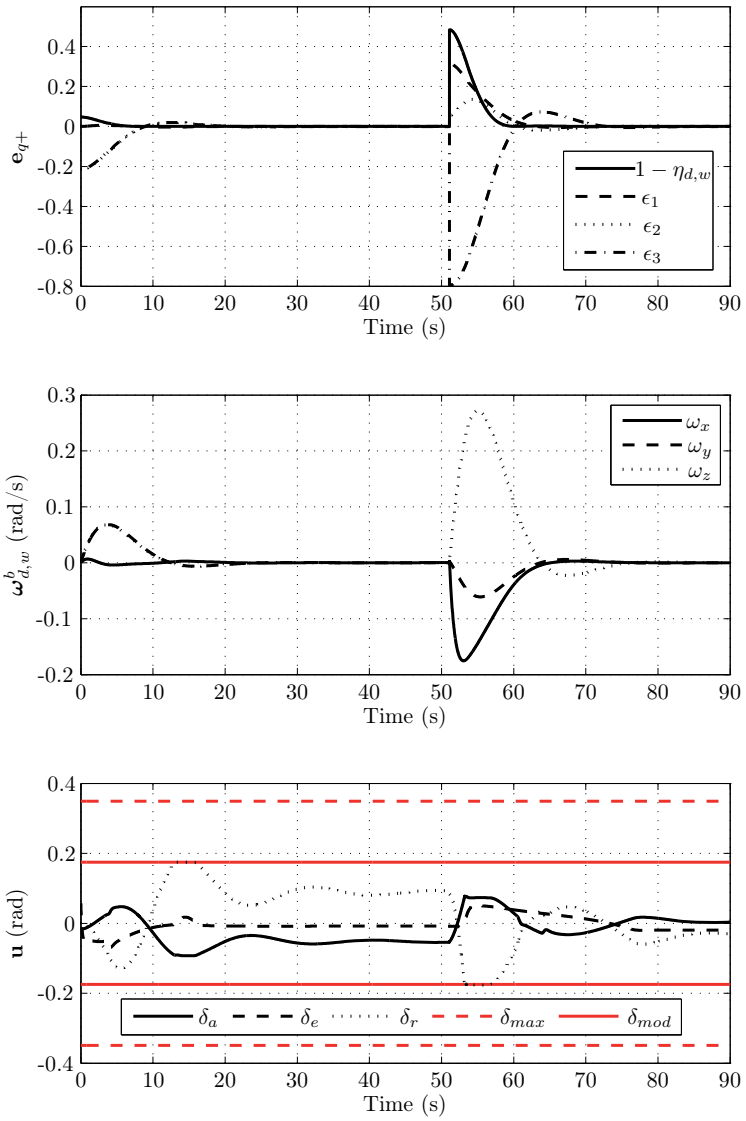

Figure 3.16: Attitude error, angular velocity error and deflection angles.

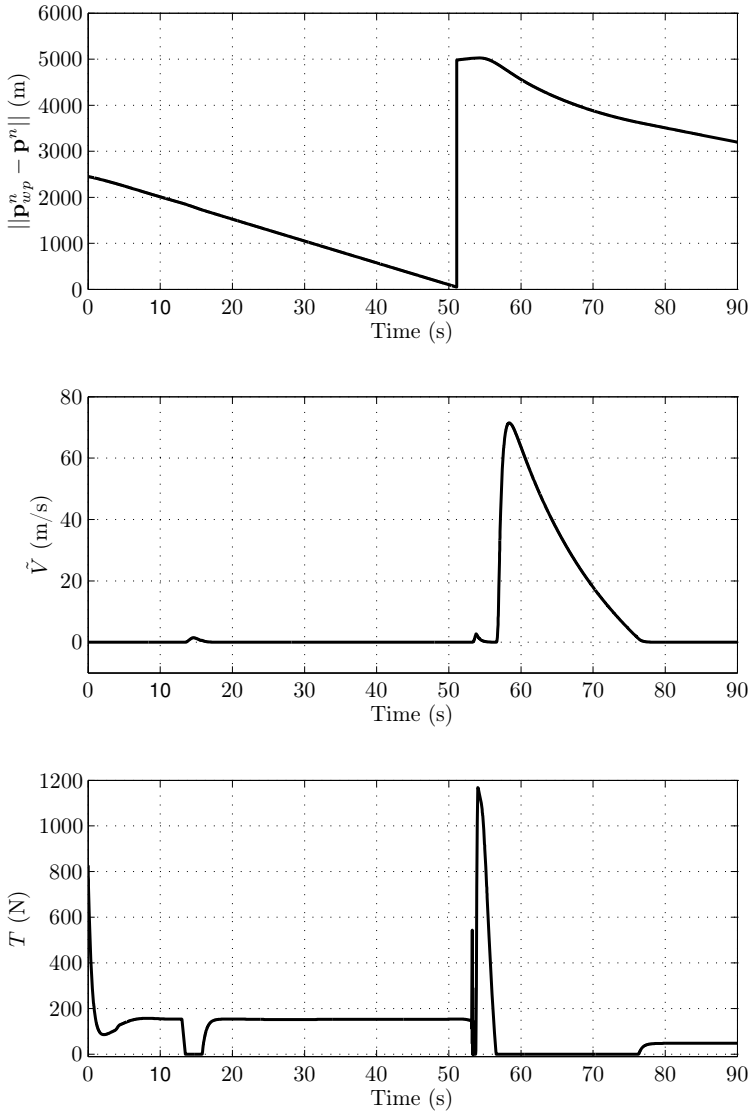

Figure 3.17: Position error, speed error and thrust.

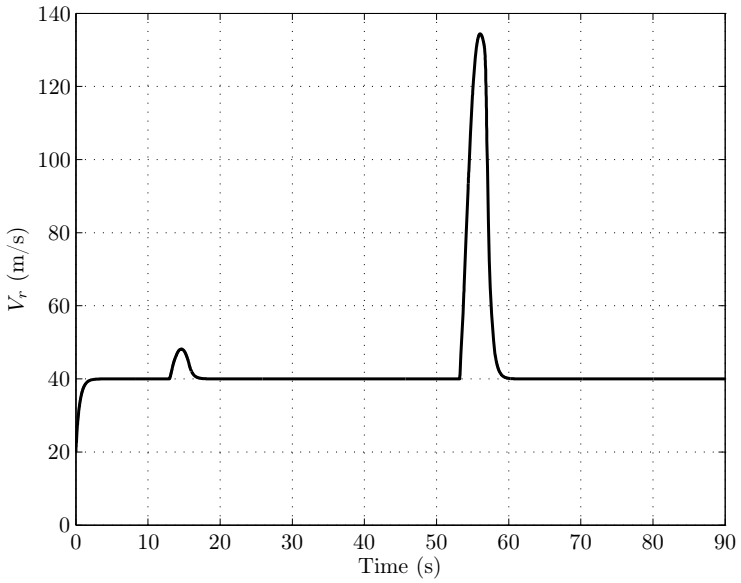

Figure 3.18: Reference speed.

Chapter 4

Guidance

> Guidance is defined as the process for guiding the path of an object towards a given point, which in general may be moving.
>
> N. A. Shneydor, 1998

This chapter is based on Oland and Kristiansen (2013*a*), Oland *et al.* (2013*a*) and Oland and Kristiansen (2014*c*) and presents different solutions for obtaining the desired states that serve as inputs to the control solutions from Chapter 3. The objective of guidance is to guide the UAV to a desired point which in general can be moving. This can be considered as two different problems, waypoint tracking and trajectory tracking. Waypoint tracking enables constant coordinates to be defined in Euclidean space that the UAV must track. As the UAV comes within a sphere of acceptance (*i.e.* sufficiently close to the waypoint), the waypoint algorithm switches to the next waypoint. Trajectory tracking on the other hand, can be considered as the problem of tracking a point that is moving as a function of time, meaning that the point is at a given position at a given time. The time dependence can be removed by introducing a path variable, which results in path following. This gives an addition degree of freedom which can be used to reduce the complexity of the control problem (*cf.* Aguiar *et al.* (2008)). In order to perform formation flight, the UAVs must be at a given position at a given time, such that this thesis focuses on waypoint tracking, trajectory tracking and formation flight, where formation flight in many ways can be seen as an application of trajectory tracking[1].

A fixed-wing UAV has only actuation along the x axis of the body frame, while the y and z axes are unactuated. This means that for example to reach a waypoint that is initially to the side of the UAV, the UAV must move in a circular trajectory to reach the desired waypoint. Using guidance, the position errors along the y and z axes are mapped to a desired orientation that makes these errors go to zero.

[1]This thesis only consider the ideal case where every UAV has perfect knowledge of the other UAVs, such that formation flight can be facilitated by tracking trajectories relative to a virtual leader. By incorporating time lags and uncertainties the problem of formation flight becomes much more challenging.

Consider for example control of ships as shown in Fossen *et al.* (2003). To make the position error in the y direction go to zero, a desired yaw angle can be chosen as $\psi_d = \text{atan2}(y_d - y, x_d - x)$ where x_d and y_d represent the desired position and atan2 ensures that $\psi_d \in (-\pi, \pi)$. This means that guidance of an underactuated rigid body can be defined as a *mapping* from the unactuated states to the actuated states (in this case the error along the y axis is mapped to a desired yaw angle which can be tracked using the rudder).

This chapter shows how to map position and velocity errors from $\mathbb{R}^3$ to $\mathbb{R}^1 \times \mathcal{S}^3$ resulting in desired states that can be tracked using the proposed controllers in Chapter 3. Firstly, waypoint tracking is considered where a desired orientation and angular velocity is designed such that the position error goes to zero. Secondly, trajectory tracking is considered, where the desired position is allowed to move as a function of time, which then can be tracked using a combination of a virtual translational controller and a mapping of the control signal to the controllable states. Thirdly, the desired trajectory can be shifted relative to a virtual leader, enabling a group of followers to perform formation flight using the proposed trajectory tracking method.

4.1 Waypoint Tracking

A desired trajectory for a UAV is commonly expressed as a set of waypoints, which the UAV shall track as accurately as possible. The simplicity of defining the trajectory through several points has made the use of waypoints very popular as it is adaptable for many missions and the operator requires little knowledge about the control system in order to complete the mission objective. This has made waypoint tracking popular for commercial flight such as over the North Atlantic, where the trajectory is defined by a set of waypoints such that the head winds are minimized and thereby reducing the propellant consumption. From a control perspective, waypoint tracking has received a lot of attention and different solutions are presented in works such as Aguiar and Pascoal (2002), Osborne and Rysdyk (2005), Børhaug and Pettersen (2005*a*), Fossen *et al.* (2003) and references therein. In Roberts and Tayebi (2009), the authors presented a method for controlling an underactuated vertical take-off and landing (VTOL) UAV which has its thrust aligned with the $\mathbf{z}^b$ axis and full rotational control. By first assuming that the VTOL-UAV has full translational control and then map the resulting control signal to a desired thrust and a desired attitude, it enables the VTOL-UAV to perform position tracking. More precisely, consider the acceleration of an underactuated VTOL-UAV in the NED frame

$$\ddot{\mathbf{p}}^n = \frac{1}{m}\mathbf{R}_b^n \begin{bmatrix} 0 \\ 0 \\ -T \end{bmatrix} + \begin{bmatrix} 0 \\ 0 \\ g \end{bmatrix} := \frac{1}{m}\mathbf{R}_b^n \mathbf{f}_t^b + \mathbf{f}_g^n \tag{4.1}$$

where the thrust is constrained along the $\mathbf{z}^b$ axis. Their approach is to first consider a fully-actuated control signal $\mathbf{f}_d^n$ which can be designed using known methods.

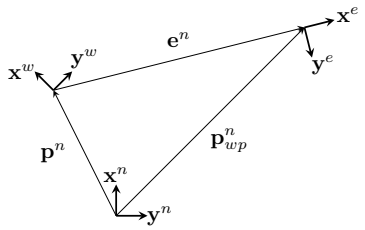

Figure 4.1: Position vectors in the xy-plane.

Then, by comparing the control signal to the actuator constraint as

$$\begin{bmatrix} 0 \\ 0 \\ -T_d \end{bmatrix} = \mathbf{R}^d_n \mathbf{f}^n_d \tag{4.2}$$

where $T_d = ||\mathbf{f}^n_d||$ and the rotation matrix $\mathbf{R}^d_n$ can be constructed using quaternions, it enables control of an underactuated VTOL-UAV by tracking the desired thrust, quaternion, angular velocity and acceleration. This approach is valid as long as $T_d \neq 0$, which is true most of the time due to the gravity vector. The desired angular velocity and acceleration can be found from the derivatives of the control law or using observers. For fixed-wing UAVs, this approach is not directly applicable since the aerodynamic force vector contains the deflection angles, and the thrust is aligned along the $\mathbf{x}^b$ axis. Instead of starting at the acceleration level as in Roberts and Tayebi (2009), it is possible to start at the position level, which can be used to facilitate waypoint tracking.

A waypoint can be defined as $\mathbf{p}^n_{wp} \in \mathbb{R}^3$ while the controllers from Chapter 3 control of the attitude, angular velocity and acceleration together with the airspeed and acceleration. A mapping is therefore required to map the tracking error from $\mathbb{R}^3$ to $\mathbb{R}^1 \times \mathcal{S}^3$ such that the UAV receives the correct inputs to track the desired waypoint. With basis in Figure 4.1 let a position error frame, denoted by superscript e, be defined through the relation

$$\mathbf{e}^e := \begin{bmatrix} ||\mathbf{e}^n|| \\ 0 \\ 0 \end{bmatrix} = \mathbf{R}^e_n \mathbf{e}^n = \mathbf{R}^e_n (\mathbf{p}^n_{wp} - \mathbf{p}^n) \tag{4.3}$$

where the objective is to make $\mathbf{e}^e \to \mathbf{0}$. To facilitate waypoint tracking, consider the following assumption and property:

Assumption 4.1 $\mathbf{w}^n = \mathbf{0}$.

Property 4.1 *The waypoint algorithm switches to the next waypoint whenever* $\Delta \geq ||\mathbf{e}^n|| \geq \delta > 0$.

Assumption 4.1 simplifies the waypoint problem and will later be removed by a correction angle, while Property 4.1 is required to avoid the singularity which exists when $\mathbf{e}^n = \mathbf{0}$. Since the origin $\mathbf{e}^n = \mathbf{0}$ is singular when determining the angular velocity, the control objective must be redefined. For waypoint tracking, it is typical to move close to the origin, and then switch to the next waypoint. Through the following lemma, a set containing the points in a shell around the origin is defined. Thus, by moving to the set, and then switch to the next waypoint, it ensures that the origin $\mathbf{e}^n = \mathbf{0}$ is never reached, but that the UAV moves sufficiently close to the origin before switching.

Lemma 4.1 *Let Assumptions 2.2 and 4.1, Property 4.1,* $||\mathbf{e}^n(t_0)|| > \delta > 0$ *hold, and let a set be defined as* $\mathcal{H}(\delta, \Delta) := \{\mathbf{x} \in \mathbb{R}^3 | \delta \leq ||\mathbf{e}^n|| \leq \Delta\}$ *where* $\delta > 0$ *represents an inner radius and* $\Delta > \delta > 0$ *represents an outer radius. Given the position error as in (4.3) and by tracking the quaternion and angular velocity*

$$\mathbf{q}_{n,e} = \begin{bmatrix} \cos\left(\frac{\vartheta_{n,e}}{2}\right) & \mathbf{k}_{n,e}^\top \sin\left(\frac{\vartheta_{n,e}}{2}\right) \end{bmatrix}^\top \tag{4.4}$$

$$\vartheta_{n,e} = \cos^{-1}\left(\frac{\mathbf{e}^e \cdot \mathbf{e}^n}{||\mathbf{e}^n||^2}\right) \quad \mathbf{k}_{n,e} = \frac{\mathbf{e}^e \times \mathbf{e}^n}{||\mathbf{e}^e \times \mathbf{e}^n||} \tag{4.5}$$

$$\boldsymbol{\omega}_{n,e}^e = \mathbf{S}^\dagger(\mathbf{e}^e)\mathbf{R}_b^e \mathbf{v}^b \tag{4.6}$$

then the set $\mathcal{H}(\delta, \Delta)$ *is uniformly asymptotically stable.*

Proof. The proof is given in Appendix E.19. ■

Remark 4.1 *The presented solution shares many similarities with the work by Børhaug and Pettersen (2005a) where the authors consider adaptive waypoint tracking for underactuated autonomous underwater vehicles. However, in this solution a quaternion based approach is applied, which has some interesting properties. Consider the case when the angular velocity and acceleration are found using filters (as in Børhaug and Pettersen (2005a)). Then; since the designed quaternions are unitary, it follows that* $\mathbf{q}_{n,e} \to \begin{bmatrix} 1 & 0 & 0 & 0 \end{bmatrix}^\top$ *as* $||\mathbf{e}^n|| \to 0$*, meaning that as long as* $||\mathbf{e}^n(t_0)|| > 0$ *the origin* $\mathbf{e}^n = \mathbf{0}$ *can be shown to be uniformly asymptotically stable. By using a desired yaw angle* $\psi_d = \tan^{-1}\left(\frac{y - y_d}{x - x_d}\right)$ *and a desired pitch angle as* $\theta_d = \tan^{-1}\left(\frac{z - z_d}{\sqrt{(x-x_d)^2 + (y-y_d)^2}}\right)$*, then the origin* $\mathbf{e}^n = \mathbf{0}$ *becomes unstable (since the desired angles are not defined at the origin) and a similar approach as in Lemma 4.1 or in Børhaug and Pettersen (2005a) should be used.*

Remark 4.2 *Using similar notation, the line of sight rate used for the proportional navigation (PN) law can be defined as (cf. Siouris (2003))*

$$\boldsymbol{\omega}_{e,n}^n = \frac{\mathbf{S}(\mathbf{e}^n)\dot{\mathbf{e}}^n}{||\mathbf{e}^n||^2} \tag{4.7}$$

and using that $\boldsymbol{\omega}_{e,n}^n = -\boldsymbol{\omega}_{n,e}^n$ *and rotating to the position error frame, the line of sight rate becomes*

$$\boldsymbol{\omega}_{n,e}^e = \frac{\mathbf{S}(\mathbf{e}^e)\mathbf{R}_b^e \mathbf{v}^b}{||\mathbf{e}^n||^2} = \mathbf{S}^\dagger(\mathbf{e}^e)\mathbf{R}_b^e \mathbf{v}^b, \tag{4.8}$$

which is identical to (4.6).

In the presence of wind and using Lemma 4.1, it is the airspeed that is aligned with the position error frame, such that the wind will perturb the tracking error. Since the objective is to track a desired position relative to the Earth, it is the ground speed that must be aligned with the position error frame, which can be done by adding a correction angle by studying the wind triangle (*cf.* Figure 2.2). Assumption 4.1 can be removed by defining a wind correction angle, $\vartheta_{e,d}$, as the angle between $\mathbf{v}^b$ and $\mathbf{v}_r^b$. Hence, by designing a quaternion as

$$\mathbf{q}_{e,d} = \begin{bmatrix} \cos\left(\frac{\vartheta_{e,d}}{2}\right) & \mathbf{k}_{e,d}^\top \sin\left(\frac{\vartheta_{e,d}}{2}\right) \end{bmatrix}^\top \tag{4.9}$$

$$\vartheta_{e,d} = \cos^{-1}\left(\frac{\mathbf{v}^b \cdot \mathbf{v}_r^b}{||\mathbf{v}^b||\ ||\mathbf{v}_r^b||}\right) \quad \mathbf{k}_{e,d} = \frac{\mathbf{v}^b \times \mathbf{v}_r^b}{||\mathbf{v}^b \times \mathbf{v}_r^b||} \tag{4.10}$$

a rotation that compensates for the wind is obtained. Since the quaternion is designed using velocity vectors, obtaining the angular velocity through differentiation requires the acceleration, which is not available. Instead the angular velocity, $\boldsymbol{\omega}_{e,d}^d$, can be found using a linear filter with saturation (*cf.* Fossen (2011)) which ensures that the angular velocity becomes bounded.

Remark 4.3 *Wind compensation is usually done using a crab angle which assumes leveled flight. Up- and downdrafts (*e.g. *mircobursts) produce wind components in the vertical plane which also affect the aircraft and are taken into account using the proposed quaternion,* $\mathbf{q}_{e,d}$.

Waypoint tracking with wind compensation can therefore be solved as the composite quaternion with the corresponding angular velocity as

$$\mathbf{q}_{n,d} = \mathbf{q}_{n,e} \otimes \mathbf{q}_{e,d} \tag{4.11}$$

$$\boldsymbol{\omega}_{n,d}^d = \mathbf{R}_e^d \boldsymbol{\omega}_{n,e}^e + \boldsymbol{\omega}_{e,d}^d \tag{4.12}$$

where $\boldsymbol{\omega}_{e,d}^d$ is found using filters.

Remark 4.4 *The waypoint algorithm produces spikes in the desired quaternion and angular velocity whenever it switches between waypoints which can make the actuators go into saturation. This can be remedied by using linear filters to smoothen the desired states (cf. Fossen (2011)).*

Remark 4.5 *The placement of waypoints is of critical importance, since by placing two waypoints too close may result in a limit cycle. The placement problem of waypoints is not considered in this thesis.*

4.1.1 Simulation

To validate the proposed approach, the backstepping controller (3.12) is used in conjunction with the proportional speed controller (3.37). The gains are chosen as $k_q = 2$, $k_z = 2$, $\kappa_p = 2$ and the waypoints are defined in Table 4.1. The

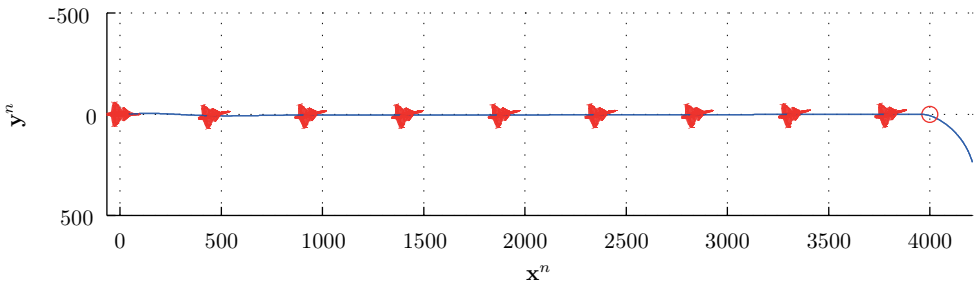

Figure 4.2: Waypoint tracking with wind compensation.

sphere of acceptance is defined by $\Delta = 50$ m, which defines when the waypoint algorithm shall switch to the next waypoint. Let the initial states be given as $\mathbf{q}_{n,b}(0) = \begin{bmatrix}1 & 0 & 0 & 0\end{bmatrix}^\top$, $\boldsymbol{\omega}_{n,b}^b(0) = \begin{bmatrix}0 & 0 & 0\end{bmatrix}^\top$ rad/s, $\mathbf{p}^n(0) = \begin{bmatrix}0 & 0 & -100\end{bmatrix}^\top$ m, $\mathbf{v}^b(0) = \begin{bmatrix}25 & 0 & 0\end{bmatrix}^\top$ m/s, $\mathbf{w}^n = \begin{bmatrix}0 & 10 & 0\end{bmatrix}^\top$ m/s and let the UAV have a desired airspeed of $V_d = 50$ m/s.

Wind Compensation

To validate the wind compensation, consider the problem of tracking a desired waypoint located at $\mathbf{p}_{wp}^n = \begin{bmatrix}4000 & 0 & -100\end{bmatrix}^\top$ while the wind is moving with a velocity of $\mathbf{w}^n = \begin{bmatrix}0 & 10 & 0\end{bmatrix}^\top$ m/s. In Figure 4.2 the UAV is able to track the desired waypoint without problems using the wind compensation, while in Figure 4.3 the guidance is not using any wind compensation and the UAV starts to drift away from the optimal trajectory. Hence, the wind compensation is required to keep the trajectory between the waypoints as short as possible.

3D Waypoint Tracking

Consider the case of tracking multiple waypoints as shown in Table 4.1. The 3D plot is shown in Figure 4.4 where the UAV perfectly tracks the desired waypoints. In Figure 4.5 the speed error, position error and thrust are shown. The speed error goes to zero during the tracking. Note that it diverges from zero at about 338

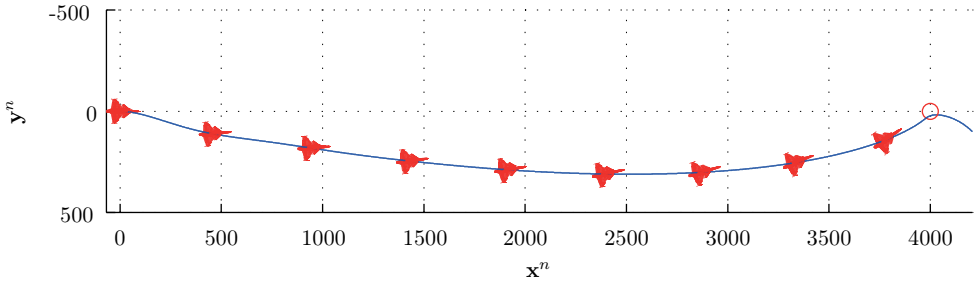

Figure 4.3: Waypoint tracking without wind compensation.

Table 4.1: List of waypoints

#	$\mathbf{p}^n_{wp}$ (m)
1	$\begin{bmatrix}2000 & 1000 & -1000\end{bmatrix}^\top$
2	$\begin{bmatrix}2000 & 4000 & -1000\end{bmatrix}^\top$
3	$\begin{bmatrix}0 & 6000 & -5000\end{bmatrix}^\top$
4	$\begin{bmatrix}0 & 7000 & -10000\end{bmatrix}^\top$
5	$\begin{bmatrix}0 & 5000 & -10000\end{bmatrix}^\top$
6	$\begin{bmatrix}-2000 & 6000 & -5000\end{bmatrix}^\top$
7	$\begin{bmatrix}0 & 0 & -2000\end{bmatrix}^\top$

seconds, which is due to the fact that the UAV is moving downwards to the next waypoint. Since the thrust is bounded between zero and a positive value, it is not able to break as it moves towards the next waypoint, and thereby it increases its speed. As the UAV regains leveled flight, the speed error goes to zero again. The position error goes to zero between each waypoint, while the thrust remains within its bounds. In Figure 4.6 the quaternion error, angular velocity error and deflection angles are shown. All errors go to zero while the deflection angles go to constant values as the errors go to zero. The quaternion error, angular velocity and deflection angles for the whole simulation are shown in Figure 4.7 where all the errors go to zero. The spikes are due to the switching between the waypoints.

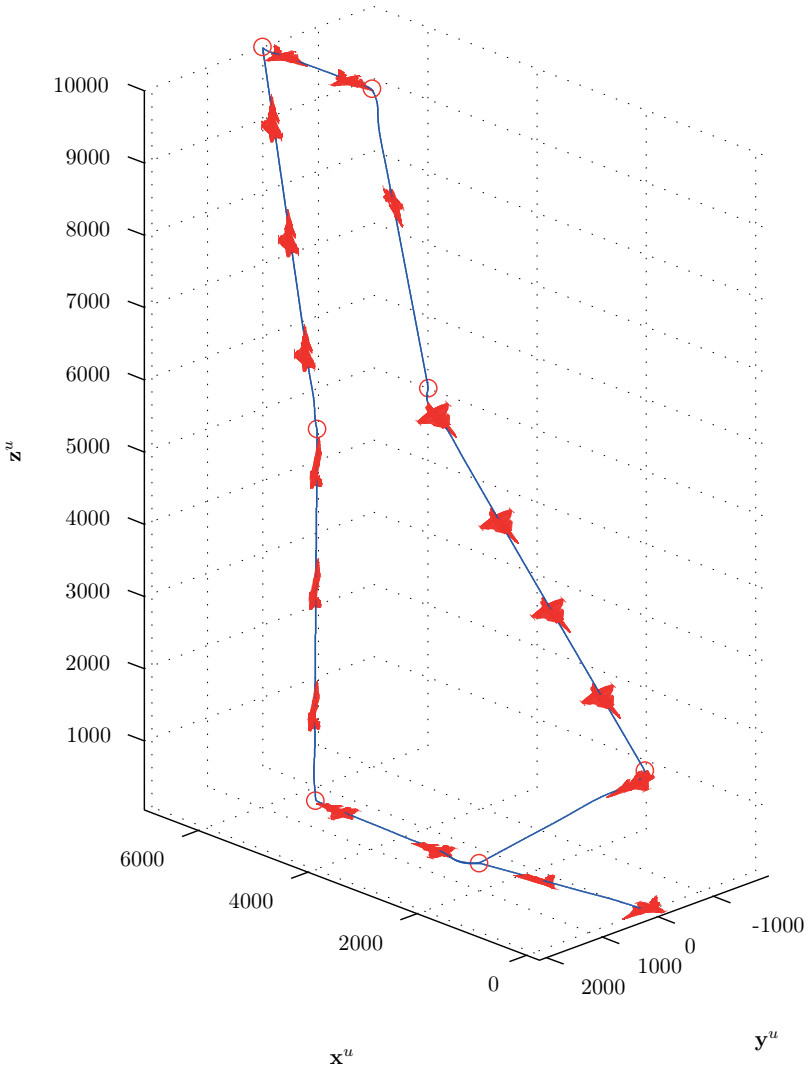

Figure 4.4: 3D Waypoint tracking.

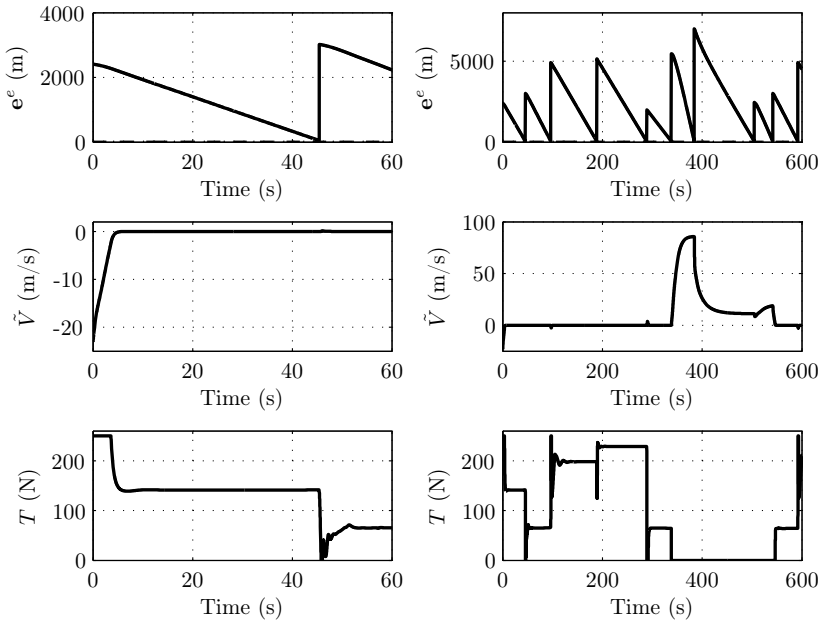

Figure 4.5: Position error, speed error and thrust.

4.2 Trajectory Tracking

The basic idea from waypoint guidance can easily be extended to that of trajectory tracking, where the errors can be mapped to desired states that can be tracked by the given control laws. First, the translational system is assumed to be fully actuated (similarly as proposed in Roberts and Tayebi (2009)), where a control law can be designed using known methods, and then the output can be mapped to controllable variables.

4.2.1 Trivial Solution

Consider the double integrator

$$\dot{\mathbf{p}}^n = \mathbf{v}^n \tag{4.13}$$

$$\dot{\mathbf{v}}^n = \mathbf{u}^n \tag{4.14}$$

where $\mathbf{p}^n$ is the position in the NED frame, $\mathbf{v}^n$ is the velocity and $\mathbf{u}^n$ is a virtual control signal that is to be designed. Let a desired trajectory be defined through $\mathbf{p}_d^n, \dot{\mathbf{p}}_d^n, \ddot{\mathbf{p}}_d^n \in \mathcal{L}_\infty$ and the tracking errors as $\mathbf{e}_1 := \mathbf{p}^n - \mathbf{p}_d^n$ and $\mathbf{e}_2 := \mathbf{v}^n - \dot{\mathbf{p}}_d^n$; then

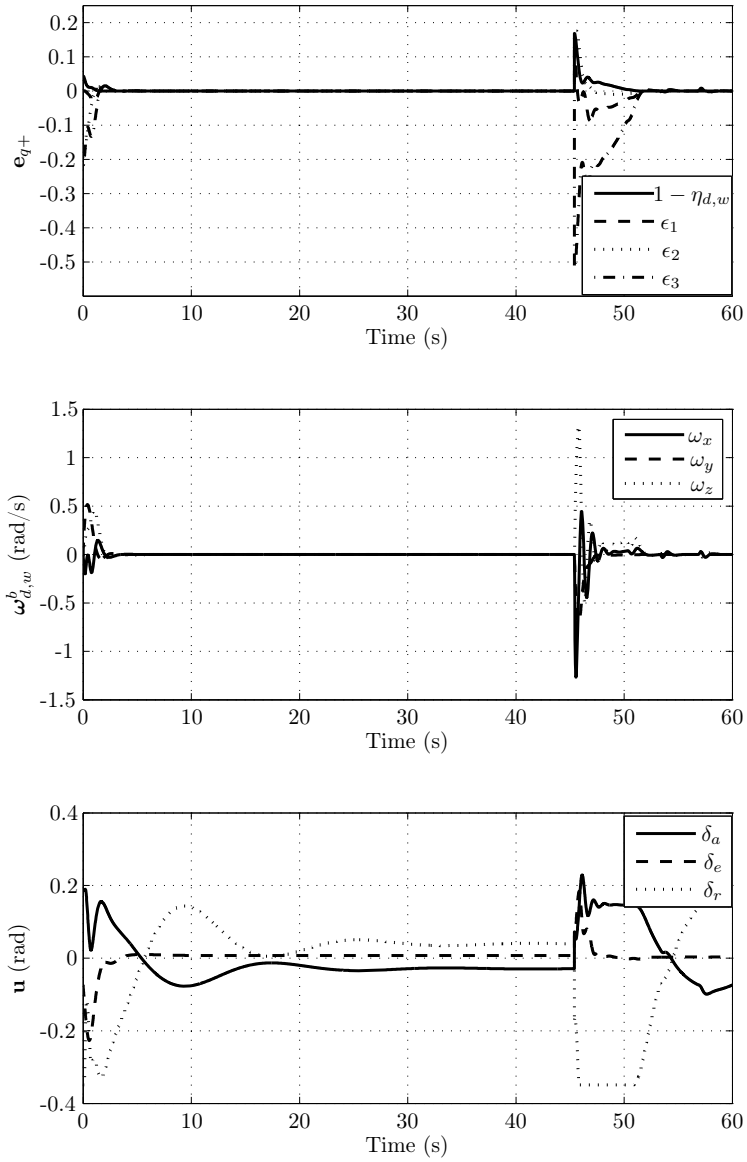

Figure 4.6: Attitude, angular velocity and deflection angles.

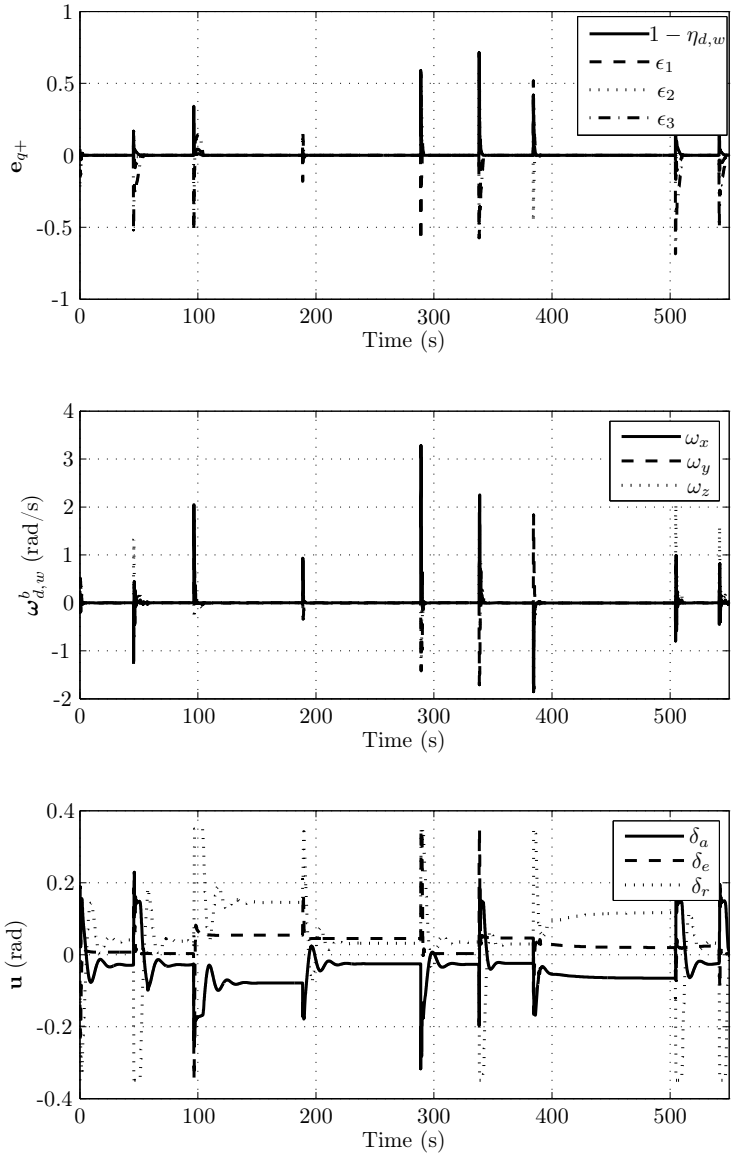

Figure 4.7: Attitude, angular velocity and deflection angles.

the tracking error dynamics can be written as

$$\dot{\mathbf{e}}_1 = \mathbf{e}_2 \tag{4.15}$$
$$\dot{\mathbf{e}}_2 = \mathbf{u}^n - \ddot{\mathbf{p}}_d^n. \tag{4.16}$$

It is now possible to use a wealth of different approaches to make the tracking error, $\mathbf{e}_1, \mathbf{e}_2 \to \mathbf{0}$ through $\mathbf{u}^n$ since it is assumed to be fully actuated. The important part is to ensure that the resulting control law is bounded, such that it does not produce commands that the attitude and speed controllers are not able to track. The virtual control law can be summarized in the following theorem:

Theorem 4.1 *Let a desired trajectory be defined through $\mathbf{p}_d^n, \dot{\mathbf{p}}_d^n, \ddot{\mathbf{p}}_d^n \in \mathcal{L}_\infty$, then the origin $(\mathbf{e}_1, \mathbf{z})$ of the dynamics (4.13)-(4.14) in closed loop with the control law*

$$\mathbf{u}^n = \ddot{\mathbf{p}}_d^n - k_p \dot{\sigma}_1(\mathbf{e}_1)\mathbf{e}_2 - k_d \sigma_2(\mathbf{z}) \tag{4.17}$$
$$\mathbf{z} = \mathbf{e}_2 + k_p \sigma_1(\mathbf{e}_1) \tag{4.18}$$

where $k_p > 0, k_d > 0$ and $\sigma_1(\cdot), \sigma_2(\cdot)$ are saturation functions, is uniformly globally asymptotically stable. Furthermore, as $\mathbf{e}_1, \mathbf{z} \to \mathbf{0}$ it follows from (4.18) that $\mathbf{e}_2 \to \mathbf{0}$.

Proof. The proof is given in Appendix E.20. ■

Note that any saturated control law can be applied to solve the trajectory tracking problem. There are several other control laws that can be applied, such as those presented in Teel (1992), Sussmann *et al.* (1994), Tyan and Bernstein (1999), Marconi and Isidori (2000), Rao (2001) and Tarbouriech *et al.* (2011). Especially note that if the term $k_p \dot{\sigma}_1(\mathbf{e}_1)\mathbf{e}_2$ is dominated through the Lyapunov analysis (which is possible), the resulting control law is similar to the nested saturation controller by Teel (1992).

4.2.2 Mapping from $\mathbb{R}^3$ to $\mathbb{R}^1 \times \mathcal{S}^3$

A fixed-wing UAV has full attitude control and only translational control in one direction, such that the control problem of performing position tracking in $\mathbb{R}^3$ must be mapped to $\mathbb{R}^1 \times \mathcal{S}^3$. Let the velocity vector $\mathbf{v}^n$ be decomposed into two parts as

$$\mathbf{v}^n := \mathbf{v}_r^n + \mathbf{w}^n \tag{4.19}$$

where $\mathbf{v}_r^n$ is the velocity vector relative the surrounding air and $\mathbf{w}^n$ is the wind vector. The relative velocity vector can now be mapped to a desired frame through the relation

$$\mathbf{v}_r^d = \begin{bmatrix} ||\mathbf{v}_r^n|| \\ 0 \\ 0 \end{bmatrix} = \mathbf{R}_n^d \mathbf{v}_r^n \tag{4.20}$$

where $\mathbf{R}_n^d$ can be constructed using quaternions. This can be summarized in the following lemma:

Lemma 4.2 *Let Assumptions 2.1 and 2.2 hold. Then, by tracking the desired quaternion, angular velocity, airspeed and acceleration*

$$\dot{\mathbf{q}}_{n,d} = \frac{1}{2}\mathbf{q}_{n,d} \otimes \begin{bmatrix} 0 \\ \boldsymbol{\omega}_{n,d}^{d} \end{bmatrix} \tag{4.21}$$

$$\boldsymbol{\omega}_{n,d}^{d} = -\mathbf{S}^{\dagger}(\mathbf{v}_r^d)\mathbf{R}_n^d\mathbf{u}^n \tag{4.22}$$

$$V_d = ||\mathbf{v}_r^n|| \tag{4.23}$$

$$\dot{V}_d = \begin{bmatrix} 1 & 0 & 0 \end{bmatrix} \mathbf{R}_n^d\mathbf{u}^n \tag{4.24}$$

where $\mathbf{u}^n$ *is given in (4.17), then the origin* $(\mathbf{e}_1, \mathbf{z}) = (\mathbf{0}, \mathbf{0})$ *is uniformly asymptotically stable.*

Proof. The proof is given in Appendix E.21. ■

Remark 4.6 *From (4.19) the relation between the ground velocity and air velocity is given. This relation enables the desired orientation to be found directly by using the relative velocity vector. The wind vector is assumed to be known, but it can be estimated by using extended matching when designing the translational control law (cf. Krstić* et al. *(1995)).*

Remark 4.7 *The desired quaternion must be properly initialized to apply the proposed mapping, i.e. it must point in the desired direction at* t_0*. For waypoint tracking, the desired quaternion is found at each instant as shown in Lemma 4.1, but it can also apply a method similar to that of trajectory tracking. Note that the desired quaternion must then be reinitialized each time the waypoint algorithm switches to a new waypoint.*

4.2.3 Simulation

The objective is to apply the virtual control law (4.17) which is mapped to a desired quaternion, angular velocity and acceleration as well as airspeed and acceleration using (4.21)-(4.24). These desired states are then tracked using the sliding surface control law and the proportional speed controller. Consider a desired circular trajectory defined as

$$\mathbf{p}_d^n = \begin{bmatrix} R\cos(\omega t) \\ R\sin(\omega t) \\ -z_d \end{bmatrix} \tag{4.25}$$

where R is the radius of the circle, ω is the angular speed of the trajectory, t is the time and z_d is a constant desired altitude. The desired velocity and acceleration are found through direct differentiation as

$$\dot{\mathbf{p}}_d^n = \begin{bmatrix} -R\omega\sin(\omega t) \\ R\omega\cos(\omega t) \\ 0 \end{bmatrix} \tag{4.26}$$

$$\ddot{\mathbf{p}}_d^n = \begin{bmatrix} -R\omega^2\cos(\omega t) \\ -R\omega^2\sin(\omega t) \\ 0 \end{bmatrix}. \tag{4.27}$$

The radius is chosen as $R = 1000$ m, the angular speed as $\omega = 0.05$ rad/s, $t_0 = 0$ s and $z_d = 100$ m. In the following simulation the sliding surface control law (3.15) is used together with the proportional speed controller (3.37) where the gains are set equal to $k_q = 2$, $k_s = 2$, $\mathbf{\Lambda} = 2\mathbf{I}$, $\kappa_p = 2$. The virtual controller (4.17), has the following gains $k_p = 0.3$, $k_d = 0.4$, $\lambda_1 = 10$, $\lambda_2 = 10$. The UAV has the following initial states: $\mathbf{q}_{n,b} = \begin{bmatrix} 1 & 0 & 0 & 0 \end{bmatrix}^\top$, $\boldsymbol{\omega}^b_{n,b}(0) = \mathbf{0}$ rad/s, $\mathbf{v}^b(0) = \begin{bmatrix} 30 & 0 & 0 \end{bmatrix}^\top$ m/s, $\mathbf{p}^n(0) = \begin{bmatrix} 0 & 0 & -50 \end{bmatrix}^\top$ m. The deflection angles are bounded as $-0.3491 \leq \delta_a, \delta_e, \delta_r \leq 0.3491$ radians, the thrust as $0 \leq T \leq 250$ N and the UAV is exposed to a constant wind vector $\mathbf{w}^n = \begin{bmatrix} 10 & 0 & 0 \end{bmatrix}^\top$ m/s.

Figure 4.8 shows the 3D plot of the simulation. The objective is to track the desired trajectory which is a point that is moving in a circular motion illustrated by the red circle. As shown in the figure, the UAV is able to track the desired trajectory. This is also highlighted in the position and velocity error plot as shown in Figure 4.9 where both the position and velocity error go to zero. The attitude, angular velocity and deflection angles are shown in Figure 4.10 where the attitude and angular velocity quickly go to zero. The deflection angles go into saturation during the initial maneuver as the UAV have to make a π radians maneuver to follow the trajectory, and as it is approaching the desired point the deflection angles remain within their bounds. In Figure 4.11 the airspeed and thrust are shown. The airspeed is perfectly tracked while the thrust remains within its bounds.

4.3 Formation Flight

Rigid body dynamics assumes that any body can be represented as a number of particles that do not move relative to each other. To enable multiple UAVs to fly in a formation, each UAV can be treated as a particle that must be located at a constant displacement, $\boldsymbol{\rho}^l_i \in \mathbb{R}^3$ away from the leader, where superscript l denotes the leader frame. The easiest way of designing a rigid formation is to let the formation be designed through the desired trajectory, such that the desired position of the i'th UAV can be chosen as

$$\mathbf{p}^n_{d,i} = \mathbf{p}^n_l + \mathbf{R}^n_l \boldsymbol{\rho}^l_i \tag{4.28}$$

where $\mathbf{p}^n_l$ is the position of a virtual leader, and $\mathbf{R}^n_l$ is the rotation matrix from the leader frame to the NED frame representing the orientation of the virtual leader. Equation (4.28) can be differentiated twice, resulting in

$$\dot{\mathbf{p}}^n_{d,i} = \dot{\mathbf{p}}^n_l + \mathbf{R}^n_l \mathbf{S}(\boldsymbol{\omega}^l_{n,l})\boldsymbol{\rho}^l_i \tag{4.29}$$

$$\ddot{\mathbf{p}}^n_{d,i} = \ddot{\mathbf{p}}^n_l + \mathbf{R}^n_l(\mathbf{S}^2(\boldsymbol{\omega}^l_{n,l})\boldsymbol{\rho}^l_i + \mathbf{S}(\dot{\boldsymbol{\omega}}^l_{n,l})\boldsymbol{\rho}^l_i). \tag{4.30}$$

where $\boldsymbol{\omega}^l_{n,l}$ is the angular velocity of the virtual leader, relative to the NED frame referenced in the leader frame. This approach enables a desired trajectory to be defined through the virtual leader by $\mathbf{p}^n_l, \dot{\mathbf{p}}^n_l, \ddot{\mathbf{p}}^n_l, \dddot{\mathbf{p}}^n_l$, which then is used to obtain desired trajectories for the followers. Note that the angular acceleration of the leader is required to find the desired translational acceleration of the i'th follower, which is one of the main motivations for using a virtual leader. Similarly as for

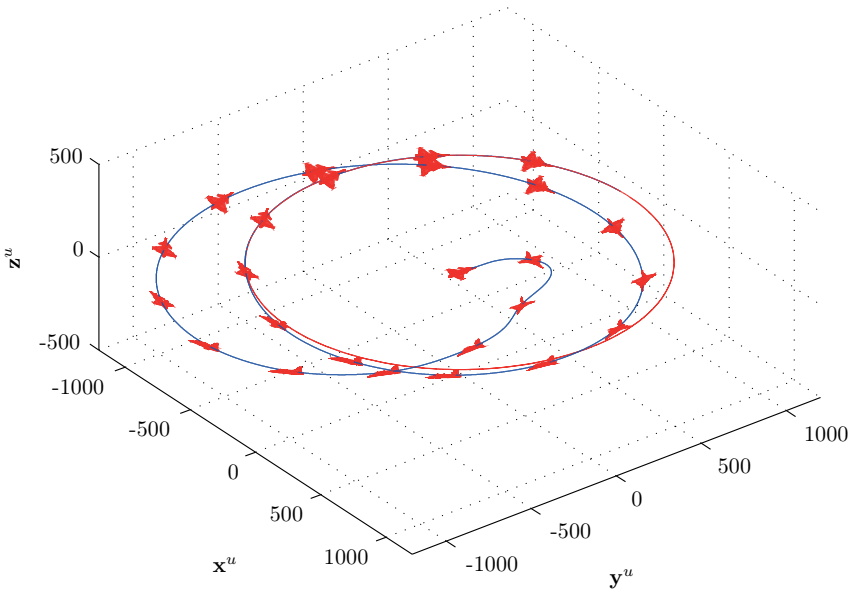

Figure 4.8: A single UAV tracking a circle.

trajectory tracking, it is possible to map the trajectory of the virtual leader to a quaternion, angular velocity and acceleration. Let the leader frame be defined through the relation

$$\dot{\mathbf{p}}_l^l = \begin{bmatrix} ||\dot{\mathbf{p}}_l^n|| \\ 0 \\ 0 \end{bmatrix} = \mathbf{R}_n^l \dot{\mathbf{p}}_l^n \tag{4.31}$$

where $\mathbf{R}_n^l$ can be constructed using quaternions. The mapping can be summarized in the following lemma:

Assumption 4.2 *Assume that* $||\dot{\mathbf{p}}_l^n|| > 0$.

Lemma 4.3 *Let Assumption 4.2 hold. Given the trajectory of the virtual leader defined by* $\mathbf{p}_l^n, \dot{\mathbf{p}}_l^n, \ddot{\mathbf{p}}_l^n, \dddot{\mathbf{p}}_l^n$*, then the velocity, acceleration and jerk can be mapped to a desired quaternion, angular velocity and acceleration as*

$$\dot{\mathbf{q}}_{n,l} = \frac{1}{2}\mathbf{q}_{n,l} \otimes \begin{bmatrix} 0 \\ \boldsymbol{\omega}_{n,l}^l \end{bmatrix} \tag{4.32}$$

$$\boldsymbol{\omega}_{n,l}^l = -\mathbf{S}^\dagger(\dot{\mathbf{p}}_l^l)\mathbf{R}_n^l \ddot{\mathbf{p}}_l^n \tag{4.33}$$

$$\dot{\boldsymbol{\omega}}_{n,l}^l = -\mathbf{S}^\dagger(\dot{\mathbf{p}}_l^l)(\mathbf{R}_n^l \dddot{\mathbf{p}}_l^n + \mathbf{S}^2(\boldsymbol{\omega}_{n,l}^l)\mathbf{R}_n^l \dot{\mathbf{p}}_l^n - 2\mathbf{S}(\boldsymbol{\omega}_{n,l}^l)\mathbf{R}_n^l \ddot{\mathbf{p}}_l^n). \tag{4.34}$$

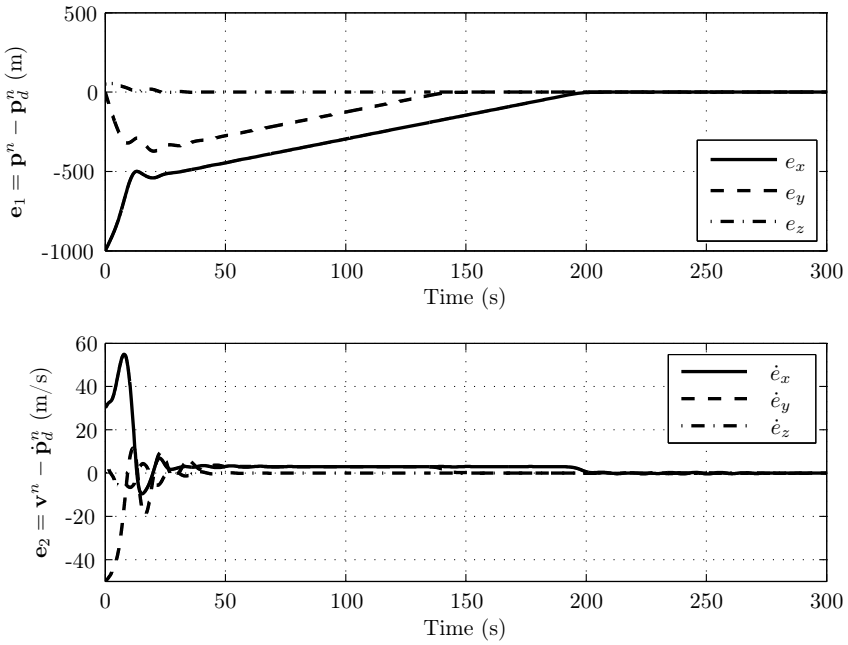

Figure 4.9: Position and velocity tracking errors.

Proof. The proof is given in Appendix E.22. ■

This approach enables desired trajectories for a group of followers to be designed relative to the virtual leader, which by properly defining the constant displacement vectors, $\boldsymbol{\rho}_i^l$, enables any rigid formation to be constructed.

Remark 4.8 *This thesis only considers rigid formations, where it is assumed that the optimal position relative to the leader that reduces the drag is constant. This might not always be the case, but can be remedied by allowing the vector $\boldsymbol{\rho}_i^l$ to be time-varying.*

4.3.1 Simulation

Consider the case of eleven UAVs that shall move in a rigid formation to exploit the aerodynamic reduction to increase their operational radius. The initial conditions are the same as for the trajectory tracking scenario, except that the gains are chosen as $k_p = k_d = 0.05$ and where the initial positions and constant displacements relative to the virtual leader are given in Table 4.2.

The virtual leader is defined through the trajectory $\mathbf{p}_l^n = \begin{bmatrix} 50t & 0 & -z_d \end{bmatrix}^\top$ m, $\dot{\mathbf{p}}_l^n = \begin{bmatrix} 50 & 0 & 0 \end{bmatrix}^\top$ m/s, which represents a trajectory moving along the $\mathbf{x}^n$ axis

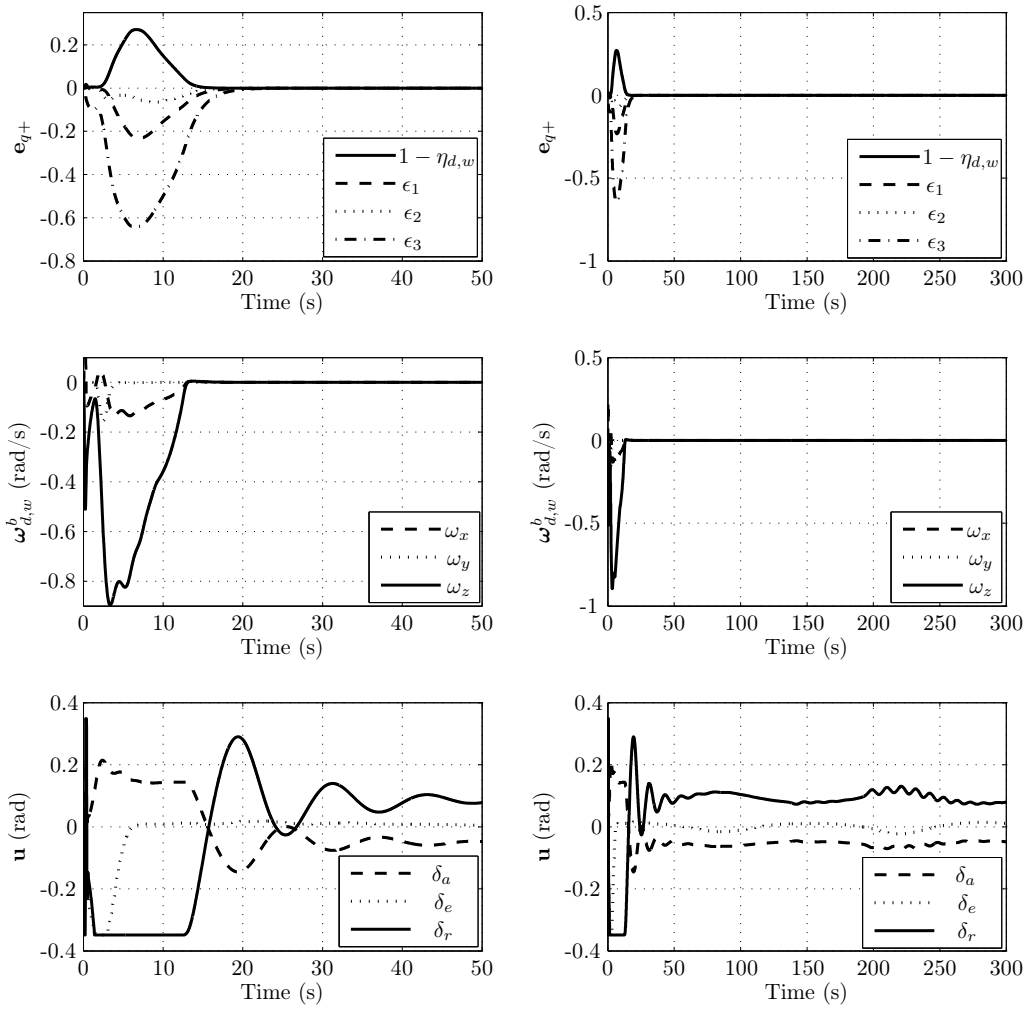

Figure 4.10: Attitude, angular velocity and deflection angles.

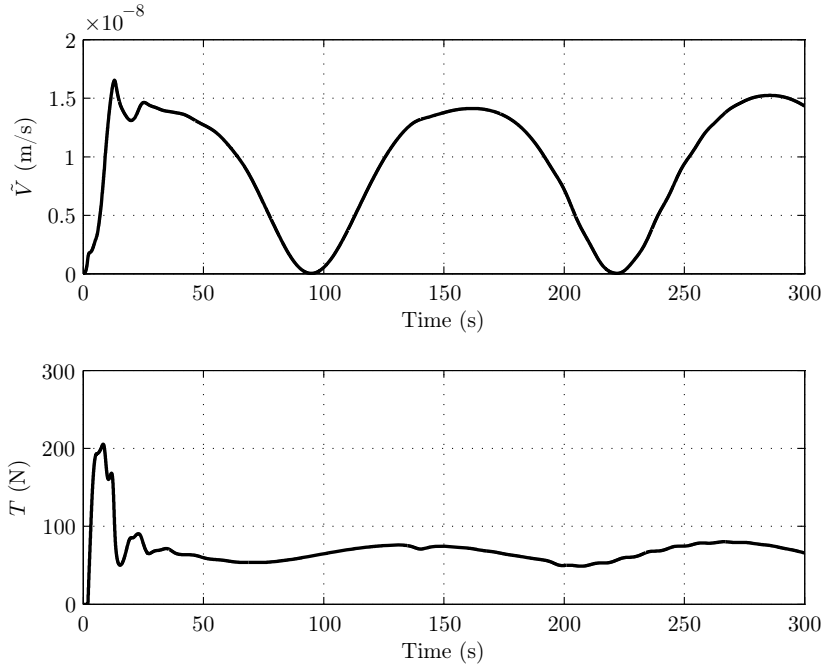

Figure 4.11: Airspeed error and thrust. Note that the airspeed in essence tracks itself through the definition of the desired frame, such that changes in speed enters through the desired acceleration.

Table 4.2: Initial positions and constant displacements of UAVs

UAV	$\mathbf{p}_i^n(0)$ (m)	$\boldsymbol{\rho}_i^l$ (m)
UAV-1	$\begin{bmatrix}100 & 100 & -50\end{bmatrix}^\top$	$\begin{bmatrix}0 & 0 & 0\end{bmatrix}^\top$
UAV-2	$\begin{bmatrix}200 & 0 & -50\end{bmatrix}^\top$	$\begin{bmatrix}-10 & -10 & 0\end{bmatrix}^\top$
UAV-3	$\begin{bmatrix}0 & 300 & -50\end{bmatrix}^\top$	$\begin{bmatrix}-10 & 10 & 0\end{bmatrix}^\top$
UAV-4	$\begin{bmatrix}300 & 300 & -50\end{bmatrix}^\top$	$\begin{bmatrix}-20 & -20 & 0\end{bmatrix}^\top$
UAV-5	$\begin{bmatrix}300 & 200 & -50\end{bmatrix}^\top$	$\begin{bmatrix}-20 & 20 & 0\end{bmatrix}^\top$
UAV-6	$\begin{bmatrix}-100 & 300 & -50\end{bmatrix}^\top$	$\begin{bmatrix}-30 & -30 & 0\end{bmatrix}^\top$
UAV-7	$\begin{bmatrix}0 & 100 & -50\end{bmatrix}^\top$	$\begin{bmatrix}-30 & 30 & 0\end{bmatrix}^\top$
UAV-8	$\begin{bmatrix}100 & 0 & -200\end{bmatrix}^\top$	$\begin{bmatrix}-40 & -40 & 0\end{bmatrix}^\top$
UAV-9	$\begin{bmatrix}0 & -100 & -200\end{bmatrix}^\top$	$\begin{bmatrix}-40 & 40 & 0\end{bmatrix}^\top$
UAV-10	$\begin{bmatrix}-100 & 0 & -200\end{bmatrix}^\top$	$\begin{bmatrix}-50 & -50 & 0\end{bmatrix}^\top$
UAV-11	$\begin{bmatrix}-100 & -100 & -200\end{bmatrix}^\top$	$\begin{bmatrix}-50 & 50 & 0\end{bmatrix}^\top$

with a speed of 50 m/s at an height of $z_d = 100$ m. Since $\ddot{\mathbf{p}}_l^n = \mathbf{0}$, it follows that both the angular velocity and acceleration of the leader relative to the NED frame is zero, simplifying the trajectories. Even though the following simulation only considers tracking a straight line, the proposed approach can easily be applied to any trajectory defined through $\mathbf{p}_l^n, \dot{\mathbf{p}}_l^n, \ddot{\mathbf{p}}_l^n, \dddot{\mathbf{p}}_l^n \in \mathcal{L}_\infty$.

The UAVs start in the positions as shown in Table 4.2, and converge to the rigid formation as shown in Figure 4.12. In Figure 4.12, the red line represents the trajectory of the virtual leader, while the final positions of the UAVs are shown as red circles. Due to the scale on the $\mathbf{y}^u$ axis, an additional plot is required to study the relative positions between the UAVs as shown in Figure 4.13 where the UAVs enter a V-formation enabling them to exploit the aerodynamic advantages and thereby increasing their operational radius. A visualization of the formation is shown in Figure 4.14 where both the position and attitude at the end of the simulation are visualized. Note that collisions between the UAVs are not considered in this simulation, but methods such as the null-space based behavioral control (Antonelli *et al.* (2005*b*)), subsumption theory (Brooks (1986)) or using potential fields (Khatib (1986)) can be used to ensure that the UAVs perform a collision free reconfiguration.

4.4 Summary

In this chapter, solutions to the problem of waypoint tracking, trajectory tracking and formation flight have been proposed and simulations have been performed to validate the proposed methods. The main observation of this chapter is that guidance of a vehicle is simply a mapping of the errors from the unactuated states to the actuated states which can be driven to zero by applying any of the control laws from Chapter 3.

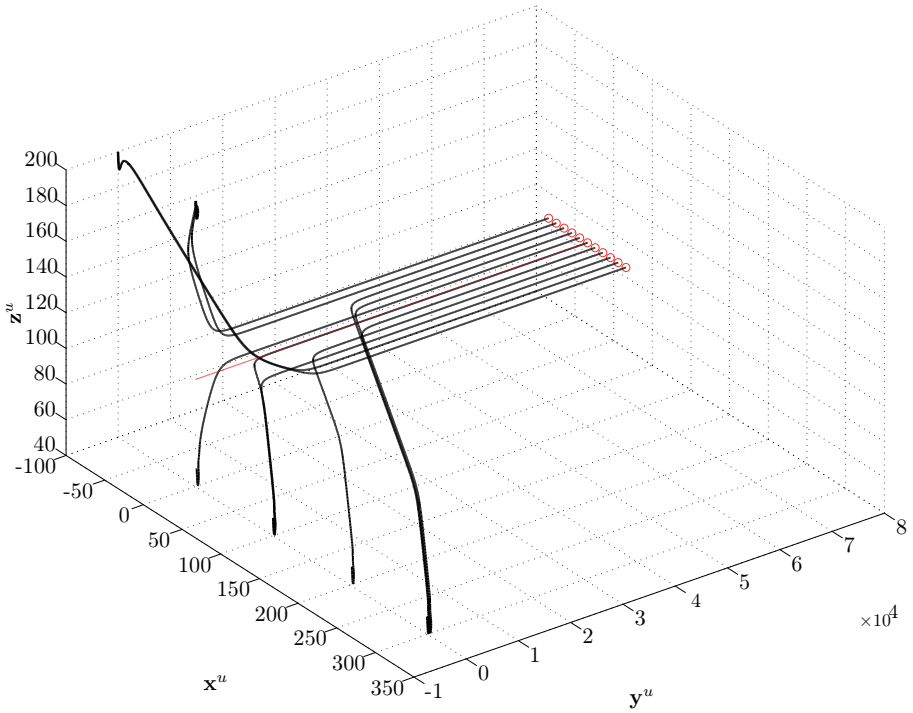

Figure 4.12: Formation flight in 3D.

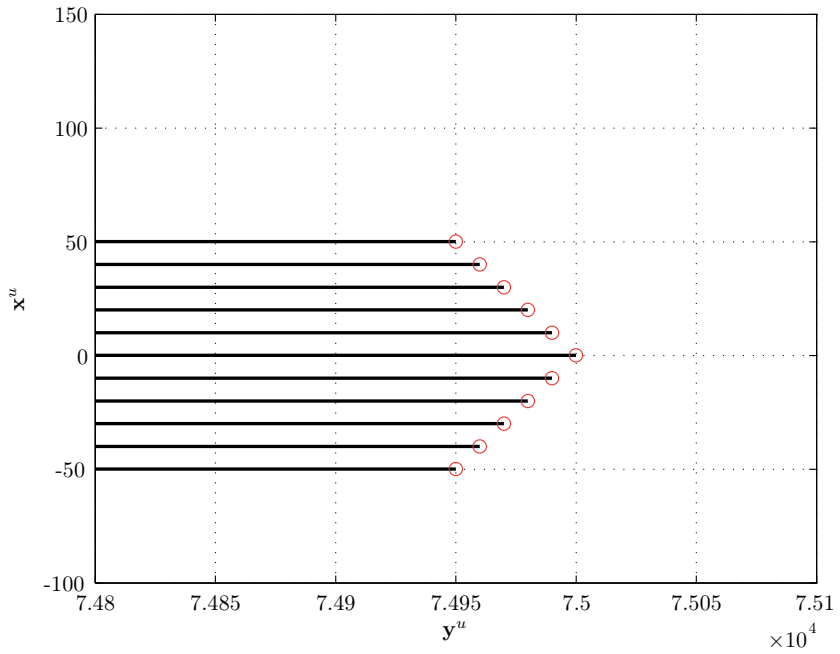

Figure 4.13: Rigid formation. The followers track the virtual leader with constant displacement vectors and enter into a V-formation which enable them to exploit the aerodynamic drag reduction.

Figure 4.14: Eleven UAVs flying in a V-formation (visualization by Tom Stian Andersen).

Chapter 5

Subsumption Architecture

> Planning is just a way of avoiding figuring out what to do next.
>
> Rodney Brooks, 1987

This chapter is based on Oland *et al.* (2014*b*) and applies the subsumption architecture to flight control through composite rotations where multiple tasks are defined as simple rotations. The approach ensures that the primary task is always fulfilled, and conflicting lower level tasks are removed by the primary rotation. The method is applied to a group of UAVs that must fly through a city without colliding with each other, the buildings nor the ground, while tracking a desired waypoint. The generality of the presented solution enables any number of tasks to be defined as simple rotations that are multiplied together producing a desired orientation.

5.1 Subsumption Architecture

To facilitate the design of a truly autonomous agent, the controller must enable the agent to perform multiple tasks in a complex dynamic environment. The layered approach to behavioral control is presented in Brooks (1986), where multiple tasks are arranged in a hierarchy and where higher level tasks subsumes lower level tasks. This ensures that the primary task is always fulfilled, while the lower level tasks are performed as the higher level tasks are completed. This layered structure enables the complex problem of behavioral control to be defined as several simple tasks that are handled using subsumption. By adding an additional layer, the competence of the agent is further augmented, increasing the apparent level of intelligence.

The basic idea has resulted in the null-space-based behavioral (NSB) control method as presented in Antonelli *et al.* (2005*b*), Arrichiello (2006) and Arrichiello *et al.* (2006*b*). The NSB method adheres to the principle of layered control, where multiple tasks can be defined as individual velocity vectors and arranged in a hierarchy where higher level tasks subsume lower level tasks. The subsumption is done by projecting conflicting lower level velocity components onto the nullspace,

thereby removing them from the resulting reference velocity vector. By following the reference velocity vector, the primary task will always be fulfilled.

When controlling a fixed-wing UAV, the use of a reference velocity vector is not directly applicable since the UAV is underactuated with only translational control in one direction. Instead of defining the tasks as velocity vectors, it is possible to design them directly as rotations that are multiplied together, producing a reference orientation that ensures that the primary task is always fulfilled.

The work presented in this chapter can be seen as an extension of the subsumption and the NSB approach, where conflicting lower level rotations are removed by the higher level rotations. Similarly as for the NSB approach, this framework only removes the conflicting parts of the lower level rotations such that *e.g.* a UAV will move toward the next waypoint while avoiding obstacles.

5.2 Layered Control

The subsumption architecture is based on a set of layers, where higher level layers subsume lower level layers. With this approach the highest active task is first pursued subsuming lower level tasks. As the highest active task is completed, the second highest task will be fully pursued and so on until the lowest level task is fully pursued. The tasks enter the system through the desired quaternion, and by designing composite rotations, each layer can be represented by a simple rotation, where the desired quaternion is a product of multiple tasks arranged in a hierarchy. For unmanned aerial vehicles, the most important task is to avoid hitting the ground, and this can be design as the primary rotation. Moving through the air at low altitudes, there can be both static and dynamic obstacles that must be avoided. This can be handled by adding an additional layer of competence which enables collision avoidance through a secondary rotation. A third layer can be added to enable the UAV to move to a desired waypoint through a tertiary rotation. These three tasks can be arranged in a hierarchy as shown in Figure 5.1 and represented using quaternions as

- Task 1: Ground avoidance, $\mathbf{q}_{c,h}$
- Task 2: Collision avoidance, $\mathbf{q}_{e,c}$
- Task 3: Waypoint tracking, $\mathbf{q}_{n,e}$

where e denotes the position error frame, c denotes the collision avoidance frame and h denotes the ground avoidance frame. The individual tasks can be written as a composite rotation with the corresponding angular velocity vector as

$$\mathbf{q}_{n,h} = \mathbf{q}_{n,e} \otimes \mathbf{q}_{e,c} \otimes \mathbf{q}_{c,h} \tag{5.1}$$

$$\boldsymbol{\omega}^h_{n,h} = \mathbf{R}^h_e \boldsymbol{\omega}^e_{n,e} + \mathbf{R}^h_c \boldsymbol{\omega}^c_{e,c} + \boldsymbol{\omega}^h_{c,h}. \tag{5.2}$$

Note that the collision avoidance quaternion is defined relative to the position error frame: that is, the output of the tertiary rotation. Similarly, the ground avoidance is defined relative to the collision avoidance frame. This enables higher level tasks to subsume lower level tasks, such that when the ground avoidance quaternion

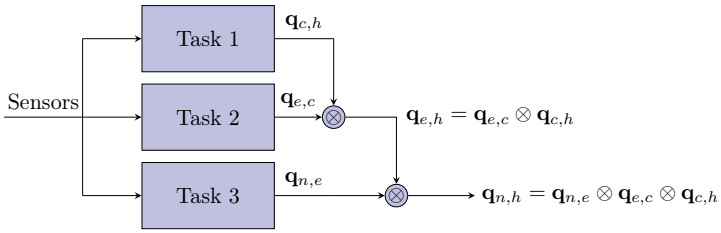

Figure 5.1: Layered control using composite rotations.

is active, the conflicting lower level rotations will be removed. Consider the case when the ground avoidance and waypoint tracking quaternions are active, while the collision avoidance quaternion is inactive. Then $\mathbf{q}_{e,c} = \begin{bmatrix} 1 & 0 & 0 & 0 \end{bmatrix}^\top$ resulting in the reference quaternion $\mathbf{q}_{n,h} = \mathbf{q}_{n,e} \otimes \mathbf{q}_{e,c} \otimes \mathbf{q}_{c,h} = \mathbf{q}_{n,e} \otimes \mathbf{q}_{c,h}$ such that the collision avoidance quaternion does not contribute to the reference. This structure enables several tasks to be defined, where it is only the active quaternions that contribute to the resulting reference quaternion.

Remark 5.1 *It is also possible to define all the rotations relative to the* NED *frame and switch between them, but then the subsumption property will be lost. Also note that this can result in an averaged desired rotation that can lead to a collision.*

Remark 5.2 *Consider the case where the position error quaternion $\mathbf{q}_{n,e}$ is represented by a desired course and flight path angle and where the collision avoidance quaternion $\mathbf{q}_{e,c}$ only performs course corrections. Then, using this framework, it is only the course that is subsumed by the collision avoidance method, enabling the* UAV *to still track the desired flight path angle. This shares similarities with the* NSB *approach where it is only conflicting velocity components that are removed.*

5.2.1 Position Error Frame

From Figure 5.2 the position tracking error can be defined as $\mathbf{e}^n = \mathbf{p}^n_{wp} - \mathbf{p}^n$ where $\mathbf{p}^n_{wp}$ is the position of a desired waypoint. The position error frame can be defined through the relation $\mathbf{e}^e = \begin{bmatrix} ||\mathbf{e}^n|| & 0 & 0 \end{bmatrix}^\top = \mathbf{R}^e_n \mathbf{e}^n$, where the rotation matrix $\mathbf{R}^e_n$ can be constructed using quaternions resulting in $\mathbf{q}_{n,e}$ and is similar to the waypoint algorithm as presented in Lemma 4.1.

5.2.2 Collision Avoidance Frame

From Figure 5.2 the position error between the UAV and an obstacle, $\mathbf{p}^n_o$, can be defined as $\mathbf{c}^n = \mathbf{p}^n_o - \mathbf{p}^n$. The collision avoidance frame can be defined through the relation $\mathbf{c}^c = \begin{bmatrix} 0 & \pm||\mathbf{c}^e|| & 0 \end{bmatrix}^\top = \mathbf{R}^c_e \mathbf{R}^e_n \mathbf{c}^n$ where the rotation matrix $\mathbf{R}^c_e$ can be constructed using quaternions resulting in $\mathbf{q}_{e,c}$. By aligning the wind frame with the collision avoidance frame, the UAV will move perpendicular to the line of

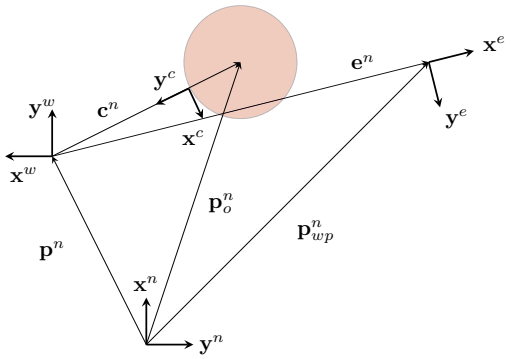

Figure 5.2: Position vectors relative to the NED frame. In the case of waypoint tracking, the objective is to align the wind frame with the position error frame which will make the position error go towards zero. In the case of collision avoidance, the objective is to align the wind frame with the collision avoidance frame, resulting in a circular motion around obstacles. By combining the two quaternions, it is possible to move to a desired waypoint without collision.

sight vector to the obstacle, and thereby avoid collision. Note that the sign of the collision avoidance frame can be chosen arbitrarily, which can be used to move left or right around an obstacle.

5.2.3 Ground Avoidance

Following a similar procedure as for the collision avoidance frame, let the closest point on the ground be denoted $\mathbf{p}_g^n$, and an error function as $\mathbf{h}^n = \mathbf{p}_g^n - \mathbf{p}^n$. The ground avoidance frame can then be defined using the relation $\mathbf{h}^h = \begin{bmatrix} 0 & 0 & ||\mathbf{h}^c|| \end{bmatrix}^\top = \mathbf{R}_c^h \mathbf{R}_e^c \mathbf{R}_n^e \mathbf{h}^n$, where $\mathbf{R}_c^h$ can be constructed using quaternions resulting in $\mathbf{q}_{c,h}$.

5.2.4 Detection Box

The performance of any collision avoidance method is naturally constrained by the method of detecting obstacles. Using only the relative distance to an obstacle is dangerous, since a high negative relative velocity may result in collision as the UAV is unable to avoid the given obstacle in time. Furthermore, the actuator constraints of a fixed-wing UAV leads to maneuverability constraints that must be taken into account. Inspired by Borenstein and Koren (1991), let a detection box be fixed with the wind frame of the UAV as shown in Figure 5.3. Then the objective of the UAV is to maneuver the detection box such that it avoids obstacles. If an obstacle is detected, the UAV checks on which side the obstacle is detected, and simply maneuvers left if the obstacle is on the right side, and to the right otherwise. A

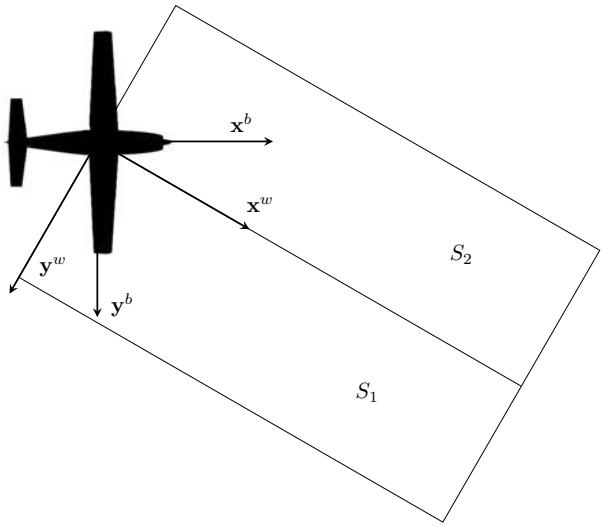

Figure 5.3: Detection box in the xy-plane. When detecting obstacles in sector S_1, the UAV will turn to the left, and if it detects an obstacle in sector S_2 it will turn to the right which is done by defining the sign of the collision avoidance frame.

similar method can be applied for ground avoidance, where the UAV pulls up if it detects the ground. This idea corresponds well with how birds navigate, who use cues from image motions that are generated during flight to detect obstacles. In Bhagavatula *et al.* (2011) the authors show that birds are able to navigate through narrow gaps by balancing the image motions that are experienced by each eye, and use that as a sensory information to avoid collisions. If the image motion on the right eye is faster than on the left eye, they change their orientation to balance the images, which relates to that of changing the detection box depending on which side the obstacle is detected.

Property 5.1 *When no obstacles are within the detection box,* $\mathbf{q}_{e,c}$ *is set equal to the identity quaternion, and* $\boldsymbol{\omega}^c_{e,c}$ *is set equal to zero. This also applies for the ground avoidance quaternion and angular velocity.*

Remark 5.3 *This detection box only considers obstacles in front of the* UAV*, but it can be extended to consider obstacles behind the* UAV*. This can allow better cooperation between the* UAV*s, as they can help each-other by reducing the risk of collision by increasing the relative distance.*

5.3 Composite Quaternion Rotations

In the following, each of the individual quaternions are derived with their corresponding angular velocities and then put together resulting in a desired quaternion and angular velocity that ensures that the primary task will always be fulfilled. The waypoint algorithm in Lemma 4.1 can be used to design the quaternion $\mathbf{q}_{n,e}$ and the angular velocity $\boldsymbol{\omega}^e_{n,e}$. Using a similar approach as for the waypoint algorithm, the collision avoidance and ground avoidance quaternions can be constructed as shown in the following lemmas:

Lemma 5.1 *Let Assumptions 2.2 and 4.1 hold. Given the position error between the closest obstacle and the* UAV *as* $\mathbf{c}^e = \mathbf{R}^e_n(\mathbf{p}^n_o - \mathbf{p}^n)$*, and by following the attitude and angular velocity*

$$\mathbf{q}_{e,c} = \begin{bmatrix} \cos\left(\frac{\vartheta_{e,c}}{2}\right) & \mathbf{k}^\top_{e,c} \sin\left(\frac{\vartheta_{e,c}}{2}\right) \end{bmatrix}^\top \tag{5.3}$$

$$\boldsymbol{\omega}^c_{e,c} = \mathbf{S}^\dagger(\mathbf{c}^c)(\mathbf{R}^c_e \mathbf{S}(\boldsymbol{\omega}^e_{n,e})\mathbf{R}^e_n \mathbf{c}^n - \mathbf{R}^c_n \dot{\mathbf{c}}^n) \tag{5.4}$$

$$\vartheta_{e,c} = \cos^{-1}\left(\frac{\mathbf{c}^c \cdot \mathbf{c}^e}{||\mathbf{c}^e||^2}\right) \quad \mathbf{k}_{e,c} = \frac{\mathbf{c}^c \times \mathbf{c}^e}{||\mathbf{c}^c \times \mathbf{c}^e||} \tag{5.5}$$

$$\mathbf{c}^c = \begin{bmatrix} 0 & \pm||\mathbf{c}^e|| & 0 \end{bmatrix}^\top = \mathbf{R}^c_e \mathbf{R}^e_n \mathbf{c}^n = \mathbf{R}^c_e \mathbf{c}^e, \tag{5.6}$$

then $||\mathbf{c}^c|| \geq \beta_c > 0 \ \forall t \geq t_0$.

Proof. The proof is given in Appendix E.23. ■

Remark 5.4 *Note that* $||\boldsymbol{\omega}^c_{e,c}|| \to \infty$ *as* $||\mathbf{c}^n|| \to 0$*, which will produce an angular velocity that will saturate the rotational control law. For waypoint guidance, this property is undesirable, but for collision avoidance it is a desirable property. By tracking the angular velocity, the actuators will go into saturation such that the* UAV *makes its best effort to avoid the obstacle. In many ways it shares the same properties as with potential fields (cf. Khatib (1986)) that go to infinity as the relative distance between an agent and an obstacle approaches zero.*

Lemma 5.2 *Let Assumptions 2.2 and 4.1 hold. Given the position error between the closest point on the ground and the* UAV *as* $\mathbf{h}^c = \mathbf{R}^c_e \mathbf{R}^e_n \mathbf{h}^n = \mathbf{R}^c_n(\mathbf{p}^n_g - \mathbf{p}^n)$*, and by following the attitude and angular velocity*

$$\mathbf{q}_{c,h} = \begin{bmatrix} \cos\left(\frac{\vartheta_{c,h}}{2}\right) & \mathbf{k}^\top_{c,h} \sin\left(\frac{\vartheta_{c,h}}{2}\right) \end{bmatrix}^\top \tag{5.7}$$

$$\boldsymbol{\omega}^h_{c,h} = \mathbf{S}^\dagger(\mathbf{h}^h)(\mathbf{R}^h_c \mathbf{S}(\boldsymbol{\omega}^c_{e,c})\mathbf{R}^c_n \mathbf{h}^n + \mathbf{R}^h_e \mathbf{S}(\boldsymbol{\omega}^e_{n,e})\mathbf{R}^e_n \mathbf{h}^n - \mathbf{R}^h_b \dot{\mathbf{h}}^n) \tag{5.8}$$

$$\vartheta_{c,h} = \cos^{-1}\left(\frac{\mathbf{h}^h \cdot \mathbf{h}^c}{||\mathbf{h}^c||^2}\right) \quad \mathbf{k}_{c,h} = \frac{\mathbf{h}^h \times \mathbf{h}^c}{||\mathbf{h}^h \times \mathbf{h}^c||} \tag{5.9}$$

$$\mathbf{h}^h = \begin{bmatrix} 0 & 0 & ||\mathbf{h}^c|| \end{bmatrix}^\top = \mathbf{R}^h_c \mathbf{R}^c_e \mathbf{R}^e_n \mathbf{h}^n = \mathbf{R}^h_c \mathbf{h}^c, \tag{5.10}$$

then $||\mathbf{h}^h|| \geq \beta_h > 0 \ \forall t \geq t_0$.

Proof. The proof is given in Appendix E.24. ■

Remark 5.5 *The lower bounds β_c and β_h are functions of initial speed, detection range, actuator constraints and the rotational control law. Hence, it is important to design the detection range to account for this, to ensure collision free trajectories.*

Theorem 5.1 *Let Assumptions 2.2 and 4.1 hold. By following the attitude and angular velocity (5.1)-(5.2) where the terms are given in lemmas 4.1, 5.1 and 5.2, then $||\mathbf{c}^c|| \geq \beta_c > 0, ||\mathbf{h}^h|| \geq \beta_h > 0 \ \forall t \geq t_0$ and $||\mathbf{e}^e|| \to \mathcal{H}(\delta, \Delta)$.*

Proof. The proof is given in Appendix E.25. ■

Remark 5.6 *The proposed approach enables collision avoidance by mapping the position errors in the $\mathbf{y}^n$ and $\mathbf{z}^n$ axes to desired orientations that result in a collision-free path. This can be extended to path following, by encompassing a virtual tube around a desired path. Instead of defining the objective as that of following the path, the objective can be defined as avoiding the walls of the virtual tube, and hence collision avoidance can be used to perform path following.*

5.3.1 Wind Compensation

Assumption 4.1 can be removed similarly as for the waypoint guidance method as shown in Section 4.1, but where the notation of the quaternion must be changed in order to fit into this framework. Let the wind correction angle be redefined as $\vartheta_{h,d}$ which is the angle between $\mathbf{v}^b$ and $\mathbf{v}_r^b$. The wind correction quaternion can thereby be designed as

$$\mathbf{q}_{h,d} = \begin{bmatrix} \cos\left(\frac{\vartheta_{h,d}}{2}\right) & \mathbf{k}_{h,d}^\top \sin\left(\frac{\vartheta_{h,d}}{2}\right) \end{bmatrix}^\top \tag{5.11}$$

$$\vartheta_{h,d} = \cos^{-1}\left(\frac{\mathbf{v}^b \cdot \mathbf{v}_r^b}{||\mathbf{v}^b||\ ||\mathbf{v}_r^b||}\right) \quad \mathbf{k}_{h,d} = \frac{\mathbf{v}^b \times \mathbf{v}_r^b}{||\mathbf{v}^b \times \mathbf{v}_r^b||} \tag{5.12}$$

which compensates for the wind. The angular velocity and acceleration are found using linear filters with saturation.

5.3.2 Desired Orientation

The tasks from the subsumption architecture defined through (5.1) and (5.2) together with wind compensation produce the desired quaternion and angular velocity as

$$\mathbf{q}_{n,d} = \mathbf{q}_{n,e} \otimes \mathbf{q}_{e,c} \otimes \mathbf{q}_{c,h} \otimes \mathbf{q}_{h,d} \tag{5.13}$$

$$\boldsymbol{\omega}_{n,d}^d = \mathbf{R}_e^d \boldsymbol{\omega}_{n,e}^e + \mathbf{R}_c^d \boldsymbol{\omega}_{e,c}^c + \mathbf{R}_h^d \boldsymbol{\omega}_{c,h}^h + \boldsymbol{\omega}_{h,d}^d \tag{5.14}$$

which also shows the extendability of the proposed approach. The addition of a new task is simply done by expanding the quaternion product, and where the resulting angular velocity is found by adding an additional term.

Lemma 5.3 *$\mathbf{q}_{n,d}$, $\boldsymbol{\omega}_{n,d}^d$ and $\dot{\boldsymbol{\omega}}_{n,d}^d$ are bounded.*

Proof. The proof is given in Appendix E.26. ■

Remark 5.7 *The rotations that have been derived in this section are based on the position errors between a* UAV *and obstacles/ground. It is therefore only possible to prove stability for stationary obstacles. Even though this is remedied by using the detection box, the desired orientations can instead be designed at a velocity level using the mapping methods from Section 4.2.2 which can enable dynamic obstacles to be avoided.*

5.4 Simulation

Each UAV has the following initial conditions: $\mathbf{q}_{n,b}(0) = \begin{bmatrix}1 & 0 & 0 & 0\end{bmatrix}^\top$, $\boldsymbol{\omega}^b_{n,b} = \begin{bmatrix}0 & 0 & 0\end{bmatrix}^\top$ rad/s, $\mathbf{v}^b(0) = \begin{bmatrix}30 & 0 & 0\end{bmatrix}^\top$ m/s, $V_d = 25$ m/s and are exposed to a constant wind vector $\mathbf{w}^n = \begin{bmatrix}3 & 0 & 0\end{bmatrix}^\top$ m/s. For the simulation, the PD+ controller (3.14) and the proportional airspeed controller (3.37) are used, where the gains are chosen as $k_q = 10$, $k_\omega = 20$ and $\kappa_p = 2$. The detection box measures 150 m in length, and each sector has a width of 10 m and a height of 40 m. To facilitate collision avoidance between the UAVs, each UAV are encompassed with a protective sphere with radius of 5 m. If the detection box of a UAV detects a point on the protective sphere from any of other the UAVs, the current UAV will maneuver to avoid collision.

5.4.1 Urban Avoidance

Consider seven UAVs that shall track a desired waypoint $\mathbf{p}^n_{wp} = \begin{bmatrix}2000 & 500 - 50\end{bmatrix}^\top$ m while moving through a city. During the maneuver, the UAVs must avoid colliding with each other, the buildings and the ground.

Figure 5.4 shows the 2D plot of the simulation where the UAVs move through the city without collision. The altitudes of the UAVs are shown in the top plot of Figure 5.5. Initially none of the UAVs are trimmed (at steady state), such that they will start to loose altitude. This makes the detection box point toward the ground such that the ground avoidance maneuver is initiated and the ground is avoided. Also note that none of the UAVs go below 40 m, which is the height of the detection box. The middle plot of Figure 5.5 shows the relative distances between the UAVs and the buildings. No UAVs come closer than 10 m, except UAV-4, which comes as close as about 8 m, before diverging from the building. The bottom plot shows the shortest distances between the UAVs, where none come closer than 10 m, and therefore no collisions have occurred. The position tracking error of all the UAVs are shown in Figure 5.6. Figure 5.7 shows the attitude dynamics of UAV-4, where the attitude and angular velocity errors go to zero, but contain several spikes throughout the simulation. These spikes are a result of the collision and ground avoidance methods which produce changes in the reference as obstacles are detected. Also note that the deflection angles go into saturation at about 19 seconds, which contribute to the fact that UAV-4 comes closer to the building than 10 m. The speed error and thrust are shown in Figure 5.8. Note the spike at about 19 seconds, which is due to the saturation of the thrust as UAV-4 moves downwards.

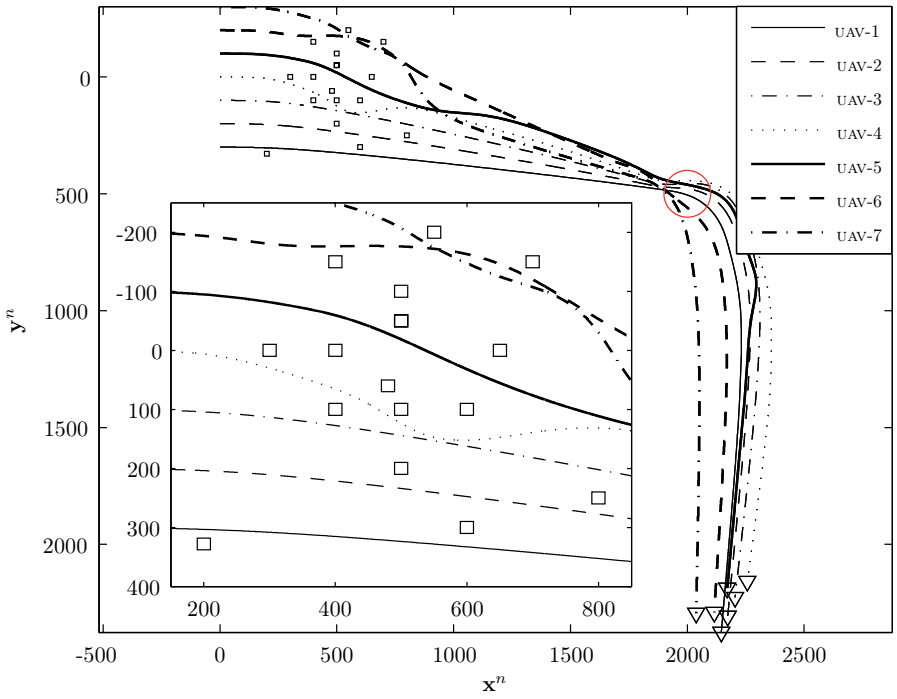

Figure 5.4: Obstacle avoidance in urban terrain where the first waypoint is shown as a red circle, the buildings are illustrated as rectangles and the final positions of the UAVs at t = 150s are shown as triangles.

5.4.2 Terrain Avoidance

The same method can be applied for terrain avoidance. Consider a fixed-wing UAV that shall avoid the ground and a radio tower located on the top of a mountain. A desired waypoint is located on the other side of the tower, and the UAV must avoid both the ground and the tower. The tower is represented as a cubic building similar as for urban avoidance, while the mountain is generated using a paraboloid representing the top of the mountain. Using the same method as for urban avoidance, the UAV is able to follow the terrain, while maneuvering around the tower as shown in Figure 5.9. No collision has occurred as shown in Figure 5.10 where the relative distance between the UAV and the mountain or the radio tower never goes below 41 m.

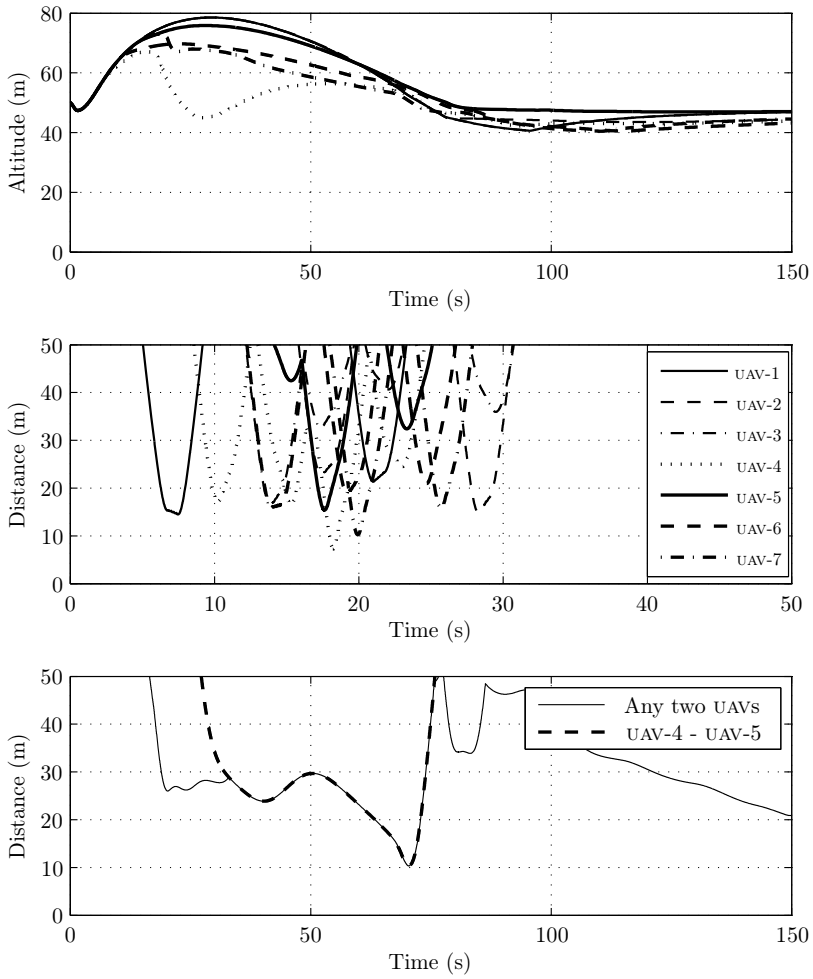

Figure 5.5: Top: altitude of each UAV. Middle: shortest distance to building. Bottom: shortest distance between any two UAVs. The same legend applied to both the top and middle plot.

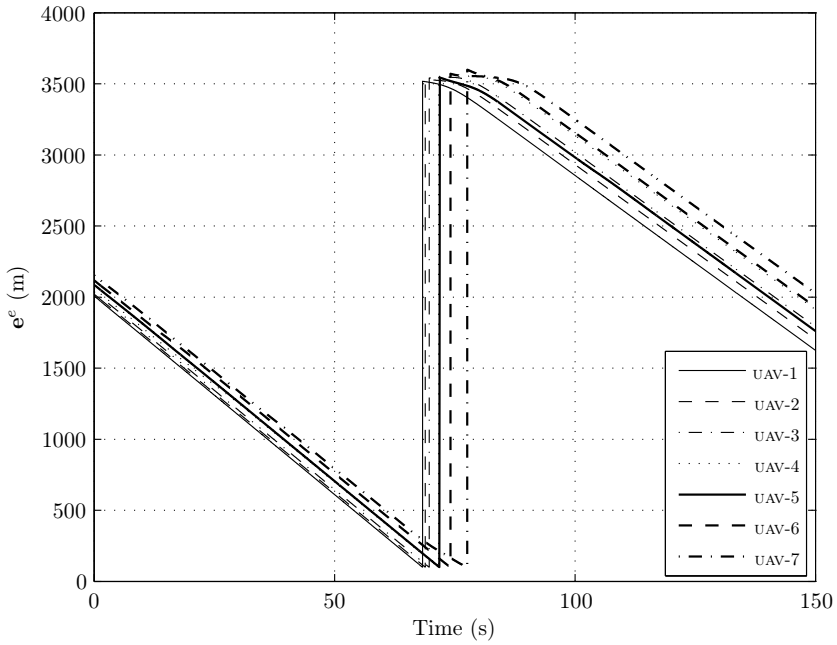

Figure 5.6: Position tracking errors.

5.5 Discussion

The problem of collision avoidance has received much attention the last decades and the most well known approach is the use of potential fields as presented in Khatib (1986). By encompassing repulsive potentials around obstacles and an attractive potential around the desired position, it enables an agent to reach the desired position without collisions by following the negative gradient of the total potential field. Even though the approach is intuitively simple and appealing, it suffers from several problems such as local minima, inability to pass through narrow gaps, and the possibility of becoming trapped as shown in Koren and Borenstein (1991). These facts motivated further research and resulted in the navigation function by Rimon and Koditschek (1992) which addresses the local minima problem, and has later has been extended to nonholonomic vehicles in Tanner *et al.* (2003) and applied for nonholonomic aircraft-like vehicles in Roussos *et al.* (2010). The problems that were pointed out in Koren and Borenstein (1991) are applicable to many of the local collision avoidance methods. As such, they deserve special attention. In this chapter, a detection box is applied for obstacle detection, similar to the vector histogram as proposed in Borenstein and Koren (1991), which enables an agent to

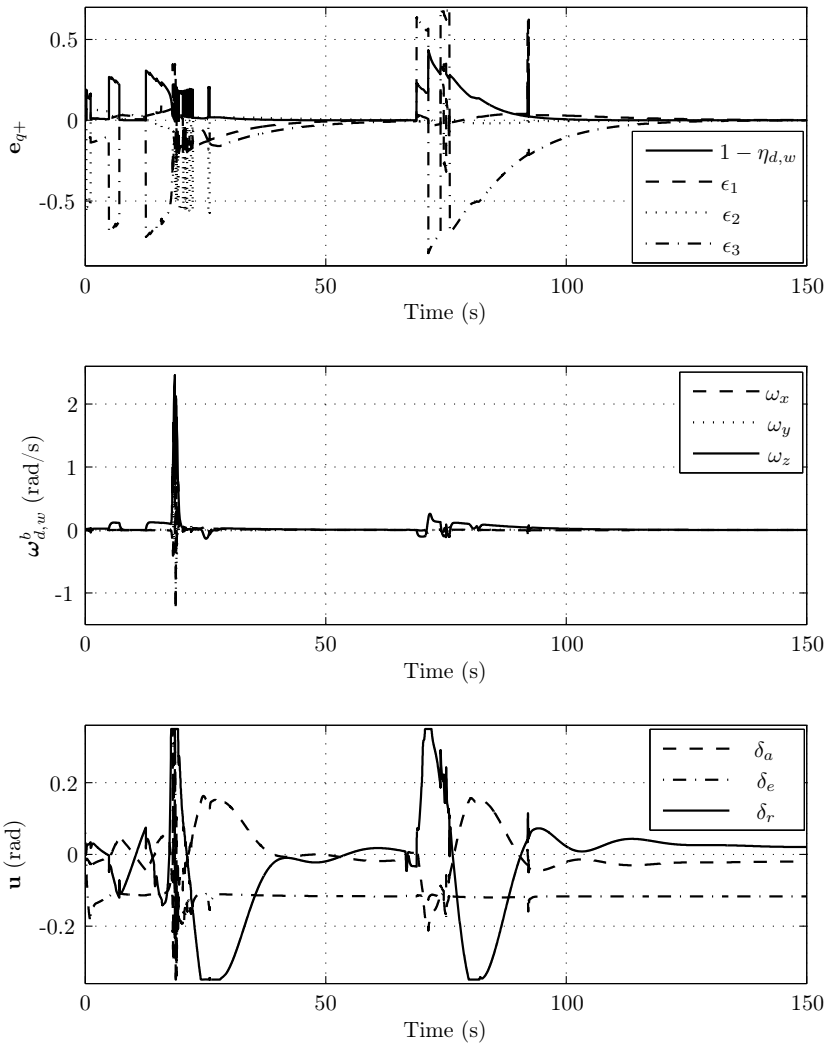

Figure 5.7: Rotational dynamics of UAV-4.

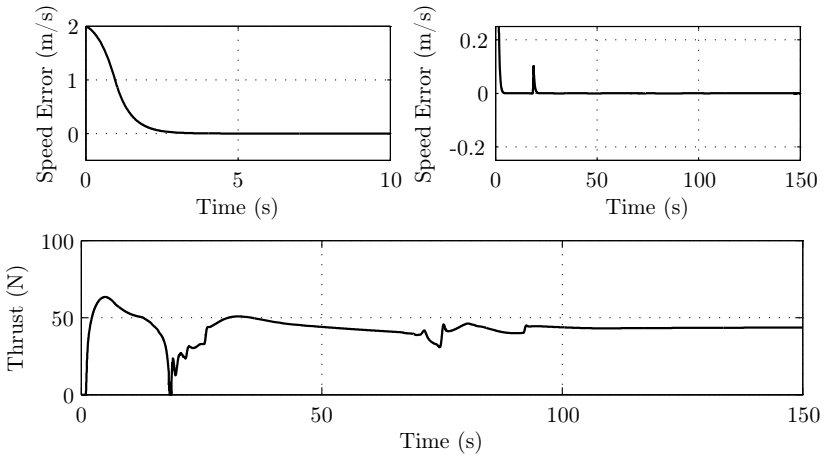

Figure 5.8: Speed error and thrust of UAV-4.

Figure 5.9: Terrain avoidance (visualization by Tom Stian Andersen).

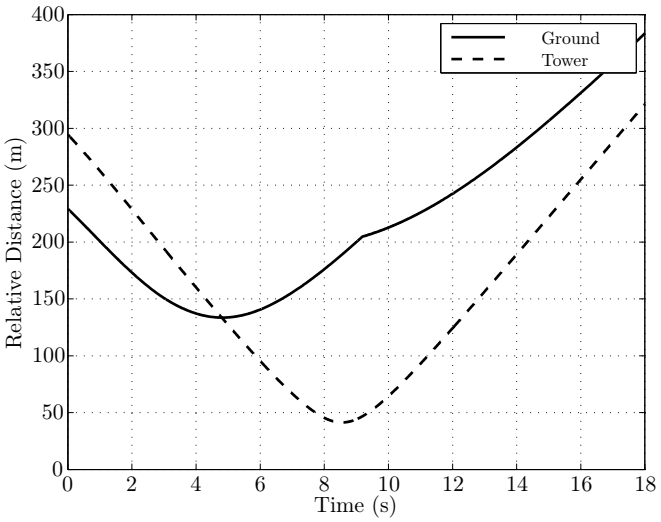

Figure 5.10: Relative distance to the the ground and the radio tower.

pass through narrow gaps. Furthermore, the subsumption architecture facilitates an arbitrary number of layers, and as such, even though it is not implemented here, it is possible to add an addition layer that serves as a global navigation function that defines no-fly-zones wherever an agent can become trapped. This highlights some of the possibilities that exist when using this framework.

5.6 Summary

In this chapter the problem of maneuvering in a complex dynamical environment has been solved using the subsumption architecture. Multiple tasks can be defined as simple rotations that are multiplied together producing a desired quaternion. The architecture ensures that the primary task will always be completed while lower level tasks will be fully pursued as higher level tasks are completed. The presented approach has been validated through simulations where the UAVs performed tasks such as collision avoidance, ground avoidance and waypoint tracking.

Chapter 6

Conclusion

This thesis has presented several solutions to the problem of flight control of fixed-wing unmanned aerial vehicles in a quaternion framework. From the basic notion that it is the speed that must be pointed in a desired direction, the translational and rotational systems were decoupled by employing a linear filter to find the higher order derivatives of the angle of attack and the sideslip angle. This decoupling enabled a rotational controller to be derived first, followed by a speed controller. To that end, several quaternion-based controllers were derived based on the Paden and Panja PD+ controller, the sliding surface controller and a regular and an adaptive backstepping controller. For speed control, both a proportional and a proportional-integral model-based controller were derived to enable the UAV to obtain a desired airspeed. The result was also improved using adaptive control in the presence of actuator saturation using a reference to move the saturation problem from the plant to the reference. Another important observation is that the airspeed directly affects the magnitude of the rotational control laws. A reference airspeed was therefore designed that enables a virtual bound to be placed on the deflection angles such that given sufficient thrust, the deflection angles remain within their linear regions and actuator saturation can be avoided.

Fixed-wing UAVs are underactuated, such that several guidance laws had to be derived in order to make the errors along the unactuated axes go to zero. First a waypoint guidance scheme was presented that mapped all the position tracking errors to one axis producing a desired quaternion and angular velocity. By moving with a positive speed and tracking the quaternion and angular velocity, a desired waypoint will be reached in finite time. This idea was then extended to trajectory tracking using a virtual saturated translational controller to make the position and velocity tracking errors go to zero. These errors were then mapped to desired states that the control laws could track, making the position and velocity errors go to zero. With the possibility of performing trajectory tracking, the approach was further augmented to enable formation flight where a formation of UAVs were shown to move in a V-formation to enable them to exploit the drag reduction that is possible using close formations.

Another important observation is that it is possible to define multiple tasks as composite rotations. This enabled the subsumption architecture to be applied for

flight control which can enable autonomous vehicles to behave more intelligently. Specifically, the approach was applied to a group of UAVs that had to perform waypoint tracking while avoiding collisions with each other, the ground and a number of buildings. The approach was also applied to a single UAV performing terrain avoidance. The subsumption architecture applied for flight control using composite rotations has a good potential to increase the overall autonomy of fixed-wing UAVs, and can be a first step towards truly autonomous unmanned aerial vehicles.

6.1 Future Work

6.1.1 Rate Saturation

One of the main delimitations of this thesis is that rate saturation has not been accounted for. It is believed that it should have relatively little impact on the derivation of the control laws, but the fact that it enables the angular acceleration $\dot{\boldsymbol{\omega}}_{b,w}^{w}$ to become bounded is a very attractive feature that is worth future research.

6.1.2 Observer-based Decoupling

Another aspect that should be augmented is the way that the higher order derivatives of the angle of attack and sideslip are found. In this thesis a simple linear filter is applied, which for some cases might be too slow to converge to the true values. A high gain observer or another approach should be studied to see if it is possible to obtain increased performance. For example, consider using a Kalman filter to estimate the position, velocity, acceleration and jerk. Then the angle of attack and sideslip can be found from the velocity vector, the angular rates from the acceleration vector and the angular accelerations from the jerk vector. The same applies for the wind quaternion that also can be handled more elegantly. Specifically, by improving the estimation of the wind quaternion, it can enable wind gusts to be accounted for, which will improve the presented solutions.

6.1.3 Extending the Quaternion Framework

One of the main contributions of this thesis is the fact that multiple tasks can be defined as simple rotations such that

$$\mathbf{q}_{d,w} = \mathbf{q}_{d,n} \otimes \mathbf{q}_{n,b} \otimes \mathbf{q}_{b,w} \tag{6.1}$$

where the desired quaternion can be expanded with multiple tasks using the subsumption architecture. This thesis has not considered the problem of state estimation such as the attitude and angular velocity of the body relative to the NED frame. This can actually be handled in the same framework by defining $\mathbf{q}_{n,b} := \mathbf{q}_{n,est} \otimes \mathbf{q}_{est,b}$ where $\mathbf{q}_{n,est}$ is a quaternion representing an estimated orientation, while $\mathbf{q}_{est,b}$ is the error between the body orientation and its estimated value. This enables observers to be applied within this framework and multiple new problems can be dealt with in a modular fashion.

6.1.4 Extending the Aerodynamics

In Appendix C an extension of the aerodynamic modeling is discussed. By using the proposed decoupling, there is no limit (from a control perspective) to the number of terms that can be added to the aerodynamics. This enables very accurate aerodynamic models to be applied. An interesting contribution would be to extend the aerodynamics to contain multiple additional terms and use it together with any of the presented control solutions to see if it is possible to obtain aerodynamic models that cover the whole flight envelope.

6.2 Acknowledgements

The 3D visualization of the aircraft in Figures 4.2, 4.3, 4.4 and 4.8 is done using "Trajectory and Attitude Plot Version 3" from Matlab File-Exchange[1] with permission by Valerio Scordamaglia. I would also like to thank the TeXample website[2] that has shared many inspirational visualization aids using the TikZ environment. The airfoil in Figure 1.2 has been created by taking basis in "Airfoil Profiles"[3] by Kjell Magne Fauske.

[1] http://www.mathworks.se/matlabcentral/fileexchange/5656-trajectory-and-attitude-plot-version-3

[2] http://www.texample.net

[3] http://www.texample.net/tikz/examples/airfoil-profiles/

Bibliography

Abdessameud, A. and A. Tayebi (2010). Formation control of VTOL UAVs without linear-velocity measurements. In: *Proceedings of the American Control Conference*. Baltimore, MD, USA.

Aguiar, A. P. and A. M. Pascoal (2002). Dynamic positioning and way-point tracking of underactuated AUVs in the presence of ocean currents. In: *Proceedings of the 41st IEEE Conference on Decision and Control*. Las Vegas, NV, USA.

Aguiar, A. P. and J. P. Hespanha (2007). Trajectory-tracking and path-following of underactuated autonomous vehicles with parametric modeling uncertainty. *Transactions on Automatic Control* **Vol. 52, No. 8**, pp. 1362–1379.

Aguiar, A. P., J. P. Hespanha and P. V. Kokotović (2008). Performance limitations in reference tracking and path following for nonlinear systems. *Automatica* **Vol. 44, No. 3**, pp. 598–610.

Akella, M. R., A. Valdivia and G. R. Kotamraju (2005). Velocity-free attitude controllers subject to actuator magnitude and rate saturations. *Journal of Guidance, Control, and Dynamics* **Vol. 28, No. 4**, pp. 659–666.

Ambrosino, G., M. Ariola, U. Ciniglio, F. Corraro, A. Pironti and M. Virgilio (2006). Algorithms for 3D UAV path generation and tracking. In: *Proceedings of the 45th IEEE Conference on Decision and Control*. San Diego, CA, USA.

Annaswamy, A. M. and J. Wong (1997). Adaptive control in the presence of saturation non-linearity. *International Journal of adaptive control and signal processing* **Vol. 11, No. 3**, pp. 3–19.

Antonelli, G., F. Arrichiello and S. Chiaverini (2005*a*). The null-space-based behavioral control for mobile robots. In: *Proceedings of IEEE International Symposium on Computational Intelligence in Robotics and Automation*. Espoo, Finland.

Antonelli, G., F. Arrichiello and S. Chiaverini (2006). Experiments of formation control with collision avoidance using the null-space-based behavioral control. In: *Proceedings of the Mediterranean Conference on Control and Automation*. Ancona, Italy.

Antonelli, G., F. Arrichiello and S. Chiaverini (2008). The null-space-based behavioral control for autonomous robotic systems. *Journal of Intelligent Service Robotics* **Vol. 1, No. 1**, pp. 27–39.

Antonelli, G., F. Arrichielo and S. Chiaverini (2005*b*). The null-space-based behavioral control for mobile robots. In: *Proceedings of the IEEE International Symposium on Computational Intelligence in Robotics and Automation*. Espoo, Finland.

Arrichiello, F. (2006). Coordination control of multiple mobile robots. PhD thesis. Universitá degli Studi di Cassino, Cassino, Italy.

Arrichiello, F., S. Chiaverini and T.I. Fossen (2006*a*). Formation control of marine surface vessels using the null-space-based behavioral control. In: *Group Coordination and Cooperative Control* (K.Y. Pettersen, T. Gravdahl and H. Nijmeijer, Eds.). Chap. 1, pp. 1–19. Springer-Verlag's Lecture Notes in Control and Information Systems series, ISBN 3-540-33468-8.

Arrichiello, F., S. Chiaverini and T.I. Fossen (2006*b*). Formation control of underactuated surface vessels using the null-space-based behavioral control. In: *Proceedings of the International Conference on Intelligent Robots and Systems*. Beijing, China.

Arrichiello, F., S. Chiaverini, G. Indiveri and P. Pedone (2009). The null-space-based behavioral control for a team of cooperative mobile robots with actuator saturations. In: *Proceedings of the International Conference on Intelligent Robots and Systems*. St. Louis, MO, USA.

Åström, K.J. and L. Rundqwist (1989). Integrator windup and how to avoid it. In: *Proceedings of the American Control Conference*. Pittsburgh, PA, USA.

Baba, Y., M. Yamaguchi and R. M. Howe (1993). Generalized guidance law for collision courses. *Journal of Guidance, Control, and Dynamics* **Vol. 16, No. 3**, pp. 511–516.

Bak, M. (2000). Control systems with constraints. PhD thesis. Technical University of Denmark, Kgs. Lyngby, Denmark.

Beard, R. W. and J. Humpherys (2011). Following straight line and orbital paths with input constraints. In: *Proceedings of the American Control Conference*. San Francisco, CA, USA.

Becker, A., P. R. Kumar and C. Wei (1985). Adaptive control with the stochastic approximation algorithm: Geometry and convergence. *IEEE Transactions on Automatic Control* **Vol. 30, No. 4**, pp. 330–338.

Berghuis, H. and H. Nijmeijer (1993). A passivity approach to controller-observer design for robots. *IEEE Transactions on Robotics and Automation* **Vol 9, No. 6**, pp. 740–754.

Betser, A., P. A. Vela, G. Pryor and A. Tannenbaum (2005). Flying in formation using a pursuit guidance algorithm. In: *Proceedings of the American Control Conference*. Portland, OR, USA.

Bhagavatula, P. S., C. Claudianos, M. R. Ibbotson and M. V. Srinivasan (2011). Optic flow cues guide flight in birds. *Current Biology* **Vol 21, No. 21**, pp. 1794–1799.

Blake, W. (2002). Drag reduction from formation flight - Flying aircraft in bird-like formations could significantly increase range. Technical report. Wright-Patterson Air Force Base, Ohio, USA.

Bloch, A. M., J. Baillieul, P. Crouch and J. Marsden (2007). *Nonholonomic mechanics and control*. Springer, ISBN 978-0-387-95535-3.

Bloch, A. M., N. E. Leonard and J. E. Mardsen (2000). Controlled Lagrangians and the stabilization of mechanical systems I: the first matching theorem. *IEEE Transactions on Automatic Control* **Vol. 45, No. 12**, pp. 2253–2270.

Borenstein, J. and Y. Koren (1991). The vector field histogram - fast obstacle avoidance for mobile robots. *IEEE Transactions on Robotics and Automation* **Vol. 7, No. 3**, pp. 278–288.

Børhaug, E. and K. Y. Pettersen (2005*a*). Adaptive way-point tracking control for underactuated autonomous vehicles. In: *Proceedings of the 44th IEEE Conference on Decision and Control*. Seville, Spain.

Børhaug, E. and K. Y. Pettersen (2005*b*). Cross-track control for underactuated autonomous vehicles. In: *Proceedings of the 44th IEEE Conference on Decision and Control*. Seville, Spain.

Borrelli, F., T. Keviczky and G. J. Balas (2004). Collision-free UAV formation flight using decentralized optimization and invariant sets. In: *Proceedings of the 43rd IEEE Conference on Decision and Control*. Atlantis, Bahamas.

Boulton, M. P. W. (1864). *On aërial locomotion*. London: Bradbury & Evans, 11, Bouviere Street.

Boulton, M. P. W. (1868). Aërial locomotion etcetera. Patent number No. 392.

Boyd, S. and S. S. Sastry (1986). Necessary and sufficient conditions for parameter convergence in adaptive control. *Automatica* **Vo. 22, No. 6**, pp. 629–639.

Breivik, M. and T. I. Fossen (2005). Guidance-based path following for autonomous underwater vehicles. In: *Proceedings of the MTS/IEEE OCEANS*. Washington, DC, USA.

Breivik, M. and T. I. Fossen (2007). Applying missile guidance concepts to motion control of marine craft. In: *Proceedings of the 7th IFAC Conference on Control Applications in Marine Systems*. Bol, Croatia.

Breivik, M. and T. I. Fossen (2008). Guidance laws for planar motion control. In: *Proceedings of the 47th IEEE Conference on Decision and Control*. Cancun, Mexico.

Breivik, M. and T. I. Fossen (2009). Guidance laws for autonomous underwater vehicles, underwater vehicles. In: *Underwater vehicles* (A. V. Inzartsev, Ed.). Chap. 4, pp. 51–76. InTech, ISBN 978-953-7619-49-7.

Brooks, R. A. (1986). A robust layered control system for a mobile robot. *IEEE Journal of Robotics and Automation* **Vol. RA-2, No. 1**, pp. 14–23.

Brooks, R. A. (1990). Elephants don't play chess. *Robotics and Autonomous Systems* **Vol. 6**, pp. 3–15.

Brooks, R. A. (1991*a*). Intelligence without reason. In: *Proceedings of the 12th International Joint Conference on Artificial Intelligence (IJCAI-91)*. Sydney, New South Wales, Australia.

Brooks, R. A. (1991*b*). Intelligence without representation. *Artificial Intelligence* **Vol. 47**, pp. 139–159.

Bullo, F. and K. M. Lynch (2001). Kinematic controllability for decoupled trajectory planning in underactuated mechanical systems. *IEEE Transactions on Robotics and Automation* **Vol. 17, No. 4**, pp. 402–412.

Burdakov, O., P. Doherty, K. Holmberg, J. Kvarnström and P. Olsson (2010). Relay positioning of unmanned aerial vehicle surveillance. *International Journal of Robotics Research* **Vol. 29, No. 8**, pp. 1069–1087.

Campa, G., Y. Gu, B. Seanor, M. R. Napolitano, L. Pollini and M. L. Fravolini (2007). Design and flight-testing of non-linear formation control laws. *Control Engineering Practice* **Vol. 15**, pp. 1077–1092.

Cetin, O. and I. Zagli (2012). Continuous airborne communication relay approach using unmanned aerial vehicles. *Journal of Intelligent and Robotic Systems* **Vol. 64, No 1-4**, pp. 549–562.

Chaillet, Antoine (2006). On the stability and robustness of nonlinear systems - applications to cascades. PhD thesis. Université Paris Sud - LSS - Supélec, Orsay.

Charlet, B., J. Levine and R. Marino (1988). Dynamic feedback linearization with application to aircraft control. In: *Proceedings of the 27th IEEE Conference on Decision and Control*. Tampa, FL, USA.

Chunyu, J., Z. Qu, E. P. and M. Falash (2009). A new reactive target-tracking control with obstacle avoidance in a dynamic environment. In: *Proceedings of the American Control Conference*. St. Louis, MO, USA.

Cui, R., S. S. Ge, B. V. E. How and Y. S. Choo (2010). Leader-follower formation control of underactuated autonomous underwater vehicles. *Ocean Engineering* **Vol. 37**, pp. 1491–1502.

Dhananjay, N. and R. Kristiansen (2012). Guidance strategy for gradient search by multiple UAVs. In: *Proceedings of the AIAA Guidance, Navigation and Control Conference*. Minneapolis, MN, USA.

Dixon, C. R. and E. W. Frew (2007). Cooperative electronic chaining using small unmanned aircraft. In: *Proceedings of the AIAA Infotech@Aerospace Conference and Exhibit*. Rohnert Park, CA, USA.

Dogan, A. and S. Venkataramanan (2005). Nonlinear control for reconfiguration of unmanned-aerial-vehicle formation. *Journal of Guidance, Control, and Dynamics* **Vol. 28, No. 4**, pp. 667–678.

Doman, D. B. and A. D. Ngo (2002). Dynamic inversion-based adaptive/reconfigurable control of the X-33 on ascent. *Journal of Guidance, Control, and Dynamics* **Vol. 25, No. 2**, pp. 275–284.

Dornheim, M. (1992). Report pinpoints factors leading to the YF-22 crash. *Aviation Week and Space Technology* **Vol. 137, No. 19**, pp. 53–54.

Dyer, S. A., Ed. (2001). *Wiley survey of instrumentation and measurement*. John Wiley & Sons, ISBN 0-471-39484-X.

Egeland, O. and J. T. Gravdahl (2002). *Modeling and simulation for automatic control*. Marine Cybernetics, Trondheim, Norway, ISBN 82-92356-01-0.

Etkin, B. (1972). *Dynamics of atmospheric flight*. Dover Publications, Inc., ISBN 0-486-44522-4.

Fantoni, I. and R. Lozano (2002). *Non-linear control for underactuated mechanical systems*. Springer-Verlag London, ISBN: 978-1-4471-1086-6.

Farrell, J., M. Sharma and M. Polycarpou (2005). Backstepping-based flight control with adaptive function approximation. *Journal of Guidance, Control, and Dynamics* **Vol. 28, No. 6**, pp. 1089–1101.

Fax, J. A. and R. M. Murray (2004). Information flow and cooperative control of vehicle formations. *IEEE Transactions on Automatic Control* **Vol. 49, No. 9**, pp. 1465–1476.

Fierro, R. and F.L. Lewis (1997). Control of nonholonomic mobile robot: backstepping kinematics into dynamics. *Journal of Robotic Systems* **Vol. 14, No. 3**, pp. 149–163.

Fierro, R., C. Belta, J. P. Desai and R. V. Kumar (2001). On controlling aircraft formations. In: *Proceedings of the 40th IEEE Conference on Decision and Control*. Orlando, FL, USA.

Fjellstad, O. (1994). Control of unmanned underwater vehicles in six degrees of freedom: A quaternion feedback approach. PhD thesis. Norges Tekniske Høgskole, Trondheim, Norway.

Fossen, T. I. (2011). *Handbook of marine craft hydrodynamics and motion control*. John Wiley & Sons Ltd., ISBN: 978-1-119-99149-6.

Fossen, T. I., M. Breivik and R. Skjetne (2003). Line-of-sight path following of underactuated marine craft. In: *Proceedings of the 6th IFAC MCMC*. Girona, Spain.

Ge, S. S. and Y. J. Cui (2000). New potential functions for mobile robot path planning. *IEEE Transactions on Robotics and Automation* **Vol. 16, No. 5**, pp. 615–620.

Giulietti, F., L. Pollini and M. Innocenti (2000). Autonomous formation flight. *IEEE Control System Magazine* **Vol. 20, No. 6**, pp. 34–44.

Godhavn, J. M. and O. Egeland (1995). Attitude control of an underactuated satellite. In: *Proceedings of the 34th IEEE Conference on Decision and Control*. New Orleans, LA, USA.

Goldman, P. (1980). Flocking as a possible predator defense in dark-eyed juncos. *The Wilson Bulletin* **Vol. 92, No. 1**, pp. 88–95.

Goodrich, M. A., J. L. Cooper, J. A. Adams, C. Humphrey, R. Zeeman and B. G. Buss (2007). Using a mini-UAV to support wilderness search and rescue: practices for human-robot teaming. In: *IEEE International Workshop on Safety, Security and Rescue Robotics*. Rome, Italy.

Grip, H. F., T. I. Fossen, T. A. Johansen and A. Saberi (2013). Nonlinear observer for GNSS-aided inertial navigation with quaternion-based attitude estimation. In: *Proceedings of the American Control Conference*. Washington, DC, USA.

Grøtli, E. (2010). Robust stability and control of spacecraft formations. PhD thesis. Norwegian University of Science and Technology, Trondheim, Norway.

Guelman, M. (1971). A qualitative study of proportional navigation. *IEEE Transaction on Aerospace and Electronic Systems* **Vol. 7, No. 4**, pp. 637–643.

Guerrero, J. A., P. Castillo, S. Salazar and R. Lozano (2012). Mini rotorcraft flight formation control using bounded inputs. *Journal of Intelligent and Robotic Systems* **Vol 65**, pp. 175–186.

Hahn, W. (1967). *Stability of Motion*. Springer-Verlag Berlin Heidelberg New York, ISBN: 978-3-642-50087-9.

Hamilton, W. R. (1844). On quaternions: or a new system of imaginaries in algebra. *Philosophical Magazine 25* pp. pp. 489–495.

Hao, Y., A. Davari and A. Manesh (2005). Differential flatness-based trajectory planning for multiple unmanned aerial vehicles using mixed-integer linear programming. In: *Proceedings of the American Control Conference*. Portland, OR, USA.

Hauser, J., S. Sastry and G. Meyer (1992). Nonlinear control design for slightly non-minimum phase systems: application to V/STOL aircraft. *Automatica* **Vol. 28, No. 4**, pp. 665–679.

Honeywell and Lockheed Martin (1996). Application of multivariable control theory to aircraft control laws. final report: multivariable control design guidelines. Technical report. Honeywell TC. and Lockheed Martin Skunk Works and Lockheed Martin TAS.

Hovakimyan, N. and C. Cao (2010). $\mathcal{L}_1$ *Adaptive Control Theory: Guaranteed Robustness with Fast Adaptation*. Society for Industrial and Applied Mathematics, ISBN 978-0-89717-04-4.

Hovakimyan, N., C. Cao, E. Kharisov, E. Xargay and I. M. Gregory (2011). $\mathcal{L}_1$ adaptive control for safety-critical systems. *IEEE Control Systems Magazine* **Vol. 31, No. 5**, pp. 54–104.

Härkegård, O. and S. T. Glad (2000). A backstepping design for flight path angle control. In: *Proceedings of the 39th Conference on Decision and Control*. Sydney, New South Wales, Australia.

Hua, M-D., T. Hamel, P. Morin and C. Samson (2009). A control approach for thrust-propelled underactuated vehicles and its application to VTOL drones. *IEEE Transactions on Automatic Control* **Vol. 54, No. 8**, pp. 1837–1853.

Huang, Y., W. C. Hoffmann, Y. Lan, W. Wu and B. K. Fritz (2009). Development of a spray system for an unmanned aerial vehicle platform. *Applied Engineering in Agriculture* **Vol. 25, No. 6**, pp. 803–809.

Ihle, I. F., J. Jouffroy and T. I. Fossen (2006). Formation control of marine surface craft: A lagrangian approach. *IEEE Journal of Oceanic Engineering* **Vol. 31, No. 4**, pp. 922–934.

Ito, D., J. Georgie, J. Valasek and D. T. Ward (2002). Reentry vehicle flight controls design guidelines: dynamic inversion. Technical report. Flight Simulation Laboratory, Texas Engineering Experiment Station, Texas A&M University, NASA.

Jadbabaie, A., J. Lin and A. S. Morse (2003). Coordination of groups of mobile autonomous agents using nearest neighbor rules. *IEEE Transactions on Automatic Control* **Vol. 48, No. 6**, pp. 988–1001.

Jeyaraman, S., A. Tsourdos, R. Zbikowski and B. White (2005). Formal techniques for the modelling and validation of a co-operating UAV team that uses Dubins set for path planning. In: *Proceedings of the American Control Conference*. Portland, OR, USA.

Jiang, Z., E. Lefeber and H. Nijmeijer (2001). Saturated stabilization and tracking of a nonholonomic mobile robot. *Systems & Control Letters* **Vol. 42**, pp. 327–332.

Johnson, E. and A. J. Calise (2000). Pseudo-control hedging: a new method for adaptive control. In: *Proceedings of the Workshop on Advances in Guidance and Control Technology*. Redstone Arsenal, Alabama, USA.

Johnson, E. N., A. Wu, J. C. Neidhoefer, S. K. Kannan and M. A. Turbe (2008). Flight-test results of autonomous airplane transitions between steady-level and hovering flight. *Journal of Guidance, Control, and Dynamics* **Vol. 31, No. 2**, pp. 358–370.

Johnson, E. N. and A. J. Calise (2001). Neural network adaptive control of systems with input saturation. In: *Proceedings of the American Control Conference*. Arlington, VA, USA.

Johnson, E. N. and A. J. Calise (2002). A six degree-of-freedom adaptive flight control architecture for trajectory following. In: *AIAA Guidance, Navigation, and Control Conference and Exhibit*. Monterey, CA, USA.

Ju, H. and C. Tsai (2007). Longitudinal axis flight control law design by adaptive backstepping. *IEEE Transactions on Aerospace and Electronic Systems* **Vol. 43, No. 1**, pp. 311–329.

Kaminer, I., A. Pascoal, E. Hallberg and C. Silvestre (1998). Trajectory tracking for autonomous vehicles: an integrated approach to guidance and control. *Journal of Guidance, Control, and Dynamics* **Vol. 21, No. 1**, pp. 29–38.

Kanayama, Y. J., Y. Kimura, F. Miyazaki and T. Noguchi (1990). A stable tracking control method for an autonomous mobile robot. In: *Proceedings of the IEEE International Conference on Robotics and Automation*.

Khalil, H. K. (2002). *Nonlinear systems*. 3rd ed., Prentice Hall, ISBN 0-13-067389-7.

Khatib, O. (1986). Real-time obstacle avoidance for manipulators and mobile robots. *The International Journal of Robotics Research* **Vol 5. No. 1**, pp. 90–98.

Kim, J. and P. K. Khosla (1992). Real-time obstacle avoidance using harmonic potential functions. *IEEE Transactions on Robotics and Automation* **Vol. 8, No. 3**, pp. 338–349.

Kingston, D. B. and R. W. Beard (2004). Real-time attitude and position estimation for small UAVs using low-cost sensors. In: *AIAA 3rd Unmanned Unlimited Technical Conference, Workshop and Exhibit*.

Koren, Y. and J. Borenstein (1991). Potential field methods and their inherent limitations for mobile robot navigation. In: *Proceedings of the IEEE Conference on Robotics and Automation*. Sacramento, CA, USA.

Kristiansen, R. (2008). Dynamic synchronization of spacecraft. PhD thesis. Norwegian University of Science and Technology, Trondheim, Norway.

Kristiansen, R., A. Loría, A. Chaillet and P. J. Nicklasson (2009*a*). Spacecraft relative rotation tracking without angular velocity measurements. *Automatica* **Vol. 45, No. 3**, pp. 750–756.

Kristiansen, R., E. Oland and D. Narayanachar (2012). Operational concepts in UAV formation monitoring of industrial emissions. In: *Proceedings of the 3rd IEEE International Conference on Cognitive Infocommunications*. Kosice, Slovakia.

Kristiansen, R., P. J. Nicklasson and J. T. Gravdahl (2008*a*). Spacecraft coordination control in 6DOF: Integrator backstepping vs. passivity-based control. *Automatica* **Vol. 44, No. 11**, pp. 2896–2901.

Kristiansen, R., P. J. Nicklasson and J. T. Gravdahl (2009*b*). Satellite attitude control by quaternion-based backstepping. *IEEE Transactions on Control Systems Technology* **Vol. 17, No. 1**, pp. 227–232.

Kristiansen, R., R. Schlanbusch and E. Oland (2011). PD+ based spacecraft attitude tracking with magnetometer rate feedback. In: *Proceedings of the 50th IEEE Conference on Decision and Control*. Orlando, FL, USA.

Kristiansen, R., T. R. Krogstad, P. J. Nicklasson and J. T. Gravdahl (2008*b*). PID+ tracking in a leader-follower spacecraft formation. In: *Proceedings of the 3rd International Symposium on Formation Flying, Missions and Technologies (ISFF)*. Estec, Holland.

Krstić, M., I. Kanellakopoulos and P. V. Kokotović (1995). *Nonlinear and adaptive control design*. John Wiley & Sons, inc., ISBN 0-471-12732-9.

Kuroki, Y., G. S. Young and S. E. Haupt (2010). UAV navigation by an expert system for contaminant mapping with a genetic algorithm. *Expert Systems with Applications* **Vol. 37, No. 6**, pp. 4687–4697.

Kyriakopoulos, K. J., P. Kakambouras and N. J. Krikelis (1995). Potential fields for nonholonomic vehicles. In: *Proceedings of the 1995 IEEE Symposium on Intelligent Control*. Monterey, CA, USA.

Kyrkjebø E. and K. Y. Pettersen (2005). Output synchronization control of Euler-Lagrange systems with nonlinear damping terms. In: *Proceedings of the 44th IEEE Conference on Decision and Control*. Seville, Spain.

Lane, S. H. and R. F. Stengel (1988). Flight control design using non-linear inverse dynamics. *Automatica* **Vol. 24, No. 4**, pp. 471–483.

Langelaan, J. W., N. Alley and J. Neidhoefer (2010). Wind field estimation for small unmanned aerial vehicles. In: *Proceedings of the AIAA Guidance, Navigation and Control Conference*. Toronto, Canada.

Lavretsky, E. and K. A. Wise (2013). *Robust and adaptive control*. Advanced Textbooks in Control and Signal Processing, Springer-Verlag London, ISBN 978-1-4471-4395-6.

Lavretsky, E. and N. Hovakimyan (2004). Positive μ-modification for stable adaption in the presence of input constraints. In: *Proceedings of the 2004 American Control Conference*. Boston, MA, USA.

Lee, D., T. C. Burg, B. Xian and D. M. Dawson (2007). Output feedback tracking control of an underactuated quad-rotor UAV. In: *Proceedings of the American Control Conference*. New York, NY, USA.

Lee, T. and Y. Kim (2001). Nonlinear adaptive flight control using backstepping and neural networks controller. *Journal of Guidance, Control and Dynamics* **Vol. 24, No. 4**, pp. 675–682.

Lee, T., M. Leok and N. H. McClamroch (2010). Geometric tracking control of a quadrotor UAV on SE(3). In: *Proceedings of the 49th IEEE Conference on Decision and Control*. Atlanta, GA, USA.

Leonard, N. E. (1995). Periodic forcing, dynamics and control of underactuated spacecraft and underwater vehicles. In: *Proceedings of 34th IEEE Conference on Decision and Control*. New Orleans, LA, USA.

Leonessa, A., W. M. Haddad and T. Hayakawa (2001). Adaptive tracking for nonlinear systems with control constraints. In: *Proceedings of the American Control Conference*. Arlington, VA, USA.

Lewis, F. L., H. Zhang, K. Hengster-Movric and A. Das (2014). *Cooperative control of multi-agent systems*. Springer, ISBN 978-1-4471-5573-7.

Lissaman, P.B.S. and C. A. Shollenberger (1970). Formation flight of birds. *Science* **Vol. 168, No. 3934**, pp. 1003–1005.

López-Martínez, M., J. Á. Acosta and J.M. Cano (2010). Non-linear sliding mode surfaces for a class of underactuated mechanical systems. *IET Control Theory and Applications* **Vol. 4, No. 10**, pp. 2195–2204.

Loría, A. (2013). Uniform global position feedback tracking control of mechanical systems without friction. In: *Proceedings of the American Control Conference*. Washington, DC, USA.

Loría, A. and E. Panteley (2002). Uniform exponential stability of linear time-varying systems: revisited. *System & Control Letters* **Vol. 47, No. 1**, pp. 13–24.

Loría, A. and E. Panteley (2005). Cascaded nonlinear time-varying systems: analysis and design. In: *Advanced Topics in Control Systems Theory*. Vol. 311 of Lecture Notes in Control and Information Sciences. Chap. 2, pp. 23–64. Springer Verlag, ISBN 1-85233-923-3.

Luyckx, L., M. Loccufier and E. Noldus (2001). On the design of nonlinear controllers for Euler-Lagrange systems. *Nonlinear Dynamics and Systems Theory* **Vol. 1, No. 1**, pp. 99–110.

MacKunis, W., P. M. Patre, M. K. Kaiser and W. E. Dixon (2010). Asymptotic tracking for aircraft via robust and adaptive dynamic inversion methods. *IEEE Transactions on Control Systems Technology* **Vol. 18, No. 6**, pp. 1448–1456.

Marconi, L. and A. Isidori (2000). Robust global stabilization of a class of uncertain feedforward nonlinear systems. *Systems & Control Letters* **41**, pp. 281–290.

Mei, J., W. Ren and G. Ma (2011). Distributed coordinated tracking with a dynamic leader for multiple Euler-Lagrange systems. *IEEE Transactions on Automatic Control* **Vol. 56, No. 6**, pp. 1415–1421.

Morelli, E. A. (1998). Global nonlinear parametric modeling with application to F-16 aerodynamics. In: *Proceedings of the American Control Conference*. Philadelphia, PA, USA.

Murray, R. M. (1999). Geometric approaches to control in the presence of magnitude and rate saturations. Technical Report 99-001. Division of Engineering and Applied Science, California Institute of Technology.

Murtaugh, S. A. and H. E. Criel (1966). Fundamentals of proportional navigation. *IEEE Spectrum* **Vol. 3, No. 12**, pp. 75–85.

Nelson, D. R., D. B. Barber, T. W. McLain and R. W. Beard (2007). Vector field path following for miniature air vehicles. *IEEE Transactions on Robotics* **Vol. 23, No. 3**, pp. 519–529.

Ngo, Anhtuan D. and David B. Doman (2001). Dynamic inversion-based adaptive/reconfigurable control of the X-33 on ascent. In: *Proceedings of the IEEE Aerospace Conference*. Big Sky, MT, USA.

Oland, E. and R. Kristiansen (2013*a*). Collision and terrain avoidance for UAVs using the potential field method. In: *Proceedings of the 34th IEEE Aerospace Conference*. Big Sky, MT, USA.

Oland, E. and R. Kristiansen (2013*b*). Quaternion based attitude control for a fixed-wing UAV using backstepping. In: *Proceedings of the 34th IEEE Aerospace Conference*. Big Sky, MT, USA.

Oland, E. and R. Kristiansen (2013*c*). Real-time particle tracking using a formation of UAVs. In: *Proceedings of the 2nd RED-UAS, Workshop on Research, Education and Development of Unmanned Aerial Systems*. Compiegne, France.

Oland, E. and R. Kristiansen (2013*d*). Underactuated translational control of a rigid spacecraft. In: *Proceedings of the 34th IEEE Aerospace Conference*. Big Sky, MT, USA.

Oland, E. and R. Kristiansen (2014*a*). Adaptive flight control with constrained actuation. In: *Proceedings of the American Control Conference*. Portland, OR, USA.

Oland, E. and R. Kristiansen (2014*b*). A decoupled approach for flight control. Submitted to Journal of Guidance, Control, and Dynamics.

Oland, E. and R. Kristiansen (2014*c*). Trajectory tracking of an underactuated fixed-wing UAV. In: *Proceedings of the ICNPAA Congress on Mathematical problems in engineering, aerospace and sciences*. Narvik, Norway.

Oland, E., R. Kristiansen and P. J. Nicklasson (2010). Spacecraft formation reconfiguration with plume avoidance. In: *Proceedings of the 31st IEEE Aerospace Conference*. Big Sky, MT, USA.

Oland, E., R. Schlanbusch and R. Kristiansen (2013*a*). Underactuated waypoint tracking of a fixed-wing UAV. In: *Proceedings of the 2nd RED-UAS, Workshop on Research, Education and Development of Unmanned Aerial Systems*. Compiegne, France.

Oland, E., T. S. Andersen and R. Kristiansen (2013*b*). Underactuated control of quadrotors with collision avoidance. In: *Proceedings of the 2nd RED-UAS, Workshop on Research, Education and Development of Unmanned Aerial Systems*. Compiegne, France.

Oland, E., T. S. Andersen and R. Kristiansen (2014*a*). Actuator desaturation for a fixed-wing UAV using speed modification. In: *Proceedings of the ICNPAA Congress on Mathematical problems in engineering, aerospace and sciences*. Narvik, Norway.

Oland, E., T. S. Andersen and R. Kristiansen (2014*b*). Subsumption architecture applied to flight control using composite rotations. Submitted to Automatica.

Olfati-Saber, R., A. Fax and R. M. Murray (2007). Consensus and cooperation in networked multi-agent systems. *Proceedings of the IEEE* **Vol. 95, No. 1**, pp. 215–233.

Olfati-Saber, Reza (2001). Nonlinear control of underactuated mechanical systems with application to robotics and aerospace vehicles. PhD thesis. Massachusetts Institute of Technology, Cambridge, MA, USA.

Ortega, R., A. Loría, P. J. Nicklasson and H. Sira-Ramírez (1998). *Passivity-based control of Euler-Lagrange systems: Mechanical, electrical and electromechanical applications*. ISBN 978-1-85233-016-3. Springer-Verlag, London.

Ortega, R. and M. W. Spong (1989). Adaptive motion control of rigid robots: A tutorial. *Automatica* **Vol. 25**, pp. 877–888.

Osborne, J. and R. Rysdyk (2005). Waypoint guidance for small UAVs in wind. In: *Proceedings of the AIAA Infotech@Aerospace*. Arlington, VA, USA.

Paden, B. and R. Panja (1988). Globally asymptotically stable 'PD+' controller for robot manipulators. *International Journal of Control* **Vol. 47, No. 6**, pp. 1697–1712.

Palumbo, N. F., R. A. Blauwkamp and J. M. Lloyd (2010). Modern homing missile guidance theory and techniques. *John Hopkins APL Technical Digest* **Vol. 29, No. 1**, pp. 42–59.

Panteley, E., A. Loría and A. Teel (2001). Relaxed persistency of excitation for uniform asymptotic stability. *IEEE Transactions on Automatic Control* **Vol. 46, No. 12**, pp. 1874–1886.

Panteley, E. and A. Loría (1998). On global uniform asymptotic stability of nonlinear time-varying systems in cascade. *Systems & Control Letters* **Vol. 33, No. 2**, pp. 131–138.

Panteley, E. and A. Loría (2010). A new characterisation of exponential stability. In: *Proceedings of the 19th International Symposium on Mathematical Theory of Networks and Systems*. Budapest, Hungary.

Park, S., J. Deyst and J. P. How (2004). A new nonlinear guidance logic for trajectory tracking. In: *Proceedings of the AIAA Guidance, Navigation and Control Conference*. Providence, RI, USA.

Paul, T., T. R. Krogstad and J. T. Gravdahl (2008). Modelling of UAV formation flight using 3D potential field. *Simulation Modelling Practice and Theory* **Vol. 16, No. 9**, pp. 1453–1462.

Pettersen, K. Y. and O. Egeland (1999). Time-varying exponential stabilization of the position and attitude of an underactuated autonomous underwater vehicle. *IEEE Transactions of Automatic Control* **Vol. 44, No. 1**, pp. 112–115.

Pettersen, K.Y. and O. Egeland (1996). Position and attitude control of an underactuated autonomous underwater vehicle. In: *Proceedings of the 35th Conference on Decision and Control*. Kobe, Japan.

Phillips, W. F. (2010). *Mechanics of flight*. John Wiley & Sons, Inc., ISBN 978-0-470-53975-0.

Qu, Z. (2009). *Cooperative control of dynamical systems*. Springer-Verlag London Limited, ISBN 978-1-84882-324-2.

Rao, V. G. (2001). Naive control of the double integrator. *IEEE Control Systems* **Vol. 21**, pp. 86–97.

Refsnes, J., A. J. Sørensen and K. Y. Pettersen (2007). Output feedback control of a slender body underactuated AUV with experimental results. In: *Proceedings of 15th Mediterranean Conference on Control and Automation*. Athens, Greece.

Reiner, J., G. J. Balas and W. L. Garrard (1996). Flight control design using robust dynamic inversion and time-scale separation. *Automatica* **Vol. 32, No. 11**, pp. 1493–1504.

Ren, W. and E. Atkins (2005). Nonlinear trajectory tracking for fixed wing UAVs via backstepping and parameter adaptation. In: *Proceedings of the AIAA Guidance, Navigation and Control Conference and Exhibit*. San Francisco, CA, USA.

Ren, W. and R. Beard (2003). CLF-based tracking control for UAV kinematic models with saturation constraints. In: *Proceedings of 42nd IEEE Conference on Decision and Control*. Maui, HI, USA.

Ren, W. and R. W. Beard (2004). Constrained nonlinear tracking control for small fixed-wing unmanned air vehicles. In: *Proceedings of the American Control Conference*. Boston, MA, USA.

Ren, W. and R. W. Beard (2008). *Distributed consensus in multi-vehicle cooperative control*. Springer-Verlag London Limited, ISBN 978-1-84800-014-8.

Reyhanoglu, M., A. van der Schaft, N. H. McClamroch and I. Kolmanovsky (1999). Dynamics and control of a class of underactuated mechanical systems. *IEEE Transactions on Automatic Control* **Vol. 44, No. 9**, pp. 1663–1671.

Reynolds, C. (1987). Flocks, herd and schools: A distributed behavioral model. *Computer Graphics* **Vol. 21, No. 4**, pp. 25–34.

Rimon, E. and D. E. Koditschek (1992). Exact robot navigation using artificial potential functions. *Transactions on Robotics and Automation* **Vol. 8, No. 5**, pp. 501 – 518.

Rizwan, Y., S. L. Waslander and C. Nielsen (2011). Nonlinear aircraft modeling and controller design for target tracking. In: *Proceedings of the American Control Conference*. San Francisco, CA, USA.

Roberts, A. and A. Tayebi (2009). Adaptive position tracking of VTOL UAVs. In: *Proceedings of the 48th IEEE Conference on Decision and Control*. Shanghai, China.

Robinson, J. W. C. (2007). Block backstepping for nonlinear flight control law design. In: *Nonlinear Analysis and Synthesis Techniques for Aircraft Control* (D. Bates and M. Hagström, Eds.). Springerlink, ISBN: 978-3-540-73718-6.

Rogers, K. J. and A. Finn (2013). Frequency estimation for 3D atmospheric tomography using unmanned aerial vehicles. In: *Proceedings of the 8th IEEE International Conference on Intelligent Sensors, Sensor Networks and Information Processing*. Melbourne, Australia.

Roussos, G., D. V. Diamarogonas and K. J. Kyriakopoulos (2010). 3D navigation and collision avoidance for nonholonomic aircraft-like vehicles. *Intl. Journal of Adaptive Control and Signal Processing* **Vol 24, No. 10**, pp. 900–920.

Rysdyk, R. (2006). Unmanned aerial vehicle path following for target observation in wind. *Journal of Guidance, Control, and Dynamics* **Vol. 29, No. 5**, pp. 1092–1100.

Samson, C. (1995). Control of chained systems application to path following and time-varying point-stabilization of mobile robots. *IEEE Transactions on Automatic Control* **Vol. 40, No. 1**, pp. 64–77.

Sato, Y., T. Yamasaki, H. Takano and Y. Baba (2006). Trajectory guidance and control for a small UAV. *KSAS International Journal* **Vol. 7, No. 2**, pp. 137–144.

Schlanbusch, R. (2012). Control of rigid bodies - with applications to leader-follower spacecraft formations. PhD thesis. Norwegian University of Science and Technology, Trondheim, Norway.

Schlanbusch, R., A. Loría and P. J. Nicklasson (2012*a*). On the stability and stabilization of quaternion equilibria of rigid bodies. *Automatica* **Vol. 48, No. 12**, pp. 3135–3141.

Schlanbusch, R., A. Loría, R. Kristiansen and P. J. Nicklasson (2012*b*). PD+ based output feedback attitude control of rigid bodies. *IEEE Transactions on Automatic Control* **Vol. 57, No. 8**, pp. 2146–2152.

Schlanbusch, R. and E. Oland (2013). Spacecraft formation reconfiguration with dynamic collision avoidance. In: *Proceedings of the 34th IEEE Aerospace Conference*. Big Sky, MT, USA.

Schlanbusch, R., E. Grøtli, A. Loría and P. J. Nicklasson (2011). Hybrid attitude tracking of output feedback controlled rigid bodies. In: *Proceedings of the 50th IEEE Conference on Decision and Control*. Orlando, FL, USA.

Schlanbusch, R., R. Kristiansen and P. J. Nicklasson (2008). Spacecraft formation reconfiguration with collision avoidance. In: *Proceedings of the 3rd International Symposium on Formation Flying, Missions and Technologies (ISFF)*. Estec, Holland.

Shaw, E. (1975). Fish in schools. *Natural History* **Vol. 84, No. 8**, pp. 40–46.

Shin, D. and Y. Kim (2006). Nonlinear discrete-time reconfigurable flight control law using neural networks. *IEEE Transactions on Control Systems Technology* **Vol. 14, No. 3**, pp. 408–422.

Shneydor, N. A. (1998). *Missile guidance and pursuit: kinematics, dynamics and control*. Woodhead Publishing, ISBN 978-1-904275-37-4.

Siciliano, B., L. Sciavicci, L. Villani and G. Oriolo (2010). *Robotics modelling, planning and control*. Springer, ISBN 978-1-84628-641-4.

Sieberling, S., Q. P. Chu and J. A. Mulder (2010). Robust flight control using incremental nonlinear dynamic inversion and angular acceleration prediction. *Journal of Guidance, Control, and Dynamics* **Vol. 33, No. 6**, pp. 1732–1742.

Simon, H. A. (1956). Dynamic programming under uncertainty with a quadratic criterion function. *Econometrica* **Vol. 24, No. 1**, pp. 74–81.

Siouris, G. M. (2003). *Missile guidance and control systems*. Springer-Verlag New York, Inc., ISBN 0-387-00726-1.

Slegers, N., J. Kyle and M. Costello (2006). Nonlinear model predictive control technique for unmanned air vehicles. *Journal of Guidance, Control and Dynamics* **Vol. 29, No. 5**, pp. 1179–1188.

Slotine, J. J. E. and W. Li (1987). On the adaptive control of robot manipulators. *International Journal of Robotics Research* **Vol. 6, No. 3**, pp. 49–59.

Slotine, J. J. E. and W. Li (1988). Adaptive manipulator control: a case study. *IEEE Transactions on Automatic Control* **Vol. 33, No. 11**, pp. 995–1003.

Slotine, J. J. E. and W. Li (1991). *Applied nonlinear control*. Prentice Hall, ISBN 0-13-040890-5.

Šmídl, V. and R. Hofman (2013). Tracking of atmospheric release of pollution using unmanned aerial vehicles. *Atmospheric Environment* **Vol. 67**, pp. 1–12.

Snell, S. A., D. F. Enns and W. L. Garrard (1992). Nonlinear inversion flight control for a supermaneuverable aircraft. *Journal of Guidance, Control, and Dynamics* **Vol. 15, No. 4**, pp. 976–984.

Sobolic, F. M. and J. P. How (2009). Nonlinear agile control test bed for a fixed-wing aircraft in a constrained environment. In: *Proceedings of the AIAA Infotech@Aerospace Conference*. Seattle, WA, USA.

Song, Y. D., Yao Li and X. H. Liao (2005). Orthogonal transformation based robust adaptive close formation control of multi-UAVs. In: *Proceedings of the American Control Conference*. Portland, OR, USA.

Sonneveldt, L. (2010). Adaptive backstepping flight control for modern fighter aircraft. PhD thesis. Delft University of Technology, Delft, The Netherlands.

Sonneveldt, L., E. R. van Oort, Q. P. Chu and J. A. Mulder (2009*a*). Nonlinear adaptive trajectory control applied to an F-16 model. *Journal of Guidance, Control and Dynamics* **Vol. 32, No. 1**, pp. 25–39.

Sonneveldt, L., E. R. van Oort, Q.P. Chu and J.A. Mulder (2009*b*). Nonlinear adaptive flight control design and handling qualities evaluation. In: *Proceedings of the 48th IEEE Conference on Decision and Control*. Shanghai, China.

Sourlas, D., J. Choi and V. Manousiouthakis (1994). Best achievable control system performance: the saturation paradox. In: *Proceedings of the 33rd IEEE Conference on Decision and Control*. Lake Buena Vista, FL, USA.

Spong, M. W. (1998). Underactuated mechanical systems. In: *Control Problems in Robotics and Automation* (B. Siciliano and K. P. Valavanis, Eds.). Springer-Verlag, London UK, ISBN 978-3-540-76220-1.

Stein, G. (2003). Respect the unstable. *IEEE Control Systems Magazine* **Vol. 23, No. 4**, pp. 12–25.

Stengel, R. F. (2004). *Flight dynamics*. Princeton University Press, ISBN 0-691-11407-2.

Stepanyan, V. and N. Hovakimyan (2007). Adaptive disturbance rejection controller for visual tracking of a maneuvering target. *Journal of Guidance, Control, and Dynamics* **Vol. 30, No. 4**, pp. 1090–1106.

Stevens, B. L. and F. L. Lewis (2003). *Aircraft control and simulation*. 2nd ed., Wiley, ISBN 978-0-471-37145-8.

Stiharu-Alexe, I. and C. Stiharu-Alexe (1993). A full-authority 4D guidance algorithm for conventional aircraft. In: *Proceedings of the American Control Conference*. San Francisco, CA, USA.

Subchan, S., B.A. White, A. Tsourdos, M. Shanmugavel and R. Zbikowski (2008). Dubins path planning of multiple UAVs for tracking contaminant cloud. In: *Proceedings of the 17th IFAC World Congress*. Seoul, Korea.

Sussmann, H. J., E. D. Sontag and Y. Yang (1994). A general result on the stabilization of linear systems using bounded controls. *IEEE Transactions on Automatic Control* **Vol. 39, No.12**, pp. 2411–2425.

Takegaki, M. and S. Arimoto (1981). A new feedback method for dynamic control of manipulators. *ASME Journal of Dynamic Systems, Measurement, and Control* **Vol. 103, No. 2**, pp. 119–125.

Tandale, M. D. and J. Valasek (2005). Adaptive dynamic inversion control with actuator saturation constraints applied to tracking spacecraft maneuvers. *The Journal of Astronautical Sciences* **Vol. 52, No. 4**, pp. 517–530.

Tanner, H. G. and K. J. Kyria (2002). Discontinuous backstepping for stabilization of nonholonomic mobile robots. In: *Proceedings of the IEEE International Conference on Robotics & Automation*. Washington, DC, USA.

Tanner, H. G., S. G. Loizou and K. J. Kyriakopoulos (2003). Nonholonomic navigation and control of cooperating mobile manipulators. *IEEE Transactions on Robotics and Automation* **Vol. 19. No. 1**, pp. 53–64.

Tarbouriech, S., G. Garcia, J. M. Gomes da Silva Jr. and I. Queinnec (2011). *Stability and stabilization of linear systems with saturating actuators*. Springer, ISBN 978-0-85729-940-6.

Tayebi, A. (2008). Unit quaternion-based output feedback for the attitude tracking problem. *IEEE Transactions on Automatic Control* **Vol. 53, No. 6**, pp. 1516–1520.

Tayebi, A. and S. McGilvray (2006). Attitude stabilization of a VTOL quadrotor aircraft. *IEEE Transaction on Control Systems Technology* **Vol. 14, No. 3**, pp. 562–571.

Tedrake, R. (2009). *Underactuated robotics: learning, planning, and control for efficient and agile machines: course notes for MIT 6.832*.

Teel, A. R. (1992). Global stabilization and restricted tracking for multiple integrators with bounded controls. *Systems & Control Letters* **Vol. 18**, pp. 165–171.

Templeton, T., D. H. Shim, C. Geyer and S. S. Sastry (2007). Autonomous vision-based landing and terrain mapping using an MPC-controlled unmanned rotorcraft. In: *Proceedings of the IEEE International Conference on Robotics and Automation*. Roma, Italy.

Toshimura, Y., T. Matsuno and S. Hokamoto (2011). Position and attitude control of an underactuated satellite with constant thrust. In: *Proceedings of the AIAA Guidance, Navigation, and Control Conference*. Portland, OR, USA.

Tsourdos, A., B. White and M. Shanmugavel (2011). *Cooperative path planning of unmanned aerial vehicles*. John Wiley & Sons, Inc., ISBN 978-0-470-74129-0.

Tyan, F. and D. S. Bernstein (1999). Global stabilization of systems containing a double integrator using a saturated linear controller. *International Journal of Robust and Nonlinear Control* **Vol. 9**, pp. 1143–1156.

van Oort, E. R., L. Sonneveldt, Q. P. Chu and J. A. Mulder (2010). Full envelope modular adaptive control of a fighter aircraft using orthogonal least squares. *Journal of Guidance, Control and Dynamics* **Vol. 33, No. 5**, pp. 1461–1472.

Visioli, A. (2003). Modified anti-windup scheme for PID controllers. In: *IEE Proceedings - Control Theory and Applications*.

Waharte, S. and N. Trigoni (2010). Supporting search and rescue operations with UAVs. In: *Proceedings of the International Conference on Emerging Security Technologies*. Canterbury, UK.

Wang, Q. and R. F. Stengel (2000). Robust nonlinear control of a hypersonic aircraft. *Journal of Guidance, Control, and Dynamics* **Vol. 23, No. 4**, pp. 577–585.

Wang, Q. and R. F. Stengel (2005). Robust nonlinear flight control of a high performance aircraft. *IEEE Transactions on Control Systems Technology* **Vol. 13, No. 1**, pp. 15–26.

Wegener, S. S., S. M. Schoenung, J. Totah, D. Sullivan, J. Frank, F. Enomoto, C. Frost and C. Theodore (2004). UAV autonomous operations for airborne science missions. In: *Proceedings of the AIAA "Unmanned Unlimited" Technical Conference, Workshop and Exhibit*. Chicago, IL, USA.

Wen, J. T. and K. Kreutz-Delgado (1991). The attitude control problem. *IEEE Transactions on Automatic Control* **Vol. 36, No. 10**, pp. 1148–1162.

Werner, G. M. and M. G. Dyer (1993). Evolution of herding behavior in artificial animals. In: *Proceedings of the 2nd International Conference on From Animals to Animats: Simulation of Adaptive Behavior*. Honolulu, HI, USA.

Wichlund, K. Y., O. J. Sørdalen and O. Egeland (1995). Control properties of underactuated vehicles. In: *Proceedings of the IEEE International Conference on Robotics and Automation*. Nagoya, Japan.

Xargay, E., V. Dobrokhodov, I. Kaminer, A. M. Pascoal, N. Hovakimyan and C. Cao (2012). Time-critical cooperative control of multiple autonomous vehicles. *IEEE Control Systems Magazine* **Vol. 32, No. 5**, pp. 49–73.

Xie, F., X. Zhang, R. Fierro and M. Motter (2005). Autopilot-based nonlinear UAV formation controller with extremum-seeking. In: *Proceedings of the 44th IEEE Conference on Decision and Control*. Seville, Spain.

Yang, C. and C. Yang (1995). Analytical solution of generalized 3D proportional navigation. In: *Proceedings of the 34th Conference on Decision and Control*. New Orleans, LA, USA.

Yang, P., R. A. Freeman and K. M. Lynch (2008). Multi-agent coordination by decentralized estimation and control. *IEEE Transactions on Automatic Control* **Vol. 53, No. 11**, pp. 2480–2496.

Yip, P. P., J.K. Hedrick and D. Swaroop (1996). The use of linear filtering to simplify integrator backstepping control of nonlinear systems. In: *Proceedings of the IEEE International Workshop on Variable Structure Systems*. Tokyo, Japan.

Yu, Z., G. Fan and J. Yi (2009). Indirect adaptive flight control based on nonlinear inversion. In: *Proceedings of the IEEE International Conference on Mechatronics and Automation*. Changchun, China.

Zhu, H., Y. Lan, W. Wu, W. C. Hoffmann, Y. Huang, X. Xue, J. Liang and B. Fritz (2010). Development of a PWM precision spraying controller for unmanned aerial vehicles. *Journal of Bionic Engineering* **Vol. 7**, pp. 276–283.

Appendix A

The YF-22 UAV Model

The UAV model that is used in the simulations is based on the nonlinear model from Campa *et al.* (2007) with the only difference being that the stabilizer is treated as an elevator. At steady flight with $V_a = 42\text{m/s}$, $\alpha = \theta = 0$, $\delta_e = -0.0175$ rad, $\delta_a = \delta_r = 0$, $T = 54.62$ N and an altitude of $h = 240$ m, the aerodynamic coefficients are given as

$m = 20.64$ kg	$J_{xx} = 1.607$ kgm^2	$J_{yy} = 7.51$ kgm^2	$J_{zz} = 7.18$ kgm^2
$J_{xz} = 0.59$ kgm^2	$b = 1.96$ m	$\bar{c} = 0.76$ m	$S = 1.37$ m^2
$C_{L_0} = -0.049$	$C_{L_\alpha} = 3.258$	$C_{L_q} = 0$	$C_{L_{\delta_e}} = 0.189$
$C_{D_0} = 0.008$	$C_{D_\alpha} = 0.508$	$C_{D_q} = 0$	$C_{D_{\delta_e}} = -0.034$
$C_{Y_0} = 0.015$	$C_{Y_\beta} = 0.272$	$C_{Y_p} = 1.215$	$C_{Y_r} = -1.161$
$C_{Y_{\delta_a}} = 0.183$	$C_{Y_{\delta_r}} = -0.459$	$C_{l_p} = -0.213$	$C_{l_r} = 0.114$
$C_{l_{\delta_a}} = -0.056$	$C_{l_{\delta_r}} = 0.014$	$C_{m_0} = 0.022$	$C_{m_\alpha} = -0.473$
$C_{m_q} = -3.449$	$C_{m_{\delta_e}} = -0.364$	$C_{n_0} = 0$	$C_{n_\beta} = 0.036$
$C_{n_p} = -0.151$	$C_{n_r} = -0.195$	$C_{n_{\delta_a}} = -0.036$	$C_{n_{\delta_r}} = -0.055$.

Appendix B

Derivation of the Aggregated Dynamics

The relative velocity can be written in the wind frame using $\mathbf{R}_w^b \mathbf{v}_r^w = \mathbf{v}_r^b$ where $\mathbf{v}_r^w = \begin{bmatrix} V_a & 0 & 0 \end{bmatrix}^\top$ and $\dot{\mathbf{v}}_r^w = \begin{bmatrix} \dot{V}_a & 0 & 0 \end{bmatrix}^\top$, and can be differentiated as

$$\mathbf{R}_w^b \mathbf{S}(\boldsymbol{\omega}_{b,w}^w)\mathbf{v}_r^w + \mathbf{R}_w^b \dot{\mathbf{v}}_r^w = \dot{\mathbf{v}}_r^b. \tag{B.1}$$

Let $\boldsymbol{\omega}_{b,w}^w := \begin{bmatrix} p_w & q_w & r_w \end{bmatrix}^\top$ and

$$\mathbf{S}(\boldsymbol{\omega}_{b,w}^w)\mathbf{v}_r^w = -\mathbf{S}(\mathbf{v}_r^w)\boldsymbol{\omega}_{b,w}^w = \begin{bmatrix} 0 & 0 & 0 \\ 0 & 0 & V_a \\ 0 & -V_a & 0 \end{bmatrix} \begin{bmatrix} p_w \\ q_w \\ r_w \end{bmatrix}; \tag{B.2}$$

then (B.1) can be rewritten using (2.21) as

$$\begin{bmatrix} \dot{V}_a \\ r_w V_a \\ -q_w V_a \end{bmatrix} = \frac{1}{m}(\mathbf{R}_b^w \mathbf{f}_{thrust}^b + \mathbf{f}_{aero}^w) + \mathbf{R}_n^w \mathbf{f}_g^n - \mathbf{R}_b^w \mathbf{S}(\boldsymbol{\omega}_{n,b}^b)\mathbf{v}_r^b, \tag{B.3}$$

which can be written using the angle of attack and sideslip rate using (2.48) as

$$\begin{bmatrix} \dot{V}_a \\ \dot{\beta} V_a \\ \dot{\alpha} V_a \cos(\beta) \end{bmatrix} = \frac{1}{m}(\mathbf{R}_b^w \mathbf{f}_{thrust}^b + \mathbf{f}_{aero}^w) + \mathbf{R}_n^w \mathbf{f}_g^n - \mathbf{R}_b^w \mathbf{S}(\boldsymbol{\omega}_{n,b}^b)\mathbf{v}_r^b, \tag{B.4}$$

which is singular with regards to the angular rates if $\beta = \pm\frac{\pi}{2}$ or $V_a = 0$. By expanding $\mathbf{R}_b^w$ and multiplying with the thrust, the equations become

$$\begin{bmatrix} \dot{V}_a \\ \dot{\beta} V_a \\ \dot{\alpha} V_a \cos(\beta) \end{bmatrix} = \frac{1}{m} \begin{bmatrix} T\cos(\alpha)\cos(\beta) \\ -T\cos(\alpha)\sin(\beta) \\ -T\sin(\alpha) \end{bmatrix} + \frac{1}{m}\mathbf{f}_{aero}^w + \mathbf{R}_n^w \mathbf{f}_g^n - \mathbf{R}_b^w \mathbf{S}(\boldsymbol{\omega}_{n,b}^b)\mathbf{v}_r^b, \tag{B.5}$$

where it is obvious that the dynamics of the airspeed become singular when solving for the thrust whenever $\alpha \vee \beta = \pm\frac{\pi}{2}$.

Appendix C

Aerodynamic Modeling

The basic forces and moments that enable flight are the aerodynamics. By properly designing the wing, a lift force is produces while flying, which compensates for the gravity vector and is crucial for flight. The aerodynamic force vector in the wind frame is defined as (*cf.* (2.17))

$$\mathbf{f}_{aero}^{w} = \frac{1}{2}\rho S V_a^2 \begin{bmatrix} -C_D \\ C_Y \\ -C_L \end{bmatrix} \tag{C.1}$$

where ρ is the air density, S is the wing area, V_a is the airspeed, C_D is the drag coefficient, C_Y is the sideforce coefficient and C_L is the lift coefficient. The coefficients are usually found through wind tunnel testing or by using estimation methods using sensor measurements and approximated using a polynomial. The lift coefficient is often defined as a function of the angle of attack, such that

$$C_L = C_{L_0} + C_{L_\alpha}\alpha \tag{C.2}$$

where C_{L_0} represents the lift coefficient when the angle of attack is zero. This approximation is valid at low angles of attack, but as the angle of attack becomes larger, this approximation becomes inaccurate. The aerodynamic polynomial is actually a truncated Taylor expansion, such that by increasing the number of terms it becomes more accurate. This has been applied from a modeling perspective in Morelli (1998), where the coefficients are modeled using a higher order Taylor series. Equation (C.2) can be augmented with additional terms,

$$C_L = C_{L_0} + C_{L_\alpha}\alpha + C_{L_{\alpha^2}}\alpha^2 + C_{L_{\alpha^3}}\alpha^3 \tag{C.3}$$

where the two additional coefficients easily can be found from wind tunnel testing or by estimation.

As a comparison, consider the lift coefficient as a function the angle of attack as shown in Figure C.1. Using the linear approximation (C.2), the coefficient is correct only in the linear region, and becomes inaccurate at high angles of attack. Adding an addition term, $C_{L_{\alpha^2}}\alpha^2$ it becomes more accurate than the linear approximation, but still it is inaccurate at high angles of attack. Finally, by using a third order

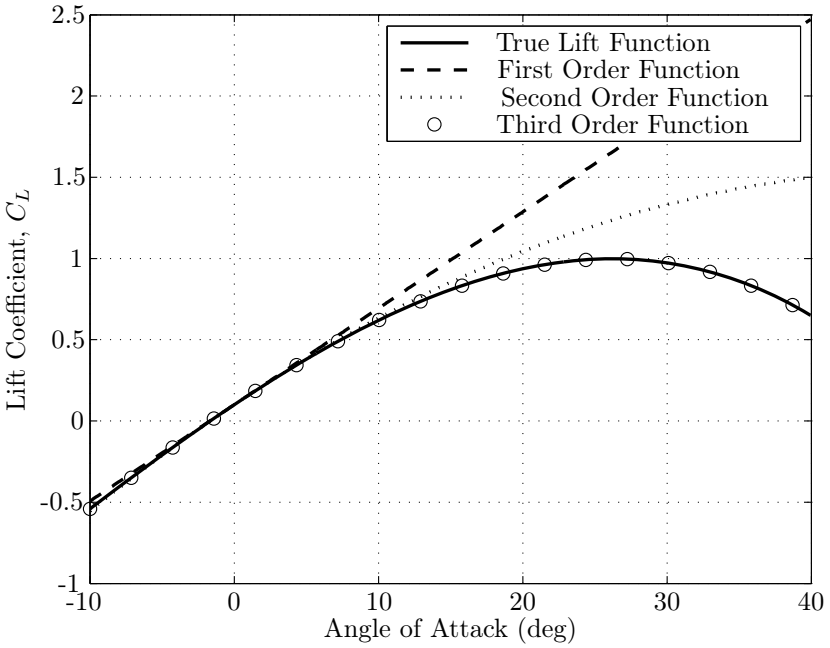

Figure C.1: Lift coefficient as a function of angle of attack.

polynomial as in (C.3), the lift coefficient is perfectly modeled, even at high angles of attack.

The lift force is not only dependent on the angle of attack, but also additional variables such as the angular velocities and the deflection angles. The aerodynamic coefficients are therefore commonly written as (*cf.* (2.18)-(2.20))

$$C_D = C_{D_0} + C_{D_\alpha}\alpha + \frac{\bar{c}}{2V_a}C_{D_q}q + C_{D_{\delta_e}}\delta_e \tag{C.4}$$

$$C_Y = C_{Y_0} + C_{Y_\beta}\beta + \frac{b}{2V_a}C_{Y_p}p + \frac{b}{2V_a}C_{Y_r}r + C_{Y_{\delta_a}}\delta_a + C_{Y_{\delta_r}}\delta_r \tag{C.5}$$

$$C_L = C_{L_0} + C_{L_\alpha}\alpha + \frac{\bar{c}}{2V_a}C_{L_q}q + C_{L_{\delta_e}}\delta_e, \tag{C.6}$$

but are still only valid close to a trimmed point, requiring either switching of coefficients or adaptive control. Since this is a truncated Taylor expansion around a

given flight condition, by applying similar arguments as for the lift coefficient, the nonlinear aerodynamics can be extended as

$$\begin{aligned}
C_D = C_{D_0} &+ C_{D_\alpha}\alpha + C_{D_{\alpha^2}}\alpha^2 + C_{D_{\alpha^3}}\alpha^3 + C_{D_{\alpha^4}}\alpha^4 + C_{D_{\alpha^5}}\alpha^5 + \dots) \\
&+ \frac{\bar{c}}{2V_a}(C_{D_q}q + C_{D_{q^2}}q^2 + C_{D_{q^3}}q^3 + C_{D_{q^4}}q^4 C_{D_{q^5}}q^5 + \dots) \\
&+ (C_{D_{\delta_e}}\delta_e + C_{D_{\delta_e^2}}\delta_e^2 + C_{D_{\delta_e^3}}\delta_e^3 + C_{D_{\delta_e^4}}\delta_e^4 + C_{D_{\delta_e^5}}\delta_e^5 + \dots) \qquad \text{(C.7)} \\
C_Y = C_{Y_0} &+ C_{Y_\beta}\beta + C_{Y_{\beta^2}}\beta^2 + C_{Y_{\beta^3}}\beta^3 + C_{Y_{\beta^4}}\beta^4 + C_{Y_{\beta^5}}\beta^5 + \dots \\
&+ \frac{b}{2V_a}(C_{Y_p}p + C_{Y_{p^2}}p^2 + C_{Y_{p^3}}p^3 + C_{Y_{p^4}}p^4 + C_{Y_{p^5}}p^5 + \dots) \\
&+ \frac{b}{2V_a}(C_{Y_r}r + C_{Y_{r^2}}r^2 + C_{Y_{r^3}}r^3 + C_{Y_{r^4}}r^4 + C_{Y_{r^5}}r^5 + \dots) \\
&+ (C_{Y_{\delta_a}}\delta_a + C_{Y_{\delta_a^2}}\delta_a^2 + C_{Y_{\delta_a^3}}\delta_a^3 + C_{Y_{\delta_a^4}}\delta_a^4 + C_{Y_{\delta_a^5}}\delta_a^5 + \dots) \\
&+ (C_{Y_{\delta_r}}\delta_r + C_{Y_{\delta_r^2}}\delta_r^2 + C_{Y_{\delta_r^3}}\delta_r^3 + C_{Y_{\delta_r^4}}\delta_r^4 + C_{Y_{\delta_r^5}}\delta_r^5 + \dots) \qquad \text{(C.8)} \\
C_L = C_{L_0} &+ C_{L_\alpha}\alpha + C_{L_{\alpha^2}}\alpha^2 + C_{L_{\alpha^3}}\alpha^3 + C_{L_{\alpha^4}}\alpha^4 + C_{L_{\alpha^5}}\alpha^5 + \dots) \\
&+ \frac{\bar{c}}{2V_a}(C_{L_q}q + C_{L_{q^2}}q^2 + C_{L_{q^3}}q^3 + C_{L_{q^4}}q^4 C_{L_{q^5}}q^5 + \dots) \\
&+ C_{L_{\delta_e}}\delta_e + C_{L_{\delta_e^2}}\delta_e^2 + C_{L_{\delta_e^3}}\delta_e^3 + C_{L_{\delta_e^4}}\delta_e^4 + C_{L_{\delta_e^5}}\delta_e^5 + \dots). \qquad \text{(C.9)}
\end{aligned}$$

Remark C.1 *This type of modeling is presented in Morelli (1998), but it is not common to use it for control. The main reason is probably due to the common approach of flight control, where the angle of attack and sideslip angles are stabilized using the angular velocity, which again are stabilized using the deflection angles in the rotational dynamics. By using this aerodynamic model, it is not possible to use the angular rates to stabilize the angle of attack and sideslip since the angular rates are represented as a power series.*

Similarly as for the aerodynamic forces, the aerodynamic moments can be extended. The common representation for the nonlinear aerodynamic moments is given as

$$\boldsymbol{\tau}^b_{aero} = \frac{1}{2}\rho S V_a^2 \begin{bmatrix} bC_l \\ \bar{c}C_m \\ bC_n \end{bmatrix} \qquad \text{(C.10)}$$

where C_l,C_m and C_n represents the aerodynamic moment coefficients and are defined as (*cf.* Etkin (1972), Stengel (2004), Campa *et al.* (2007))

$$C_l = C_{l_0} + C_{l_\beta}\beta + \frac{b}{2V_a}C_{l_p}p + \frac{b}{2V_a}C_{l_r}r + C_{l_{\delta_a}}\delta_a + C_{l_{\delta_r}}\delta_r \qquad \text{(C.11)}$$

$$C_m = C_{m_0} + C_{m_\alpha}\alpha + \frac{\bar{c}}{2V_a}C_{m_q}q + C_{m_{\delta_e}}\delta_e \qquad \text{(C.12)}$$

$$C_n = C_{n_0} + C_{n_\beta}\beta + \frac{b}{2V_a}C_{n_p}p + \frac{b}{2V_a}C_{n_r}r + C_{n_{\delta_a}}\delta_a + C_{n_{\delta_r}}\delta_r. \qquad \text{(C.13)}$$

Similarly as for the forces, the aerodynamic moment equations can be extended as

$$C_l = C_{l_{ext}} + \frac{b}{2V_a} C_{l_p} p + \frac{b}{2V_a} C_{l_r} r + C_{l_{\delta_a}} \delta_a + C_{l_{\delta_r}} \delta_r \tag{C.14}$$

$$C_m = C_{m_{ext}} + \frac{\bar{c}}{2V_a} C_{m_q} q + C_{m_{\delta_e}} \delta_e \tag{C.15}$$

$$C_n = C_{n_{ext}} + \frac{b}{2V_a} C_{n_p} p + \frac{b}{2V_a} C_{n_r} r + C_{n_{\delta_a}} \delta_a + C_{n_{\delta_r}} \delta_r \tag{C.16}$$

with

$$\begin{aligned} C_{l_{ext}} = {} & C_{l_0} + C_{l_\beta}\beta + C_{l_{\beta^2}}\beta^2 + C_{l_{\beta^3}}\beta^3 + C_{l_{\beta^4}}\beta^4 + C_{l_{\beta^5}}\beta^5 + \dots \\ & + \frac{b}{2V_a}(C_{l_{p^2}} p^2 + C_{l_{p^3}} p^3 + C_{l_{p^4}} p^4 + C_{l_{p^5}} p^5 + \dots) \\ & + \frac{b}{2V_a}(C_{l_{r^2}} r^2 + C_{l_{r^3}} r^3 + C_{l_{r^4}} r^4 + C_{l_{r^5}} r^5 + \dots) \end{aligned} \tag{C.17}$$

$$\begin{aligned} C_{m_{ext}} = {} & C_{m_0} + C_{m_\alpha}\alpha + C_{m_{\alpha^2}}\alpha^2 + C_{m_{\alpha^3}}\alpha^3 + C_{m_{\alpha^4}}\alpha^4 + C_{m_{\alpha^5}}\alpha^5 + \dots \\ & + \frac{\bar{c}}{2V_a}(C_{m_{q^2}} q^2 + C_{m_{q^3}} q^3 + C_{m_{q^4}} q^4 + C_{m_{q^5}} q^5 + \dots) \end{aligned} \tag{C.18}$$

$$\begin{aligned} C_{n_{ext}} = {} & C_{n_0} + C_{n_\beta}\beta + C_{n_{\beta^2}}\beta^2 + C_{n_{\beta^3}}\beta^3 + C_{n_{\beta^4}}\beta^4 + C_{n_{\beta^5}}\beta^5 + \dots \\ & + \frac{b}{2V_a}(C_{n_{p^2}} p^2 + C_{n_{p^3}} p^3 + C_{n_{p^4}} p^4 + C_{n_{p^5}} p^5 + \dots) \\ & + \frac{b}{2V_a}(C_{n_{r^2}} r^2 + C_{n_{r^3}} r^3 + C_{n_{r^4}} r^4 + C_{n_{r^5}} r^5 + \dots) \end{aligned} \tag{C.19}$$

enabling the aerodynamic moments to be written in compact form as

$$\boldsymbol{\tau}^b_{aero} = \mathbf{f}_{ext}(\mathbf{x}) - \mathbf{D}(\mathbf{x})\boldsymbol{\omega}^b_{n,b} + \mathbf{G}(\mathbf{x})\mathbf{u} \tag{C.20}$$

where $\mathbf{D}(\mathbf{x})$ and $\mathbf{G}(\mathbf{x})$ are defined in Section 2.4 and

$$\mathbf{f}_{ext}(\mathbf{x}) = \frac{1}{2}\rho S V_a^2 \begin{bmatrix} bC_{l_{ext}} \\ \bar{c}C_{m_{ext}} \\ bC_{n_{ext}} \end{bmatrix}. \tag{C.21}$$

Remark C.2 *Note that the deflection angles have not been extended in order to be able to use them for control. It is worth mentioning that the aerodynamics can be augmented using actuator dynamics ($\dot{\delta}_a, \dot{\delta}_e, \dot{\delta}_r$) for control, which then would allow the deflection angles themselves to be extended similarly as the other variables.*

Remark C.3 *It is well established that dynamics containing terms of even powers provide a destabilizing effect to the system. Since there is full control of the speed and the attitude, these terms can simply be removed from the closed loop system by properly designing the control law, and as such do not pose a problem from a control point of view.*

Remark C.4 *Note that cross terms can also be included into these aerodynamic models, since all undesirable terms can be removed.*

Remark C.5 *There is an upper bound on the number of terms used for parameterizations, where an over-parametrization degrades the aerodynamic model (cf. Morelli (1998)).*

The main point with this appendix is to emphasize that using the decoupling method such that the rotational controller can be designed before a translational controller, it enables the aerodynamics to contain multiple additional terms without increasing the control problem.

Appendix D

Lyapunov Stability

This appendix contains the different theorems and lemmas that are used to prove stability. It is based on the work by Khalil (2002), and is included to allow the thesis to be self-sustained. On a general level all desired states are assumed to be time-varying, such that this thesis considers non-autonomous systems.

D.1 Non-autonomous Systems

Definition D.1 (Khalil (2002)) *Consider the non-autonomous system*

$$\dot{\mathbf{x}} = f(t, \mathbf{x}) \tag{D.1}$$

where $f : [0, \infty) \times \mathcal{D} \to \mathbb{R}^n$ is piecewise continuous in t and locally Lipschitz in $\mathbf{x}$ on $[0, \infty) \times \mathcal{D}$, and $\mathcal{D} \subset \mathbb{R}^n$ is a domain that contains the origin $\mathbf{x} = \mathbf{0}$. The origin is an equilibrium point for (D.1) at $t = 0$ if

$$f(t, \mathbf{0}) = \mathbf{0}, \quad \forall t \geq 0. \tag{D.2}$$

Lemma D.1 (Khalil (2002)) *If $f(t, \mathbf{x})$ and $\frac{\partial f}{\partial \mathbf{x}}(t, \mathbf{x})$ are continuous on $[a, b] \times \mathcal{D}$, for some domain $\mathcal{D} \subset \mathbb{R}^n$, then f is locally Lipschitz in $\mathbf{x}$ on $[a, b] \times \mathcal{D}$.*

Lemma D.2 (Khalil (2002)) *If $f(t, \mathbf{x})$ and $\frac{\partial f}{\partial \mathbf{x}}(t, \mathbf{x})$ are continuous on $[a, b] \times \mathbb{R}^n$, then f is globally Lipschitz in $\mathbf{x}$ on $[a, b] \times \mathbb{R}^n$ if and only if $\frac{\partial f}{\partial \mathbf{x}}$ is uniformly bounded on $[a, b] \times \mathbb{R}^n$.*

Definition D.2 (Khalil (2002)) *A continuous function $\alpha : [0, a) \to [0, \infty)$ is said to belong to class $\mathcal{K}$ if it is strictly increasing and $\alpha(0) = 0$. It is said to belong to class $\mathcal{K}_\infty$ if $a = \infty$ and $\alpha(r) \to \infty$ as $r \to \infty$.*

Definition D.3 (Khalil (2002)) *A continuous function $\beta : [0, a) \times [0, \infty) \to [0, \infty)$ is said to belong to class $\mathcal{KL}$ if, for each fixed s, the mapping $\beta(r, s)$ belongs to class $\mathcal{K}$ with respect to r and, for each fixed r, the mapping $\beta(r, s)$ is decreasing with respect to s and $\beta(r, s) \to 0$ as $s \to \infty$.*

Definition D.4 (Khalil (2002)) *The equilibrium point $\mathbf{x} = \mathbf{0}$ of (D.1) is*

- *stable if, for each* $\epsilon > 0$*, there is* $\delta = \delta(\epsilon, t_0) > 0$ *such that*

$$||\mathbf{x}(t_0)|| < \delta \Rightarrow ||\mathbf{x}(t)|| < \epsilon, \quad \forall\ t \geq t_0 \geq 0 \tag{D.3}$$

- *uniformly stable if, for each* $\epsilon > 0$*, there is* $\delta = \delta(\epsilon) > 0$*, independent of* t_0*, such that (D.3) is satisfied.*
- *unstable if it is not stable.*

- *asymptotically stable if it is stable and there is a positive constant* $c = c(t_0)$ *such that* $\mathbf{x}(t) \to \mathbf{0}$ *as* $t \to \infty$*, for all* $||\mathbf{x}(t_0)|| < c$*.*
- *uniformly asymptotically stable if it is uniformly stable and there is a positive constant* c*, independent of* t_0*, such that for all* $||\mathbf{x}(t_0)|| < c, \mathbf{x}(t) \to \mathbf{0}$ *as* $t \to \infty$*, uniformly in* t_0*; that is, for each* $\eta > 0$*, there is* $T = T(\eta) > 0$ *such that*

$$||\mathbf{x}(t)|| < \eta, \quad \forall\ t \geq t_0 + T(\eta),\ \forall\ ||\mathbf{x}(t_0)|| < c \tag{D.4}$$

- *uniformly globally asymptotically stable (*UGAS*) if it is uniformly stable,* $\delta(\epsilon)$ *can be chosen to satisfy* $\lim_{\epsilon \to \infty} \delta(\epsilon) = \infty$*, and, for each pair of positive numbers* η *and* c*, there is* $T = T(\eta, c) > 0$ *such that*

$$||\mathbf{x}(t)|| < \eta, \quad \forall\ t \geq t_0 + T(\eta, c),\ \forall\ ||\mathbf{x}(t_0)|| < c. \tag{D.5}$$

Theorem D.1 (Khalil (2002)) *Let* $\mathbf{x} = \mathbf{0}$ *be an equilibrium point for (D.1) and* $\mathcal{D} \subset \mathbb{R}^n$ *be a domain containing* $\mathbf{x} = \mathbf{0}$*. Let* $V := [0, \infty) \times \mathcal{D} \to \mathbb{R}$ *be a continuously differentiable function, such that*

$$W_1(\mathbf{x}) \leq V(t, \mathbf{x}) \leq W_2(\mathbf{x}) \tag{D.6}$$

$$\frac{\partial V}{\partial t} + \frac{\partial V}{\partial \mathbf{x}} f(t, \mathbf{x}) \leq 0 \tag{D.7}$$

$\forall\ t \geq 0$ *and* $\forall\ \mathbf{x} \in \mathcal{D}$*, where* $W_1(\mathbf{x})$ *and* $W_2(\mathbf{x})$ *are continuous positive definite functions on* $\mathcal{D}$*. Then,* $\mathbf{x} = \mathbf{0}$ *is uniformly stable.*

Theorem D.2 (Khalil (2002)) *Suppose the assumptions for Theorem D.1 are satisfied with inequality (D.7) strengthened to*

$$\frac{\partial V}{\partial t} + \frac{\partial V}{\partial \mathbf{x}} f(t, \mathbf{x}) \leq -W_3(\mathbf{x}) \tag{D.8}$$

$\forall\ t \geq 0$ *and* $\forall\ \mathbf{x} \in \mathcal{D}$*, where* $W_3(\mathbf{x})$ *is a continuous positive definite function on* $\mathcal{D}$*. Then,* $\mathbf{x} = \mathbf{0}$ *is uniformly asymptotically stable. Moreover, if* r *and* c *are chosen such that* $\mathcal{B}_r = \{||\mathbf{x}|| \leq r\} \subset \mathcal{D}$ *and* $c < \min_{||\mathbf{x}||=r} W_1(\mathbf{x})$*, then every trajectory starting in* $\{\mathbf{x} \in \mathcal{B}_r | W_2(\mathbf{x}) \leq c\}$ *satisfies*

$$||\mathbf{x}(t)|| \leq \beta(||\mathbf{x}(t_0)||, t - t_0), \quad \forall t \geq t_0 \geq 0 \tag{D.9}$$

for some class $\mathcal{KL}$ *function* β*. Finally, if* $\mathcal{D} = \mathbb{R}^n$ *and* $W_1(\mathbf{x})$ *is radially unbounded, then* $\mathbf{x} = \mathbf{0}$ *is uniformly globally asymptotically stable.*

Theorem D.3 (Khalil (2002)) *Let $\mathbf{x} = \mathbf{0}$ be an equilibrium point of (D.1) and $\mathcal{D} \subset \mathbb{R}^n$ be a domain containing $\mathbf{x} = \mathbf{0}$. Let $V : [0, \infty) \times \mathcal{D} \to \mathbb{R}$ be a continuously differentiable function such that*

$$k_1||\mathbf{x}||^a \leq V(t, \mathbf{x}) \leq k_2||\mathbf{x}||^a \tag{D.10}$$

$$\frac{\partial V}{\partial t} + \frac{\partial V}{\partial \mathbf{x}} f(t, \mathbf{x}) \leq -k_3||\mathbf{x}||^a \tag{D.11}$$

$\forall\ t \geq 0$ and $\forall\ \mathbf{x} \in \mathcal{D}$, where k_1, k_2, k_3 and a are positive constants. Then, $\mathbf{x} = \mathbf{0}$ is uniformly exponentially stable[1]. If the assumptions hold globally, then $\mathbf{x} = \mathbf{0}$ is uniformly globally exponentially stable.

Theorem D.4 (Matrosov, Hahn (1967)) *Let two functions $V(t, \mathbf{x})$, $W(t, \mathbf{x})$ be given which are continuous on the domain $\mathcal{D}$ and satisfy:*

1. *$V(t, \mathbf{x})$ is positive definite and decrescent.*
2. *The derivative $\dot{V}$ can be estimated from above by a non-positive continuous t-independent function*

$$\dot{V} \leq U(\mathbf{x}) \leq 0 \tag{D.12}$$

3. *The function $W(t, \mathbf{x})$ is bounded.*
4. *The derivative $\dot{W}$ is definitely non-zero on the set $\mathcal{N} := \{\mathbf{x} : U(\mathbf{x}) = 0\}$.*

Then the equilibrium $\mathbf{x} = \mathbf{0}$ of (D.1) is uniformly asymptotically stable.

Definition D.5 (Khalil (2002)) *The solutions of (D.1) are*

- *Uniformly bounded if there exists a positive constant c, independent of $t_0 \geq 0$, and for every $a \in (0, c)$, there is $\beta = \beta(a) > 0$, independent of t_0, such that*

$$||\mathbf{x}(t_0)|| \leq a \Rightarrow ||\mathbf{x}(t)|| \leq \beta, \forall\ t \geq t_0. \tag{D.13}$$

- *Uniformly globally bounded if (D.13) holds for arbitrarily large a.*
- *Uniformly ultimately bounded with ultimate bound b if there exists positive constants b and c, independent of $t_0 \geq 0$, and for every $a \in (0, c)$, there is $T = T(a, b) \geq 0$, independent of t_0, such that*

$$||\mathbf{x}(t_0)|| \leq a \Rightarrow ||\mathbf{x}(t)|| \leq b\ \forall\ t \geq t_0 + T. \tag{D.14}$$

- *Uniformly globally ultimately bounded if (D.14) holds for arbitrary large a.*

[1] Even though Khalil (2002) does not use the term "uniformly" exponentially stable, it is included here to follow the definitions by Loría and Panteley (2002). The same theorem is presented in Panteley and Loría (2010) where "uniformly" is included.

Theorem D.5 (Khalil (2002)) *Let $\mathcal{D} \subset \mathbb{R}^n$ be a domain that contains the origin and $V : [0, \infty) \times \mathcal{D} \to \mathbb{R}$ be a continuously differentiable function such that*

$$\alpha_1(||\mathbf{x}||) \leq V(t, \mathbf{x}) \leq \alpha_2(||\mathbf{x}) \tag{D.15}$$

$$\frac{\partial V}{\partial t} + \frac{\partial V}{\partial \mathbf{x}} f(t, \mathbf{x}) \leq -W_3(\mathbf{x}), \forall\ ||\mathbf{x}|| \geq \mu > 0 \tag{D.16}$$

$\forall\ t \geq 0$ and $\forall\ \mathbf{x} \in \mathcal{D}$, where α_1 and α_2 are class $\mathcal{K}$ functions and $W_3(\mathbf{x})$ is a continuous positive definite function. Take $r > 0$ such that $\mathcal{B}_r \subset \mathcal{D}$ and suppose that

$$\mu < \alpha_2^{-1}(\alpha_1(r)). \tag{D.17}$$

Then, there exists a class $\mathcal{KL}$ function β and for every initial state $\mathbf{x}(t_0)$, satisfying $||\mathbf{x}(t_0)|| \leq \alpha_2^{-1}(\alpha_1(r))$, there is $T \geq 0$ (dependent on $\mathbf{x}(t_0)$ and μ) such that the solution of (D.1) satisfies

$$||\mathbf{x}(t_0)|| \leq \beta(||\mathbf{x}(t_0)||, t - t_0), \forall\ t_0 \leq t \leq t_0 + T \tag{D.18}$$

$$||\mathbf{x}(t)|| \leq \alpha_1^{-1}(\alpha_2(\mu)), \forall t \geq t_0 + T. \tag{D.19}$$

Moreover, if $\mathcal{D} = \mathbb{R}^n$ and α_1 belongs to class $\mathcal{K}_\infty$, then (D.18) and (D.19) hold for any initial state $\mathbf{x}(t_0)$, with no restriction on how large μ is.

D.2 Input-to-State Stability

Consider the system

$$\dot{\mathbf{x}} = f(t, \mathbf{x}, \mathbf{u}) \tag{D.20}$$

where $f : [0, \infty) \times \mathbb{R}^n \times \mathbb{R}^m \to \mathbb{R}^n$ is a piecewise continuous in t and locally Lipschitz in $\mathbf{x}$ and $\mathbf{u}$. The input $\mathbf{u}(t)$ is a piecewise continuous, bounded function of t for all $t \geq 0$.

Definition D.6 (Khalil (2002)) *The system (D.20) is said to be input-to-state stable if there exit a class $\mathcal{KL}$ function β and a class $\mathcal{K}$ function γ such that for any initial state $\mathbf{x}(t_0)$ and any bounded input $\mathbf{u}(t)$, the solutions $\mathbf{x}(t)$ exists for $t \geq t_0$ and satisfies*

$$||\mathbf{x}(t)|| \leq \beta(||\mathbf{x}(t_0)||, t - t_0) + \gamma(\sup_{t_0 \geq \tau \geq t} ||\mathbf{u}(\tau)||). \tag{D.21}$$

Theorem D.6 (Khalil (2002)) *Let $V : [0, \infty) \times \mathbb{R}^n \to \mathbb{R}$ be a continuous differentiable function such that*

$$\alpha_1(||\mathbf{x}||) \leq V(t, \mathbf{x}) \leq \alpha_2(||\mathbf{x}||) \tag{D.22}$$

$$\frac{\partial V}{\partial t} + \frac{\partial V}{\partial \mathbf{x}} f(t, \mathbf{x}, \mathbf{u}) \leq -W_3(\mathbf{x}), \quad \forall\ ||\mathbf{x}|| \geq \rho(||\mathbf{x}||) > 0 \tag{D.23}$$

$\forall\ (t, \mathbf{x}, \mathbf{u}) \in [0, \infty) \times \mathbb{R}^n \times \mathbb{R}^m$, where α_1, α_2 are class $\mathcal{K}_\infty$ functions, ρ is a class $\mathcal{K}$ function, and $W_3(\mathbf{x})$ is a continuously positive definite function on $\mathbb{R}^n$. Then, the system (D.20) is input-to-state stable with $\gamma = \alpha_1^{-1} \circ \alpha_2 \circ \rho$.

D.3 Stability of Cascades

An interconnected cascaded system is commonly expressed as (Loría and Panteley (2005))

$$\Sigma_1 : \dot{\mathbf{x}}_1 = f_1(t, \mathbf{x}_1) + g(t, \mathbf{x})\mathbf{x}_2 \tag{D.24}$$

$$\Sigma_2 : \dot{\mathbf{x}}_2 = f_2(t, \mathbf{x}_2) \tag{D.25}$$

where $\mathbf{x}_1 \in \mathbb{R}^n$, $\mathbf{x}_2 \in \mathbb{R}^m$, $\mathbf{x} = \begin{bmatrix} \mathbf{x}_1^\top & \mathbf{x}_2^\top \end{bmatrix}^\top$ and the functions $f_1(t, \mathbf{x}_1), f_2(t, \mathbf{x}_2)$ and $g(t, \mathbf{x})$ are continuous in their arguments, locally Lipschitz in $\mathbf{x}$, uniformly in t, and $f_1(t, \mathbf{x}_2)$ is continuously differentiable in both arguments. The use of cascade theory, enables a divide and conquer approach to be applied, where each problem can be solved in a modular fashion. This enables the stability of the system

$$\dot{\mathbf{x}}_1 = f_1(t, \mathbf{x}_1). \tag{D.26}$$

to be determined first and independently from the cascade. Then the stability properties of the driving system (D.25) can be established followed by an analysis of the interconnection term $g(t, \mathbf{x})$ to determine the stability of the cascaded system (D.24)-(D.25). In the following, a lemma and a theorem will be presented based on the work by Panteley and Loría (1998) and Loría and Panteley (2005) that enable the stability properties of cascaded systems to be determined.

Lemma D.3 (Loría and Panteley (2005)) *The cascade (D.24)-(D.25) is* UGAS *if and only if the system (D.25) and (D.26) are* UGAS *and the solutions of (D.24)-(D.25) are uniformly globally bounded.*

Assumption D.1 *There exist constants $c_1, c_2, \eta > 0$ and a Lyapunov function $V(t, \mathbf{x}_1)$ for (D.26) such that $V : \mathbb{R}_{\geq 0} \times \mathbb{R}^n \to \mathbb{R}_{\geq 0}$ is positive definite and radially unbounded, which satisfies:*

$$\left|\left|\frac{\partial V}{\partial \mathbf{x}_1}\right|\right| ||\mathbf{x}_1|| \leq c_1 V(t, \mathbf{x}_1) \quad \forall \ ||\mathbf{x}_1|| \geq \eta \tag{D.27}$$

$$\left|\left|\frac{\partial V}{\partial \mathbf{x}_1}\right|\right| \leq c_2 \quad \forall \ ||\mathbf{x}_1|| \leq \eta. \tag{D.28}$$

Assumption D.2 *There exist two continuous functions $\theta_1, \theta_2 : \mathbb{R}_{\geq 0} \to \mathbb{R}_{\geq 0}$, such that $g(t, \mathbf{x})$ satisfies*

$$||g(t, \mathbf{x})|| \leq \theta_1(||\mathbf{x}_2||) + \theta_2(||\mathbf{x}_2||)||\mathbf{x}_1||. \tag{D.29}$$

Assumption D.3 *There exists a class $\mathcal{K}$ function $\alpha(\cdot)$ such that, for all $t_0 \geq 0$, the trajectories of the system (D.25) satisfy*

$$\int_{t_0}^{\infty} ||\mathbf{x}_2(t, t_0, \mathbf{x}_2(t_0))||dt \leq \alpha(||\mathbf{x}_2(t_0)||). \tag{D.30}$$

Theorem D.7 *Under assumptions D.1-D.3 the origin of the cascaded system is uniformly asymptotically stable if the respective origins of (D.25) and (D.26) are uniformly asymptotically stable; see Panteley and Loría (1998).*

To consider input-to-state stability for cascaded systems, let the system be written as

$$\dot{\mathbf{x}}_1 = f_1(t, \mathbf{x}_1, \mathbf{x}_2) \tag{D.31}$$
$$\dot{\mathbf{x}}_2 = f_2(t, \mathbf{x}_2) \tag{D.32}$$

where $f_1 : [0, \infty) \times \mathbb{R}^{n_1} \times \mathbb{R}^{n_2} \to \mathbb{R}^{n_1}$ and $f_2 : [0, \infty) \times \mathbb{R}^{n_2} \to \mathbb{R}^{n_2}$ are piecewise continuous in t and locally Lipschitz in $\mathbf{x} = \begin{bmatrix} \mathbf{x}_1^\top & \mathbf{x}_2^\top \end{bmatrix}^\top$, and where the unforced system can be written as

$$\dot{\mathbf{x}}_1 = f_1(t, \mathbf{x}_1, \mathbf{0}). \tag{D.33}$$

Lemma D.4 (Khalil (2002)) *If the system (D.31), with $\mathbf{x}_2$ as input, is input-to-state stable and the origins (D.32) and (D.33) are uniformly globally asymptotically stable, then the origin of the cascaded system (D.31) and (D.32) is uniformly globally asymptotically stable.*

Appendix E

Detailed Proofs

E.1 Proof of Lemma 3.1

The drag force is a positive force that is working in the opposite direction of motion and is defined as $D = \frac{1}{2}\rho S V_a^2 C_D$ *cf.* (2.17). Since the air density, surface area and airspeed are positive, it follows that the drag coefficient must be positive. From (B.5) the linear acceleration can be written as

$$\dot{V}_a = \frac{1}{m}(T\cos(\alpha)\cos(\beta) - \frac{1}{2}\rho S V_a^2 C_D + \begin{bmatrix} m & 0 & 0 \end{bmatrix} \mathbf{R}_n^w \mathbf{f}_g^n) \tag{E.1}$$

which can be rewritten as

$$\dot{V}_a = -\frac{1}{2m}\rho S C_D V_a^2 + \gamma(T, \alpha, \beta, \mathbf{q}_{n,b}, g) \tag{E.2}$$

where the first term provides damping while the second term is a bounded function. The thrust is physically bounded, $0 \leq T \leq T_{max}$, the angle of attack and the sideslip angle are bounded by $\pm\frac{\pi}{2}$, $||\mathbf{q}_{n,b}|| = 1$ and $||\mathbf{f}_g^n|| = g$. A Lyapunov function candidate can now be proposed as

$$V := \frac{1}{2}V_a^2 \ > 0 \quad \forall\ V_a \neq 0. \tag{E.3}$$

and by differentiating (E.3) and inserting (E.2), it results in

$$\dot{V} = -\frac{1}{2m}\rho S C_D V_a^3 + V_a \gamma(T, \alpha, \beta, \mathbf{q}_{n,b}, g) \tag{E.4}$$

$$\dot{V} \leq -\frac{1}{2m}\rho S C_D V_a^3 \quad \forall\ V_a \geq \frac{2m||\gamma(T, \alpha, \beta, \mathbf{q}_{n,b}, g)||}{\rho S C_D}, \tag{E.5}$$

and by applying Assumption 2.2 it follows that $V_a > 0\ \forall\ t \geq t_0$ such that the first term will always provide damping to the system. Hence, by applying Theorem D.5 and Definition D.5 it follows that all the solutions are uniformly globally ultimately bounded[1].

[1] Note that Theorem D.5 requires that $a \in (0, c)$ with c as a constant, while $V_a \geq \beta_v > 0$, such that this is a slight abuse of the theorem.

E.2 Proof of Lemma 3.2

The actuators are physically upper and lower bounded by a maximum and minimum deflection angle, such that $||\mathbf{u}|| \leq \beta_{\mathbf{u}}$. Let a Lyapunov function candidate be chosen as

$$V = \frac{1}{2}(\boldsymbol{\omega}_{n,b}^{b})^{\top}\mathbf{J}\boldsymbol{\omega}_{n,b}^{b} > 0 \quad \forall\ \boldsymbol{\omega}_{n,b}^{b} \neq \mathbf{0} \tag{E.6}$$

and by differentiation of (E.6) and inserting (2.32) it becomes

$$\dot{V} = -(\boldsymbol{\omega}_{n,b}^{b})^{\top}\mathbf{D}(\mathbf{x})\boldsymbol{\omega}_{n,b}^{b} + (\boldsymbol{\omega}_{n,b}^{b})^{\top}(\mathbf{f}(\mathbf{x}) + \mathbf{G}(\mathbf{x})\mathbf{u}) \tag{E.7}$$

$$\leq -\beta_D||\boldsymbol{\omega}_{n,b}^{b}||^2 \quad \forall\ ||\boldsymbol{\omega}_{n,b}^{b}|| \geq \frac{||\mathbf{f}(\mathbf{x})|| + ||\mathbf{G}(\mathbf{x})||\beta_{\mathbf{u}}}{\beta_D}, \tag{E.8}$$

where β_D is the smallest eigenvalue of the damping matrix $\mathbf{D}(\mathbf{x})$ when $V_a = \beta_v$. Hence, by applying Theorem D.5 and Definition D.5 it follows that all the solutions are uniformly globally ultimately bounded.

E.3 Proof of Lemma 3.3

Let $\boldsymbol{\omega}_{b,w}^{w} := \begin{bmatrix} p_w & q_w & r_w \end{bmatrix}^{\top}$. From (B.3), the translational dynamics can be written as

$$\begin{bmatrix} \dot{V}_a \\ r_w V_a \\ -q_w V_a \end{bmatrix} = \frac{1}{m}(\mathbf{R}_b^w \mathbf{f}_{thrust}^b + \mathbf{f}_{aero}^w) + \mathbf{R}_n^w \mathbf{f}_g^n - \mathbf{R}_b^w \mathbf{S}(\boldsymbol{\omega}_{n,b}^b)\mathbf{v}_r^b, \tag{E.9}$$

where m is constant, $||\mathbf{R}_b^w|| = ||\mathbf{R}_n^w|| = 1$, $||\mathbf{f}_{thrust}^b|| = |T| \leq T_{max}$ using its physical constraint, $||\mathbf{f}_g^n|| = g$ which is a constant, $||\boldsymbol{\omega}_{n,b}^b|| \leq \beta_{\boldsymbol{\omega}}$ as shown in Lemma 3.2 and $||\mathbf{v}_r^b|| = V_a \leq \beta_{V_{max}}$ by applying Lemma 3.1, and $||\mathbf{f}_{aero}^b|| \leq \beta_{f_{aero}}$ since the aerodynamics are a function of bounded variables. Hence, all the terms of the translational dynamics are bounded, and hence it follows that $\dot{V}_a, r_w$ and q_w are bounded. Furthermore, the angular velocity between the wind and body frame can be expanded using (2.48) as

$$\boldsymbol{\omega}_{b,w}^{w} = \begin{bmatrix} p_w \\ q_w \\ r_w \end{bmatrix} = \begin{bmatrix} -\dot{\alpha}\sin(\beta) \\ -\dot{\alpha}\cos(\beta) \\ \dot{\beta} \end{bmatrix} \tag{E.10}$$

where $\frac{p_w}{q_w} = \tan(\beta)$ such that $p_w = q_w \tan(\beta)$ indicating that p_w is also bounded. Hence, all the terms of $\boldsymbol{\omega}_{b,w}^{w}$ are bounded.

E.4 Proof of Lemma 3.4

Expanding the terms it becomes

$$\mathbf{e}_{q\pm}^{\top}\mathbf{T}_e\mathbf{T}_e^{\top}\mathbf{e}_{q\pm} = \frac{1}{4}\boldsymbol{\epsilon}^{\top}\boldsymbol{\epsilon} \geq \frac{1}{8}\left((1 \mp \eta)^2 + \boldsymbol{\epsilon}^{\top}\boldsymbol{\epsilon}\right) = \frac{1}{8}\mathbf{e}_{q\pm}^{\top}\mathbf{e}_{q\pm} \tag{E.11}$$

where the inequality in (E.11) is found by

$$\frac{1}{8}\left((1\mp\eta)^2+\boldsymbol{\epsilon}^\top\boldsymbol{\epsilon}\right)\leq\frac{1}{4}\boldsymbol{\epsilon}^\top\boldsymbol{\epsilon} \tag{E.12}$$

$$(1\mp\eta)^2\leq\boldsymbol{\epsilon}^\top\boldsymbol{\epsilon}=1-\eta^2 \tag{E.13}$$

$$1\mp2\eta+\eta^2\leq1-\eta^2 \tag{E.14}$$

$$\mp2\eta\leq0, \tag{E.15}$$

and it follows that the inequality holds for $\mathbf{e}_{q+}\ \forall\ 0\leq\eta\leq1$ and $\mathbf{e}_{q-}\ \forall\ -1\leq\eta\leq0$.

E.5 Proof of Theorem 3.1

Without loss of generality, consider the positive equilibrium point and let $\mathbf{e}_q:=\mathbf{e}_{q+}$ and $\mathbf{T}_e:=\mathbf{T}_e(\mathbf{e}_{q+})$. A Lyapunov function candidate can now be chosen as

$$V_1=\frac{1}{2}\mathbf{e}_q^\top\mathbf{e}_q>0\quad\forall\ \mathbf{e}_q\neq\mathbf{0} \tag{E.16}$$

which can be differentiated and by inserting (3.4) it becomes

$$\dot{V}_1=\mathbf{e}_q^\top\mathbf{T}_e\mathbf{R}_b^w\boldsymbol{\omega}_{d,w}^b \tag{E.17}$$

$$=\mathbf{e}_q^\top\mathbf{T}_e\mathbf{R}_b^w(\boldsymbol{\omega}_{n,b}^b-\mathbf{R}_d^b\boldsymbol{\omega}_{n,d}^d+\mathbf{R}_w^b\boldsymbol{\omega}_{b,w}^w). \tag{E.18}$$

The angular velocity $\boldsymbol{\omega}_{n,b}^b$ can now be used for control, and using standard backstepping procedure (*cf.* Krstić *et al.* (1995)), let

$$\boldsymbol{\omega}_{n,b}^b:=\mathbf{R}_d^b\boldsymbol{\omega}_{n,d}^d-\mathbf{R}_w^b\boldsymbol{\omega}_{b,w}^w-k_q\mathbf{R}_w^b\mathbf{T}_e^\top\mathbf{e}_q+\mathbf{z} \tag{E.19}$$

where $k_q>0$ is a gain and $\mathbf{z}$ is a new variable to be defined. Inserting (E.19) into (E.18), the Lyapunov derivative becomes

$$\dot{V}_1=-k_q\mathbf{e}_q^\top\mathbf{T}_e\mathbf{T}_e^\top\mathbf{e}_q+\mathbf{e}_q^\top\mathbf{T}_e\mathbf{R}_b^w\mathbf{z} \tag{E.20}$$

which is negative definite as long as $\mathbf{z}=\mathbf{0}$. To stabilize the dynamics of the new variable, it can be written using (E.19) as

$$\mathbf{J}\mathbf{z}=\mathbf{J}\boldsymbol{\omega}_{n,b}^b-\mathbf{J}\mathbf{R}_d^b\boldsymbol{\omega}_{n,d}^d+\mathbf{J}\mathbf{R}_w^b\boldsymbol{\omega}_{b,w}^w+k_q\mathbf{J}\mathbf{R}_w^b\mathbf{T}_e^\top\mathbf{e}_q \tag{E.21}$$

and by differentiating (E.21), inserting (2.32) and using (E.19) it becomes

$$\begin{aligned}\mathbf{J}\dot{\mathbf{z}}=&-\mathbf{S}(\boldsymbol{\omega}_{n,b}^b)\mathbf{J}\boldsymbol{\omega}_{n,b}^b+\mathbf{f}(\mathbf{x})-\mathbf{D}(\mathbf{x})(\mathbf{R}_d^b\boldsymbol{\omega}_{n,d}^d-\mathbf{R}_w^b\boldsymbol{\omega}_{b,w}^w-k_q\mathbf{R}_w^b\mathbf{T}_e^\top\mathbf{e}_q)\\&-\mathbf{D}(\mathbf{x})\mathbf{z}+\mathbf{G}(\mathbf{x})\mathbf{u}+\mathbf{J}\mathbf{S}(\boldsymbol{\omega}_{n,b}^b)\mathbf{R}_d^b\boldsymbol{\omega}_{n,d}^d-\mathbf{J}\mathbf{R}_d^b\dot{\boldsymbol{\omega}}_{n,d}^d+\mathbf{J}\mathbf{R}_w^b\dot{\boldsymbol{\omega}}_{b,w}^w\\&+k_q\mathbf{J}\mathbf{R}_w^b\mathbf{S}(\boldsymbol{\omega}_{b,w}^w)\mathbf{T}_e^\top\mathbf{e}_q+\frac{k_q}{2}\mathbf{J}\mathbf{R}_w^b\dot{\boldsymbol{\epsilon}}_{d,w}\end{aligned} \tag{E.22}$$

where $\mathbf{T}_e^\top\mathbf{e}_q=\frac{\boldsymbol{\epsilon}_{d,w}}{2}$ has been used. Let a second Lyapunov function candidate be defined as

$$V_2=V_1+\frac{1}{2}\mathbf{z}^\top\mathbf{J}\mathbf{z}>0\quad\forall\ \mathbf{e}_q,\mathbf{z}\neq\mathbf{0} \tag{E.23}$$

which by using (E.20) and (E.22) can be differentiated as

$$\begin{aligned}\dot{V}_2 = &-k_q \mathbf{e}_q^\top \mathbf{T}_e \mathbf{T}_e^\top \mathbf{e}_q + \mathbf{e}_q^\top \mathbf{T}_e \mathbf{R}_b^w \mathbf{z} \\ &+ \mathbf{z}^\top (-\mathbf{S}(\boldsymbol{\omega}_{n,b}^b)\mathbf{J}\boldsymbol{\omega}_{n,b}^b + \mathbf{f}(\mathbf{x}) - \mathbf{D}(\mathbf{x})(\mathbf{R}_d^b \boldsymbol{\omega}_{n,d}^d - \mathbf{R}_w^b \boldsymbol{\omega}_{b,w}^w - k_q \mathbf{R}_w^b \mathbf{T}_e^\top \mathbf{e}_q) \\ &- \mathbf{D}(\mathbf{x})\mathbf{z} + \mathbf{G}(\mathbf{x})\mathbf{u} + \mathbf{J}\mathbf{S}(\boldsymbol{\omega}_{n,b}^b)\mathbf{R}_d^b \boldsymbol{\omega}_{n,d}^d - \mathbf{J}\mathbf{R}_d^b \dot{\boldsymbol{\omega}}_{n,d}^d + \mathbf{J}\mathbf{R}_w^b \dot{\boldsymbol{\omega}}_{b,w}^w \\ &+ k_q \mathbf{J}\mathbf{R}_w^b \mathbf{S}(\boldsymbol{\omega}_{b,w}^w)\mathbf{T}_e^\top \mathbf{e}_q + \frac{k_q}{2}\mathbf{J}\mathbf{R}_w^b \dot{\boldsymbol{\epsilon}}_{d,w}). \end{aligned} \tag{E.24}$$

Inserting the control law (3.12) into (E.24) the Lyapunov derivative becomes

$$\dot{V}_2 = -k_q \mathbf{e}_q^\top \mathbf{T}_e \mathbf{T}_e^\top \mathbf{e}_q - \mathbf{z}^\top (\mathbf{D}(\mathbf{x}) + k_\omega \mathbf{I})\mathbf{z} \tag{E.25}$$

and using Lemma 3.4 it reduces to

$$\dot{V}_2 \leq -\frac{k_q}{8}||\mathbf{e}_q||^2 - (\beta_D + k_\omega)||\mathbf{z}||^2 \tag{E.26}$$

which is negative definite. The damping matrix $\mathbf{D}(\mathbf{x})$ is positive definite as long as $V_a > 0$ and can be lower bounded using Assumption 2.2 as $\beta_D \leq \lambda_{min}(\mathbf{D}(\mathbf{x}_{min}))$ where $\lambda_{min}(\mathbf{D}(\mathbf{x}_{min}))$ is the smallest eigenvalue of the damping matrix where $\mathbf{x}_{min} = \begin{bmatrix}\beta_v & 0 & 0\end{bmatrix}^\top$. Given $\mathbf{q}_{n,d} \in \mathcal{S}^3$ and $\boldsymbol{\omega}_{n,d}^d, \dot{\boldsymbol{\omega}}_{n,d}^d \in \mathcal{L}_\infty$ it follows using Theorem D.3 that the origin $(\mathbf{e}_q, \mathbf{z}) = (\mathbf{0}, \mathbf{0})$ is uniformly exponentially stable. A similar proof can be shown for the negative equilibrium point by defining $\mathbf{e}_q := \mathbf{e}_{q-}$ and $\mathbf{T}_e := \mathbf{T}_e(\mathbf{e}_{q-})$.

E.6 Proof of Theorem 3.2

Without loss of generality, consider the positive equilibrium point such that $\mathbf{e}_q := \mathbf{e}_{q+}$ and $\mathbf{T}_e := \mathbf{T}_e(\mathbf{e}_{q+})$. Let a Lyapunov function candidate be defined as

$$V = \frac{1}{2}k_q \mathbf{e}_q^\top \mathbf{e}_q + (\boldsymbol{\omega}_{d,w}^b)^\top \mathbf{J}\boldsymbol{\omega}_{d,w}^b > 0 \quad \forall\ \mathbf{e}_q, \boldsymbol{\omega}_{d,w}^b \neq \mathbf{0} \tag{E.27}$$

where k_q is a positive scalar gain. Equation (E.27) can be differentiated, and by inserting (3.4) and (3.8) it becomes

$$\begin{aligned}\dot{V} = &k_q \mathbf{e}_q^\top \mathbf{T}_e \mathbf{R}_b^w \boldsymbol{\omega}_{d,w}^b + (\boldsymbol{\omega}_{d,w}^b)^\top (-\mathbf{S}(\boldsymbol{\omega}_{n,b}^b)\mathbf{J}\boldsymbol{\omega}_{n,b}^b + \mathbf{f}(\mathbf{x}) - \mathbf{D}(\mathbf{x})\boldsymbol{\omega}_{d,w}^b \\ &- \mathbf{D}(\mathbf{x})(\mathbf{R}_d^b \boldsymbol{\omega}_{n,d}^d - \mathbf{R}_w^b \boldsymbol{\omega}_{b,w}^w) + \mathbf{G}(\mathbf{x})\mathbf{u} + \mathbf{J}\mathbf{S}(\boldsymbol{\omega}_{n,b}^b)\mathbf{R}_d^b \boldsymbol{\omega}_{n,d}^d \\ &- \mathbf{J}\mathbf{R}_d^b \dot{\boldsymbol{\omega}}_{n,d}^d + \mathbf{J}\mathbf{R}_w^b \dot{\boldsymbol{\omega}}_{b,w}^w). \end{aligned} \tag{E.28}$$

By inserting the control law (3.14) into (E.28), the Lyapunov derivative becomes

$$\dot{V} = -(\boldsymbol{\omega}_{d,w}^b)^\top (\mathbf{D}(\mathbf{x}) + k_\omega \mathbf{I})\boldsymbol{\omega}_{d,w}^b \leq -(\beta_D + k_\omega)||\boldsymbol{\omega}_{d,w}^b||^2 \tag{E.29}$$

which is negative semidefinite and where β_D is a smallest eigenvalue of the damping matrix $\mathbf{D}(\mathbf{x})$ when $V_a = \beta_v$. Given $\mathbf{q}_{n,d}, \boldsymbol{\omega}_{n,d}^d, \dot{\boldsymbol{\omega}}_{n,d}^d \in \mathcal{L}_\infty$ and by applying Theorem D.1, it follows that the origin $(\mathbf{e}_q, \boldsymbol{\omega}_{d,w}^b) = (\mathbf{0}, \mathbf{0})$ is uniformly stable. The closed loop dynamics are found by inserting (3.14) into (3.8) as

$$\mathbf{J}\dot{\boldsymbol{\omega}}_{d,w}^b = -k_q \mathbf{R}_w^b \mathbf{T}_e^\top \mathbf{e}_q - (\mathbf{D}(\mathbf{x}) + k_\omega \mathbf{I})\boldsymbol{\omega}_{d,w}^b. \tag{E.30}$$

To show that $\mathbf{e}_q \to \mathbf{0}$, the Matrosov theorem can be applied (*cf.* Hahn (1967)). Let an auxiliary function be defined as

$$W := \mathbf{e}_q^\top \mathbf{T}_e \mathbf{R}_b^w \mathbf{J} \boldsymbol{\omega}_{d,w}^b \tag{E.31}$$

which is continuous and bounded since $||\mathbf{e}_q|| \leq 1$, $||\mathbf{R}_b^w|| = 1$ and $||\boldsymbol{\omega}_{d,w}^b|| \leq \beta_{\omega_e}$ using (E.29). The auxiliary function can be differentiated and by inserting (E.30) and evaluating it in the set $\mathcal{N} = \{\mathbf{e}_q \in \mathcal{S}_e^3 \ | \boldsymbol{\omega}_{d,w}^b = \mathbf{0}\}$ it becomes

$$\dot{W} = -k_q \mathbf{e}_q^\top \mathbf{T}_e \mathbf{T}_e^\top \mathbf{e}_q \leq -\frac{k_q}{8} \mathbf{e}_q^\top \mathbf{e}_q \tag{E.32}$$

where Lemma 3.4 has been used. The Lyapunov function (E.27) is decrescent and positive definite, and $\dot{V}$ is negative semidefinite and can be bounded by a time-independent function. The auxiliary function, W, is bounded and its derivative, $\dot{W}$, is definitely non-zero in the set $\mathcal{N}$. Thus, all conditions of Theorem D.4 are met, and it follows that the origin $(\mathbf{e}_q, \boldsymbol{\omega}_{d,w}^b) = (\mathbf{0}, \mathbf{0})$ is uniformly asymptotically stable. A similar proof can be done for the negative equilibrium point by defining $\mathbf{e}_q := \mathbf{e}_{q-}$ and $\mathbf{T}_e := \mathbf{T}_e(\mathbf{e}_{q-})$.

E.7 Proof of Theorem 3.3

Without loss of generality, consider the positive equilibrium point and let $\mathbf{e}_q := \mathbf{e}_{q+}$ and $\mathbf{T}_e := \mathbf{T}_e(\mathbf{e}_{q+})$. The sliding variable is defined as

$$\mathbf{s} = \boldsymbol{\omega}_{n,b}^b - \boldsymbol{\omega}_{n,r}^b \tag{E.33}$$

$$\boldsymbol{\omega}_{n,r}^b = \mathbf{R}_d^b \boldsymbol{\omega}_{n,d}^d - \mathbf{R}_w^b \boldsymbol{\omega}_{b,w}^w - \boldsymbol{\Lambda} \mathbf{R}_w^b \mathbf{T}_e^\top \mathbf{e}_q \tag{E.34}$$

where $\boldsymbol{\Lambda} = \lambda \mathbf{I}$ with $\lambda > 0$, enabling the angular velocity error to be written as

$$\boldsymbol{\omega}_{d,w}^b = \mathbf{s} - \boldsymbol{\Lambda} \mathbf{R}_w^b \mathbf{T}_e^\top \mathbf{e}_q, \tag{E.35}$$

and the sliding variable can be differentiated using (2.32) and (E.33) as

$$\mathbf{J}\dot{\mathbf{s}} = -\mathbf{S}(\boldsymbol{\omega}_{n,b}^b)\mathbf{J}\boldsymbol{\omega}_{n,b}^b + \mathbf{f}(\mathbf{x}) - \mathbf{D}(\mathbf{x})\mathbf{s} - \mathbf{D}(\mathbf{x})\boldsymbol{\omega}_{n,r}^b + \mathbf{G}(\mathbf{x})\mathbf{u} - \mathbf{J}\dot{\boldsymbol{\omega}}_{n,r}^b. \tag{E.36}$$

A Lyapunov function candidate be now chosen as

$$V_1 = \frac{k_q}{2} \mathbf{e}_q^\top \mathbf{e}_q + \frac{1}{2} \mathbf{s}^\top \mathbf{J} \mathbf{s} > 0 \quad \forall \mathbf{e}_q, \mathbf{s} \neq \mathbf{0} \tag{E.37}$$

where $k_q > 0$ is a scalar gain. Equation (E.37) can be differentiated using (3.4), (E.35) and (E.36) as

$$\begin{aligned} \dot{V}_1 = &-k_q \mathbf{e}_q^\top \mathbf{T}_e \boldsymbol{\Lambda} \mathbf{T}_e^\top \mathbf{e}_q + k_q \mathbf{e}_q^\top \mathbf{T}_e \mathbf{R}_b^w \mathbf{s} \\ &+ \mathbf{s}^\top (-\mathbf{S}(\boldsymbol{\omega}_{n,b}^b)\mathbf{J}\boldsymbol{\omega}_{n,b}^b + \mathbf{f}(\mathbf{x}) - \mathbf{D}(\mathbf{x})\mathbf{s} - \mathbf{D}(\mathbf{x})\boldsymbol{\omega}_{n,r}^b + \mathbf{G}(\mathbf{x})\mathbf{u} - \mathbf{J}\dot{\boldsymbol{\omega}}_{n,r}^b) \end{aligned} \tag{E.38}$$

and by inserting (3.15) into (E.38) it results in

$$\begin{aligned} \dot{V}_1 &= -k_q \mathbf{e}_q^\top \mathbf{T}_e \boldsymbol{\Lambda} \mathbf{T}_e^\top \mathbf{e}_q - \mathbf{s}^\top (\mathbf{D}(\mathbf{x}) + k_s \mathbf{I}) \mathbf{s} \\ &\leq -\frac{k_q \lambda}{8} ||\mathbf{e}_q||^2 - (\beta_D + k_s) ||\mathbf{s}||^2 \end{aligned} \tag{E.39}$$

where Lemma 3.4 has been used and where β_D is the smallest eigenvalue of the damping matrix $\mathbf{D}(\mathbf{x})$ when $V_a = \beta_v$. The Lyapunov Function (E.37) is positive definite and decrescent while its derivative (E.39) is negative definite. Given $\mathbf{q}_{n,d}, \boldsymbol{\omega}^d_{n,d}, \dot{\boldsymbol{\omega}}^d_{n,d} \in \mathcal{L}_\infty$ it follows by applying Theorem D.3 that the origin $(\mathbf{e}_q, \mathbf{s}) = (\mathbf{0}, \mathbf{0})$ is uniformly exponentially stable. A similar proof can be done for the negative equilibrium point by defining $\mathbf{e}_q := \mathbf{e}_{q-}$ and $\mathbf{T}_e := \mathbf{T}_e(\mathbf{e}_{q-})$.

E.8 Proof of Lemma 3.5

Without loss of generality let $\mathbf{e}_{q_r} = \mathbf{e}_{q_r+}$ and $\mathbf{T}_{e_r} = \mathbf{T}_{e_r}(\mathbf{e}_{q_r+})$. A Lyapunov function candidate can be defined as

$$V_1 = \frac{1}{2}\mathbf{e}_{q_r}^\top \mathbf{e}_{q_r} > 0 \quad \forall \mathbf{e}_{q_r} \neq \mathbf{0} \tag{E.40}$$

and differentiated along the trajectories of (3.21) as

$$\dot{V}_1 = \mathbf{e}_{q_r}^\top \mathbf{T}_{e_r}(\boldsymbol{\omega}^r_{n,r} - \mathbf{R}^r_d \boldsymbol{\omega}^d_{n,d}). \tag{E.41}$$

Using backstepping (*cf.* Krstić *et al.* (1995)), the reference angular velocity can be chosen as

$$\boldsymbol{\omega}^r_{n,r} = \mathbf{R}^r_d \boldsymbol{\omega}^d_{n,d} - k_1 \mathbf{T}_{e_r}^\top \mathbf{e}_{q_r} + \mathbf{z}_r \tag{E.42}$$

where $k_1 > 0$ is a gain and $\mathbf{z}_r$ is a new variable to be defined. By inserting (E.42) into (E.41), the Lyapunov derivative becomes

$$\dot{V}_1 = -k_1 \mathbf{e}_{q_r}^\top \mathbf{T}_{e_r} \mathbf{T}_{e_r}^\top \mathbf{e}_{q_r} + \mathbf{e}_{q_r}^\top \mathbf{T}_{e_r} \mathbf{z}_r, \tag{E.43}$$

which is negative definite as long as $\mathbf{z}_r = \mathbf{0}$. The new variable is found using (E.42) as

$$\mathbf{z}_r = \boldsymbol{\omega}^r_{n,r} - \mathbf{R}^r_d \boldsymbol{\omega}^d_{n,d} + k_1 \mathbf{T}_{e_r}^\top \mathbf{e}_{q_r} \tag{E.44}$$

and its derivative is found as

$$\dot{\mathbf{z}}_r = \dot{\boldsymbol{\omega}}^r_{n,r} + \mathbf{S}(\boldsymbol{\omega}^r_{n,r}) \mathbf{R}^r_d \boldsymbol{\omega}^d_{n,d} - \mathbf{R}^r_d \dot{\boldsymbol{\omega}}^d_{n,d} + k_1 \frac{\dot{\boldsymbol{\epsilon}}_{d,r}}{2} \tag{E.45}$$

where $\mathbf{T}_{e_r}^\top \mathbf{e}_{q_r} = \frac{1}{2}\boldsymbol{\epsilon}_{d,r}$ has been used. A second Lyapunov function candidate can now be defined as

$$V_2 = V_1 + \frac{1}{2}\mathbf{z}_r^\top \mathbf{z}_r > 0 \quad \forall\ \mathbf{e}_{q_r}, \mathbf{z}_r \neq \mathbf{0}. \tag{E.46}$$

By differentiating (E.46) and inserting (E.43) and (E.45), it becomes

$$\begin{aligned} \dot{V}_2 = &- k_1 \mathbf{e}_{q_r}^\top \mathbf{T}_{e_r} \mathbf{T}_{e_r}^\top \mathbf{e}_{q_r} + \mathbf{e}_{q_r}^\top \mathbf{T}_{e_r} \mathbf{z}_r + \mathbf{z}_r^\top \left(\dot{\boldsymbol{\omega}}^r_{n,r} + \mathbf{S}(\boldsymbol{\omega}^r_{n,r}) \mathbf{R}^r_d \boldsymbol{\omega}^d_{n,d} \right. \\ &\left. - \mathbf{R}^r_d \dot{\boldsymbol{\omega}}^d_{n,d} + k_1 \frac{\dot{\boldsymbol{\epsilon}}_{d,r}}{2} \right), \end{aligned} \tag{E.47}$$

and by inserting (3.24) into (E.47) it results in

$$\dot{V}_2 = -k_1 \mathbf{e}_{q_r}^\top \mathbf{T}_{e_r} \mathbf{T}_{e_r}^\top \mathbf{e}_{q_r} - k_2 \mathbf{z}_r^\top \mathbf{z}_r + \mathbf{z}_r^\top \boldsymbol{\xi}_1 \tag{E.48}$$

$$\leq -\frac{k_1}{8} ||\mathbf{e}_{q_r}||^2 - k_2 ||\mathbf{z}_r||^2 \quad \forall \; ||\mathbf{z}_r|| \geq \left|\left| \frac{\boldsymbol{\xi}_1}{k_2} \right|\right| \tag{E.49}$$

where Lemma 3.4 has been used. Let $\dot{\mathbf{x}}_r := \begin{bmatrix} \dot{\mathbf{e}}_{q_r}^\top & \dot{\mathbf{z}}_r^\top \end{bmatrix}^\top$ denote the system. Consider the case when $\boldsymbol{\xi}_1$ is nonzero and perturbs the system. The Lyapunov function (E.46) is positive definite and decrescent, while its derivative (E.49) is negative definite $\forall \; ||\mathbf{z}_r|| \geq \left|\left| \frac{\boldsymbol{\xi}_1}{k_2} \right|\right|$ and the function $\boldsymbol{\xi}_1$ is bounded. By applying Theorem D.6 it is concluded that the system $\dot{\mathbf{x}}_r$ is input-to-state stable. Being input-to-state stable, it follows from Definition D.6 that the solution $\mathbf{x}_r(t)$ exists for all $t \geq t_0$ and satisfies

$$||\mathbf{x}_r(t)|| \leq \beta(||\mathbf{x}_r(t_0)||, t - t_0) + \gamma \left(\sup_{t_0 \leq \tau \leq t} ||\boldsymbol{\xi}_1(\tau)|| \right) \tag{E.50}$$

where β is a class $\mathcal{KL}$ function while γ is a class $\mathcal{K}$ function. As the bounded function $\boldsymbol{\xi}_1 \to \mathbf{0}$, equation (E.50) reduces to

$$||\mathbf{x}_r(t)|| \leq \beta(||\mathbf{x}_r(t_0)||, t - t_0) \tag{E.51}$$

showing that the origin $(\mathbf{e}_{q_r}, \mathbf{z}_r) = (\mathbf{0}, \mathbf{0})$ is uniformly asymptotically stable when $\boldsymbol{\xi}_1 = \mathbf{0}$. A similar proof can be done for the negative equilibrium point by defining $\mathbf{e}_{q_r} = \mathbf{e}_{q_r -}$ and $\mathbf{T}_{e_r} = \mathbf{T}_{e_r}(\mathbf{e}_{q_r -})$.

E.9 Proof of Theorem 3.4

Without loss of generality, let $\mathbf{e}_q := \mathbf{e}_{q+}$ and $\mathbf{T}_e := \mathbf{T}_e(\mathbf{e}_{q+})$. A Lyapunov function candidate can be defined as

$$V_1 := \frac{1}{2} \mathbf{e}_q^\top \mathbf{e}_q > 0 \quad \forall \; \mathbf{e}_q \neq \mathbf{0}. \tag{E.52}$$

Equation (E.52) can be differentiated as

$$\dot{V}_1 = \mathbf{e}_q^\top \mathbf{T}_e \mathbf{R}_b^w \boldsymbol{\omega}_{r,w}^b \tag{E.53}$$

where $\boldsymbol{\omega}_{r,w}^b$ can be used for control. Using backstepping, let the angular velocity error be chosen as

$$\boldsymbol{\omega}_{r,w}^b := -k_3 \mathbf{R}_w^b \mathbf{T}_e^\top \mathbf{e}_q + \mathbf{z} \tag{E.54}$$

where $k_3 > 0$ is a gain and $\mathbf{z}$ is a new variable, then

$$\dot{V}_1 = -k_3 \mathbf{e}_q^\top \mathbf{T}_e \mathbf{T}_e^\top \mathbf{e}_q + \mathbf{e}_q^\top \mathbf{T}_e \mathbf{R}_b^w \mathbf{z} \tag{E.55}$$

which is negative definite as long as $\mathbf{z} = \mathbf{0}$. The new variable is found from (E.54) and differentiated using (3.29) as

$$\mathbf{z} = \boldsymbol{\omega}_{n,b}^{b} - \mathbf{R}_{r}^{b}\boldsymbol{\omega}_{n,r}^{r} + \mathbf{R}_{w}^{b}\boldsymbol{\omega}_{b,w}^{w} + k_3\mathbf{R}_{w}^{b}\mathbf{T}_{e}^{\top}\mathbf{e}_q \tag{E.56}$$

$$\begin{aligned}\dot{\mathbf{z}} = \mathbf{J}^{-1}(&-\mathbf{S}(\boldsymbol{\omega}_{n,b}^{b})\mathbf{J}\boldsymbol{\omega}_{n,b}^{b} + \hat{\mathbf{f}}(\mathbf{x}) - \hat{\mathbf{D}}(\mathbf{x})\boldsymbol{\omega}_{n,b}^{b} + \hat{\mathbf{G}}(\mathbf{x})\mathbf{u} + \hat{\mathbf{G}}(\mathbf{x})\tilde{\mathbf{u}} - \boldsymbol{\Phi}_2\tilde{\boldsymbol{\theta}}_2 \\ &- \boldsymbol{\Phi}_3\tilde{\boldsymbol{\theta}}_3) + \mathbf{S}(\boldsymbol{\omega}_{n,b}^{b})\mathbf{R}_{r}^{b}\boldsymbol{\omega}_{n,r}^{r} - \mathbf{R}_{r}^{b}(\mathbf{R}_{d}^{r}\dot{\boldsymbol{\omega}}_{n,d}^{d} - \mathbf{S}(\boldsymbol{\omega}_{n,r}^{r})\mathbf{R}_{d}^{r}\boldsymbol{\omega}_{n,d}^{d} - k_1\frac{\dot{\boldsymbol{\epsilon}}_{d,r}}{2} \\ &- \mathbf{T}_{e_r}^{\top}\mathbf{e}_{q_r} - k_2\mathbf{z}_r + \boldsymbol{\xi}_1) + \mathbf{R}_{w}^{b}\dot{\boldsymbol{\omega}}_{b,w}^{w} + k_3\mathbf{R}_{w}^{b}\mathbf{S}(\boldsymbol{\omega}_{b,w}^{w})\mathbf{T}_{e}^{\top}\mathbf{e}_q + \frac{k_3}{2}\mathbf{R}_{w}^{b}\dot{\boldsymbol{\epsilon}}_{r,w}.\end{aligned} \tag{E.57}$$

A second Lyapunov function candidate can be defined as

$$V_2 := V_1 + \frac{1}{2}\mathbf{z}^{\top}\mathbf{z} + \frac{1}{2}\tilde{\boldsymbol{\theta}}_2^{\top}\boldsymbol{\Gamma}_2^{-1}\tilde{\boldsymbol{\theta}}_2 + \frac{1}{2}\tilde{\boldsymbol{\theta}}_3^{\top}\boldsymbol{\Gamma}_3^{-1}\tilde{\boldsymbol{\theta}}_3 > 0 \quad \forall\ \mathbf{e}_q, \mathbf{z}, \tilde{\boldsymbol{\theta}}_2, \tilde{\boldsymbol{\theta}}_3 \neq \mathbf{0} \tag{E.58}$$

where $\boldsymbol{\Gamma}_2 > \mathbf{0}$ and $\boldsymbol{\Gamma}_3 > \mathbf{0}$ are adaptive gain matrices. Differentiating (E.58) and inserting (E.55) and (E.57), the Lyapunov derivative becomes

$$\begin{aligned}\dot{V}_2 = &-k_3\mathbf{e}_q^{\top}\mathbf{T}_e\mathbf{T}_e^{\top}\mathbf{e}_q + \mathbf{e}_q^{\top}\mathbf{T}_e\mathbf{R}_b^{w}\mathbf{z} + \mathbf{z}^{\top}(\mathbf{J}^{-1}(-\mathbf{S}(\boldsymbol{\omega}_{n,b}^{b})\mathbf{J}\boldsymbol{\omega}_{n,b}^{b} + \hat{\mathbf{f}}(\mathbf{x}) \\ &- \hat{\mathbf{D}}(\mathbf{x})\boldsymbol{\omega}_{n,b}^{b} + \hat{\mathbf{G}}(\mathbf{x})\mathbf{u} + \hat{\mathbf{G}}(\mathbf{x})\tilde{\mathbf{u}} - \boldsymbol{\Phi}_2\tilde{\boldsymbol{\theta}}_2 - \boldsymbol{\Phi}_3\tilde{\boldsymbol{\theta}}_3) + \mathbf{S}(\boldsymbol{\omega}_{n,b}^{b})\mathbf{R}_{r}^{b}\boldsymbol{\omega}_{n,r}^{r} \\ &- \mathbf{R}_{r}^{b}(\mathbf{R}_{d}^{r}\dot{\boldsymbol{\omega}}_{n,d}^{d} - \mathbf{S}(\boldsymbol{\omega}_{n,r}^{r})\mathbf{R}_{d}^{r}\boldsymbol{\omega}_{n,d}^{d} - k_1\frac{\dot{\boldsymbol{\epsilon}}_{d,r}}{2} - \mathbf{T}_{e_r}^{\top}\mathbf{e}_{q_r} - k_2\mathbf{z}_r + \boldsymbol{\xi}_1) \\ &+ \mathbf{R}_{w}^{b}\dot{\boldsymbol{\omega}}_{b,w}^{w} + k_3\mathbf{R}_{w}^{b}\mathbf{S}(\boldsymbol{\omega}_{b,w}^{w})\mathbf{T}_{e}^{\top}\mathbf{e}_q + \frac{k_3}{2}\mathbf{R}_{w}^{b}\dot{\boldsymbol{\epsilon}}_{r,w}) + \tilde{\boldsymbol{\theta}}_2^{\top}\boldsymbol{\Gamma}_2^{-1}\dot{\tilde{\boldsymbol{\theta}}}_2 + \tilde{\boldsymbol{\theta}}_3^{\top}\boldsymbol{\Gamma}_3^{-1}\dot{\tilde{\boldsymbol{\theta}}}_3.\end{aligned} \tag{E.59}$$

The first problem that can be solved is to remove the saturation problem from the closed loop dynamics and into the reference trajectory by defining $\boldsymbol{\xi}_1$ as in (3.31). The control law (3.30) and the two adaption laws (3.33)-(3.34) can now be inserted, resulting in the Lyapunov derivative as

$$\dot{V}_2 \leq -\frac{k_3}{8}||\mathbf{e}_q||^2 - k_4||\mathbf{z}||^2 < 0 \quad \forall\ \mathbf{e}_q, \mathbf{z} \neq \mathbf{0}, \tag{E.60}$$

which is negative semi-definite. Given $\mathbf{q}_{n,d} \in \mathcal{S}^3$ and $\boldsymbol{\omega}_{n,d}^{d}, \dot{\boldsymbol{\omega}}_{n,d}^{d} \in \mathcal{L}_\infty$ it follows by using Theorem D.1 that the origin $(\mathbf{e}_q, \mathbf{z}, \tilde{\boldsymbol{\theta}}_2, \tilde{\boldsymbol{\theta}}_3) = (\mathbf{0}, \mathbf{0}, \mathbf{0}, \mathbf{0})$ is uniformly stable, indicating that the terms $\mathbf{e}_q, \mathbf{z}, \tilde{\boldsymbol{\theta}}_2$ and $\tilde{\boldsymbol{\theta}}_3$ are bounded. To show that the origin is uniformly asymptotically stable, Matrosov's theorem will be applied. The closed loop error dynamics can now be found as

$$\dot{\mathbf{e}}_q = -k_3\mathbf{R}_{w}^{b}\mathbf{T}_{e}^{\top}\mathbf{e}_q + \mathbf{T}_e\mathbf{R}_{b}^{w}\mathbf{z} \tag{E.61}$$

$$\dot{\mathbf{z}} = -\mathbf{R}_{w}^{b}\mathbf{T}_{e}^{\top}\mathbf{e}_q - k_4\mathbf{z} - \mathbf{J}^{-1}(\boldsymbol{\Phi}_2\tilde{\boldsymbol{\theta}}_2 + \boldsymbol{\Phi}_3\tilde{\boldsymbol{\theta}}_3) \tag{E.62}$$

$$\dot{\tilde{\boldsymbol{\theta}}}_2 = \boldsymbol{\Gamma}_2\boldsymbol{\Phi}_2^{\top}\mathbf{J}^{-1}\mathbf{z} \tag{E.63}$$

$$\dot{\tilde{\boldsymbol{\theta}}}_3 = \text{proj}(\boldsymbol{\Gamma}_3\boldsymbol{\Phi}_2^{\top}\mathbf{J}^{-1}\mathbf{z}), \tag{E.64}$$

and a continuous bounded auxiliary function can now be chosen as

$$W := \mathbf{e}_q^{\top}\mathbf{T}_e\mathbf{R}_{b}^{w}(\boldsymbol{\Phi}_2\tilde{\boldsymbol{\theta}}_2 + \boldsymbol{\Phi}_3\tilde{\boldsymbol{\theta}}_3) + \mathbf{z}^{\top}\mathbf{J}^{-1}(\boldsymbol{\Phi}_2\tilde{\boldsymbol{\theta}}_2 + \boldsymbol{\Phi}_3\tilde{\boldsymbol{\theta}}_3) \tag{E.65}$$

Note that $\boldsymbol{\Phi}_2 = \boldsymbol{\Phi}_2(V_a, \alpha, \beta, \boldsymbol{\omega}^b_{n,b})$ and $\boldsymbol{\Phi}_3 = \boldsymbol{\Phi}_3(V_a, \delta_a, \delta_e, \delta_r)$. The angle of attack, α, and the sideslip angle β are bounded by $\pm\frac{\pi}{2}$, V_a is shown to be bounded in Lemma 3.1, the angular velocity, $\boldsymbol{\omega}^b_{n,b}$ is shown to be bounded in Lemma 3.2 and the deflection angles are physically bounded. The remaining terms are bounded since the origin is shown to be uniformly stable. Equation E.65 can now be differentiated, and by evaluating it in the set $\mathcal{N} := \{\tilde{\boldsymbol{\theta}}_2 \in \mathbb{R}^{11}, \tilde{\boldsymbol{\theta}}_3 \in \mathbb{R}^5 | \mathbf{e}_q = \mathbf{0}, \mathbf{z} = \mathbf{0}\}$, it becomes

$$\begin{aligned}\dot{W} &= -(\mathbf{J}^{-1}(\boldsymbol{\Phi}_2\tilde{\boldsymbol{\theta}}_2 + \boldsymbol{\Phi}_3\tilde{\boldsymbol{\theta}}_3))^\top(\mathbf{J}^{-1}(\boldsymbol{\Phi}_2\tilde{\boldsymbol{\theta}}_2 + \boldsymbol{\Phi}_3\tilde{\boldsymbol{\theta}}_3)) \\ &\leq -\left|\left|\mathbf{J}^{-1}(\boldsymbol{\Phi}_2\tilde{\boldsymbol{\theta}}_2 + \boldsymbol{\Phi}_3\tilde{\boldsymbol{\theta}}_3)\right|\right|^2, \end{aligned} \tag{E.66}$$

which is definitely non-zero as long as the matrices $\boldsymbol{\Phi}_2$ and $\boldsymbol{\Phi}_3$ are persistently exciting (Assumption 3.4). The Lyapunov function (E.58) is positive definite and decrescent while its derivative (E.60) is negative semi-definite and can be bounded by a time-independent function. The auxiliary function (E.65) is bounded and its derivative (E.66) is definitely non-zero in the set $\mathcal{N}$. Hence, all the conditions of Theorem D.4 are fulfilled, and it follows that the origin $(\mathbf{e}_q, \mathbf{z}, \tilde{\boldsymbol{\theta}}_2, \tilde{\boldsymbol{\theta}}_3) = (\mathbf{0}, \mathbf{0}, \mathbf{0}, \mathbf{0})$ is uniformly asymptotically stable. A similar proof can be done for the negative equilibrium point by defining $\mathbf{e}_q := \mathbf{e}_{q-}$ and $\mathbf{T}_e := \mathbf{T}_e(\mathbf{e}_{q-})$.

E.10 Proof of Lemma 3.6

The error functions are naturally constrained $||\mathbf{e}_q||, ||\mathbf{e}_{q_r}|| \leq 2$, the rotation matrices $||\mathbf{R}|| = 1$ and the inertia matrix is constant. From the Lyapunov function (E.58) and its derivative (E.60) it follows that $\mathbf{e}_q, \mathbf{z}, \tilde{\boldsymbol{\theta}}_1, \tilde{\boldsymbol{\theta}}_2$ are bounded. Since $\boldsymbol{\theta}_1$ and $\boldsymbol{\theta}_2$ are assumed to be constants, it follows that $||\hat{\boldsymbol{\theta}}_1|| \leq \beta_{\hat{\boldsymbol{\theta}}_1}$ and $||\hat{\boldsymbol{\theta}}_2|| \leq \beta_{\hat{\boldsymbol{\theta}}_2}$ implying that $\hat{\mathbf{f}}(\mathbf{x}), \hat{\mathbf{D}}(\mathbf{x}), \hat{\mathbf{G}}(\mathbf{x})$ are bounded. Using Assumption 2.2, the airspeed becomes lower bounded, such that $||\hat{\mathbf{G}}^{-1}(\mathbf{x})|| \leq \beta_{\hat{\mathbf{G}}}$. Lemma 3.2 can be used to show that $||\boldsymbol{\omega}^b_{n,b}|| \leq \beta_{\boldsymbol{\omega}}$ and by design it follows that $\mathbf{q}_{n,d} \in \mathcal{S}^3$ and $\boldsymbol{\omega}^d_{n,d}, \dot{\boldsymbol{\omega}}^d_{n,d} \in \mathcal{L}_\infty$. The angular velocity between the wind and the body frame can be shown to be bounded by using Lemma 3.3 such that $||\boldsymbol{\omega}^w_{b,w}|| \leq \beta_{\boldsymbol{\omega}_w}$ while its angular acceleration can be shown to be bounded by imposing rate saturation or using filters with saturation to ensure that $||\dot{\boldsymbol{\omega}}^w_{b,w}|| \leq \beta_{\dot{\boldsymbol{\omega}}_w}$. By expanding $\boldsymbol{\omega}^b_{r,w} = -\mathbf{R}^b_r\boldsymbol{\omega}^r_{n,r} - \mathbf{R}^b_d\boldsymbol{\omega}^d_{n,d} + \boldsymbol{\omega}^b_{n,b} + \mathbf{R}^b_w\boldsymbol{\omega}^w_{b,w}$, where all the terms have been shown to be bounded except $\boldsymbol{\omega}^r_{n,r}$ it follows that $\boldsymbol{\omega}^r_{n,r}$ must also be bounded. With $||\boldsymbol{\omega}^r_{n,r}|| \leq \beta_{\boldsymbol{\omega}_r}$, the reference variable $\mathbf{z}_r$ can be expanded as $\mathbf{z}_r = \boldsymbol{\omega}^r_{n,r} - \mathbf{R}^r_d\boldsymbol{\omega}^d_{n,d} + k_1\mathbf{T}^\top_{e_r}\mathbf{e}_{q_r}$, where $||\mathbf{T}^\top_{e_r}\mathbf{e}_{q_r}|| = ||\frac{\boldsymbol{\epsilon}_{d,r}}{2}|| \leq \frac{1}{2}$ indicating that $||\mathbf{z}_r|| \leq \beta_{\mathbf{z}_r}$. The quaternion vector rates can be written as $||\dot{\boldsymbol{\epsilon}}_{r,w}|| = ||(\eta_{r,w}\mathbf{I} + \mathbf{S}(\boldsymbol{\epsilon}_{r,w}))\boldsymbol{\omega}^w_{r,w}|| \leq \beta_{\dot{\boldsymbol{\epsilon}}}$ and similar for $||\dot{\boldsymbol{\epsilon}}_{d,r}|| = ||(\eta_{d,r}\mathbf{I} + \mathbf{S}(\boldsymbol{\epsilon}_{d,r}))\boldsymbol{\omega}^r_{d,r}|| = ||(\eta_{d,r}\mathbf{I} + \mathbf{S}(\boldsymbol{\epsilon}_{d,r}))(\boldsymbol{\omega}^r_{n,r} - \mathbf{R}^r_d\boldsymbol{\omega}^d_{n,d})|| \leq \beta_{\dot{\boldsymbol{\epsilon}}_r}$. Hence all the terms of the control law (3.30) are bounded and consequently, $||\mathbf{u}|| \leq \beta_{\mathbf{u}}$.

E.11 Proof of Lemma 3.7

The function is given as $\boldsymbol{\xi}_1 = \mathbf{R}^r_b\mathbf{J}^{-1}\hat{\mathbf{G}}(\mathbf{x})(\sigma(\mathbf{u}) - \mathbf{u})$ where $||\mathbf{u}|| \leq \beta_{\mathbf{u}}$ by using Lemma 3.6, the saturated control signal is bounded by its physical bound, $||\mathbf{R}^r_b|| = 1$, the inertia matrix is constant and nonsingular, and $\hat{\mathbf{G}}$ is shown to be bounded as

part of the proof of Lemma 3.6. Hence, all the parts of the function $\boldsymbol{\xi}_1$ are bounded and consequently, $||\boldsymbol{\xi}_1|| \leq \beta_{\boldsymbol{\xi}_1}$.

E.12 Proof of Theorem 3.5

Let a Lyapunov function candidate be chosen as

$$V_1 = \frac{1}{2}\tilde{V}^2 > 0 \quad \forall\ \tilde{V} \neq 0 \tag{E.67}$$

which can be differentiated using (3.9) as

$$\dot{V}_1 = \tilde{V}\left(\frac{u}{mV_a}T + \frac{(\mathbf{v}_r^b)^\top}{V_a}\left(\frac{1}{m}\mathbf{R}_w^b\mathbf{f}_{aero}^w + \mathbf{R}_n^b\mathbf{f}_g^n\right) - \dot{V}_d\right) \tag{E.68}$$

and by inserting (3.37), the Lyapunov derivative becomes

$$\dot{V}_1 = -\kappa_p\tilde{V}^2 \tag{E.69}$$

which is negative definite. Given $V_d, \dot{V}_d \in \mathcal{L}_\infty$, it follows by applying Theorem D.3 that the origin ($\tilde{V} = 0$) is uniformly exponentially stable. Since the thrust is constrained between zero and an upper bound, the stability does not hold globally.

E.13 Proof of Theorem 3.6

With $x_1 = \int_0^t (V_a - V_d(\tau))d\tau$ and $x_2 = V_a - V_d(\tau)$, the airspeed tracking error dynamics can be written using (3.9) as

$$\dot{x}_1 = x_2 \tag{E.70}$$

$$\dot{x}_2 = \frac{u}{mV_a}T + \frac{(\mathbf{v}_r^b)^\top}{V_a}\left(\frac{1}{m}\mathbf{R}_w^b\mathbf{f}_{aero}^w + \mathbf{R}_n^b\mathbf{f}_g^n\right) - \dot{V}_d. \tag{E.71}$$

Using backstepping, let a Lyapunov function candidate be defined as

$$V_1 := \frac{1}{2}x_1^2 > 0 \quad \forall\ x_1 \neq 0 \tag{E.72}$$

which can be differentiated as

$$\dot{V}_1 = x_1x_2 \tag{E.73}$$

and where x_2 can be used for control. Let $x_2 := -\kappa_1 x_1 + z$ where $\kappa_1 > 0$ and z is a new variable, then

$$\dot{V}_1 = -\kappa_1 x_1^2 + x_1 z. \tag{E.74}$$

The dynamics of the new variable are found through differentiation, and by inserting (E.71) it becomes

$$\dot{z} = \frac{u}{mV_a}T + \frac{(\mathbf{v}_r^b)^\top}{V_a}\left(\frac{1}{m}\mathbf{R}_w^b\mathbf{f}_{aero}^w + \mathbf{R}_n^b\mathbf{f}_g^n\right) - \dot{V}_d + \kappa_1 x_2. \tag{E.75}$$

Let a second Lyapunov function candidate be defined as

$$V_2 := V_1 + \frac{1}{2}z^2 > 0 \quad \forall\, x_1, z \neq 0 \tag{E.76}$$

which can be differentiated, and by using (E.74) and (E.75) it becomes

$$\dot{V}_2 = -\kappa_1 x_1^2 + x_1 z + z\left(\frac{u}{mV_a}T + \frac{(\mathbf{v}_r^b)^\top}{V_a}\left(\frac{1}{m}\mathbf{R}_w^b\mathbf{f}_{aero}^w + \mathbf{R}_n^b\mathbf{f}_g^n\right) - \dot{V}_d + \kappa_1 x_2\right). \tag{E.77}$$

The control law can now be chosen as

$$T := \frac{mV_a}{u}\left(\dot{V}_d - \kappa_1 x_2 - x_1 - \kappa_2 z - \frac{(\mathbf{v}_r^b)^\top}{V_a}\left(\frac{1}{m}\mathbf{R}_w^b\mathbf{f}_{aero}^w + \mathbf{R}_n^b\mathbf{f}_g^n\right)\right) \tag{E.78}$$

where $\kappa_2 > 0$ and which can be written in original coordinates as in (3.38) where $\kappa_p = \kappa_1 + \kappa_2$ and $\kappa_i = 1 + \kappa_1\kappa_2$. Inserting (E.78) into (E.77), the Lyapunov derivative becomes

$$\dot{V}_2 = -\kappa_1 x_1^2 - \kappa_2 z^2 \leq -\kappa_1 ||x_1||^2 - \kappa_2 ||z||^2 \tag{E.79}$$

which is negative definite. Given $V_d, \dot{V}_d \in \mathcal{L}_\infty$, it follows by applying Theorem D.3 that the origin $(x_1, z) = (0, 0)$ is uniformly exponentially stable. Since the thrust is constrained between zero and an upper bound, the stability does not hold globally.

E.14 Proof of Lemma 3.8

Let a Lyapunov function candidate be defined as

$$V := \frac{1}{2}\tilde{V}_r^2 > 0 \quad \forall\, \tilde{V}_r \neq 0 \tag{E.80}$$

which is positive definite, decrescent and radially unbounded. By differentiating (E.80) and inserting (3.39) the Lyapunov derivative becomes

$$\dot{V} = -\kappa_r \tilde{V}_r^2 + \tilde{V}_r \xi_2 \tag{E.81}$$

$$\dot{V} \leq -\kappa_r |\tilde{V}_r|^2 \quad \forall\, |\tilde{V}_r| \geq \frac{|\xi_2|}{\kappa_r} \tag{E.82}$$

which is negative definite if $\xi_2 = 0$ (unforced system). To take ξ_2 into account, consider the closed loop error dynamics which can be written as

$$\dot{\tilde{V}}_r = -\kappa_r \tilde{V}_r + \xi_2 := f(\tilde{V}_r, \xi_2). \tag{E.83}$$

The function ξ_2 is bounded and has the property that $\xi_2(0) = 0$, such that it is a class $\mathcal{K}$ function. The Lyapunov function (E.80) is positive definite and decrescent, while its derivative (E.82) is negative definite when $|\tilde{V}_r| \geq \frac{|\xi_2|}{\kappa_r}$, hence by applying Theorem D.6 it follows that the system $f(\tilde{V}_r, \xi_2)$ is input-to-state stable. Being

input-to-state stable, it follows from Definition D.6 that the solution $\tilde{V}_r(t)$ exists for all $t \geq t_0$ and satisfies

$$|\tilde{V}_r(t)| \leq \beta(|\tilde{V}_r(t_0)|, t - t_0) + \gamma\left(\sup_{t_0 \leq \tau \leq t} |\xi_2(\tau)|\right) \tag{E.84}$$

where β is a class $\mathcal{KL}$ function while γ is a class $\mathcal{K}$ function. As the bounded function $\xi_2 \to 0$, equation (E.84) reduces to

$$|\tilde{V}_r(t)| \leq \beta(|\tilde{V}_r(t_0)|, t - t_0) \tag{E.85}$$

showing that the origin ($\tilde{V}_r = 0$) of the unforced system is uniformly globally asymptotically stable.

E.15 Proof of Theorem 3.7

Let a Lyapunov function candidate be defined as

$$V := \frac{1}{2}\tilde{V}^2 + \frac{1}{2}\tilde{\boldsymbol{\theta}}_1^\top \boldsymbol{\Gamma}_1^{-1}\tilde{\boldsymbol{\theta}}_1 > 0 \quad \forall\ \tilde{V} \neq 0, \tilde{\boldsymbol{\theta}} \neq \mathbf{0} \tag{E.86}$$

which is positive definite, radially unbounded and decrescent. Differentiating (E.86) and inserting (2.56) and (3.39) the derivative is found as

$$\begin{aligned}\dot{V} = \tilde{V}\Bigg(&\frac{u}{mV_a}T + \frac{u}{mV_a}\tilde{T} - \dot{V}_d + \kappa_r\tilde{V}_r - \xi_2 \\ &+\frac{(\mathbf{v}_r^b)^\top}{V_a}\left(\frac{1}{m}\mathbf{R}_w^b\boldsymbol{\Phi}_1\hat{\boldsymbol{\theta}}_1 - \frac{1}{m}\mathbf{R}_w^b\boldsymbol{\Phi}_1\tilde{\boldsymbol{\theta}}_1 + \mathbf{R}_n^b\mathbf{f}_g^n\right)\Bigg) + \tilde{\boldsymbol{\theta}}_1^\top\boldsymbol{\Gamma}_1^{-1}\dot{\tilde{\boldsymbol{\theta}}}_1\end{aligned} \tag{E.87}$$

and by inserting (3.40), (3.41) and (3.42) it reduces to

$$\dot{V} \leq -\kappa_p\tilde{V}^2 < 0 \quad \forall\ \tilde{V} \neq 0, \tag{E.88}$$

which is negative semi-definite. By applying Theorem D.1 it follows that the origin $(\tilde{V}, \tilde{\boldsymbol{\theta}}_1) = (0, \mathbf{0})$ is uniformly stable. To show that the origin is uniformly asymptotically stable, Matrosov's theorem will be applied. To that end, the closed loop error dynamics can be written as

$$\dot{\tilde{V}} = -\kappa_p\tilde{V} - \frac{(\mathbf{v}_r^b)^\top}{mV_a}\mathbf{R}_w^b\boldsymbol{\Phi}_1\tilde{\boldsymbol{\theta}}_1, \tag{E.89}$$

and a continuous bounded auxiliary function can be chosen as

$$W := \tilde{V}(\mathbf{v}_r^b)^\top\mathbf{R}_w^b\boldsymbol{\Phi}_1\tilde{\boldsymbol{\theta}}_1. \tag{E.90}$$

The terms $\tilde{V}$ and $\tilde{\boldsymbol{\theta}}_1$ are bounded through (E.88); $||\mathbf{v}_r^b|| = V_a \leq \beta_{V_{max}}$ by using Lemma 3.1 and $||\mathbf{R}_w^b|| = 1$. The regressor matrix $\boldsymbol{\Phi}_1 = \boldsymbol{\Phi}_1(V_a, \alpha, \beta, \boldsymbol{\omega}_{n,b}^b, \mathbf{u})$ where α, β are bounded by $\pm\frac{\pi}{2}$, the angular velocity, $\boldsymbol{\omega}_{n,b}^b$, is shown to be bounded in Lemma 3.2 and the deflection angles, $\mathbf{u}$, are physically bounded. Hence, all the

terms of (E.90) are bounded. The auxiliary function can now be differentiated and by inserting (E.89) and evaluating it in the set $\mathcal{N} = \{\tilde{\boldsymbol{\theta}}_1 \in \mathbb{R}^{14} | \tilde{V} = 0\}$ it becomes

$$\dot{W} = -\left(\frac{(\mathbf{v}_r^b)^\top}{mV_a}\mathbf{R}_w^b\boldsymbol{\Phi}_1\tilde{\boldsymbol{\theta}}_1\right)\left((\mathbf{v}_r^b)^\top\mathbf{R}_w^b\boldsymbol{\Phi}_1\tilde{\boldsymbol{\theta}}_1\right) = -\left|\left|\frac{(\mathbf{v}_r^b)^\top}{mV_a}\mathbf{R}_w^b\boldsymbol{\Phi}_1\tilde{\boldsymbol{\theta}}_1\right|\right|^2 \tag{E.91}$$

which is definitely non-zero in the set $\mathcal{N}$ as long as $\boldsymbol{\Phi}_1$ is not zero (which is fulfilled through Assumption 3.4). The Lyapunov function (E.86) is decrescent and positive definite, while its derivative (E.88) is negative semi-definite. The auxiliary function is continuous and bounded, while its derivative is definitely non-zero in the set $\mathcal{N}$. Hence, it follows by applying Theorem D.4 that the origin $(\tilde{V}, \tilde{\boldsymbol{\theta}}_1) = (0, \mathbf{0})$ is uniformly asymptotically stable.

E.16 Proof of Lemma 3.9

From the Lyapunov function (E.86) and its derivative (E.88) it follows that $|\tilde{V}| \leq \beta_{\tilde{V}}$ and $||\tilde{\boldsymbol{\theta}}_1|| \leq \beta_{\tilde{\boldsymbol{\theta}}_1}$. Using Lemma 3.1 it follows that $||\mathbf{v}_r^b|| = V_a \leq \beta_{V_{max}}$ and consequently using $|\tilde{V}| = |V_a - V_r| \leq \beta_{\tilde{V}}$ it follows that $|V_r| \leq \beta_{V_r}$. The desired acceleration is bounded $\dot{V}_d \in \mathcal{L}_\infty$, the rotation matrices as $||\mathbf{R}_w^b|| = ||\mathbf{R}_n^b|| = 1$, the estimation error is bounded as $||\tilde{\boldsymbol{\theta}}_1|| \leq \beta_{\tilde{\boldsymbol{\theta}}_1}$, and with constant coefficients it follows that $||\hat{\boldsymbol{\theta}}_1|| \leq \beta_{\hat{\boldsymbol{\theta}}_1}$. The matrix $\boldsymbol{\Phi}_1$ is a function of bounded variables $(V_a, \alpha, \beta, \boldsymbol{\omega}_{n,b}^b, \mathbf{u})$ and is therefore bounded, the gravity vector is bounded as $||\mathbf{f}_g^n|| = g$ and using Assumption 2.2 and the fact that $u >> v, w$ it follows that $u > 0$ and $V_a > 0$. Hence, all the terms in the control law are bounded, and consequently $T \leq \beta_T$.

E.17 Proof of Lemma 3.10

Expanding ξ_2, it can be written as $\xi_2 = \frac{u}{mV_a}(\sigma(T) - T)$ where $T \leq \beta_T$ is shown to be bounded in Lemma 3.9 and $\sigma(T) \leq T_{max}$ by imposing its physical constraints. Using Assumption 2.2 the airspeed is lower bounded as $V_a \geq \beta_v > 0$ and using Lemma 3.1 it follows that $V_a \leq \beta_{V_{max}}$ and as a consequence $|u| \leq \beta_u$, such that $|\xi_2| \leq \frac{\beta_u}{m\beta_v}(T_{max} + \beta_T)$ and hence the function is bounded.

E.18 Proof of Theorem 3.8

The dual equilibrium points $(\mathbf{e}_{q\pm}, \mathbf{s}, \tilde{V}) = (\mathbf{0}, \mathbf{0}, 0)$ can be shown to be uniformly exponentially stable by applying Theorem 3.3 and 3.5. To show that the reference asymptotically tracks the desired speed, let $\tilde{V}_r := (V_r - V_d)$ and a Lyapunov function candidate as

$$V := \frac{1}{2}\tilde{V}_r^2 > 0 \quad \forall\ \tilde{V}_r \neq 0. \tag{E.92}$$

By differentiating (E.92) and inserting (3.54), the Lyapunov derivative becomes

$$\dot{V} = -\kappa_r \tilde{V}_r^2 + \kappa_u u_{max} \tilde{V}_r \tag{E.93}$$

$$\dot{V} \leq -\kappa_r |\tilde{V}_r|^2 \quad \forall\ |\tilde{V}_r| \geq \frac{\kappa_u}{\kappa_r} |u_{max}|. \tag{E.94}$$

The Lyapunov function (E.92) is positive definite and radially unbounded, while its derivative (E.94) is negative definite when $u_{max} = 0$ (unforced system), and by applying Theorem D.3, it follows that the the origin ($\tilde{V}_r = 0$) is uniformly globally exponentially stable. To take the function u_{max} into account, the closed loop system can be written as $\dot{\tilde{V}}_r = -\kappa_r \tilde{V}_r + \kappa_u u_{max} := f(\tilde{V}_r, u_{max})$. The Lyapunov function (E.92) is positive definite and decrescent, while its derivative (E.94) is negative definite for all $|\tilde{V}_r| \geq \frac{\kappa_u}{\kappa_r}|u_{max}|$ where u_{max} is a class $\mathcal{K}$ function[2]. By applying Theorem D.6 it is concluded that the system $f(\tilde{V}_r, u_{max})$ is input-to-state stable. Being input-to-state stable, it follows from Definition D.6 that the solution $\tilde{V}_r(t)$ exists for all $t \geq t_0$ and satisfies

$$|\tilde{V}_r(t)| \leq \beta(|\tilde{V}_r(t_0)|, t - t_0) + \gamma\left(\sup_{t_0 \leq \tau \leq t} |u_{max}(\tau)|\right) \tag{E.95}$$

where β is a class $\mathcal{KL}$ function while γ is a class $\mathcal{K}$ function. As the bounded function $u_{max} \to 0$, equation (E.95) reduces to

$$|\tilde{V}_r(t)| \leq \beta(|\tilde{V}_r(t_0)|, t - t_0) \tag{E.96}$$

indicating that $|\tilde{V}_r(t)| \to 0$ as $t \to \infty$. When $u_{max} \neq 0$, the reference airspeed increases and diverges from the desired airspeed. This will make $V_a \to \infty$ which makes $u_{max} \to 0$ removing the second term of (E.93), and the exponential stability properties of the origin is thereby regained which makes the reference track the desired speed profile. As $u_{max} \to 0$, the deflection angles will desaturate.

E.19 Proof of Lemma 4.1

The following proof first designs the position error frame by taking basis in $\mathbf{e}^e = \mathbf{R}_n^e \mathbf{e}^n$, and then the stability of the set $\mathcal{H}(\delta, \Delta)$ is shown by looking at the error function

$$\mathbf{e}_\delta^e = \begin{bmatrix} ||\mathbf{e}^n||_\delta & 0 & 0 \end{bmatrix}^\top = \mathbf{R}_n^e \mathbf{e}^n \tag{E.97}$$

$$||\mathbf{e}^n||_\delta = \inf_{\mathbf{x} \in \mathcal{H}} ||\mathbf{x} - \mathbf{p}^n||, \tag{E.98}$$

which considers all errors except a small ball around the origin of $\mathbf{e}^n = \mathbf{0}$. Consider the position error which can be defined in the position error frame as

$$\mathbf{e}^e = \begin{bmatrix} ||\mathbf{e}^n|| & 0 & 0 \end{bmatrix}^\top = \mathbf{R}_n^e \mathbf{e}^n = \mathbf{R}_n^e (\mathbf{p}_{wp}^n - \mathbf{p}^n) \tag{E.99}$$

[2]By design $u_{max}(0) = 0$. The function is bounded since by increasing the reference speed the airspeed becomes increased, and consequently the output from the rotational control law is decreased; making $u_{max} \to 0$

where the rotation matrix $\mathbf{R}_n^e$ can be constructed with quaternions using (4.4). The angular velocity can be found by differentiating (E.99) resulting in

$$\dot{\mathbf{e}}^e = \mathbf{S}(\mathbf{e}^e)\boldsymbol{\omega}_{n,e}^e - \mathbf{R}_b^e\mathbf{v}^b \tag{E.100}$$

where $-\mathbf{S}(\boldsymbol{\omega}_{n,e}^e)\mathbf{e}^e = \mathbf{S}(\mathbf{e}^e)\boldsymbol{\omega}_{n,e}^e$ and $\dot{\mathbf{p}}_{wp}^n = \mathbf{0}$ and $\dot{\mathbf{p}}^n = \mathbf{R}_b^n\mathbf{v}^b$ have been used. The skew symmetric matrix can be expressed as

$$\mathbf{S}(\mathbf{e}^e)\boldsymbol{\omega}_{n,e}^e = \begin{bmatrix} 0 & 0 & 0 \\ 0 & 0 & -||\mathbf{e}^n|| \\ 0 & ||\mathbf{e}^n|| & 0 \end{bmatrix} \boldsymbol{\omega}_{n,e}^e, \tag{E.101}$$

and its pseudoinverse as

$$\mathbf{S}^\dagger(\mathbf{e}^e) = \begin{bmatrix} 0 & 0 & 0 \\ 0 & 0 & -\frac{1}{||\mathbf{e}^n||} \\ 0 & \frac{1}{||\mathbf{e}^n||} & 0 \end{bmatrix} \tag{E.102}$$

where superscript $\dagger$ denotes the pseudoinverse. Notice that the pseudoinverse matrix removes any components along the $\mathbf{x}^e$ axis, such that $\mathbf{S}^\dagger(\mathbf{e}^e)\dot{\mathbf{e}}^e = \mathbf{0}$. This can be exploited to solve (E.100) for the angular velocity as

$$\boldsymbol{\omega}_{n,e}^e = \mathbf{S}^\dagger(\mathbf{e}^e)\mathbf{R}_b^e\mathbf{v}^b. \tag{E.103}$$

Notice that as $||\mathbf{e}^n|| \to 0$ the angular velocity $||\boldsymbol{\omega}_{n,e}^e|| \to \infty$, such that a switching algorithm must be applied to ensure that the angular velocity does not go to infinity. More precisely, as long as $||\mathbf{e}^n|| \geq \delta > 0$, the angular velocity will remain bounded. To that end, the set $\mathcal{H}(\delta, \Delta)$ is defined as a shell around the origin $\mathbf{e}^n = \mathbf{0}$, such that by using Property 4.1, the UAV will never reach the interior of the shell which ensures that $||\mathbf{e}^n|| \geq \delta > 0$ such that the angular velocity (4.6) is upper bounded as $||\boldsymbol{\omega}_{n,e}^e|| \leq \frac{1}{\delta}V_{max}$ and the equality (E.97) holds for all $||\mathbf{e}^n|| \geq \delta$. Equation (E.97) can be differentiated as

$$\dot{\mathbf{e}}_\delta^e = -\mathbf{S}(\boldsymbol{\omega}_{n,e}^e)\mathbf{e}_\delta^e + \mathbf{R}_n^e(\dot{\mathbf{p}}_{wp}^n - \dot{\mathbf{p}}^n) \tag{E.104}$$

where by using Assumption 4.1 it follows that $\mathbf{v}^b = \mathbf{v}_r^b = \mathbf{R}_w^b\mathbf{v}_r^w$ where $\mathbf{v}_r^w := \begin{bmatrix} V_a & 0 & 0 \end{bmatrix}^\top$ with $V_a \geq \beta_v$ using Assumption 2.2. The waypoint is a fixed point, such that $\dot{\mathbf{p}}_{wp}^n = \mathbf{0}$, enabling the position error kinematics to be written as

$$\dot{\mathbf{e}}_\delta^e = -\mathbf{S}(\boldsymbol{\omega}_{n,e}^e)\mathbf{e}_\delta^e - \mathbf{R}_w^e\mathbf{v}_r^w. \tag{E.105}$$

By inserting the rotation matrix $\mathbf{R}_w^e = \mathbf{I} + 2\eta_{e,w}\mathbf{S}(\boldsymbol{\epsilon}_{e,w}) + 2\mathbf{S}^2(\boldsymbol{\epsilon}_{e,w})$ into (E.105) it is obtained that

$$\dot{\mathbf{e}}_\delta^e = -\mathbf{S}(\boldsymbol{\omega}_{n,e}^e)\mathbf{e}_\delta^e - \mathbf{v}_r^w - (2\eta_{e,w}\mathbf{S}(\boldsymbol{\epsilon}_{e,w}) + 2\mathbf{S}^2(\boldsymbol{\epsilon}_{e,w}))\mathbf{v}_r^w \tag{E.106}$$

where the term $\mathbf{v}_r^w$ provides damping to the system. Using Assumption 4.1, it follows that $\mathbf{q}_{n,d} = \mathbf{q}_{n,e}$, *i.e.* there is no quaternion for wind compensation. Thus, by making the error $(\mathbf{e}_{q\pm}, \boldsymbol{\omega}_{d,w}^b) \to (\mathbf{0}, \mathbf{0})$ the quaternion $\mathbf{q}_{e,w} \to \begin{bmatrix} 1 & 0 & 0 & 0 \end{bmatrix}^\top$

such that the last term in (E.106) will disappear. The system can now be written on cascaded form as

$$\dot{\mathbf{x}}_1 = f_1(t, \mathbf{x}_1) + g(t, \mathbf{x})\mathbf{x} \tag{E.107}$$
$$\dot{\mathbf{x}}_2 = f_2(t, \mathbf{x}_2) \tag{E.108}$$

where $\mathbf{x} = \begin{bmatrix}\mathbf{x}_1^\top & \mathbf{x}_2^\top\end{bmatrix}^\top$, $\mathbf{x}_1 := \mathbf{e}_\delta^e$, $\mathbf{x}_2 = \begin{bmatrix}\mathbf{e}_{q\pm}^\top & (\boldsymbol{\omega}_{d,w}^b)^\top\end{bmatrix}^\top$,

$$f_1(t, \mathbf{x}_1) := -\mathbf{S}(\boldsymbol{\omega}_{n,e}^e)\mathbf{e}_\delta^e - \mathbf{v}_r^w \tag{E.109}$$
$$g(t, \mathbf{x}) := \begin{bmatrix}\mathbf{0} & 2\eta_{e,w}\mathbf{S}(\mathbf{v}_r^w) + 2\mathbf{S}(\boldsymbol{\epsilon}_{e,w})\mathbf{S}(\mathbf{v}_r^w) & \mathbf{0}\end{bmatrix}, \tag{E.110}$$

and where $f_2(t, \mathbf{x}_2)$ represents the rotational dynamics in closed loop with any of the rotational control laws from Chapter 3. Consider first the unforced system $\dot{\mathbf{x}}_1 = f_1(t, \mathbf{x}_1)$ which can be written as

$$\dot{\mathbf{x}}_1 = -\mathbf{S}(\boldsymbol{\omega}_{n,e}^e)\mathbf{x}_1 - \mathbf{v}_r^w. \tag{E.111}$$

Let a Lyapunov function candidate be defined as

$$V := \frac{1}{2}\mathbf{x}_1^\top\mathbf{x}_1 > 0 \quad \forall\ \mathbf{x}_1 \neq 0 \tag{E.112}$$

which through differentiation and inserting (E.111) becomes

$$\dot{V} = -\mathbf{x}_1^\top(\mathbf{S}(\boldsymbol{\omega}_{n,e}^e)\mathbf{x}_1 + \mathbf{v}_r^w) \tag{E.113}$$
$$\dot{V} = -\mathbf{x}_1^\top\mathbf{v}_r^w \tag{E.114}$$

since $\mathbf{x}_1^\top\mathbf{S}(\boldsymbol{\omega}_{n,e}^e)\mathbf{x}_1 = 0$. Note that both $\mathbf{x}_1 = \begin{bmatrix}||\mathbf{e}^n||_\delta & 0 & 0\end{bmatrix}^\top$ and $\mathbf{v}_r^w = \begin{bmatrix}V_a & 0 & 0\end{bmatrix}^\top$ are positive with only components on the x-axis, such that the Lyapunov derivative can be written as

$$\dot{V} = -||\mathbf{x}_1||\beta_v \tag{E.115}$$

where β_v represents the lower bound of the airspeed. This means that as $\mathbf{x}_1(t) \to \mathbf{0}$, the trajectories will converge to the set $\mathcal{H}(\delta, \Delta)$. Hence, it follows by using Theorem D.2 that the set $\mathcal{H}(\delta, \Delta)$ is uniformly asymptotically stable when $\mathbf{x}_2 = \mathbf{0}$.

To prove that the cascade is uniformly asymptotically stable, Assumptions D.1-D.3 must be fulfilled in order to invoke Theorem D.7. Since the set $\mathcal{H}(\delta, \Delta)$ of the system $\dot{\mathbf{x}}_1 = f_1(t, \mathbf{x}_1)$ is uniformly asymptotically stable, it follows from converse theorems (*e.g.* Khalil (2002)) that there exist a suitable $V(t, \mathbf{x}_1)$, and as such the Assumption D.1 is fulfilled. The second assumption requires that the interconnection term $g(t, \mathbf{x})$ has a linear growth bound. The interconnection term can be bounded as

$$||g(t, \mathbf{x})|| \leq \begin{bmatrix}\mathbf{0} & 2||\eta_{e,w}\mathbf{S}(\mathbf{v}_r^w)|| + 2||\mathbf{S}(\boldsymbol{\epsilon}_{e,w})\mathbf{S}(\mathbf{v}_r^w)|| & \mathbf{0}\end{bmatrix}, \tag{E.116}$$

where $|\eta_{e,w}| \leq 1$, $||\boldsymbol{\epsilon}_{e,w}|| \leq 1$, $||\mathbf{v}_r^w|| \leq \beta_{V_{max}}$ (*cf.* Lemma 3.1), and consequently Assumption D.2 is fulfilled. The third assumption states that the trajectories of

system (E.108) must converge sufficiently fast to the origin through an integrability constraint. Any of the rotational control laws from Chapter 3 (except the adaptive controller) in closed loop with (2.25) and (2.32) results in uniformly exponential stability of the equilibrium $\mathbf{x}_2 = \mathbf{0}$. This means that $||\mathbf{x}_2|| \to 0$ exponentially, and as such Assumption D.3 is fulfilled. With Assumptions D.1-D.3 fulfilled, it follows by invoking Theorem D.7 that the set $\mathcal{C} := \{\mathbf{x}_1 \in \mathbb{R}^3, \mathbf{x}_2 \in \mathcal{S}_e^3 \times \mathbb{R}^3 | \delta \leq ||\mathbf{x}_1|| \leq \Delta, \mathbf{x}_2 = \mathbf{0}\}$ of the cascaded system (E.107)-(E.108) is uniformly asymptotically stable.

E.20 Proof of Theorem 4.1

Let a Lyapunov function candidate be chosen as

$$V_1 = \frac{1}{2}\mathbf{e}_1^\top \mathbf{e}_1 > 0 \quad \forall\ \mathbf{e}_1 \neq \mathbf{0} \tag{E.117}$$

which can be differentiated as

$$\dot{V}_1 = \mathbf{e}_1^\top \mathbf{e}_2. \tag{E.118}$$

The error term $\mathbf{e}_2$ can be used for control and chosen as

$$\mathbf{e}_2 := -k_p \sigma_1(\mathbf{e}_1) + \mathbf{z} \tag{E.119}$$

where $k_p > 0$ and $\mathbf{z}$ is a new variable, and where

$$\sigma_1(\mathbf{e}_1) = \lambda_1 \tanh\left(\frac{\mathbf{e}_1}{\lambda_1}\right) = \begin{bmatrix}\lambda_1 \tanh(\frac{e_x}{\lambda_1}) & \lambda_1 \tanh(\frac{e_y}{\lambda_1}) & \lambda_1 \tanh(\frac{e_z}{\lambda_1})\end{bmatrix}^\top \tag{E.120}$$

with λ_1 as a constant bound. Note that $\mathbf{e}_1^\top \sigma_1(\mathbf{e}_1) > 0$. Inserting (E.119) into the (E.118) the Lyapunov derivative becomes

$$\dot{V}_1 = -\mathbf{e}_1^\top (k_p \sigma_1(\mathbf{e}_1) - \mathbf{z}) \tag{E.121}$$

which is negative definite as long as $||\mathbf{z}|| \leq k_p \lambda_1$. The dynamics of the new variable are found using (E.119) and (4.16) as

$$\dot{\mathbf{z}} = \mathbf{u}^n - \ddot{\mathbf{p}}_d^n + k_p \dot{\sigma}_1(\mathbf{e}_1)\mathbf{e}_2 \tag{E.122}$$

where

$$k_p \dot{\sigma}_1(\mathbf{e}_1)\mathbf{e}_2 = k_p \left(\mathbf{I} - \begin{bmatrix}\tanh^2(\frac{e_x}{\lambda_1}) & 0 & 0 \\ 0 & \tanh^2(\frac{e_y}{\lambda_1}) & 0 \\ 0 & 0 & \tanh^2(\frac{e_z}{\lambda_1})\end{bmatrix}\right)\mathbf{e}_2 \tag{E.123}$$

which is zero when the position tracking error is in saturation. A second Lyapunov function candidate can be chosen as

$$V_2 = V_1 + \frac{1}{2}\mathbf{z}^\top \mathbf{z} > 0 \quad \forall\ \mathbf{e}_1, \mathbf{z} \neq \mathbf{0} \tag{E.124}$$

and differentiated as

$$\dot{V}_2 = -\mathbf{e}_1^\top(k_p\sigma_1(\mathbf{e}_1) - \mathbf{z}) + \mathbf{z}^\top(\mathbf{u}^n - \ddot{\mathbf{p}}_d^n + k_p\dot{\sigma}_1(\mathbf{e}_1)\mathbf{e}_2). \tag{E.125}$$

Inserting the control law (4.17) into (E.125), the Lyapunov derivative becomes

$$\dot{V}_2 = -\mathbf{e}_1^\top(k_p\sigma_1(\mathbf{e}_1) - \mathbf{z}) - k_d\mathbf{z}^\top\sigma_2(\mathbf{z}) \tag{E.126}$$

$$\dot{V}_2 \leq -k_p\mathbf{e}_1^\top\sigma_1(\mathbf{e}_1) - k_d\mathbf{z}^\top\sigma_2(\mathbf{z}) \quad \forall\ ||\mathbf{z}|| \leq k_p\lambda_1. \tag{E.127}$$

The second saturation function is defined as $\sigma_2(\mathbf{z}) = \lambda_2 \tanh\left(\frac{\mathbf{z}}{\lambda_2}\right)$. Applying Theorem D.2 it follows that the origin $(\mathbf{e}_1, \mathbf{z}) = (\mathbf{0}, \mathbf{0})$ is uniformly asymptotically stable. When $||\mathbf{z}(0)|| \geq k_p\lambda_1$, the Lyapunov function is not negative definite, and by using Lemma 3.1 it follows that $||\mathbf{z}|| \leq \beta_{V_{max}} + ||\dot{\mathbf{p}}_d^n|| + k_p\lambda_1$. With $\mathbf{z}$ bounded, its trajectories have no finite escape time. Hence, $\exists\ t_1 \geq t_0$ such that $||\mathbf{z}(t_1)|| \leq k_p\lambda_1$, from where the origin becomes asymptotically attractive. This means that initially the trajectories may diverge, but after a time t_1, the trajectories will converge to the origin.

The stability properties of the origin can be further studied by considering the closed loop system as a cascade, which can be written as

$$\dot{\mathbf{e}}_1 = -k_p\sigma(\mathbf{e}_1) + \mathbf{z} \tag{E.128}$$

$$\dot{\mathbf{z}} = -k_d\sigma(\mathbf{z}). \tag{E.129}$$

Let $\mathbf{x}_1 := \mathbf{e}_1$ and $\mathbf{x}_2 := \mathbf{z}$, then the cascaded system is obtained as

$$\dot{\mathbf{x}}_1 = f(t, \mathbf{x}_1, \mathbf{x}_2) \tag{E.130}$$

$$\dot{\mathbf{x}}_2 = f(t, \mathbf{x}_2). \tag{E.131}$$

Both (E.131) and $\dot{\mathbf{x}}_1 = f(t, \mathbf{x}_1, \mathbf{0})$ have uniformly globally asymptotically stable equilibrium points at their respective origins. Furthermore, with $\mathbf{z}$ and consequently $\mathbf{x}_2$ bounded, it follows that

$$||\mathbf{x}_1(t)|| \leq \beta(||\mathbf{x}_1(t_0)||, t - t_0) + \gamma(\sup_{t_0 \leq \tau \leq t} ||\mathbf{x}_2||) \tag{E.132}$$

implying that the system (E.130) is input-to-state stable. Hence, it follows by applying Lemma D.4 that the origin of the cascaded system $(\mathbf{x}_1, \mathbf{x}_2) = (\mathbf{e}_1, \mathbf{z}) = (\mathbf{0}, \mathbf{0})$ is uniformly globally asymptotically stable.

E.21 Proof of Lemma 4.2

Equation (4.20) can be differentiated as

$$\dot{\mathbf{v}}_r^d = -\mathbf{S}(\boldsymbol{\omega}_{n,d}^d)\mathbf{v}_r^d + \mathbf{R}_n^d\mathbf{u}^n \tag{E.133}$$

which can be solved for the angular velocity as

$$\boldsymbol{\omega}_{n,d}^d = -\mathbf{S}^\dagger(\mathbf{v}_r^d)\mathbf{R}_n^d\mathbf{u}^n \tag{E.134}$$

since $\mathbf{S}^\dagger(\mathbf{v}_r^d)\dot{\mathbf{v}}_r^d = \mathbf{0}$. Also note that with constant wind, the relative acceleration is found as

$$\mathbf{v}_r^n = \mathbf{v}^n - \mathbf{w}^n \tag{E.135}$$
$$\dot{\mathbf{v}}_r^n = \mathbf{u}^n. \tag{E.136}$$

The desired airspeed is found as $V_d = ||\mathbf{v}_r^n||$ while its acceleration is found using (E.133) by noting that the term $\mathbf{S}(\boldsymbol{\omega}_{n,d}^d)\mathbf{v}_r^d$ does not produce any $\mathbf{x}^d$ components, such that the desired acceleration is found as

$$\dot{V}_d = \begin{bmatrix} 1 & 0 & 0 \end{bmatrix} \mathbf{R}_n^d \mathbf{u}^n. \tag{E.137}$$

Since this is a simple mapping, the same stability results as for Theorem 4.1 holds.

E.22 Proof of Lemma 4.3

The velocity vector (4.31) can be differentiated as

$$\ddot{\mathbf{p}}_l^l = -\mathbf{S}(\boldsymbol{\omega}_{n,l}^l)\dot{\mathbf{p}}_l^l + \mathbf{R}_n^l \ddot{\mathbf{p}}_l^n \tag{E.138}$$
$$\boldsymbol{\omega}_{n,l}^l = -\mathbf{S}^\dagger(\dot{\mathbf{p}}_l^l)\mathbf{R}_n^l \ddot{\mathbf{p}}_l^n \tag{E.139}$$

where $\mathbf{S}^\dagger(\dot{\mathbf{p}}_l^l)\ddot{\mathbf{p}}_l^l = \mathbf{0}$ has been used. Similarly, by differentiating (E.138) the jerk is found as

$$\dddot{\mathbf{p}}_l^l = -\mathbf{S}(\dot{\boldsymbol{\omega}}_{n,l}^l)\dot{\mathbf{p}}_l^l - \mathbf{S}(\boldsymbol{\omega}_{n,l}^l)\ddot{\mathbf{p}}_l^l - \mathbf{S}(\boldsymbol{\omega}_{n,l}^l)\mathbf{R}_n^l \ddot{\mathbf{p}}_l^n + \mathbf{R}_n^l \dddot{\mathbf{p}}_l^n \tag{E.140}$$

and by inserting (E.138) it becomes

$$\dddot{\mathbf{p}}_l^l = -\mathbf{S}(\dot{\boldsymbol{\omega}}_{n,l}^l)\dot{\mathbf{p}}_l^l + \mathbf{S}^2(\boldsymbol{\omega}_{n,l}^l)\dot{\mathbf{p}}_l^l - 2\mathbf{S}(\boldsymbol{\omega}_{n,l}^l)\mathbf{R}_n^l \ddot{\mathbf{p}}_l^n + \mathbf{R}_n^l \dddot{\mathbf{p}}_l^n \tag{E.141}$$

which can now be solved for the angular acceleration as

$$\dot{\boldsymbol{\omega}}_{n,l}^l = -\mathbf{S}^\dagger(\dot{\mathbf{p}}_l^l)(\mathbf{R}_n^l \dddot{\mathbf{p}}_l^n + \mathbf{S}^2(\boldsymbol{\omega}_{n,l}^l)\mathbf{R}_n^l \dot{\mathbf{p}}_l^n - 2\mathbf{S}(\boldsymbol{\omega}_{n,l}^l)\mathbf{R}_n^l \ddot{\mathbf{p}}_l^n). \tag{E.142}$$

E.23 Proof of Lemma 5.1

The quaternion can be found by studying (5.6) where the rotation matrix $\mathbf{R}_e^c$ can be constructed using quaternions as shown in (5.3). Equation (5.6) can be differentiated as

$$\dot{\mathbf{c}}^c = -\mathbf{S}(\boldsymbol{\omega}_{e,c}^c)\mathbf{c}^c - \mathbf{R}_e^c \mathbf{S}(\boldsymbol{\omega}_{n,e}^e)\mathbf{R}_n^e \mathbf{c}^n + \mathbf{R}_n^c \dot{\mathbf{c}}^n \tag{E.143}$$

where $\mathbf{S}(\boldsymbol{\omega}_{e,c}^c)\mathbf{c}^c = -\mathbf{S}(\mathbf{c}^c)\boldsymbol{\omega}_{e,c}^c$ with

$$\mathbf{S}(\mathbf{c}^c) = \begin{bmatrix} 0 & 0 & \mp||\mathbf{c}^e|| \\ 0 & 0 & 0 \\ \pm||\mathbf{c}^e|| & 0 & 0 \end{bmatrix} \tag{E.144}$$

which filters out any $\mathbf{y}^c$ components such that $\mathbf{S}^\dagger(\mathbf{c}^c)\dot{\mathbf{c}}^c = \mathbf{0}$. Solving (E.143) for the angular velocity results in

$$\boldsymbol{\omega}^c_{e,c} = \mathbf{S}^\dagger(\mathbf{c}^c)(\mathbf{R}^c_e\mathbf{S}(\boldsymbol{\omega}^e_{n,e})\mathbf{R}^e_n\mathbf{c}^n - \mathbf{R}^c_n\dot{\mathbf{c}}^n). \tag{E.145}$$

Consider static obstacles, that is $\dot{\mathbf{p}}^n_o = \mathbf{0}$, then equation (E.143) can be rewritten as

$$\dot{\mathbf{c}}^c = -\mathbf{S}(\boldsymbol{\omega}^c_{e,c})\mathbf{c}^c - \mathbf{R}^c_e\mathbf{S}(\boldsymbol{\omega}^e_{n,e})\mathbf{R}^e_n\mathbf{c}^n - \mathbf{R}^c_w\mathbf{v}^w_r \tag{E.146}$$

where $\dot{\mathbf{p}}^n = \mathbf{R}^n_b\mathbf{v}^b = \mathbf{R}^n_b\mathbf{v}^b_r = \mathbf{R}^n_w\mathbf{v}^w_r$ follows from Assumption 4.1. Let the rotation matrix be written as $\mathbf{R}^c_w = \mathbf{I} + 2\eta_{c,w}\mathbf{S}(\boldsymbol{\epsilon}_{c,w}) + 2\mathbf{S}^2(\boldsymbol{\epsilon}_{c,w})$, which can be inserted into (E.146) as

$$\dot{\mathbf{c}}^c = -\mathbf{S}(\boldsymbol{\omega}^c_{e,c})\mathbf{c}^c - \mathbf{R}^c_e\mathbf{S}(\boldsymbol{\omega}^e_{n,e})\mathbf{R}^e_n\mathbf{c}^n - (\mathbf{I} + 2\eta_{c,w}\mathbf{S}(\boldsymbol{\epsilon}_{c,w}) + 2\mathbf{S}^2(\boldsymbol{\epsilon}_{c,w}))\mathbf{v}^w_r. \tag{E.147}$$

Let the collision avoidance quaternion be the primary task, such that $\mathbf{q}_{n,d} = \mathbf{q}_{n,c}$, then by making $(\mathbf{e}_{q\pm}, \boldsymbol{\omega}^b_{d,w}) \to (\mathbf{0}, \mathbf{0})$ through rotational control, it follows that $\mathbf{q}_{c,w} \to \begin{bmatrix}1 & 0 & 0 & 0\end{bmatrix}^\top$. The system can now be written on cascaded form as

$$\dot{\mathbf{x}}_1 = f_1(t, \mathbf{x}_1) + g(t, \mathbf{x})\mathbf{x} \tag{E.148}$$

$$\dot{\mathbf{x}}_2 = f_2(t, \mathbf{x}_2) \tag{E.149}$$

where $\mathbf{x} = \begin{bmatrix}\mathbf{x}_1^\top & \mathbf{x}_2^\top\end{bmatrix}^\top$, $\mathbf{x}_1 := \mathbf{c}^c$, $\mathbf{x}_2 = \begin{bmatrix}\mathbf{e}^\top_{q\pm} & (\boldsymbol{\omega}^b_{d,w})^\top\end{bmatrix}^\top$,

$$f_1(t, \mathbf{x}_1) := -\mathbf{S}(\boldsymbol{\omega}^c_{e,c})\mathbf{c}^c - \mathbf{R}^c_e\mathbf{S}(\boldsymbol{\omega}^e_{n,e})\mathbf{R}^e_n\mathbf{c}^n - \mathbf{v}^w_r \tag{E.150}$$

$$g(t, \mathbf{x}) := \begin{bmatrix}\mathbf{0} & 2\eta_{c,w}\mathbf{S}(\mathbf{v}^w_r) + 2\mathbf{S}(\boldsymbol{\epsilon}_{c,w})\mathbf{S}(\mathbf{v}^w_r) & \mathbf{0}\end{bmatrix}, \tag{E.151}$$

and where $f_2(t, \mathbf{x}_2)$ represents the rotational dynamics in closed loop with any of the rotational control laws from Chapter 3. Consider the unforced system $\dot{\mathbf{x}}_1 = f_1(t, \mathbf{x}_1)$ which can be written in original coordinates as[3]

$$\dot{\mathbf{c}}^c = -\mathbf{S}(\boldsymbol{\omega}^c_{e,c})\mathbf{c}^c - \mathbf{R}^c_e\mathbf{S}(\boldsymbol{\omega}^e_{n,e})\mathbf{R}^e_n\mathbf{c}^n - \mathbf{v}^w_r. \tag{E.152}$$

Let a Lyapunov function candidate be defined as

$$V = \frac{1}{2}(\mathbf{c}^c)^\top\mathbf{c}^c \tag{E.153}$$

which by differentiation and inserting (E.152) results in

$$\dot{V} = (\mathbf{c}^c)^\top(-\mathbf{S}(\boldsymbol{\omega}^c_{e,c})\mathbf{c}^c - \mathbf{R}^c_e\mathbf{S}(\boldsymbol{\omega}^e_{n,e})\mathbf{R}^e_n\mathbf{c}^n - \mathbf{v}^w_r). \tag{E.154}$$

The terms can be shown to be zero as

$$(\mathbf{c}^c)^\top(\mathbf{S}(\boldsymbol{\omega}^c_{e,c})\mathbf{c}^c = 0 \tag{E.155}$$

$$(\mathbf{c}^c)^\top\mathbf{R}^c_e\mathbf{S}(\boldsymbol{\omega}^e_{n,e})\mathbf{R}^e_n\mathbf{c}^n = (\mathbf{c}^c)^\top\mathbf{R}^c_e\mathbf{S}(\boldsymbol{\omega}^e_{n,e})\mathbf{R}^e_c\mathbf{c}^c = 0 \tag{E.156}$$

$$(\mathbf{c}^c)^\top\mathbf{v}^w_r = \begin{bmatrix}0 & \pm||\mathbf{c}^e|| & 0\end{bmatrix}\begin{bmatrix}V_a \\ 0 \\ 0\end{bmatrix} = 0 \tag{E.157}$$

[3]To avoid confusion with the different frames, the system is kept in its original coordinates.

such that

$$\dot{V} = 0. \tag{E.158}$$

This means that as long as the collision avoidance quaternion is perfectly tracked, the relative distance between the obstacle and the UAV will neither increase nor decrease, such that the UAV will move in a circular trajectory around the obstacle. Furthermore it follows that the unforced system $\dot{\mathbf{x}}_1 = f_1(t, \mathbf{x}_1)$ is bounded. The interconnection term can be bounded as

$$||g(t, \mathbf{x})|| \leq \begin{bmatrix} \mathbf{0} & 2||\eta_{c,w}\mathbf{S}(\mathbf{v}_r^w)|| + 2||\mathbf{S}(\boldsymbol{\epsilon}_{c,w})\mathbf{S}(\mathbf{v}_r^w)|| & \mathbf{0} \end{bmatrix}, \tag{E.159}$$

where $|\eta_{c,w}| \leq 1$, $||\mathbf{v}_r^w|| \leq \beta_{V_{max}}$ using Lemma 3.1 and $||\boldsymbol{\epsilon}_{c,w}|| \leq 1$. The origin of the rotational error dynamics $\dot{\mathbf{x}}_2 = f_2(t, \mathbf{x})$ can be shown to be uniformly exponentially stable by using any of the rotational control laws in Chapter 3 (except the adaptive controller). Even though Theorem D.7 considers the *stability* of cascades, similar arguments can be applied to prove collision avoidance. From (E.158) the Lyapunov derivative is zero whenever the collision avoidance quaternion is perfectly tracked. The collision avoidance quaternion and corresponding angular velocity are fed back through the desired trajectories to the rotational control laws, which are tracked by the control laws making $\mathbf{x}_2 \to \mathbf{0}$ exponentially fast. As $\mathbf{x}_2 \to \mathbf{0}$, $\dot{V} \to 0$ it follows that the distance to the obstacle goes to a constant, $\beta_c > 0$. Hence, it follows that the position error between the obstacle and the UAV becomes lower bounded as $||\mathbf{c}^c|| \geq \beta_c > 0$, and collision with the obstacle is avoided.

E.24 Proof of Lemma 5.2

This proof follows the same lines as for collision avoidance. The quaternion can be found by studying (5.10) where the rotation matrix $\mathbf{R}_c^h$ can be constructed using quaternions as shown in (5.7). Equation (5.10) can be differentiated as

$$\dot{\mathbf{h}}^h = -\mathbf{S}(\boldsymbol{\omega}_{c,h}^h)\mathbf{h}^h - \mathbf{R}_c^h\mathbf{S}(\boldsymbol{\omega}_{e,c}^c)\mathbf{R}_n^c\mathbf{h}^n - \mathbf{R}_e^h\mathbf{S}(\boldsymbol{\omega}_{n,e}^e)\mathbf{R}_n^e\mathbf{h}^n + \mathbf{R}_n^h\dot{\mathbf{h}}^n \tag{E.160}$$

where $\mathbf{S}(\boldsymbol{\omega}_{c,h}^h)\mathbf{h}^h = -\mathbf{S}(\mathbf{h}^h)\boldsymbol{\omega}_{c,h}^h$ with

$$\mathbf{S}(\mathbf{h}^h) = \begin{bmatrix} 0 & -||\mathbf{h}^c|| & 0 \\ ||\mathbf{h}^c|| & 0 & 0 \\ 0 & 0 & 0 \end{bmatrix} \tag{E.161}$$

which filters out any $\mathbf{z}^h$ components such that $\mathbf{S}^\dagger(\mathbf{h}^h)\dot{\mathbf{h}}^h = \mathbf{0}$. Solving (E.160) for the angular velocity results in

$$\boldsymbol{\omega}_{c,h}^h = \mathbf{S}^\dagger(\mathbf{h}^h)(\mathbf{R}_c^h\mathbf{S}(\boldsymbol{\omega}_{e,c}^c)\mathbf{R}_n^c\mathbf{h}^n + \mathbf{R}_e^h\mathbf{S}(\boldsymbol{\omega}_{n,e}^e)\mathbf{R}_n^e\mathbf{h}^n - \mathbf{R}_b^h\dot{\mathbf{h}}^n). \tag{E.162}$$

Since the ground is stationary, $\dot{\mathbf{p}}_g^n = \mathbf{0}$, such that equation (E.160) can be rewritten as

$$\dot{\mathbf{h}}^h = -\mathbf{S}(\boldsymbol{\omega}_{c,h}^h)\mathbf{h}^h - \mathbf{R}_c^h\mathbf{S}(\boldsymbol{\omega}_{e,c}^c)\mathbf{R}_n^c\mathbf{h}^n - \mathbf{R}_e^h\mathbf{S}(\boldsymbol{\omega}_{n,e}^e)\mathbf{R}_n^e\mathbf{h}^n - \mathbf{R}_w^h\mathbf{v}_r^w \tag{E.163}$$

where $\dot{\mathbf{p}}^n = \mathbf{R}_b^n \mathbf{v}^b = \mathbf{R}_b^n \mathbf{v}_r^b = \mathbf{R}_w^n \mathbf{v}_r^w$ follows from Assumption 4.1. Let the rotation matrix be written as $\mathbf{R}_w^h = \mathbf{I} + 2\eta_{h,w}\mathbf{S}(\boldsymbol{\epsilon}_{h,w}) + 2\mathbf{S}^2(\boldsymbol{\epsilon}_{h,w})$, which can be inserted into (E.163) as

$$\begin{aligned}\dot{\mathbf{h}}^h = &-\mathbf{S}(\boldsymbol{\omega}_{c,h}^h)\mathbf{h}^h - \mathbf{R}_c^h\mathbf{S}(\boldsymbol{\omega}_{e,c}^c)\mathbf{R}_n^c\mathbf{h}^n - \mathbf{R}_e^h\mathbf{S}(\boldsymbol{\omega}_{n,e}^e)\mathbf{R}_n^e\mathbf{h}^n \\ &- (\mathbf{I} + 2\eta_{h,w}\mathbf{S}(\boldsymbol{\epsilon}_{h,w}) + 2\mathbf{S}^2(\boldsymbol{\epsilon}_{h,w}))\mathbf{v}_r^w. \end{aligned} \tag{E.164}$$

Let the ground avoidance quaternion be the primary task, such that $\mathbf{q}_{n,d} = \mathbf{q}_{n,h}$, then by making $(\mathbf{e}_{q\pm}, \boldsymbol{\omega}_{d,w}^w) \to (\mathbf{0}, \mathbf{0})$ through rotational control, it follows that $\mathbf{q}_{h,w} \to \begin{bmatrix}1 & 0 & 0 & 0\end{bmatrix}^\top$. The system can now be written on cascaded form as

$$\dot{\mathbf{x}}_1 = f_1(t, \mathbf{x}_1) + g(t, \mathbf{x})\mathbf{x} \tag{E.165}$$

$$\dot{\mathbf{x}}_2 = f_2(t, \mathbf{x}_2) \tag{E.166}$$

where $\mathbf{x} = \begin{bmatrix}\mathbf{x}_1^\top & \mathbf{x}_2^\top\end{bmatrix}^\top$, $\mathbf{x}_1 := \mathbf{h}^h$, $\mathbf{x}_2 = \begin{bmatrix}\mathbf{e}_{q\pm}^\top & (\boldsymbol{\omega}_{d,w}^b)^\top\end{bmatrix}^\top$,

$$f_1(t, \mathbf{x}_1) := -\mathbf{S}(\boldsymbol{\omega}_{c,h}^h)\mathbf{h}^h - \mathbf{R}_c^h\mathbf{S}(\boldsymbol{\omega}_{e,c}^c)\mathbf{R}_n^c\mathbf{h}^n - \mathbf{R}_e^h\mathbf{S}(\boldsymbol{\omega}_{n,e}^e)\mathbf{R}_n^e\mathbf{h}^n - \mathbf{v}_r^w \tag{E.167}$$

$$g(t, \mathbf{x}) := \begin{bmatrix}\mathbf{0} & 2\eta_{h,w}\mathbf{S}(\mathbf{v}_r^w) + 2\mathbf{S}(\boldsymbol{\epsilon}_{h,w})\mathbf{S}(\mathbf{v}_r^w) & \mathbf{0}\end{bmatrix}, \tag{E.168}$$

and where $f_2(t, \mathbf{x}_2)$ represents the rotational dynamics in closed loop with any of the rotational control laws from Chapter 3. Consider the unforced system $\dot{\mathbf{x}}_1 = f_1(t, \mathbf{x}_1)$ which can be written in original coordinates as[4]

$$\dot{\mathbf{h}}^h = -\mathbf{S}(\boldsymbol{\omega}_{c,h}^h)\mathbf{h}^h - \mathbf{R}_c^h\mathbf{S}(\boldsymbol{\omega}_{e,c}^c)\mathbf{R}_n^c\mathbf{h}^n - \mathbf{R}_e^h\mathbf{S}(\boldsymbol{\omega}_{n,e}^e)\mathbf{R}_n^e\mathbf{h}^n - \mathbf{v}_r^w. \tag{E.169}$$

Let a Lyapunov function candidate be defined as

$$V = \frac{1}{2}(\mathbf{h}^h)^\top\mathbf{h}^h \tag{E.170}$$

which by differentiation and inserting (E.169) results in

$$\dot{V} = (\mathbf{h}^h)^\top(-\mathbf{S}(\boldsymbol{\omega}_{c,h}^h)\mathbf{h}^h - \mathbf{R}_c^h\mathbf{S}(\boldsymbol{\omega}_{e,c}^c)\mathbf{R}_n^c\mathbf{h}^n - \mathbf{R}_e^h\mathbf{S}(\boldsymbol{\omega}_{n,e}^e)\mathbf{R}_n^e\mathbf{h}^n - \mathbf{v}_r^w). \tag{E.171}$$

The terms can be shown to be zero as

$$(\mathbf{h}^h)^\top\mathbf{S}(\boldsymbol{\omega}_{c,h}^h)\mathbf{h}^h = 0 \tag{E.172}$$

$$(\mathbf{h}^h)^\top\mathbf{R}_c^h\mathbf{S}(\boldsymbol{\omega}_{e,c}^c)\mathbf{R}_n^c\mathbf{h}^n = (\mathbf{h}^h)^\top\mathbf{R}_c^h\mathbf{S}(\boldsymbol{\omega}_{e,c}^c)\mathbf{R}_h^c\mathbf{h}^h = 0 \tag{E.173}$$

$$(\mathbf{h}^h)^\top\mathbf{R}_e^h\mathbf{S}(\boldsymbol{\omega}_{n,e}^e)\mathbf{R}_n^e\mathbf{h}^n = (\mathbf{h}^h)^\top\mathbf{R}_e^h\mathbf{S}(\boldsymbol{\omega}_{n,e}^e)\mathbf{R}_h^e\mathbf{h}^h = 0 \tag{E.174}$$

$$(\mathbf{h}^h)^\top\mathbf{v}_r^w = \begin{bmatrix}0 & 0 & ||\mathbf{h}^c||\end{bmatrix}\begin{bmatrix}V_a \\ 0 \\ 0\end{bmatrix} = 0 \tag{E.175}$$

such that

$$\dot{V} = 0. \tag{E.176}$$

[4]To avoid confusion with the different frames, the system is kept in its original coordinates.

This means that as long as the ground avoidance quaternion is perfectly tracked ($\mathbf{x}_2 = \mathbf{0}$), the relative distance between the ground and the UAV will neither increase nor decrease, such that the UAV will move tangentially to the ground. Furthermore it follows that the unforced system $\dot{\mathbf{x}}_1 = f_1(t, \mathbf{x}_1)$ is bounded. The interconnection term can be bounded as

$$||g(t,\mathbf{x})|| \leq \begin{bmatrix}\mathbf{0} & 2||\eta_{h,w}\mathbf{S}(\mathbf{v}_r^w)|| + 2||\mathbf{S}(\boldsymbol{\epsilon}_{h,w})\mathbf{S}(\mathbf{v}_r^w)|| & \mathbf{0}\end{bmatrix}, \tag{E.177}$$

where $|\eta_{h,w}| \leq 1$, $||\mathbf{v}_r^w|| \leq \beta_{V_{max}}$ using Lemma 3.1 and $||\boldsymbol{\epsilon}_{h,w}|| \leq 1$. The origin of the rotational error dynamics $\dot{\mathbf{x}}_2 = f_2(t, \mathbf{x})$ can be shown to be uniformly exponentially stable by using any of the rotational control laws in Chapter 3 (except the adaptive controller). From (E.176) the Lyapunov derivative is zero whenever the ground avoidance quaternion is perfectly tracked. The ground avoidance quaternion and corresponding angular velocity are fed back through the desired trajectories to the rotational control laws, which are tracked by the control laws making $\mathbf{x}_2 \to \mathbf{0}$ exponentially fast. As $\mathbf{x}_2 \to \mathbf{0}$, $\dot{V} \to 0$ such that the distance to the ground goes to a constant $\beta_h > 0$. Hence, it follows that the position relative the ground becomes lower bounded as $||\mathbf{h}^h|| \geq \beta_h > 0$, and collision with the ground is avoided.

E.25 Proof of Theorem 5.1

The quaternion is given as $\mathbf{q}_{n,h} = \mathbf{q}_{n,e} \otimes \mathbf{q}_{e,c} \otimes \mathbf{q}_{c,h}$. When the primary task is active, it follows from Lemma 5.2 that $||\mathbf{h}^c|| \geq \beta_h > 0 \; \forall t \geq t_0$. As the primary task is completed, it follows from Property 5.1 that $\mathbf{q}_{c,h} = \begin{bmatrix}1 & 0 & 0 & 0\end{bmatrix}^\top$ reducing the quaternion to $\mathbf{q}_{n,h} = \mathbf{q}_{n,c} = \mathbf{q}_{n,e} \otimes \mathbf{q}_{e,c}$ where the secondary task becomes active. Using Lemma 5.1, the secondary task ensures that $||\mathbf{c}^c|| \geq \beta_c > 0 \; \forall t \geq t_0$. As the secondary task is completed, Property 5.1 reduces the quaternion to $\mathbf{q}_{n,h} = \mathbf{q}_{n,e}$ which by using Lemma 4.1 ensures that $||\mathbf{e}^e|| \to \mathcal{H}(\delta, \Delta)$.

E.26 Proof of Lemma 5.3

The quaternion $\mathbf{q}_{n,d}$ is naturally constrained to the set $\mathcal{S}^3$ such that $||\mathbf{q}_{n,d}|| = 1$. The angular velocity vector can be written as $\boldsymbol{\omega}_{n,d}^d = \mathbf{R}_e^d\boldsymbol{\omega}_{n,e}^e + \mathbf{R}_c^d\boldsymbol{\omega}_{e,c}^c + \mathbf{R}_h^d\boldsymbol{\omega}_{c,h}^h + \boldsymbol{\omega}_{h,d}^d$ where the the rotation matrices are bounded as $||\mathbf{R}|| = 1$ and where $\boldsymbol{\omega}_{h,d}^d$ is bounded by design such that $||\boldsymbol{\omega}_{h,d}^d|| \leq \beta_{\omega_w}$. From (E.103) $\boldsymbol{\omega}_{n,e}^e = \mathbf{S}^\dagger(\mathbf{e}^e)\mathbf{R}_b^e\mathbf{v}^b$ where by using Lemma 3.1 and Assumption 2.1 the ground velocity becomes bounded as $||\mathbf{v}^b|| \leq \beta_{V_{max}} + \beta_{V_{wind}}$ and by using Property 4.1 it follows that $||\mathbf{e}^e|| > 0$, such that $||\boldsymbol{\omega}_{n,e}^e|| \leq \beta_{\omega_e}$. From (E.145) $\boldsymbol{\omega}_{e,c}^c = \mathbf{S}^\dagger(\mathbf{c}^c)(\mathbf{R}_e^c\mathbf{S}(\boldsymbol{\omega}_{n,e}^e)\mathbf{R}_n^e\mathbf{c}^n - \mathbf{R}_n^c\dot{\mathbf{c}}^n)$ where $||\mathbf{c}^c|| \geq \beta_c$ from Lemma 5.1, $||\dot{\mathbf{c}}^n|| = ||\mathbf{R}_b^n\mathbf{v}^b|| \leq \beta_{V_{max}} + \beta_{V_{wind}}$, $||\mathbf{c}^n|| \leq \beta_{c,max}$ since obstacles outside the detection box are ignored, and hence $||\boldsymbol{\omega}_{e,c}^c|| \leq \beta_{\omega_c}$. From (E.162) $\boldsymbol{\omega}_{c,h}^h = \mathbf{S}^\dagger(\mathbf{h}^h)(\mathbf{R}_c^h\mathbf{S}(\boldsymbol{\omega}_{e,c}^c)\mathbf{R}_n^c\mathbf{h}^n + \mathbf{R}_e^h\mathbf{S}(\boldsymbol{\omega}_{n,e}^e)\mathbf{R}_n^e\mathbf{h}^n + \mathbf{R}_b^h\mathbf{v}^b)$ where $||\mathbf{h}^h|| > 0$ using Lemma 5.2, $||\mathbf{h}^n|| \leq \beta_{h,max}$ since points of the ground outside the detection box are ignored, and hence $||\boldsymbol{\omega}_{c,h}^h|| \leq \beta_{\omega_h}$. It follows that $||\boldsymbol{\omega}_{n,d}^d|| \leq \beta_{\omega_e} + \beta_{\omega_c} + \beta_{\omega_h} + \beta_{\omega_w} \leq \beta_{\omega_d}$, and where the the angular acceleration is found using a saturated filter which ensures that $||\dot{\boldsymbol{\omega}}_{n,d}^d|| \leq \beta_{\dot{\omega}_d}$.